Contents

Journal of Agricultural Machinery

Vol. 15   **No. 1**   **2025**

Contents

Artificial Neural Network (ANN) Modeling of Plasma and Ultrasound-assisted Air Drying of Cumin Seeds

M. Namjoo [ID] [1], M. Moradi [ID] [2*], M. A. Nematollahi [ID] [2], H. Golbakhshi [ID] [3]

1- Department of Mechanical Engineering of Biosystems, Faculty of Agriculture, University of Jiroft, Jiroft, Iran
2- Department of Biosystems Engineering, College of Agriculture, Shiraz University, Shiraz, Iran
3- Department of Mechanical Engineering, University of Jiroft, Jiroft, Iran
(*- Corresponding Author Email: moradih@shirazu.ac.ir)

Abstract

In this study, the air drying of cumin seeds was boosted by cold plasma pre-treatment (CPt) followed by high-power ultrasound waves (USp). To examine the impact of included effects, different CP exposure times (0, 15, and 30 s), sonication powers (0, 60, 120, and 180 W), and drying air temperatures (30, 35, and 40 °C) were selected as input variables. A series of well-designed experiments were conducted to evaluate drying time, effective moisture diffusivity, and energy consumption, as well as color change and rupture force of dried seeds for each drying program. Numerical investigations can effectively bypass the challenges associated with experimental analysis. Therefore, the wavelet-based neural network (WNN), the multilayer perceptron neural network (MLPNN), and the radial-basis function neural network (RBFNN), as three well-known artificial neural networks models, were used to map the inputs and output data and the results were compared with the Multiple Quadratic Regression (MQR) analysis. According to the results, the WNN model with an average correlation coefficient of $R^2 > 0.92$ for the train data set, and $R^2 > 0.83$ for the test data set provided the most beneficial tool for evaluating the drying process of cumin seeds.

Keywords: Artificial neural network, Cold plasma, Cumin seeds, Drying, Ultrasound

Nomenclature	
MR	Moisture ratio (-)
M_t	Time-dependent moisture content of the seeds (-)
M_0	Primary moisture content of the seeds (-)
M_e	Equilibrium Moisture content (-)
D_{eff}	Diffusion coefficient (m^{2}s^{-1})
t	Drying time (min)
M	Moisture concentration (-w.b.)
ΔE	Total color change (-)
L^*	Whiteness/darkness (-)
a^*	Redness/greenness (-)
b^*	Yellowness/blueness (-)
L	Half thickness of the drying body (m)
y	Dependent variable (-)
x	Independent variable (-)
β	Constant term (-)

Introduction

Cumin seed (*Cuminum Cyminum* L.) is a seed from the *Apiaceae* family, formerly called Umbelliferae. Umbelliferous seeds are rich in essential oil content, offering valuable applications in the food, perfume, cosmetic, and pharmaceutical sectors of the industry (Guo, An, Jia, & Xu, 2018; Merah *et al.,* 2020). Thanks to the high levels of petroselinic acid and other bioactive molecules in cumin seed, it is valued for its medicinal and therapeutic properties. Moreover, cumin seeds are widely used as a spice in cooking due to their strong aroma and warm bitterish taste (Namjoo, Moradi, Niakousari, & Karparvarfard, 2022), dominated by the flavor compound cumin aldehyde. The drying process has a crucial role in the production of high-quality cumin seeds. This process also reduces the bulk volume and facilitates the transportation and disposal of end-products (Khalo ahmadi, Roustapour, & Borghaee, 2022). In initial drying, the freshly harvested plants are exposed to sunlight for easier separation of cumin seeds. Then, the drying process should be continued, whether by sun or dryer, until the final level of moisture content of seeds reaches 10% on the wet basis (Namjoo, Dibagar, Golbakhshi, Figiel, & Masztalerz, 2024).

The essential oil of cumin has outstanding chemical and biological characteristics which may be badly affected by heating (Guo *et al.,* 2018). Shortening the drying period is an effective approach to minimize the exposure time of samples to the harmful effects of dehydration. Therefore, to accelerate the drying process and preserve the natural characteristics of the samples, some physical-based treatments, prior to the main single or hybrid drying procedures, have been investigated by researchers (Tabibian, Labbafi, Askari, Rezaeinezhad, & Ghomi, 2020).

The cold plasma (CP) and the ultrasound waves (US) are two physical-field techniques which have widespread applications in the drying process. These non-thermal and non-chemical technologies can improve the performance of drying systems, without leaving any adverse effects on chemical structure and physical properties of samples (Zhou *et al.,* 2020). By exposing the food materials to CP, some surface reactions occur and alters the surface topography of the skin layer (Miraei Ashtiani et al., 2020; Osloob, Moradi, & Niakousari, 2023). The internal microstructure may also be changed by propagation of high-power ultrasound waves during the air-drying process. As a result, when the CP pretreated samples are dried in a US-assisted air drying system, the effective moisture diffusivity significantly increases, resulting in a higher rate of water evaporation compared to the performance of single dryers (Moghimi, Farzaneh, & Bakhshabadi, 2018; Shashikanthalu, Ramireddy, & Radhakrishnan, 2020).

Besides the effective moisture diffusivity and drying time, the amount of consumed energy, as well as the total color change, and rupture force of end-products may also be evaluated for assessing the performance of the upgraded system (Moradi, Ghasemi, & Azimi-Nejadian, 2021; Namjoo, Moradi, Niakousari, *et al.,* 2022). In this case, conducting a comprehensive experimental investigation appears to be daunting and could require significant time and resources. Forecasting the dehydration process of various crops by numerical modeling is a more practical approach for improving the performance of the drying systems (Sun, Zhang, & Mujumdar, 2019).

Based on the results of the limited number of experiments, some regression-based methods such as multiple linear regressions (MQR) can establish a proper relationship between inputs and outputs and predict the performance of a system for non-inspected drying conditions (Meerasri & Sothornvit, 2022). The artificial neural network (ANN) is another category of data-driven methods that is developed based on the biological neural systems in the human body. This class of computing models is also coupled with artificial intelligence to improve the correlation between inputs and outputs. In the

nonlinear problems with more than one input parameter, ANN can readily forecast the values of desired output variables (Kaveh, Abbaspour Gilandeh, Amiri Chayjan, & Mohammadigol, 2019). Recently, ANN has been widely used to investigate the drying process of various crops, including pumpkin seeds (Dhurve, Tarafdar, & Arora, 2021), basil seeds(Amini, Salehi, & Rasouli, 2021), ginkgo biloba seeds (Bai, Xiao, Ma, & Zhou, 2018), potato slice (Rezaei, Behroozi-Khazaei, & Darvishi, 2021), pistachio nuts, squash, and cantaloupe seeds (Mohammad Kaveh, Chayjan, & Khezri, 2018), mushroom slices (Liu *et al.*, 2019), and green tea leaves (Kalathingal, Basak, & Mitra, 2020).

As mentioned earlier, in case of cumin seed drying, the quality of end-products, the energy costs, and production rate may significantly improve by CP pretreatment followed by ultrasound-assisted air drying. To the best knowledge of authors, there is no predicting model developed for estimating the positive influence of cold plasma and high-power ultrasound waves on the drying of cumin seeds. To fill this gap, the drying of cumin seeds is investigated in the current research and through several experiments, drying time, effective moisture diffusivity, energy consumption, total color change, and rupture force (as the output variables) were measured for different drying air temperature, CP exposure time (CPt), and ultrasound power (USp). Then, the wavelet-based neural network (WNN), the multilayer perceptron (MLP), and radial basis function (RBF) neural networks were employed for mapping the input and output data. For evaluating the accuracy of predictions, the results of multiple linear regressions (MQR) were also obtained and compared with the results of neural network-based models.

Materials and Methods

Sample Preparation and CP Pretreatment

In this research, freshly harvested cumin seeds were provided from a local farm in Khatam County in Yazd province, central Iran to certify genetic purity. The samples were characterized by longitudinal ridges, are yellow-brown, and have 69.4% (d.b.) initial moisture content. For uniform distribution of moisture throughout the samples, the healthy seeds were wrapped in polythene plastic bags and kept refrigerated at 4±1 °C and relative humidity of 53±1%. The CP device (Nik Plasma Tech Co., Tehran, Iran) in the excitation mode of Dielectric Barrier Discharge (DBD) was used to pretreat the seeds. Before each drying run, 60 g of cumin seed sample was used for CP pretreatment at different exposure times of 15 or 30 s. After CP pretreatment, 10 g of the sample was separated to determine the moisture content as well as to evaluate the color characteristics of the pretreated seeds to ensure that no significant alteration occurred in the initial moisture level and color quality of the samples. The rest of the pretreated sample, 50 g, was placed in the drying chamber and exposed to different drying programs for further analysis. Runs with no CP pretreatment (CPt: 0 s) were also conducted as control experiments. At the laboratory site, the temperature and relative humidity of the ambient air were 25 °C and 50%, respectively.

Ultrasound-Assisted Air-Drying Process

To conduct the main drying experiment, a hybrid ultrasound-assisted convective dryer was constructed at the Faculty of Agriculture, Shiraz University, Shiraz, Iran, as demonstrated in Figure 1. The drying unit is equipped with a centrifugal fan (2200 RPM, 550 m^3 h^{-1}, and BEF-14-7V2SP), controller unit of input variables, multifunction monitoring system (humidity, temperature, energy, and weight), electrical heater (including 3 kW electrical heating coils), drying chamber, sonication unit (20 kHz), and inverter. The sonication unit (Farasot Zagros Co., Iran) contained a 1200 W generator, power meter (Model Delta power, Ziegler Co., Germany), transducer, and horn. The piezoelectric transducer was made up of four piezoceramic rings with an outer diameter of 50 mm, an inner diameter of 20 mm, and a thickness of 6 mm. Additionally, a thermal

velocity probe was used to measure the linear air flow rate. The forward one-phase centrifugal fan propelled the drying air toward the electric heater, warming it to achieve the desired temperature. For online moisture content control, the samples enclosed in the cylindrical mesh basket were weighed every 3 minutes. A detailed description of the main hybrid drying unit can be found in Namjoo et al., (2022). Each drying trial lasted until the final moisture level of about 10±1% (d.b.) was attained. Table 1 renders a detailed description of the drying programs at the constant air velocity of 0.6 m s⁻¹. The experimental results comparing the effects of single and combined applications of cold plasma and ultrasound waves on the air drying of cumin seeds were analyzed against a control group.

Measured Parameters

Drying Time (DT)

This study utilizes a first-order kinetic model to describe the moisture transfer during the drying process of cumin seeds, providing essential experimental data on drying kinetics, as follows (X. Wang et al., 2023):

$$MR = \frac{Mt - M_e}{M_0 - M_e} \qquad (1)$$
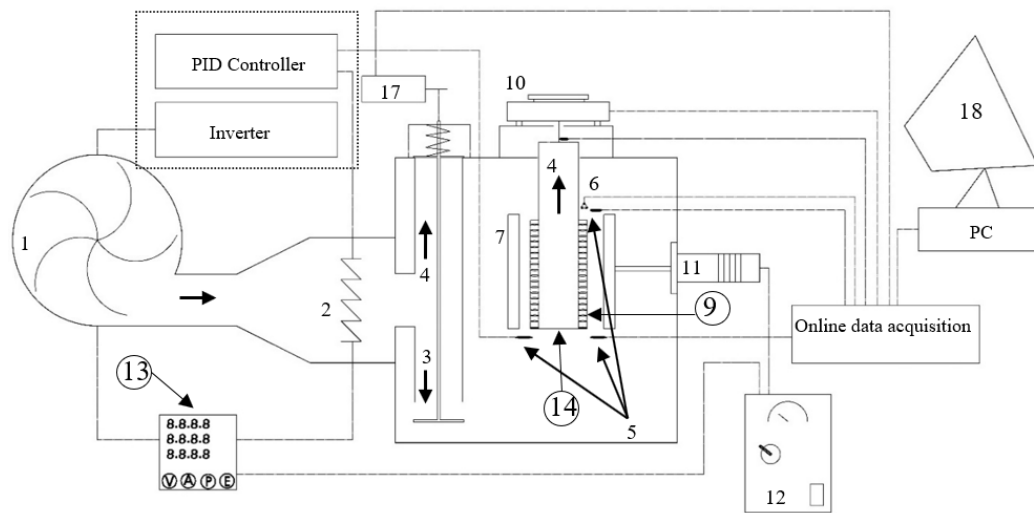
Fig. 1. A schematic view of the developed ultrasound assisted air dryer: 1- Centrifugal fan, 2- Thermal element, 3- Air in, 4- Air out, 5- Temperature and relative humidity sensor, 6- Laser sighting infrared sensor, 7- Cylindrical vibrating element (ultrasonic horn), 8- Cylindrical drying chamber, 9- Mesh screen, 10- Digital balance, 11- Ultrasonic transducer, 12- Ultrasonic generator, 13- Power meter, 14- Drying samples, 15- PID controller, 16- Electrical panel, 17- Gearbox DC motor, and 18- Monitor (Namjoo, Moradi, Dibagar, & Niakousari, 2022)

Table 1- A detailed description of the different seed drying programs designed for this research

Program description	Drying program	Drying air temperature (T)	Ultrasound power (USp)	Cold plasma pretreatment time (CPt)
Convective drying (Control group)	CV	30, 35, and 40 °C	0	0
Convective drying assisted by ultrasound waves	USCV	30, 35, and 40 °C	60, 120, and 180 W	0
Convective drying with cold plasma pretreatment	CPCV	30, 35, and 40 °C	0	15 and 30 s
Convective drying assisted by ultrasound waves with cold plasma pretreatment	CPUSCV	30, 35, and 40 °C	60, 120, and 180 W	15 and 30 s

Where, MR is the moisture ratio (-), M is the moisture content (% d.b.), and subscripts t, e, and 0 describe the instantaneous, equilibrium, and initial values, respectively. The experiments were performed to acquire data for the seed's moisture content as a function of time. Cumin seeds with an initial moisture content of 69.4±1% (d.b.) were dried to reach the final moisture level of 10±1% (d.b.). The required time was recorded in the drying program as the drying duration.

Effective Moisture Diffusivity (D_{eff})

Fick's second law was used to determine effective moisture diffusivity as suggested in the papers on drying foods. Here, the effective moisture diffusivity of the drying body was calculated by establishing a graphical method and assuming one-dimensional moisture movement, uniform initial moisture distribution, negligible shrinkage, and constant diffusion coefficient. The actual geometry of the drying body was a cylindrical mesh basket with the thickness and height of 8 and 130 mm, respectively, which was assumed similar to a rectangular slab with an airflow perpendicular to the samples. Therefore, the analytical solution for the drying body as a slab object is given in Eq. (2) (Chatzilia, Kaderides, & Goula, 2023; Lingayat, VP, & VRK, 2021):

$$MR = \frac{8}{\pi^2} \sum_{n=0}^{\infty} \frac{1}{(2n+1)^2} \exp\left(\frac{-(2n+1)^2 \pi^2 D_{eff}\cdot t}{4L^2}\right) \quad (2)$$

where L represents half of the thickness of the drying body (m), and n is a positive integer that stands for drying terms. By substituting n= 0 into Eq. (2), an excellent proximate solution is given in long drying times as follows (Gong *et al.,* 2020):

$$\ln(MR) = \ln\left(\frac{8}{\pi^2}\right) - \left(\frac{\pi^2 D_{eff}\cdot t}{4L^2}\right) \quad (3)$$

The effective moisture diffusivity (D_{eff}) is typically established by a graphical method. This way, the experimental result is presented in terms of the natural logarithm of the moisture ratio (MR) as a function of drying time, as displayed in Eq. (4). The outcome is a linear regression ($A \times k_1 + B$), in which the slope of the line (k_1) is used to compute the effective moisture diffusivity as follows (Dibagar, Kowalski, Chayjan, & Figiel, 2020):

$$k_1 = -\frac{\pi^2 D_{eff}}{4L^2} \quad (4)$$

Energy Consumption (EC)

In this research, energy consumption refers to the energy, which was supplied for the electrical elements of the main drying system, including fan, heating unit, sonication unit, etc. This amount of energy is required to remove water from the cumin seeds and attain the final moisture content of 10% (d.b.) in each experimental run. In this regard, a Power Meter instrument (Model Delta power, Ziegler Co., Germany) was utilized, and the consumed energy was directly recorded in kilowatt-hours (kWh).

Total Color Change (ΔE)

A new colorimetric system was employed to characterize the color quality of the fresh and dried cumin seeds. The color was determined using image processing technique. To ensure an acceptable image quality, a good camera and proper illumination were applied. The device, developed for measuring total color change, consisted of four main elements of a rectangular chamber (35 ×25 ×25 cm), sample holder, camera (Canon EOS 4000D) with three detectors per pixel: Red, Green, and Blue, and LED lamps. After locating the fresh and dried samples on the holder in the chamber's center, digital images were captured by the camera from the top. The images were then stored on a PC and processed with algorithms written in the toolbox of MATLAB R2013a to translate the color space of RGB to the reference zone L^* (whiteness/darkness), a^* (redness/greenness), and b^* (yellowness/blueness), followed by calculating the change in the color values of samples (ΔE) as follows (Izli & Polat, 2019; Özkan Karabacak, 2019):

$$\Delta E = \sqrt{(L^* - L_0^*)^2 + (a^* - a_0^*)^2 + (b^* - b_0^*)^2} \qquad (5)$$

where, index 0 denotes the color specifications of the fresh cumin seeds. Higher values of ΔE stand for the significant difference between the color of fresh and dried seed samples.

Rupture Force (RF)

The spice industry relies on the size reduction of herbaceous plants, achieved through various forces to create particles with precise shapes and dimensions. Size reduction, one of the most energy-consuming processes in the food industry, is directly linked to microbiological and chemical stability and convenience (Saiedirad & Mirsalehi, 2010). Rupture force is defined as the amount of force needed to trigger the rupture of a product. It is related to the firmness and brittleness of the sample (Saiedirad *et al.,* 2008). The rupture force of the dried cumin seeds was assessed by an Instron Universal Testing Machine (Model STM-20, SANTAM Co., Iran) equipped with a compression load cell (Model DBBP-20, BONGSHIN Co., Korea), with an accuracy of ±0.01 N in force and ±0.001 mm in deformation. The mechanical test was repeated ten times for each drying point and reported in N.

Artificial Neural Network Modeling

The MLPNN training

The well-known multilayer perceptron neural network (MLPNN) is schematically described in Fig. 2. As can be seen, different layers with several neurons are considered in this model. The adjacent neurons are connected by weights (w_{ij}). The weights are corrected in an iterative back-propagation algorithm and in each iteration (q) are estimated as follows (Habibi & Nematollahi, 2019; Moosavi, Nematollahi, & Rahimi, 2021; Nematollahi, Jamali, & Hosseini, 2020; Nematollahi & Mousavi Khaneghah, 2019;

Sun *et al.,* 2019; Zakeri, Naghavi, & Safavi, 2009):

$$w_{ij}(q + 1) = w_{ij}(q) + \Delta w_{ij}(q) \qquad (6)$$

In order to minimize the error in prediction of output variables, the generalized delta-learning rule is employed, and the following equation is proposed for computing the values of $\Delta w_{ji}(q)$:

$$\Delta w_{ji}(q) = \gamma f'_j(.) x_i \sum_{k=1}^{K} \left\{ \left[(P_m)_k - (P_p)_k \right] f'_k(.) w_{kj}(q) \right\} + \alpha \Delta w_{ji}(q-1) \qquad (7)$$

where P_p is the value predicted by NN, P_m is the experimentally measured data, and γ is the learning rate. The derivative of transfer function relative to its input variable x_i is denoted by $f'(.)$, and α is the momentum value and is a positive number between 0 and 1.

The RBFNN training

In the radial basis function neural network (RBFNN), two feed-forward layers are used for fast training of NNs. RBFNN considers the Gaussian basis function φ for weighted sum of input data vector $\mathbf{X}$. Then, the components of output vector Y_k are computed as (Nematollahi & Mousavi Khaneghah, 2019):

$$Y_k(\mathbf{X}) = \sum_{j=1}^{n} w_{kj} \varphi_j \left(\left\| \mathbf{X} - U_j \right\| \right) + b_k \qquad (8)$$

Where, U is the vector of center of basis function φ.

The WNN training

The WNN is developed based on wavelet basis functions for training data and estimating the outputs. The wavelet algorithm is not iterative and compared to the conventional MLPNN, the learning time and the accuracy of the results improve greatly. The employed basis functions also allow for inclusion of multiresolution frameworks in the structure of WNN (Safavi & Romagnoli, 1997).
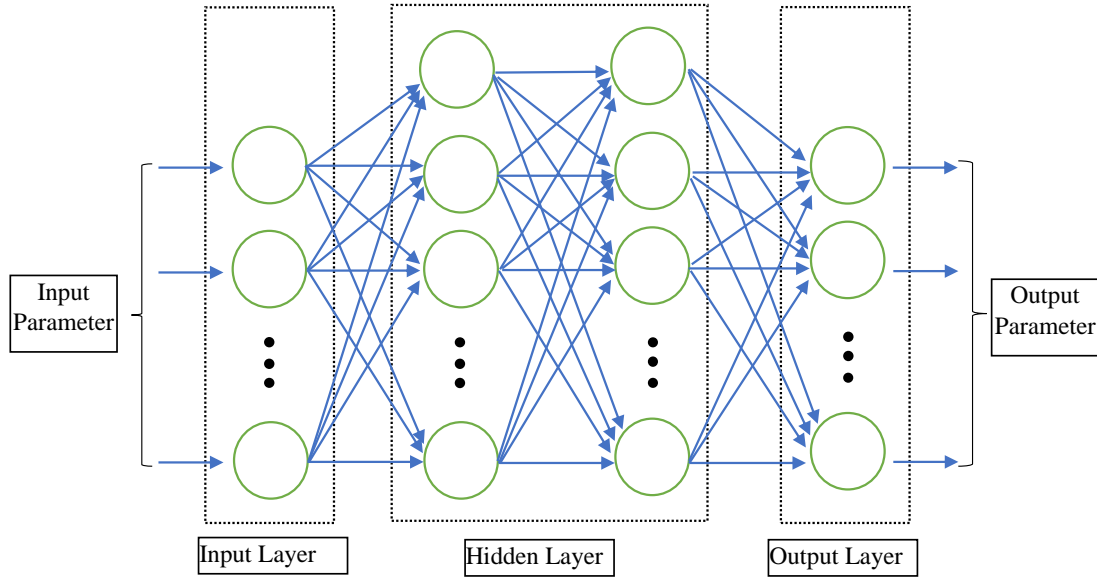
Fig. 2. Schematic illustration of the multilayer perceptron neural networks (MLPNNs).

In the WNN approach, the outputs of any function $\mathbf{F}(\mathbf{X}) \in L^2(R)$ are estimated as:

$$\mathbf{F}(\mathbf{X}) = \sum_{s=-\infty}^{s=+\infty} a_{0,s} \phi_{0,s}(\mathbf{X}) + \sum_{r=-\infty}^{0} \sum_{s=-\infty}^{s=+\infty} d_{r,s} \psi_{r,s}(\mathbf{X}) \qquad (9)$$

Where $a_{0,s}$ and $d_{r,s}$ are constant coefficients, and the scaling functions $\phi_{r,s}$ and the wavelet functions $\psi_{r,s}$ are given by:

$$\psi_{r,s}(\mathbf{X}) = 2^{-r/2} \psi(2^{-r/2}\mathbf{X} - s) \quad r, s \in Z \qquad (10)$$

$$\phi_{r,s}(\mathbf{X}) = 2^{-r/2} \phi(2^{-r/2}\mathbf{X} - s) \quad r, s \in Z \qquad (11)$$

in which r and s are, respectively, the dilation and translation factors.

In order to evaluate the unknown coefficients "a" and "d", Safavi and Romagnoli (1997) rearranged Eq. (9) into the following form:

$$\mathbf{F}(\mathbf{X}) - \mathbf{F}_r(\mathbf{X}) = \sum_{s=-\infty}^{s=+\infty} c_{r,s} \theta_{r,s}(\mathbf{X}) \qquad (12)$$

Then the set of linear equations were derived for the problem from:

$$\overline{\mathbf{F}}(\mathbf{X}) = \mathbf{AC} \qquad (13)$$

Where,

$$\overline{\mathbf{F}} = \begin{bmatrix} \overline{\mathbf{F}}(X_1) \\ \overline{\mathbf{F}}(X_2) \\ \vdots \\ \overline{\mathbf{F}}(X_n) \end{bmatrix}, \quad \mathbf{A} = \begin{bmatrix} \theta_1(X_1) & \cdots & \theta_k(X_1) \\ \vdots & & \vdots \\ \theta_1(X_n) & \cdots & \theta_k(X_n) \end{bmatrix}, \quad \mathbf{C} = \begin{bmatrix} c_1 \\ c_2 \\ \vdots \\ c_k \end{bmatrix} \qquad (14)$$

The variable θ in Eq. (14) includes both scaling and wavelet functions. As a result, the vector C is found as:

$$\mathbf{C} = ((\mathbf{A^T A})^{-1} \mathbf{A^T}) \overline{\mathbf{F}} = \mathbf{A^+} \overline{\mathbf{F}} \qquad (15)$$

Where $\mathbf{A^+}$ denotes the pseudo-inverse of matrix $\mathbf{A}$.

For more details about the WNN methodology and its training process, one could refer to. Figure 3 clearly shows the training process in WNN.

Multiple Quadratic Regression (MQR) Analysis

In addition to artificial neural networks, the Multiple Quadratic Regression (MQR) method is also used in this study to develop the predicting models. In this regard, the performance of the drying system, described by output variables y, is correlated by the following expression to the input parameters x_i (CPt, T and USp):

$$y = \beta_{11}x_1^2 + \beta_{22}x_2^2 + \beta_{33}x_3^2 + \beta_{12}x_1x_2 + \beta_{13}x_1x_3 + \beta_{23}x_2x_3 + \beta_1x_1 + \beta_2x_2 + \beta_3x_3 + \beta_0$$

$$(16)$$
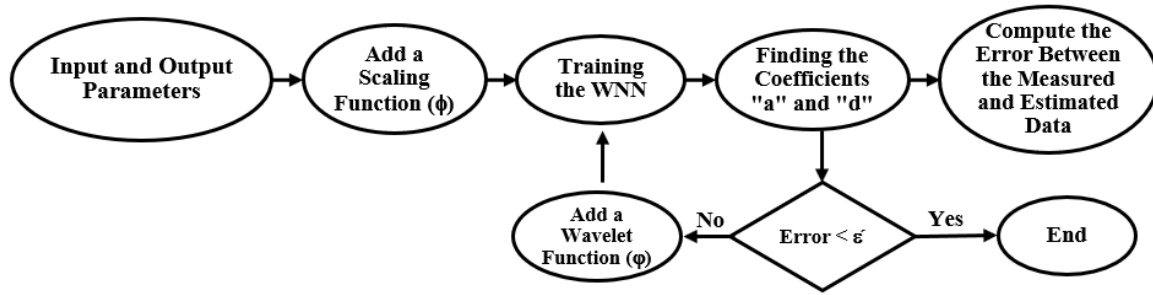
Fig. 3. The training process in WNN

where β_0 is a constant, and β_i, β_{ii}, and β_{ij} are the linear, pure quadratic, and interaction coefficients, respectively (Namjoo, Golbakhshi, Kamandar, & Beigi, 2024).

All aforementioned numerical modeling types were carried out using MATLAB software (Matlab, 2016). In order to develop and validate the models, 80% of the experimentally measured data was used for training and the remaining 20% was used for the test phase.

ANN and MQR Models Validation

To show the goodness of fit and performance of the used models, indices of the correlation coefficient (R), root mean square error (RMSE), the mean absolute percentage error (MAPE), and the mean absolute error (MAE) were calculated using Eqs. (17)-(20), respectively (Wang, Tian, & An, 2022).

$$R = \frac{\sum_{i=1}^{n}(Y_{pre\,i}-\overline{Y_{pre}})(Y_{exp\,i}-\overline{Y_{exp}})}{\sqrt{\sum_{i=1}^{n}(Y_{pre\,i}-\overline{Y_{pre}})^2 \sum_{i=1}^{n}(Y_{exp\,i}-\overline{Y_{exp}})^2}},$$ (17)

i=1,2,3,.., N

$$RMSE = \left[\frac{1}{n}\sum_{i=1}^{n}(Y_{pre\,i}-Y_{exp\,i})^2\right]^{\frac{1}{2}},$$ (18)

i=1,2,3,.., N

$$MAPE = \frac{1}{n}\sum_{i=1}^{n}\left|\frac{Y_{pre\,i}-Y_{exp\,i}}{Y_{exp\,i}}\right| \times 100,$$ (19)

i=1,2,3,.., N

$$MAE = \frac{1}{n}\sum_{i=1}^{n}|Y_{pre,i}-Y_{exp,i}|,$$ (20)

$$i = 1,2,3,..,N$$

where, $Y_{exp,i}$ and $Y_{pre,i}$ denote the ith experimental (measured) and predicted values, respectively. $\overline{Y_{exp}}$ and $\overline{Y_{pre}}$ are the corresponding mean values of $Y_{exp,i}$ and $Y_{pre,i}$, respectively. High values of R and lower RMSE, MAPE, and MAE outcomes confirm that the proposed model fits well to the experimental drying data, and it can be applied for prediction (Dotto, Souza, Simoes, Morejon, & Moreira, 2017; Nematollahi & Mousavi Khaneghah, 2019).

Results and Discussion

The experimental drying data underwent statistical analysis using IBM SPSS software (version 26). Statistical assessment of the results was performed using a factorial design to find the effect of drying air temperature (T) at three levels (30, 35, and 40 ºC), CPt at three levels (0, 15, and 30 s) and USp at four levels (0, 60, 120, and 180 W) on drying time, effective moisture diffusivity, energy consumption, total color change, and rupture force of dried cumin seeds during drying (Table 2). The experiment was conducted in a complete randomized design (CRD) with three replicates. The degree of freedom, sum squares, means squares, and F-values of the individual linear and interaction terms of CPt, T, and USp were generated through the analysis of variance (ANOVA) table. Additionally, the significance of each program evaluated was analyzed using ANOVA, with the results presented in Table 2.

Table 2- ANOVA results for the main and interaction effects of CPt, T, and USp on the studied parameters.

S.O.V.	D.F.	DT	D_{eff}	EC	ΔE	RF
CPt	2	13758.176^{**}	$1.910E-7^{**}$	1.152^{**}	114.093^{**}	316.732^{**}
T	2	16289.065^{**}	$3.694E-7^{**}$	1.604^{**}	11.901^{**}	18.307^{**}
USp	3	16952.012^{**}	$1.524E-7^{**}$	1.386^{**}	9.916^{**}	464.006^{**}
USp×T	4	136.343^{*}	$1.197E-8^{**}$	0.017^{*}	0.942^{*}	4.286^{**}
CPt×USp	6	1698.744^{**}	$1.101E-8^{**}$	0.077^{**}	0.491^{ns}	25.624^{**}
CPt×T	6	1489.262^{**}	$4.717E-9^{**}$	0.125^{**}	0.468^{ns}	4.267^{**}
CPt×T×USp	12	71.577^{ns}	$1.628E-9^{ns}$	0.018^{**}	0.066^{ns}	0.250^{ns}
Error	72	51.167	1.329E-9	0.005	0.318	0.990
Total	107					

**: significant at 0.01, *: significant at 0.05, and ^{ns}: not significant

Results of the WNN, MLPNN, RBFNN, and MQR models

In this research, we aimed to develop some predicting models for correlating the inputs parameters (CP exposure time, drying air temperature, and ultrasound power) and outputs variables (drying time, effective moisture diffusivity, energy consumption, total color change, and rupture force). These models can readily reveal the optimal dehydration process for cumin seeds. In this regard, three well-known neural networks-based models, namely the MLPNN, RBFNN, and WNN were employed.

In order to minimize the error of MLPNN predictions, sufficient number of hidden layers and neurons should be considered for the architecture of network. In this regard, two hidden layers were used, and the sigmoid function was adopted as the transfer function. In an iterative learning procedure, the number of included neurons was systematically increased for improving the accuracy of predictions. The training process for the network was conducted using the Levenberg–Marquardt algorithm. Then it was found that by using 11 neurons within the hidden layers, acceptable accuracy may be achieved and adding more neurons did not provide any significant contribution.

To calibrate the outputs of the model with the prepared experimental data, the WNN model should be trained by selecting appropriate wavelet and examining different layers of resolution. In the special case of cumin seed drying, the second resolution and the Gaussian type wavelet were found to be the optimal parameters for the WNN.

The performances of WNN, MLPNN, and RBFNN, along with the regression-based MQR model, were evaluated, and their results are given in Table 3. As can be seen, MQR failed to provide accurate predictions, especially very poor results were obtained in this model for the total change in color of dried samples. MLP and RBF models provided sufficient estimations for drying time and energy consumption. However, the average accuracy of MLP was 2.28% better than that achieved in the RBF model. In this study, the most accurate predictions for the performance of drying system were evaluated by the WNN model. The average accuracy of results in WNN for all defined output variables was 3.02% and 5.37% better than MLP and RBF models, respectively. Furthermore, WNN enjoys a non-iterative learning algorithm for training neural networks. This greatly reduces the computational time and provides an important advantage for WNN. Therefore, in the subsequent sections of this paper, we used a WNN model for evaluating the effects of various input parameters on drying time, effective moisture diffusivity, energy consumption, total color change, and rupture force of dried seeds.

Table 3- The performance of the applied MQR and ANN models in prediction of cumin seeds drying parameters.

ANN models	Output variable	R²		RMSE		MAPE		MAE	
		Train	Test	Train	Test	Train	Test	Train	Test
WNN	DT	0.9767	0.9399	5.9701	7.8990	2.0350	3.3251	4.5388	7.1591
	D_{eff}	0.9532	0.8943	$2.4736e^{-10}$	$3.4032e^{-10}$	2.0416	3.6538	$1.3357e^{-10}$	$1.9685e^{-10}$
	EC	0.9718	0.9251	0.0596	0.0797	1.7936	2.0066	0.0473	0.0478
	ΔE	0.9341	0.8339	0.5929	0.8167	3.0305	3.5292	0.3686	0.4643
	RF	0.9532	0.8943	0.3403	0.24736	2.0416	3.0538	0.2519	0.5418
	Avg.	0.9577	0.8971	1.39258	1.808552	2.18846	3.1137	1.04132	1.6426
MLP	DT	0.9681	0.9239	6.3331	8.9526	2.4853	3.522	5.1258	7.2562
	D_{eff}	0.9264	0.8679	0.2274×10^{-9}	0.1895×10^{-9}	2.4963	3.8158	0.1387×10^{-9}	0.1732×10^{-9}
	EC	0.9602	0.9065	0.0650	0.0834	3.1129	2.3476	0.0666	0.0505
	ΔE	0.9256	0.9076	0.5282	0.4661	4.1017	3.6409	0.3694	0.4817
	RF	0.9080	0.8214	1.1574	0.858	2.2521	3.1619	0.9851	0.6942
	Avg.	0.9296	0.9523	2.6804	1.93055	3.40526	2.64444	2.181225	1.559975
RBF	DT	0.9415	0.9594	9.5866	6.4513	4.2339	2.8297	8.5242	5.4283
	D_{eff}	0.8970	0.9378	0.2704×10^{-9}	0.1677×10^{-9}	3.8022	2.9022	0.2878×10^{-9}	0.1776×10^{-9}
	EC	0.9308	0.9430	0.1879	0.1461	3.5674	2.6835	0.124	0.0947
	ΔE	0.8712	0.9183	0.8764	0.6352	5.5838	3.9035	0.7387	0.5475
	RF	0.9050	0.9528	1.8599	0.9688	4.1379	2.7375	1.2427	0.8326
	Avg.	0.9089	0.9422	3.1277	2.05035	4.26504	3.01128	2.6574	1.725775
MQR	DT	0.8379	0.8477	13.7969	12.9660	5.4473	5.4126	11.4930	10.6436
	D_{eff}	0.8325	0.8425	3.27×10^{-10}	3.01×10^{-10}	4.9575	4.3275	2.63×10^{-10}	2.39×10^{-10}
	EC	0.8499	0.8574	0.1220	0.1168	4.4976	4.5901	0.0995	0.0961
	ΔE	0.7936	0.7916	0.7264	0.6798	6.0722	6.0306	0.6203	0.5824
	RF	0.8593	0.8763	1.7927	1.4871	4.6907	4.0843	1.4681	1.1990
	Avg.	0.83464	0.8431	3.2876	3.0500	5.1331	4.8890	2.736175	2.5042

Drying time

The neural network developed on the basis of WNN is used in this section for predicting the impact of various drying programs on the time duration of cumin seeds. As can be seen in Fig. 4, the R^2-values for the training and test data were found to be 0.9681 and 0.9432, respectively. This clearly indicates that the WNN model can properly predict the linear and complex correlations between drying time and the influential input variables. Our results are consistent with the outcomes reported in

earlier related studies. Specifically, the obtained R²-values are in good agreement with the findings of Potisate *et al.* (2014) which

varied between 0.81 and 0.98 across different drying treatments of moringa leaves.
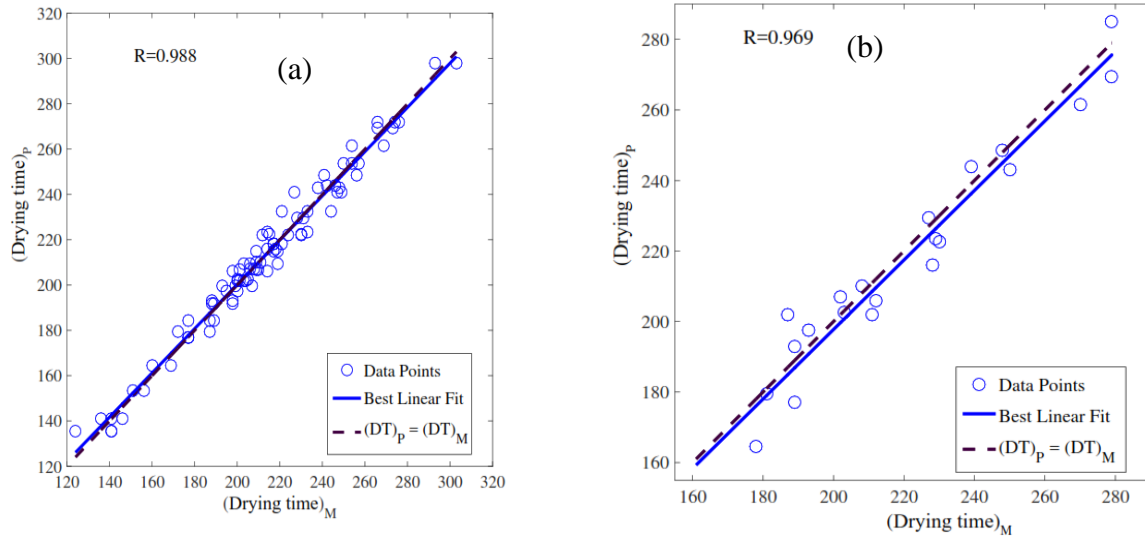
Fig. 4. The regression of the measured and predicted drying time: a) Train data, and b) Test data
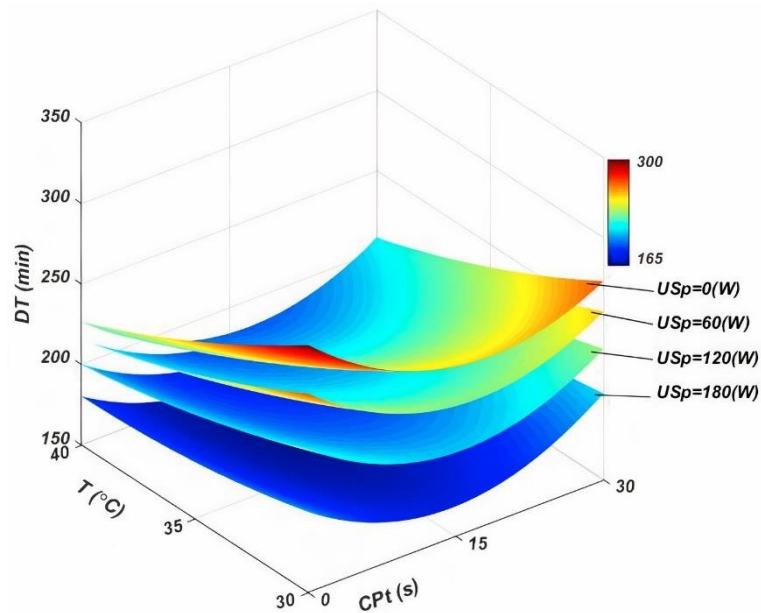
Fig. 5. Response surface plots for the effect of independent variables on drying time of cumin seeds during the drying process

The drying time of cumin seeds was assessed across various drying temperatures, USp, and CPt, with results presented in Fig. 5. In pure convective drying, drying times ranged from 219 to 293 minutes, with higher temperatures leading to faster drying. Introducing ultrasound waves accelerated

drying, with total drying times ranging from 124 to 303 minutes, depending on temperature and ultrasound power. CPt before drying reduced drying times by 11.65% to 15.29% at various temperatures. Combining CP and ultrasound technologies further reduced drying times, with a minimum of 124 minutes

observed. However, longer CPt increased drying times due to surface hardening and increased evaporative resistance. Excessive CPt may disrupt cell walls and hinder water removal. Overall, CPt for 15 seconds significantly reduced drying times in an ultrasound-assisted system.

Effective moisture diffusivity

The results of the WNN model for effective moisture diffusivity were evaluated in Fig 6. The correlation coefficient (R^2) for train and test data was obtained as 0.9264 and 0.9421, respectively. Other introduced statistical measures were also used for further improvement of the model. To this end, the learning procedure continued until the values 0.2274×10^{-9}, 3.1278, and 0.1732×10^{-9} were attained, respectively, for the root mean square error (RMSE), mean absolute percentage error (MAPE), and mean absolute error (MAE). Then, RMSE, MAPE, and MAE were found to be 0.1895×10^{-9}, 2.4963, and 0.1387×10^{-9} for the test data, respectively. Similar conclusions were also made by Onwude *et al.* (2018) and Khanlari *et al.* (2020) for sweet potato and celery drying, respectively.
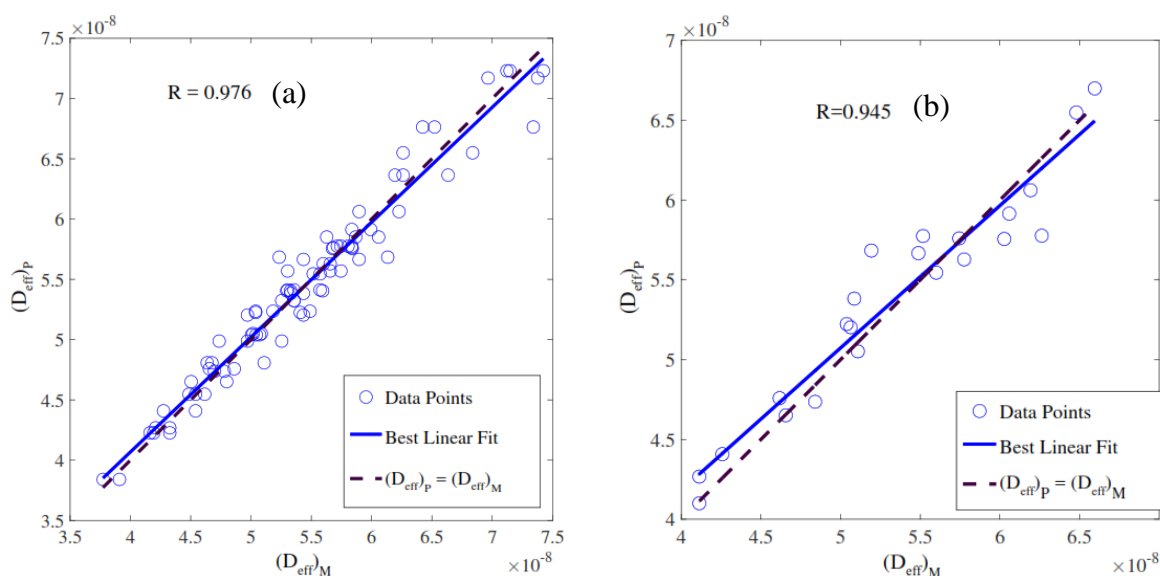
Fig. 6. The regression of the measured and predicted effective moisture diffusivity of cumin seeds: a) Train data, and b) Test data

Figure 7 illustrates the influence of various independent variables on enhancing the effective moisture diffusivity of samples. In a traditional drying setup, elevating the temperature resulted in increased seed diffusivity, reaching a maximum value of 9.29×10^{-10} m² s^{-1} at 40 °C, while the lowest diffusivity of 6.29×10^{-10} m² s^{-1} was observed at 30 °C.

In a combined drying system, varying ultrasound powers led to an increase in moisture diffusivity. The highest diffusivity (1.24×10^{-9} m² s^{-1}) was achieved at 40 °C with an ultrasound power of 180 W, while the lowest (7.51×10^{-10} m² s^{-1}) was observed at 30 °C with 60 W. Exposure to CP for 30 seconds enhanced seed moisture diffusivity. However, ultrasound power contributed more significantly to diffusivity enhancement at the same air temperatures, with longer exposure times (30 s) providing less modification. This suggests that excessive exposure to CP can increase diffusion resistance at the seed's surface.

Energy consumption

The results of experimental analysis for energy consumption were categorized into two test and train datasets and depicted in Figure 8. Two well-suited linear regression functions were proposed based on WNN. The error indices were evaluated in Table 3 for verifying

the predictions. As can be seen, RMSE, MAPE, and MAE for the training data are slightly more than those obtained for the test results. However, the correlation coefficient of results ($R^2 = 0.9722$ for train, and $R^2 = 0.9254$ for test data) demonstrated that the calculated values for energy consumption agree with the experimental results. The energetic investigations for drying of potato (Aghbashlo, Kianmehr, & Arabhosseini, 2008; Akpinar, Midilli, & Bicer, 2005), carrot slices (Nazghelichi, Kianmehr, & Aghbashlo, 2010), kodo millet grains, and fenugreek seeds (Yogendrasasidhar & Setty, 2018) also led to similar results.

Under different drying conditions, the results for energy consumption are given in Fig. 9. Various drying conditions were tested, and energy consumption was analyzed. In conventional convective drying, energy consumption ranged from 2.27 to 2.93 kWh, with lower temperatures resulting in higher energy usage due to longer drying times. Ultrasound-assisted drying showed a range of 1.95-2.93 kWh, with lower consumption at higher temperatures and ultrasound powers. Combining cold plasma pretreatment with ultrasound/convective drying significantly

reduced energy usage to 1.42-2.85 kWh. CP pretreatment alone showed some energy savings, but the combination of CP and ultrasound provided the most efficient drying method, reducing energy consumption while maintaining product quality.

Color change

The results of experimental analysis and the WNN model for the change in color of dried seeds were illustrated in Fig. 10. The predictions of neural network for this variable had $R^2 = 0.9256$ for testing data, and $R^2 = 0.9076$ for training set. So, WNN can provide reliable predictions for the case which have not been experimentally investigated. Guiné *et al.* (2015), showed that for different drying treatments, artificial neural network modeling can precisely evaluate the color change of the banana variety. Bai *et al.* (2018) developed an ANNs model for investigating the drying kinetics and color changes of Ginkgo biloba seeds during microwave drying. The ANN models showed strong correlation to the experimental data, with correlation coefficients ranging from 0.956 to 0.9834. The models also had low mean square errors, between 0.0014 and 2.2044.
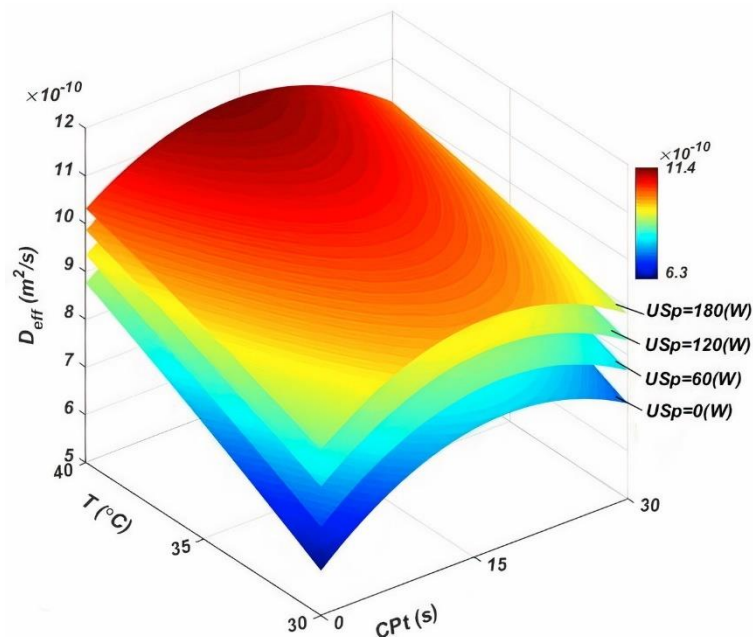
Fig. 7. Response surface plots for the effect of independent variables on moisture diffusivity of cumin seeds during the drying process
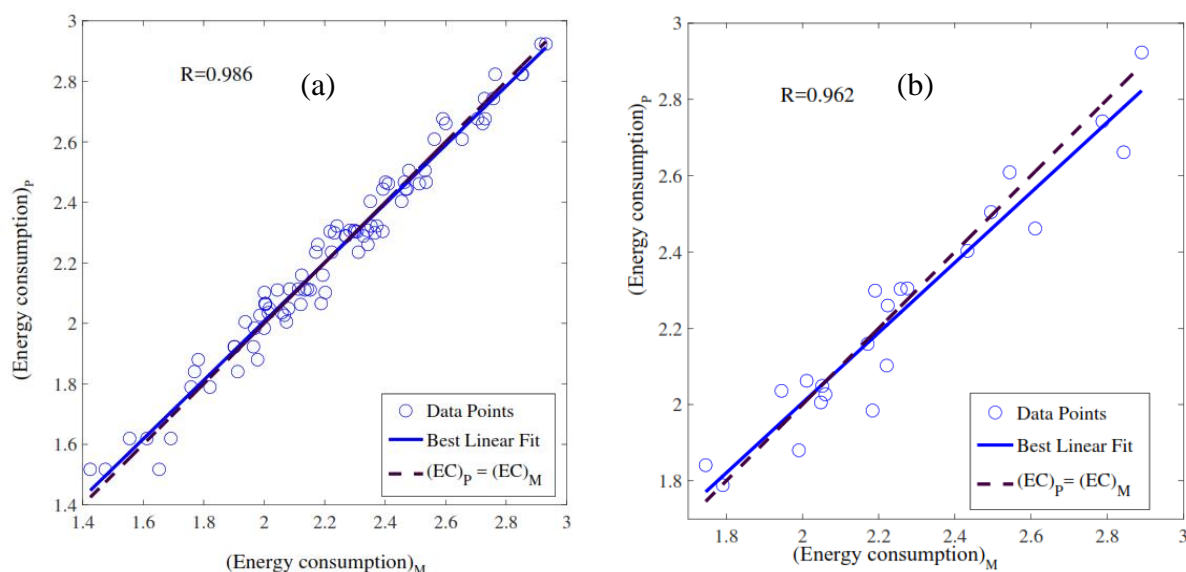
Fig. 8. The regression of the measured and predicted energy consumption: a) Train data, and b) Test data
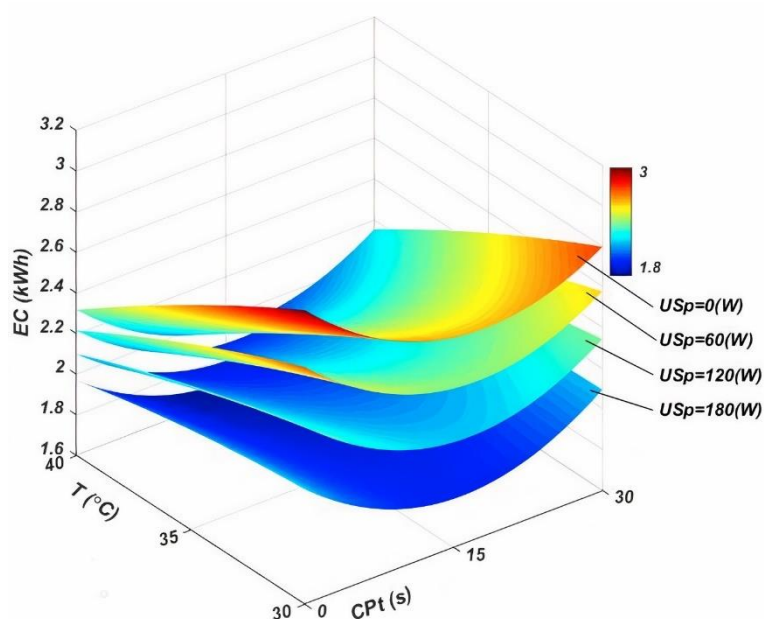
Fig. 9. Response surface plots for the effect of independent variables on the energy consumption of cumin seeds during the drying process

In this section, the changes in the color of cumin seeds were investigated, and the results were given in Fig. 11. In conventional drying, higher temperatures lead to greater color change, indicating potential degradation of quality. Introducing ultrasound reduces color change, with lower temperatures and higher ultrasound power showing the least change in color. CPt results in significant color change reduction, but prolonged exposure may have

adverse effects. Combining CP pretreatment and ultrasound shows the most effective preservation of color, with minimal change observed at lower temperatures and higher ultrasound power. This indicates that integrating both CP and ultrasound technologies, while meticulously managing the parameters, presents the most effective method for maintaining seed quality.
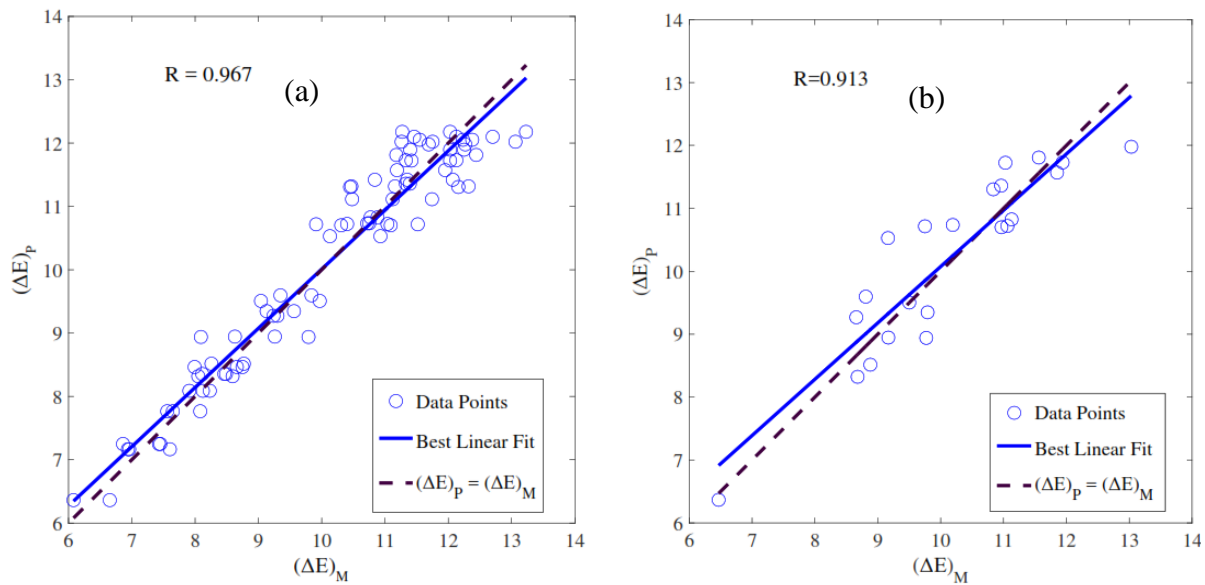
Fig. 10. The regression of the measured and predicted color change: a) Train data, and b) Test data
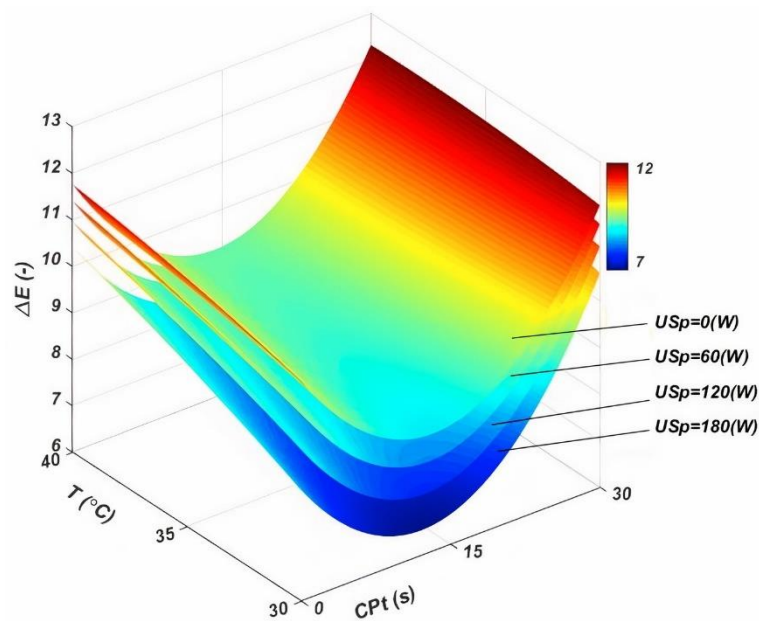
Fig. 11. Response surface plots for the effect of independent variables on the color change of cumin seeds during the drying process

Rupture force

The experimental data for the rupture force of dried seeds were displayed in Figure 12. Using the developed WNN model, the regression analysis was performed for mapping the input parameters with the desired variable. For both train and test datasets, the values of R^2 were found to be more than 0.90, and therefore best-fitting lines were proposed for the rupture force. The obtained values for RMSE, MAPE, and MAE (see Table 3) also reaffirmed that the WNN model suitably predicted the impact of drying conditions on the quality of end-products. The overall results are also found to be in very good agreement with the results of available investigations in the literature (Barreiro, Steinmetz, & Ruiz-Altisent, 1997; Saeidirad, Rohani, & Zarifneshat, 2013).
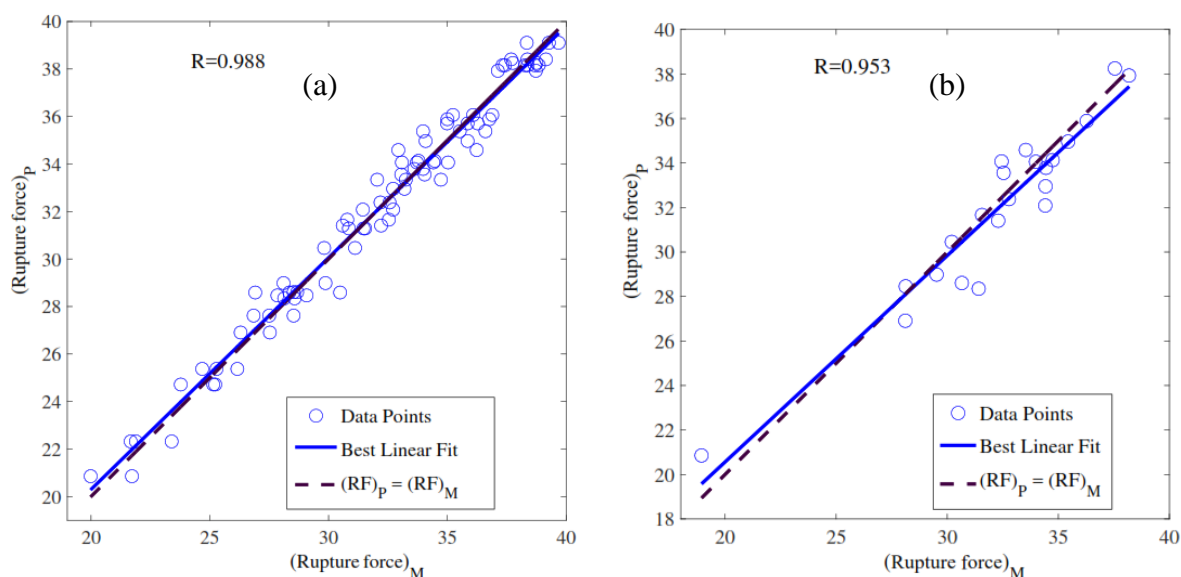
Fig. 12. The regression of the measured and predicted rupture force: a) Train data, and b) Test data

The effect of drying temperature, as well as exposing the seeds to US and CP, were evaluated and the results for the rupture force were given in Fig. 13. Convective drying temperatures showed minimal impact on seed crispiness. Introducing ultrasound led to cell collapse and increased ease of seed crushing. Higher ultrasound power resulted in significantly reduced rupture force. CPt had a lesser impact on reducing rupture force compared to ultrasound. Combining CPt with hybrid ultrasound/convective drying resulted in varying rupture forces depending on CP exposure time and ultrasound power. The scheme with CP pretreatment time of 15 seconds and ultrasound power of 180 W proved most effective in reducing rupture force.
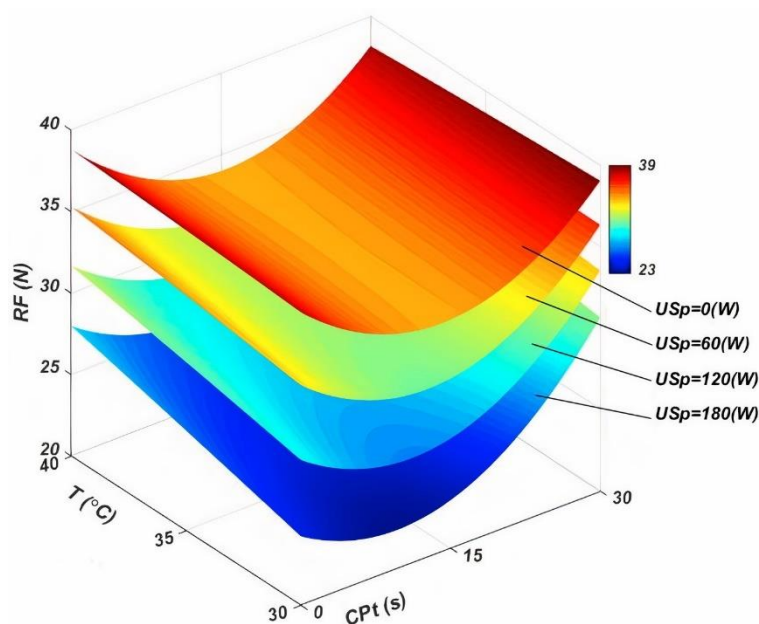
Fig. 13. Response surface plots for the effect of independent variables on the rupture force of cumin seeds during the drying process

**Sensitivity analysis**

Sensitivity analysis is a technique for evaluating the weight of each input parameter on output variables defined in the model. In this analysis, the inputs are systematically varying and the change in outputs are studied. This reveals which inputs inflict prominent impacts on the variation in outputs. Sensitivity analysis quantifies input uncertainty propagation and identifies influential parameters (Bhaskaran, Chennippan, & Subramaniam, 2020). In this section, the influence of input variables on DT, EC, ΔE, RF, and D_{eff} were studied, and the results were graphically shown in Fig. 14. It is evident that the drying temperature conveniently stimulated the moisture diffusivity D_{eff} but had no significant effects on the color change and rupture force.
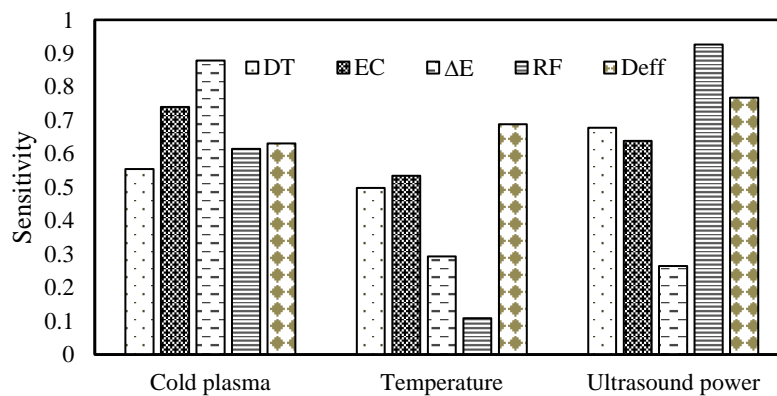
Fig. 14. Results of sensitivity analysis for hybrid drying of cumin seed

This raises the need for extra drying sources for improving the dehydration process. According to the results of sensitivity analysis, the average contribution of CP, temperature, and ultrasound to the output variables is 3.4176, 2.1227, and 3.2752, respectively. This clearly demonstrates the superiority of hybrid drying programs to the pure hot-air convective drying, and the CP was recognized as the most prominent factor. The maximum improvement in energy consumption EC and color change ΔE were created by exposing the seeds to CP. However, Fig. 9 shows that the ultrasound provided 21.73 and 50.73% more increase in D_{eff} and RF compared with those achieved CP. But contrary to CP, the ultrasonic power also had a negligible effect on the color change of cumin seed during the drying process.

Conclusion

In this study, some numerical predicting models were developed for investigating the contribution of cold plasma and high-power ultrasound waves for improving the convective air drying of cumin seeds. Three neural network models, namely MLPNN, RBFNN, and WNN, were used for predicting the performance of drying systems. The drying air temperature, CP exposing time, and the sonication power were selected as the input variables. The dehydration process was described by drying time, effective moisture diffusivity, energy consumption, color change, and the rupture force of dried seeds. The available experimental data was used for training and testing the models. The results of the regression-based MQR model were also evaluated and compared with the results of neural network models. Among all developed models, MLPNN and WNN showed the best fitting with the experimental data. The average values of $R^2 = 0.9523$ and RMSE = 1.93055 were found for the results of MLPNN, while the error indices obtained for the predictions of

WNN were estimated as $R^2 = 0.8972$ and RMSE = 1.808552. However, the WNN model used a non-iterative learning algorithm with a significantly shorter computational time. Therefore, this model was recognized as the most appropriate predicting tool for investigating the hybrid convective drying of cumin seeds.

Data availability statement

The data that support the findings of this study are available from the corresponding author, upon reasonable request.

Declaration of competing interests

The authors declare that they have no conflict of interest.

Authors Contribution

M. Namjoo: Data acquisition, Data pre and post processing, Writing- Original draft, Statistical analysis.

M. Moradi: Supervision, Technical advice, Review and editing services

M. A. Nematollahi: Numerical/computer simulation, Validation, Writing- Original draft

H. Golbakhshi: Review and editing services

References

1. Aghbashlo, M., Kianmehr, M. H., & Arabhosseini, A. (2008). Energy and exergy analyses of thin-layer drying of potato slices in a semi-industrial continuous band dryer. *Drying Technology, 26*(12), 1501-1508. https://doi.org/10.1080/07373930802412231
2. Akpinar, E. K., Midilli, A., & Bicer, Y. (2005). Energy and exergy of potato drying process via cyclone type dryer. *Energy Conversion and Management, 46*(15-16), 2530-2552. https://doi.org/10.1016/j.enconman.2004.12.008
3. Amini, G., Salehi, F., & Rasouli, M. (2021). Drying kinetics of basil seed mucilage in an infrared dryer: Application of GA-ANN and ANFIS for the prediction of drying time and moisture ratio. *Journal of Food Processing and Preservation, 45*(3), e15258. https://doi.org/10.1111/jfpp.15258
4. Bai, J.-W., Xiao, H.-W., Ma, H.-L., & Zhou, C.-S. (2018). Artificial Neural Network Modeling of Drying Kinetics and Color Changes of Ginkgo Biloba Seeds during Microwave Drying Process. *Journal of Food Quality, 2018*, 3278595. https://doi.org/10.1155/2018/3278595
5. Barreiro, P., Steinmetz, V., & Ruiz-Altisent, M. (1997). Neural bruise prediction models for fruit handling and machinery evaluation. *Computers and Electronics in Agriculture, 18*(2-3), 91-103. https://doi.org/10.1016/s0168-1699(97)00022-7
6. Bhaskaran, P. E., Chennippan, M., & Subramaniam, T. (2020). Future prediction & estimation of faults occurrences in oil pipelines by using data clustering with time series forecasting. *Journal of Loss Prevention in the Process Industries, 66*, 104203. https://doi.org/10.1016/j.jlp.2020.104203
7. Chatzilia, T., Kaderides, K., & Goula, A. M. (2023). Drying of peaches by a combination of convective and microwave methods. *Journal of Food Process Engineering, 46*(4), e14296. https://doi.org/10.1111/jfpe.14296
8. Dhurve, P., Tarafdar, A., & Arora, V. K. (2021). Vibro-Fluidized Bed Drying of Pumpkin Seeds: Assessment of Mathematical and Artificial Neural Network Models for Drying Kinetics. *Journal of Food Quality, 2021*, 7739732. https://doi.org/10.1155/2021/7739732
9. Dibagar, N., Kowalski, S. J., Chayjan, R. A., & Figiel, A. (2020). Accelerated convective drying of sunflower seeds by high-power ultrasound: Experimental assessment and optimization approach. *Food and Bioproducts Processing, 123*, 42-59. https://doi.org/10.1016/j.fbp.2020.05.014
10. Dotto, G. L., Souza, T. B., Simoes, M. R., Morejon, C. F., & Moreira, M. F. P. (2017). Diffusive-convective model considering the shrinkage applied for drying of pears (*pyrus*). *Journal of Food Process Engineering, 40*(4), e12503. https://doi.org/10.1111/jfpe.12503

11. Gong, C., Liao, M., Zhang, H., Xu, Y., Miao, Y., & Jiao, S. (2020). Investigation of hot air–assisted radio frequency as a final-stage drying of pre-dried carrot cubes. *Food and Bioprocess Technology, 13*(3), 419-429. https://doi.org/10.1007/s11947-019-02400-0

12. Guiné, R. P., Barroca, M. J., Gonçalves, F. J., Alves, M., Oliveira, S., & Mendes, M. (2015). Artificial neural network modelling of the antioxidant activity and phenolic compounds of bananas submitted to different drying treatments. *Food Chemistry, 168*, 454-459. https://doi.org/10.1016/j.foodchem.2014.07.094

13. Guo, Y.-R., An, Y.-M., Jia, Y.-X., & Xu, J.-G. (2018). Effect of drying methods on chemical composition and biological activity of essential oil from cumin (*Cuminum cyminum*). *Journal of Essential Oil Bearing Plants, 21*(5), 1295-1302. https://doi.org/10.1080/0972060x.2018.1538818

14. Habibi, S., & Nematollahi, M. (2019). Position and mass identification in nanotube mass sensor using neural networks. *Proceedings of the Institution of Mechanical Engineers, Part C: Journal of Mechanical Engineering Science, 233*(15), 5377-5387. https://doi.org/10.1177/0954406219841075

15. Izli, N., & Polat, A. (2019). Freeze and convective drying of quince (*Cydonia oblonga*): Effects on drying kinetics and quality attributes. *Heat and Mass Transfer, 55*, 1317-1326. https://doi.org/10.1007/s00231-018-2516-y

16. Kalathingal, M. S. H., Basak, S., & Mitra, J. (2020). Artificial neural network modeling and genetic algorithm optimization of process parameters in fluidized bed drying of green tea leaves. *Journal of Food Process Engineering, 43*(1), e13128. https://doi.org/10.1111/jfpe.13128

17. Kaveh, M., Abbaspour Gilandeh, Y., Amiri Chayjan, R., & Mohammadigol, R. (2019). Comparison of Mathematical Modeling, Artificial Neural Networks and Fuzzy Logic for Predicting the Moisture Ratio of Garlic and Shallot in a Fluidized Bed Dryer. *Journal of Agricultural Machinery, 9*(1), 99-112. https://doi.org/10.22067/jam.v9i1.66231

18. Kaveh, M., Chayjan, R. A., & Khezri, B. (2018). Modeling drying properties of pistachio nuts, squash and cantaloupe seeds under fixed and fluidized bed using data-driven models and artificial neural networks. *International Journal of Food Engineering, 14*(1), 10-23. https://doi.org/10.1515/ijfe-2017-0248

19. Khalo ahmadi, A., Roustapour, O. R., & Borghaee, A. M. (2022). Design and Construction of a Cabinet Dryer for Food Waste and Evaluation of its Kinetics and Energy Consumption. *Journal of Agricultural Machinery, 12*(4), 467-480. https://doi.org/10.22067/jam.2021.69918.1037

20. Khanlari, A., Güler, H. Ö., Tuncer, A. D., Şirin, C., Bilge, Y. C., Yılmaz, Y., & Güngör, A. (2020). Experimental and numerical study of the effect of integrating plus-shaped perforated baffles to solar air collector in drying application. *Renewable energy, 145*, 1677-1692. https://doi.org/10.1016/j.renene.2019.07.076

21. Lingayat, A., VP, C., & VRK, R. (2021). Drying kinetics of tomato (*Solanum lycopersicum*) and Brinjal (*Solanum melongena*) using an indirect type solar dryer and performance parameters of dryer. *Heat and Mass Transfer, 57*, 853-872. https://doi.org/10.1007/s00231-020-02999-3

22. Liu, Z.-L., Bai, J.-W., Wang, S.-X., Meng, J.-S., Wang, H., Yu, X.-L., ..., & Xiao, H.-W. (2019). Prediction of energy and exergy of mushroom slices drying in hot air impingement dryer by artificial neural network. *Drying Technology*. https://doi.org/10.1080/07373937.2019.1607873

23. Matlab, S. (2016). Matlab. *The MathWorks, Natick, MA*.

24. Meerasri, J., & Sothornvit, R. (2022). Artificial neural networks (ANNs) and multiple linear regression (MLR) for prediction of moisture content for coated pineapple cubes. *Case Studies in Thermal Engineering, 33*, 101942. https://doi.org/10.1016/j.csite.2022.101942

25. Merah, O., Sayed-Ahmad, B., Talou, T., Saad, Z., Cerny, M., Grivot, S., ..., & Hijazi, A. (2020). Biochemical composition of cumin seeds, and biorefining study. *Biomolecules, 10*(7), 1054. https://doi.org/10.3390/biom10071054

26. Miraei Ashtiani, S.-H., Rafiee, M., Mohebi Morad, M., Khojastehpour, M., Khani, M. R., Rohani, A., ..., & Martynenko, A. (2020). Impact of gliding arc plasma pretreatment on drying efficiency and physicochemical properties of grape. *Innovative Food Science & Emerging Technologies, 63*, 102381. https://doi.org/10.1016/j.ifset.2020.102381

27. Moghimi, M., Farzaneh, V., & Bakhshabadi, H. (2018). The effect of ultrasound pretreatment on some selected physicochemical properties of black cumin (*Nigella Sativa*). *Nutrire, 43*(1), 1-8. https://doi.org/10.1186/s41110-018-0077-y

28. Moosavi, A. A., Nematollahi, M. A., & Rahimi, M. (2021). Predicting water sorptivity coefficient in calcareous soils using a wavelet–neural network hybrid modeling approach. *Environmental Earth Sciences, 80*, 1-19. https://doi.org/10.1007/s12665-021-09518-5

29. Moradi, M., Ghasemi, J., & Azimi-Nejadian, H. (2021). Energy and Exergy Analysis of Drying Process of Lemon Verbena Leaves in a Solar Dryer. *Journal of Agricultural Machinery, 11*(2), 423-433. https://doi.org/10.22067/jam.v11i2.85801

30. Namjoo, M., Dibagar, N., Golbakhshi, H., Figiel, A., & Masztalerz, K. (2024). RSM-Based Optimization Analysis for Cold Plasma and Ultrasound-Assisted Drying of Caraway Seed. *Foods, 13*(19), 3084. https://doi.org/10.3390/foods13193084

31. Namjoo, M., Golbakhshi, H., Kamandar, M. R., & Beigi, M. (2024). Multi-Objective Investigation and Optimization of Paddy Processing in a Hot Air Dryer. *Periodica Polytechnica Chemical Engineering*. https://doi.org/10.3311/PPch.24100

32. Namjoo, M., Moradi, M., Dibagar, N., & Niakousari, M. (2022). Cold plasma pretreatment prior to ultrasound-assisted air drying of cumin seeds. *Food and Bioprocess Technology, 15*(9), 2065-2083. https://doi.org/10.1007/s11947-022-02863-8

33. Namjoo, M., Moradi, M., Niakousari, M., & Karparvarfard, S. H. (2022). Ultrasound-assisted air drying of cumin seeds: modeling and optimization by response surface method. *Heat and Mass Transfer*. https://doi.org/10.1007/s00231-022-03306-y

34. Nazghelichi, T., Kianmehr, M. H., & Aghbashlo, M. (2010). Thermodynamic analysis of fluidized bed drying of carrot cubes. *Energy, 35*(12), 4679-4684. https://doi.org/10.1016/j.energy.2010.09.036

35. Nematollahi, M. A., Jamali, B., & Hosseini, M. (2020). Fluid velocity and mass ratio identification of piezoelectric nanotube conveying fluid using inverse analysis. *Acta Mechanica, 231*(2), 683-700.https://doi.org/10.1007/s00707-019-02554-0

36. Nematollahi, M. A., & Mousavi Khaneghah, A. (2019). Neural network prediction of friction coefficients of rosemary leaves. *Journal of Food Process Engineering, 42*(6), e13211. https://doi.org/10.1111/jfpe.13211

37. Onwude, D. I., Hashim, N., Abdan, K., Janius, R., & Chen, G. (2018). Investigating the influence of novel drying methods on sweet potato (*Ipomoea batatas*): Kinetics, energy consumption, color, and microstructure. *Journal of Food Process Engineering, 41*(4), e12686. https://doi.org/10.1111/jfpe.12686

38. Osloob, F., Moradi, M., & Niakousari, M. (2023). Cold Plasma: A Novel Pretreatment Method for Drying Canola Seeds: Kinetics Study and Superposition Modeling. *Journal of Agricultural Machinery, 13*(1), 41-53. https://doi.org/10.22067/jam.2022.75630.1096

39. Özkan Karabacak, A. (2019). Effects of different drying methods on drying characteristics, colour and in-vitro bioaccessibility of phenolics and antioxidant capacity of blackthorn pestil (leather). *Heat and Mass Transfer, 55*, 2739-2750. https://doi.org/10.1007/s00231-019-02611-3

40. Potisate, Y., Phoungchandang, S., & Kerr, W. L. (2014). The effects of predrying treatments and different drying methods on phytochemical compound retention and drying characteristics

of Moringa leaves (*Moringa oleifera*). *Drying Technology, 32*(16), 1970-1985. https://doi.org/10.1080/07373937.2014.926912

41. Rezaei, S., Behroozi-Khazaei, N., & Darvishi, H. (2021). Modeling of Potato Slice Drying Process in a Microwave Dryer using Artificial Neural Network and Machine Vision. *Journal of Agricultural Machinery, 11*(2), 263-275. https://doi.org/10.22067/jam.v11i2.78709

42. Saeidirad, M. H., Rohani, A., & Zarifneshat, S. (2013). Predictions of viscoelastic behavior of pomegranate using artificial neural network and Maxwell model. *Computers and Electronics in Agriculture, 98*, 1-7. https://doi.org/10.1016/j.compag.2013.07.009

43. Safavi, A. A., & Romagnoli, J. A. (1997). Application of wavelet-based neural networks to the modelling and optimisation of an experimental distillation column. *Engineering Applications of Artificial Intelligence, 10*(3), 301-313. https://doi.org/10.1016/S0952-1976(97)00009-2

44. Saiedirad, M., & Mirsalehi, M. (2010). Prediction of mechanical properties of cumin seed using artificial neural networks. *Journal of Texture studies, 41*(1), 34-48. https://doi.org/10.1111/j.1745-4603.2009.00211.x

45. Saiedirad, M., Tabatabaeefar, A., Borghei, A., Mirsalehi, M., Badii, F., & Varnamkhasti, M. G. (2008). Effects of moisture content, seed size, loading rate and seed orientation on force and energy required for fracturing cumin seed (*Cuminum cyminum*) under quasi-static loading. *Journal of Food Engineering, 86*(4), 565-572. https://doi.org/10.1016/j.jfoodeng.2007.11.021

46. Shashikanthalu, S. P., Ramireddy, L., & Radhakrishnan, M. (2020). Stimulation of the germination and seedling growth of Cuminum cyminum L. seeds by cold plasma. *Journal of Applied Research on Medicinal and Aromatic Plants, 18*, 100259. https://doi.org/10.1016/j.jarmap.2020.100259

47. Sun, Q., Zhang, M., & Mujumdar, A. S. (2019). Recent developments of artificial intelligence in drying of fresh food: A review. *Critical Reviews in Food Science and Nutrition, 59*(14), 2258-2275. https://doi.org/10.1080/10408398.2018.1446900

48. Tabibian, S. A., Labbafi, M., Askari, G. H., Rezaeinezhad, A. R., & Ghomi, H. (2020). Effect of gliding arc discharge plasma pretreatment on drying kinetic, energy consumption and physico-chemical properties of saffron. *Journal of food engineering, 270*, 109-117. https://doi.org/10.1016/j.jfoodeng.2019.109766

49. Wang, C., Tian, S., & An, X. (2022). The effects of drying parameters on drying characteristics, colorimetric differences, antioxidant components of sliced chinese jujube. *Heat and Mass Transfer, 58*(9), 1561-1571. https://doi.org/10.1007/s00231-023-03412-5

50. Wang, X., Zhong, J., Han, M., Li, F., Fan, X., & Liu, Y. (2023). Drying characteristics and moisture migration of ultrasound enhanced heat pump drying on carrot. *Heat and Mass Transfer*, 1-12. https://doi.org/10.1007/s00231-023-03564-1

51. Yogendrasasidhar, D., & Setty, Y. P. (2018). Drying kinetics, exergy and energy analyses of Kodo millet grains and Fenugreek seeds using wall heated fluidized bed dryer. *Energy, 151*, 799-811. https://doi.org/10.1016/j.energy.2018.03.089

52. Zakeri, V., Naghavi, V., & Safavi, A. A. (2009). Developing real-time wave-net models for non-linear time-varying experimental processes. *Computers & Chemical Engineering, 33*(8), 1379-1385. https://doi.org/10.1016/j.compchemeng.2009.02.003

53. Zhou, Y.-H., Vidyarthi, S. K., Zhong, C.-S., Zheng, Z.-A., An, Y., Wang, J., ..., & Xiao, H.-W. (2020). Cold plasma enhances drying and color, rehydration ratio and polyphenols of wolfberry via microstructure and ultrastructure alteration. *LWT, 134*, 110173. https://doi.org/10.1016/j.lwt.2020.110173

مدل‌سازی اثر توام پلاسمای سرد و توان فراصوت بر خشک شدن دانه‌های زیره سبز در یک خشک‌کن هوای گرم با استفاده از شبکه عصبی مصنوعی

مسلم نامجو [iD] ۱، مهدی مرادی [iD] ۲*، محمدامین نعمت اللهی [iD] ۲، حسین گلبخشی [iD] ۳

چکیده

این مطالعه به‌منظور بررسی اثر زمان پلاسمای سرد (CPt) و توان امواج فراصوت (USp) بر خشک شدن دانه زیره سبز در یک خشک‌کن هـوای گرم انجام شد. در این راستا، از یک دستگاه تولید پلاسمای سرد و یک خشک‌کن هیبریدی هوای گرم– فراصوت در مقیاس آزمایشگاهی استفاده شـد و روش‌های خشک کردن به گونه‌ای برنامه‌ریزی شد که اثرات CPt و USp در خشک کردن دانه‌ها به‌صورت منفرد یـا ترکیبـی دخالـت داشـته باشـند. زمان‌های مختلف پیش‌تیمار پلاسمای سرد (۱۵ و ۳۰ ثانیه)، توان‌های امواج فراصوت (۶۰، ۱۲۰ و ۱۸۰ وات) و دمای هوای خشک شدن (۳۰، ۳۵ و ۴۰ درجه سانتی‌گراد) برای مطالعه تغییرات زمان خشک کردن، ضریب نفوذپذیری مؤثر رطوبت، مصرف انرژی، تغییر رنگ کل، نیروی گسیختگی بذر زیـره سبز انجام گرفت. از سه شبکه عصبی مصنوعی معروف شامل شبکه عصبی مبتنی بر موجک (WNN)، پرسپترون چندلایه (MLPNNs)، تـابع پایـه شعاعی (RBFNNs) و تحلیل رگرسیون چندگانه درجه دوم (MQR) برای مدل‌سازی ورودی‌های مذکور و پارامترهای خشک‌کردن استفاده شـد. بـر اساس نتایج مدل‌سازی، بهترین برازش خطی بین داده‌های تجربی و مقادیر پیش‌بینی‌شده توسط مدل‌سازی شبکه عصبی WNN با حـداکثر R^2 ۰/۹۲ و ۰/۸۳ به‌ترتیب برای داده‌های آموزش و تست به‌دست آمد.

واژه‌های کلیدی: پلاسمای سرد، خشک کردن، دانه‌های زیره سبز، شبکه عصبی مصنوعی، فراصوت

۱- گروه مکانیک بیوسیستم، دانشکده کشاورزی، دانشگاه جیرفت، جیرفت، ایران

۲- گروه مهندسی بیوسیستم، دانشکده کشاورزی، دانشگاه شیراز، شیراز، ایران

۳- گروه مکانیک، دانشگاه جیرفت، جیرفت، ایران

(Email: moradih@shirazu.ac.ir :نویسنده مسئول -*)

Optimization of Cumulative Energy, Exergy Consumption and Environmental Life Cycle Assessment Modification of Corn Production in Lorestan Province, Iran

M. Soleymani [ID] [1*], **A. Asakereh** [ID] [1], **M. Safaieenejad** [2]

1- Department of Biosystems Engineering, Shahid Chamran University of Ahvaz, Ahvaz, Iran
2- Agricultural Mechanization Management Department of Lorestan Province Agricultural Jihad Organization, Khorramabad, Iran
(*- Corresponding Author Email: m.soleymani@scu.ac.ir)

Abstract

Optimal use of resources, including energy, is one of the most important principles in modern and sustainable agricultural systems. Exergy analysis and life cycle assessment were used to study the efficient use of inputs, energy consumption reduction, and various environmental effects in the corn production system in Lorestan province, Iran. The required data were collected from farmers in Lorestan province using random sampling. The Cobb-Douglas equation and data envelopment analysis were utilized for modeling and optimizing cumulative energy and exergy consumption (CEnC and CExC) and devising strategies to mitigate the environmental impacts of corn production. The Cobb-Douglas equation results revealed that electricity, diesel fuel, and N-fertilizer were the major contributors to CExC in the corn production system. According to the Data Envelopment Analysis (DEA) results, the average efficiency of all farms in terms of CExC was 94.7% in the CCR model and 97.8% in the BCC model. Furthermore, the results indicated that there was excessive consumption of inputs, particularly potassium and phosphate fertilizers. By adopting more suitable methods based on DEA of efficient farmers, it was possible to save 6.47, 10.42, 7.40, 13.32, 31.29, 3.25, and 6.78% in the exergy consumption of diesel fuel, electricity, machinery, chemical fertilizers, biocides, seeds, and irrigation, respectively.

Keywords: DEA, Energy in agriculture, LCA, Renewability, Sustainability

Introduction

The agriculture sector has become increasingly reliant on energy due to the widespread use of agricultural machinery and inputs in mechanized agriculture, particularly in developing countries where there has been a shift from traditional to mechanized farming methods. Mechanization is the main factor in the consumption of non-renewable energy in agriculture (Leiva & Morris, 2001). In addition to reducing non-renewable resources, this situation has also had adverse effects on the environment (Nemecek, Dubois, Huguenin-Elie, & Gaillard, 2011; Nikkhah, Khojastehpour, Emadi, Taheri-Rad, & Khorramdel, 2015). Since the agricultural sector, on the other hand, is responsible for the food security of the growing population, a balance must be struck between the use of resources and the production of agricultural products (Alam, Alam, & Islam, 2005). The consumption of resources should be such that it does not threaten the food security of future generations (Alam *et al.*, 2005).

Increasing agricultural productivity is not possible without the proper, wise, and timely use of inputs. Using more inputs, whether directly or indirectly, leads to a rise in energy consumption. Therefore, to determine effective methods for the optimal use of agricultural inputs, it is necessary to first identify them accurately and comprehensively (Mani, Kumar, Panwar, & Kant, 2007). Energy is one of the most important resources in agricultural activities and due to the limited resources, greenhouse gas emissions, and possible harmful effects on the environment, it should be used optimally and effectively (Alam *et al.,* 2005). On the other hand, the scarcity of natural resources and the impact of intensive agriculture on the environment raise concerns about the ecological sustainability of agriculture. A careful equilibrium must be established between energy usage and its availability in the agricultural sector (Leiva & Morris, 2001).

Today, achieving sustainability in agricultural production systems is one of the main policies in the agricultural sector, with the aim of increasing productivity and reducing adverse effects on the environment. Sustainability in agriculture is achieved when the food needs of the present population is met without threatening the food security of future generations. This type of agriculture emphasizes the protection of the environment and natural resources, and the optimal use of non-renewable resources. To evaluate possible practical measures and promote agricultural sustainability, it is critical to identify the actual flow of various inputs and outputs in agricultural production systems. The optimal use of inputs is one of the principles of sustainable agricultural systems (Ahamed *et al.,* 2011). This situation is even more necessary in the case of energy as one of the most important agricultural inputs, especially in developing countries that are highly dependent on non-renewable resources (Apazhev *et al.,* 2019; Jat *et al.,* 2020; Parihar *et al.,* 2018; Shah *et al.,* 2021). Therefore, identifying optimal patterns of energy consumption in agriculture is necessary and

can develop sustainable agriculture as an economic production system (Hatirli, Ozkan, & Fert, 2005). The evaluation of the flow of energy consumption in the production system of agricultural products is the basis of energy analysis. The main goals of energy analysis are to reduce energy consumption, identify non-renewable energy sources for replacement with renewable sources, reduce production costs, and use environmentally friendly production methods as part of an optimal management system (Gezer, Acaroğlu, & Haciseferoğullari, 2003).

Production in agriculture is always associated with the main goal of increasing yield and reducing costs (Gezer *et al.,* 2003). Therefore, optimal energy consumption requires comprehensive planning in this regard. Optimization is a process in which the greatest benefit is obtained by changing the input or output values of a system (Thankappan, Midmore, & Jenkins, 2006). Optimization of energy consumption in agriculture is possible by increasing productivity and maintaining the level of energy input or saving energy consumption without reducing productivity (Bhunia *et al.,* 2021; Vlontzos, Niavis, & Manos, 2014). A lot of research has been done on the optimization of agricultural systems from different perspectives. Optimizing energy consumption is one of these perspectives in which the highest performance with the lowest amount of input energy is desired (Thankappan *et al.,* 2006). However, this approach considers the analysis and amount of energy consumed based on the first law of thermodynamics without considering the quality of energy consumed and does not clearly show the loss of energy in energy conversion processes (Sartor & Dewallef, 2017). For this reason, in recent years, exergy analysis methods that measure the quantity and quality of energy and material flow based on common units have been used (Juárez-Hernández, Usón, & Pardo, 2019). Exergy is the maximum useful work that can be obtained from the system during a process that brings the system into thermodynamic equilibrium

with its environment (Juárez-Hernández *et al.,* 2019). Exergy analysis, based on the principles of mass and energy conservation and the second law of thermodynamics, is more useful than energy analysis in determining system efficiency. This procedure provides a useful tool to examine the impact of the use of energy resources on the environment (Ahamed *et al.,* 2011). In previous studies, exergy analysis, cumulative degree of perfection (CDP) and renewability index (RI) were used to evaluate the effects of agricultural production systems on the environment (KhojastehpourTroujeni, Esmailpour, Vahedi, & Emadi, 2018; Yildizhan & Taki, 2018). It also determines the location, types, and magnitude of actual exergy losses (Dincer & Cengel, 2001; Yildizhan, 2018). Exergy is a thermodynamic balance indicator and a unified scale for evaluating different forms of energy carriers and materials, which is suitable for evaluating the sustainability of various production processes and systems (Bösch, Hellweg, Frischknecht, & Huijbregts, 2007; Juárez-Hernández *et al.,* 2019). Several researchers have used the exergy analysis to better understand the efficiency and sustainability of the agricultural production system (Al-Ghandoor & Jaber, 2009; Amiri, Asgharipour, Campbell, & Armin, 2020; EsmaeilpourTroujeni, Rohani, & Khojastehpour, 2021; Juárez-Hernández *et al.,* 2019; Ordikhani, Parashkoohi, Zamani, & Ghahderijani, 2021; Pelvan & Özilgen, 2017; Shahhoseini, Ramroudi, Kazemi, & Amiri, 2021; Yildizhan & Taki, 2018). Saving cumulative exergy consumption (CExC) in agricultural production means less consumption of energy and natural resources and less pollution (Yildizhan, 2018).

Energy consumption in Iran's agricultural sector has almost doubled from 2001 to 2018, mainly due to the increase in the use of agricultural machinery, chemical and mineral materials, and irrigation, as well as the increase in cultivated area, reaching 58.1 million barrels of crude oil equivalent. The sources of this energy are mainly non-renewable (diesel and fossil-based electricity).

Accordingly, the agricultural sector in Iran is one of the most important sectors in the emission of pollutants in the environment (for example, more than one-third of N2O emissions in Iran) (Anonymous, 2018). Studies have shown that increasing the use of energy and inputs in agriculture may increase yield, but reduce energy efficiency and exacerbate some of the harmful effects of agricultural systems on the environment (Mohammadi *et al.,* 2013). Therefore, increasing the efficiency of energy consumption in agricultural production systems is very effective to achieve sustainable agriculture. There are various techniques to optimize energy consumption in production units and systems. Data Envelopment Analysis (DEA) is a linear programming method that constructs the efficiency frontier by using the information of production units as the decision-making unit and determines the degree of inefficiency of each decision-making unit based on the distance of that unit to the efficient frontier. DEA has been widely used to measure the efficiency of agricultural production in terms of energy and to determine the optimal amount of input consumption (Bhunia *et al.,* 2021; Kaab, Sharifi, Mobli, Nabavi-Pelesaraei, & Chau, 2019; Powar *et al.,* 2020; Gurdeep Singh, Sodhi, & Tiwari, 2021; Vlontzos *et al.,* 2014).

Several studies have analyzed energy consumption in corn production, mostly based on the first law of thermodynamics (Banaeian & Zangeneh, 2011; Komleh Pishgar, Keyhani, Rafiee, & Sefeedpary, 2011; Mani *et al.,* 2007; Su, Shao, Tian, Li, & Huang, 2021; Yousefi, Khoramivafa, & Mondani, 2014). In this study, optimization of inputs consumption, reduction of energy consumption, and reduction of various environmental effects of the corn production system are investigated based on exergy analysis and life cycle assessment of corn production. The DEA method was used to determine the optimal amount of input consumption based on the CExC and to minimize the environmental effects of corn production while maintaining the current level of performance.

Materials and Methods

The general steps and the boundary of the studied system are shown in Fig. **1**. In the first step, the analysis of exergy and energy in corn production system was performed based on CExC, cumulative energy consumption (CEnC), and exergy and energy evaluation indicators. Finally, the CExC was modeled using the Cobb-Douglas model. In the next step, DEA was used to measure the efficiency of inputs used in each farm (production unit) in terms of CExC and to determine the effective consumption of inputs and CExC in corn farms. The Life Cycle Analysis (LCA) of the corn production system was investigated in the final step.
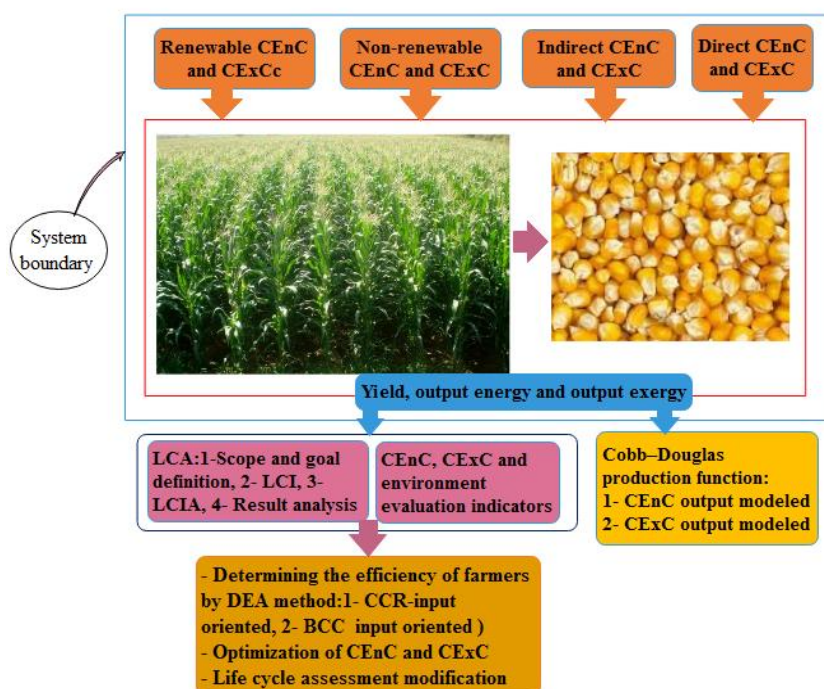
Fig. 1. System boundary and general stages of the study

Data and studied area

The required data were collected from corn farmers in Lorestan province, Iran. About 780 thousand hectares of the province's area are agricultural lands, and it is one of the most important corn production areas in Iran. A total of 214 farmers were randomly selected (Equation (1), (William G. Cochran, 1991)) to interview and collect the necessary data.

$$n = \frac{Nt^2s^2}{Nd^2 + t^2s^2} \tag{1}$$

Where:

n – The sample size

N – The size of the statistical population (total corn farmers in the province)

t – The reliability coefficient (1.96 which represents the 95% confidence interval) and the permissible error in the sample size was defined to be 5% for 95% confidence level

d – The precision where (x – X) or mid-confidence interval

S^2 – the variance of the surveyed factor of the population

For exergy analysis, all materials and input energy carriers were quantified based on energy and exergy coefficients. Diesel fuel, electricity, human power, chemical fertilizers, biocides, machinery and tools, irrigation, seeds, and infrastructure (such as irrigation canals) are considered inputs that demand energy or cost at various stages of land

preparation, planting, harvesting, and transportation.

Energy and exergy analysis

CExC and CEnC are the sums of total exergy and energy used in all processes required to produce a product, respectively. Therefore, CEnC and CExC were calculated in corn production by considering all categories of inputs and energy carriers. CEnC and CExC in the production of agricultural products are divided into renewable and non-renewable, direct and indirect. Diesel and electricity, which are direct carriers of energy, are direct components of CEnC and CExC in agricultural systems, and the rest of the inputs are of indirect types. On the other hand, agricultural machinery, diesel fuel, chemical fertilizers, biocides and electricity (which is mainly fossil-based in Iran) are non-renewable components of CEnC and CExC in corn production. Table 1 shows the specific equivalents of CEnC and CExC extracted from relevant references. These values for each input are obtained using work and heat interaction processes (EsmaeilpourTroujeni *et al.,* 2021; Yildizhan, 2018). Only inputs for which cost or energy are used were considered in this study, and other inputs and energies such as solar energy, energy received from air and soil, and microorganisms were excluded.

Table 1- CEnC and CExC equivalents of inputs and outputs in corn production system

Items		Specific CEnC		Specific CExC	
		Quantity	Reference	Quantity	Reference
Input	Diesel fuel	56.3 MJ lit^{-1}	(Erdal, Esengün, Erdal, & Gündüz, 2007)	53.2 MJ lit^{-1}	(KhojastehpourTroujeni *et al.,* 2018; Yildizhan, 2018)
	Electricity	12 MJ kWh^{-1}	(Ordikhani *et al.,* 2021)	4.17 MJ kWh^{-1}	(Amiri *et al.,* 2020)
	Nitrogen fertilizer (N)	76.14 MJ kg^{-1}	(Yilmaz, Akcaoz, & Ozkan, 2005)	32.7 MJ kg^{-1}	(Amiri *et al.,* 2020)
	Phosphate fertilizer (P$_2$O$_5$)	12.4 MJ kg^{-1}	(Yilmaz *et al.,* 2005)	7.52 MJ kg^{-1}	(Amiri *et al.,* 2020; EsmaeilpourTroujeni *et al.,* 2021)
	Potassium fertilizer (K$_2$O)	11.15 MJ kg^{-1}	(Ordikhani *et al.,* 2021)	4.7 MJ kg^{-1}	(Pelvan & Özilgen, 2017)
	Herbicides	120 MJ lit^{-1}	(Beheshti Tabar, Keyhani, & Rafiee, 2010)	32.7 MJ lit^{-1}	(EsmaeilpourTroujeni *et al.,* 2021)
	Pesticides	363.6 MJ lit^{-1}	(Kaab *et al.,* 2019)	7.52 MJ lit^{-1}	(Yildizhan & Taki, 2018)
	Fungicides	198 MJ lit^{-1}	(Yildizhan & Taki, 2018)	4.56 MJ lit^{-1}	(Yildizhan & Taki, 2018)
	Machinery	9 MJ kg^{-1} year^{-1}	(Kaab *et al.,* 2019)	7.1 MJ kg^{-1}	(Michalakakis, Fouillou, Lupton, Gonzalez Hernandez, & Cullen, 2021)
	Irrigation	0.00102 MJ kg^{-1}	(Yildizhan & Taki, 2018)	0.00425 MJ kg^{-1}	(Amiri *et al.,* 2020)
	Human labor	1.96 MJ h^{-1}	(Kaab *et al.,* 2019)	-	
	Corn seed	100 MJ kg^{-1}	(Kitani, 1999)	21.7 MJ kg^{-1}	(Juárez-Hernández *et al.,* 2019)
Output	Corn grain	18.3 MJ kg^{-1}	(Ptasinski, 2016)	21.7 MJ kg^{-1}	(Juárez-Hernández *et al.,* 2019)

One of the important indicators in evaluating energy consumption in the production of agricultural products is the ratio of output CEnC to input CEnC, ER (Equation (2)). This index is considered as a criterion for measuring energy usage efficiency in agricultural production systems (Yuan, Peng, Wang, & Man, 2018). The higher the index, the higher the efficiency of energy use (Ordikhani *et al.,* 2021). A value greater than 1 for this index indicates that the energy output of the production system is greater than CEnC (Banaeian & Zangeneh, 2011; Bhunia *et al.,* 2021; Mobtaker, Keyhani, Mohammadi, Rafiee, & Akram, 2010; Mousavi-Avval, Rafiee, Jafari, & Mohammadi, 2011b; Royan, Khojastehpour, Emadi, & Mobtaker, 2012; Gurdeep Singh *et al.,* 2021; Vlontzos *et al.,* 2014). Since only inputs for which energy or cost have been spent are considered, the value of this index can be higher than 1. Other important indicators that are used in the

evaluation of energy consumption in agricultural systems include Energy Intensity (EI), Energy Productivity (EP), and Net Energy Gained (NEG), which are calculated using Equations (3), (4), and (5), respectively (Kaab *et al.,* 2019; Ordikhani *et al.,* 2021). EI and EP are the two contrasting indicators. EI shows the amount of CEnC used to produce one unit of product, which is mostly used in the perspective of industrial agriculture, while EP shows the amount of product per unit of CEnC, and is mostly used to compare the production system of different agricultural products. The higher the EP and the lower the EI, the more efficient the agricultural production process is in terms of energy consumption. NEG is equal to the output energy minus CEnC. When NEG is greater than zero, more energy has been produced than consumed. The higher this index is, the more efficient the production system is. A comprehensive study of all these indicators (ER, EP, and EI) is useful to compare and show the potential environmental impacts of agricultural production systems (Khan *et al.,* 2009).

$$Energy\ ratio\ (ER)$$
$$= \frac{Equivalent\ energy\ produced\ (MJ\ ha^{-1})}{Input\ CEnC\ (MJ\ ha^{-1})} \quad (2)$$

Energy intensity (EI)
$$= \frac{Input\ CEnC\ (MJ\ ha^{-1})}{Yield\ (kg\ ha^{-1})} \quad (3)$$

$$Energy\ productivity\ (EP)$$
$$= \frac{Yield\ (kg\ ha^{-1})}{Input\ CEnC\ (MJ\ ha^{-1})} \quad (4)$$

Cumulative net energy gain$(CNEnG)$
$$= Output\ CEnC\ (MJ\ ha^{-1}) \quad (5)$$
$$- Input\ CEnC\ (MJ\ ha^{-1})$$

In the current study, the cumulative exergy approach and obtained Cumulative Degree of Perfection (CDP), as well as renewability index were used to evaluate the renewability and sustainability of corn production processes and the efficiency of exergy consumption (Ahamed *et al.,* 2011; EsmaeilpourTroujeni *et al.,* 2021). The RI is the ratio of renewable resources to non-renewable resources. A

higher value of RI means that the production system produces in a more renewable way (Hai *et al.,* 2023). In the calculation of exergy efficiency, all controllable and uncontrollable inputs are considered, while in CDP, only the controllable inputs are considered (EsmaeilpourTroujeni *et al.,* 2021). Since only controllable inputs are usually considered in agricultural systems, CDP is preferable. CDP is equal to the ratio of exergy obtained from the agricultural production system to the CExC of controllable inputs in the agricultural production system (Equation (6), (Ahamed *et al.,* 2011; EsmaeilpourTroujeni *et al.,* 2021)). Since in agricultural production systems, the produced crops are in equilibrium with the environment, the exergy of the crops is considered equal to their chemical exergy (KhojastehpourTroujeni *et al.,* 2018; Yildizhan, 2018). This index, together with the RI, provides a powerful tool for evaluating and comparing the harmful effects of production processes on the environment and is used as an index to monitor the level of environmental sustainability of the processes (EsmaeilpourTroujeni *et al.,* 2021).

CDP
$$= \frac{Exergy\ in\ products\ ((m \times b)_{products})}{\sum(m \times CExC)_{raw\ materials} + \sum(m \times CExC)_{fuels}} \quad (6)$$

Where, m represents mass, and b represents chemical exergy

The Renewability Index (RI) is used to determine the renewability of processes, evaluate the intensity of resource stress, and analyze the environmental impact of a production system. This index, which is obtained based on Equation (7) (KhojastehpourTroujeni *et al.,* 2018; Pelvan & Özilgen, 2017; Yildizhan & Taki, 2018), shows the 4 states of processes in terms of renewability. The negative value of this index indicates that the process is completely non-renewable, and the zero value indicates that the restoration work is equal to the amount of exergy produced in the system. Process renewability increases from zero until it reaches its highest value of 1, which represents

a fully renewable process. In general, the higher the value of this index for a system, the lower its harmful effects on the environment (KhojastehpourTroujeni *et al.,* 2018; Yildizhan & Taki, 2018).

$$RI = \frac{E_{ch} - W_r}{E_{ch}} \qquad (7)$$

Where, E_{ch} and W_r represent the chemical exergy of final products and restoration work, respectively.

Excessive exploitation of resources, especially non-renewable ones, can have harmful effects on the environment. In some cases when the effect is insignificant, nature can tolerate it and neutralize the risks caused by it. In the processing of resources, non-renewable energy sources are destroyed and restoring them to their initial states requires work (Berthiaume, Bouchard, & Rosen., 2001). This restoration work (W_r) is estimated by summing the net exergy consumption in the process and the net exergy consumption for waste treatment. In an agricultural crop production process, the exergy of all consumed non-renewable resources is calculated to estimate the restoration work (EsmaeilpourTroujeni *et al.,* 2021; Pelvan & Özilgen, 2017; Yildizhan & Taki, 2018, 2019).

Regression modeling

Regression analysis is a statistical method in which the relationship between two or more quantitative variables is used to predict a variable with the help of another variable or variables. In this study, regression method was used to investigate the relationship between energy consumption and cumulative exergy, and crop yield. For this purpose, the Cobb-Douglas function was chosen due to its simplicity, compatibility with physical logic, and generalization power. This function has been widely used in energy research (Banaeian & Zangeneh, 2011; Bhunia *et al.,* 2021; Mobtaker *et al.,* 2010; Mousavi-Avval *et al.,* 2011b; Royan *et al.,* 2012; Gurdeep Singh *et al.,* 2021; Vlontzos *et al.,* 2014). The best statistically significant estimates and the expected signs of the parameters are obtained from this function, which is expressed as Equations (8) and (9) (Mobtaker *et al.,* 2010).

$$Y = f(x)\exp(u) \qquad (8)$$

$$LnY_i = a + \sum_{j=1}^{n} \propto_J lnX_{ij} + e_i \qquad (9)$$

where, Y is the corn yield, X is the energy and exergy inputs used in the production processes, α is the coefficient of energy and exergy inputs, e is the error coefficient, and a is a constant value.

To change the inputs and their effects on the output, the returns to scale index was used. This index shows how much the output value changes for each unit increase in all input consumption. The sum of the regression coefficients obtained in the Cobb-Douglas equation indicates the returns to scale index; a value greater than 1 indicates increasing returns to scale, a value less than 1 signifies decreasing returns to scale, and a value equal to 1 denotes constant returns to scale (Mobtaker *et al.,* 2010).

Life Cycle Assessment (LCA)

LCA is a standard and widely used environmental assessment method for evaluating processes, products, and services. LCA is an analytical tool that assesses the environmental burden and impacts related to the entire life cycle of a product or process (extraction and processing of raw materials, manufacturing, distribution and use, and recycling or final disposal of all residuals of main and by-products). LCA is a "cradle to grave" approach to assess all inputs, outputs, and wastes of a product, process, or service, and their impacts on human health and the environment, and finally, interpret the assessment results throughout the entire life cycle (Ordikhani *et al.,* 2021; Prasad *et al.,* 2020). This method serves as an effective approach for assessing the impact of a process on various categories of environmental effects and assists managers in promoting the development of products with minimal adverse environmental impacts (Kaab *et al.,* 2019). A complete LCA is performed in four steps: 1- goal and scope definition, 2- life cycle inventory (LCI), 3- life cycle impact assessment (LCIA), and 4- interpretation of results (Prasad *et al.,* 2020). The purpose of

the life cycle assessment in this study was to examine environmental impact groups per kilogram of corn product (as a functional unit). The studied impact categories were: Acidification (AC), Eutrophication (EP), Global Warming Potential (GWP), Ozone Layer Depletion (OLD), Human Toxicity (HT), Fresh Water Aquatic Ecotoxicity (FWAE), Marine Aquatic Ecotoxicity (MAE), Terrestrial Ecotoxicity (TE), and Photochemical Oxidation (PO).

In LCI, all the inputs, outputs, wastes, their amount, and the probable emissions to the environment in the corn production system were determined based on the functional unit (FU). The main inputs at this stage were diesel fuel, electricity, machinery, nitrogen fertilizer, phosphate fertilizer, potassium fertilizer, biocides, irrigation water, and infrastructures, whose environmental impacts were estimated based on existing standards (Finkbeiner, Inaba, Tan, Christiansen, & Klüppel, 2006). Accurate estimation of the amount of pollutants released into the soil, water, and air is challenging. Therefore, instead of measurement, emission factors of pollutants are often used to estimate the average emission of pollutants (Tzilivakis, Warner, May, Lewis, & Jaggard, 2005). Accordingly, the emission factors of pollutants caused by the use of inputs in agricultural production systems were obtained from relevant references (Brentrup, Küsters, Lammel, Barraclough, & Kuhlmann, 2004; IPCC, 2006; Nikkhah *et al.,* 2015; Ordikhani *et al.,* 2021).

The third stage (LCIA) includes the classification and characterization, normalization ranking, grouping, and weighting, of which the first two are mandatory, and the last three are optional. In the classification, impact category groups are defined, and then the released pollutants audited in the LCI stage are placed in the corresponding impact groups based on the type of pollutant released. Then, the coefficient or weight of each pollutant is applied for different impact categories. For this purpose, a characteristic factor is determined for each type of pollutant in the impact groups according to the functioning of

the ecosystem (Brentrup *et al.,* 2004; A. Singh *et al.,* 2010). Finally, in the last stage of LCA, interpretation, the results obtained in LCI and LCIA are summarized, important issues are identified, and recommendations are given especially for reducing the harmful effects of hazardous pollutants (Arts, Ruijten, Aelst, Trullemans, & Sels, 2021; Ashby, 2013; Cao, 2017; Hernandez, Oregi, Longo, & Cellura, 2019; Kylili, Seduikyte, & Fokaides, 2018; Papapetrou & Kosmadakis, 2022; Prasad *et al.,* 2020). In the current study, the CML 2 baseline 2000 V2.05/universe technique was used to perform LCA in the Simapro 8.4.0.0. Software.

Data Envelopment Analysis (DEA)

DEA is a non-parametric method for estimating production functions based on a series of optimizations using linear programming (Adler, Friedman, & Sinuany-Stern, 2002). It is a powerful tool in the field of improving productivity and calculating the efficiency of Decision-Making Units (DMUs). This technique was used to evaluate the efficiency of farms in energy and exergy consumption in corn production, and based on this, the efficient amount of energy and exergy consumption was determined, while maintaining the current production level. In this method, DMUs (Adler *et al.,* 2002) can be made efficient in an input or output oriented manner. In the input-oriented mode, by maintaining the output level, the consumption of inputs is minimized, and in the output-oriented mode, by keeping the input values constant, the output value and production are maximized (Mousavi-Avval, Rafiee, Jafari, & Mohammadi, 2011a; Mousavi-Avval *et al.,* 2011b). The production of agricultural products relies on limited and scarce resources. Hence, in similar studies, the use of input-oriented DEA models has been preferred to reduce the inputs used in agricultural production systems (Chauhan, Mohapatra, & Pandey, 2006; Malana & Malano, 2006; Mohammadi *et al.,* 2014; Mousavi-Avval *et al.,* 2011a, 2011b). Therefore, in this research, the input-oriented method was used and the CExC of controllable inputs and corn grain

yield were defined as input and output variables, respectively. Each farm was considered as a DMU and the two models of Constant Returns to Scale (CCR) and Variable Returns to Scale (BCC), were used as input-oriented models to calculate efficiency. In the constant returns to scale model, with one percent change in the input values, the outputs also change by one percent (decrease or increase), while in the variable returns to scale model, with one percent change in the inputs, the outputs change with different percentages (increase or decrease) (Mousavi-Avval *et al.,* 2011b; P. Singh, Singh, & Sodhi, 2019). The efficiency of using inputs in the CCR model is called Technical Efficiency (TE), and in the BCC model it is called Pure Technical Efficiency (PTE) (Gurdeep Singh *et al.,* 2021). Scale efficiency (SE) is calculated by dividing the TE by the PTE, and its value is at most 1. When SE is 1, it means that the farmer produces at the most efficient scale, and the TE and PTE of production are equal (Chauhan *et al.,* 2006; Malana & Malano, 2006; Mohammadi *et al.,* 2014; Mousavi-Avval *et al.,* 2011a, 2011b). DEA Solver software was used to calculate efficiency and analyze data.

Results and Discussion

Energy consumption and cumulative exergy

CEnC and CExC in grain corn production systems were calculated to be 68.9 and 29.6 GJ/ha, respectively. Also, CEnC and CExC for the production of one tonne of corn seeds were calculated as 6644 and 2854 MJ, respectively. The results are comparable with the energy consumption for silage corn production in Tehran province, Iran, which is 68.93 GJ ha^{-1} (Komleh Pishgar *et al.,* 2011). As a result of increasing agricultural mechanization and chemical use such as fertilizers, energy consumption for corn production in Iran is increasing and has reached 63.64 GJ ha^{-1}, from 40.98 GJ ha^{-1} in 2001 (Banaeian & Zangeneh, 2011). Electricity, diesel fuel, and nitrogen fertilizer have the largest share in CEnC with 57.58, 10.19, and 12.21%, respectively. In similar studies, diesel fuel, chemical fertilizers, and electricity used in irrigation have been reported as the main energy inputs in corn production (Banaeian & Zangeneh, 2011; Pishgar-Komleh, Keyhani, Mostofi-Sarkari, & Jafari, 2012; Yousefi, Mahdavi, & Mahmud, 2014). Fig. **2** shows the contribution of inputs in energy consumption and cumulative exergy of corn production. As can be seen from this figure in terms of CExC, electricity, diesel fuel, and nitrogen fertilizer are the highest exergy input to the system with 46.57, 22.41, and 12.21%, respectively.
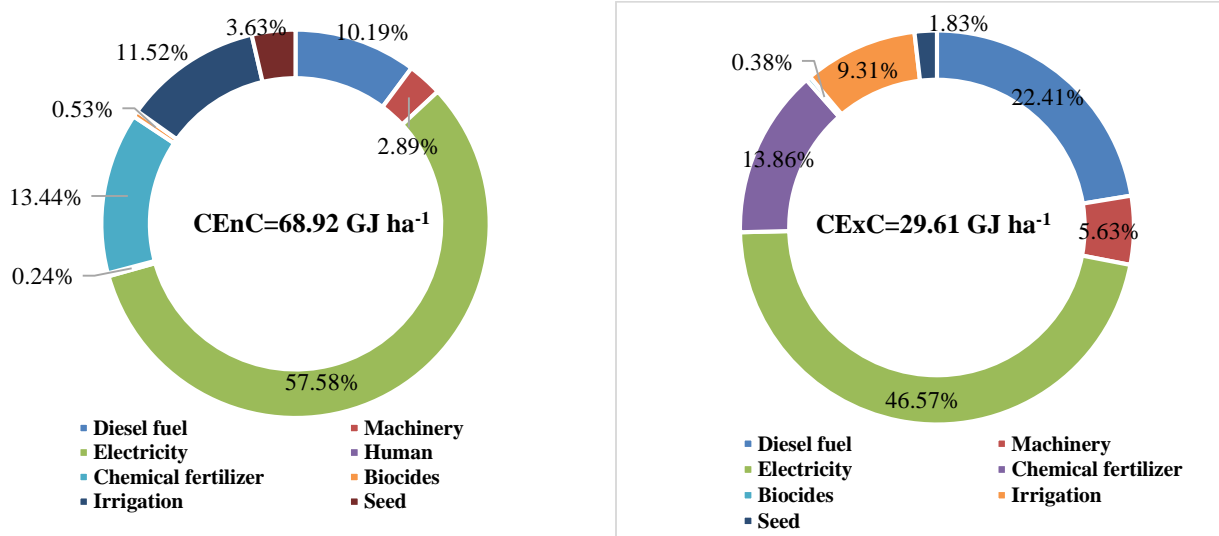

Fig. 2. Contribution of inputs in energy consumption and cumulative exergy in corn production

Autocorrelation of the data, used to estimate the relationship between energy inputs and corn yield, using the Cobb-Douglas production function, was tested by the Durbin-Watson statistic (Hatirli *et al.,* 2005; Mobtaker *et al.,* 2010). The value of this statistic for the model of CEnC and CExC was equal to 1.87 and 1.73, respectively, which shows that the autocorrelation of the data in both models is not significant (α= 5%). The regression results for the Cobb-Douglas model based on CEnC and CExC are shown in Table 2. The value of R^2 for Cobb-Douglas model estimated based on CEnC (model 1) was equal to 0.94, which shows that this model has the ability to predict and explain 94% of the yield changes by 6 inputs of electricity, labor, fuel, machinery, and phosphorus and nitrogen fertilizers. Among the inputs, electrical energy has the greatest effect on yield with a coefficient of 0.578, which means that with an increase of 1 unit of electricity consumed within the model's data range, corn yield increases by about 0.58 units. Phosphorus and nitrogen fertilizers are in the next ranks with coefficients of 0.242 and 0.228, respectively. The negative input coefficients for human energy and nitrogen fertilizer indicate that increasing the consumption of each megajoule of these inputs, based on the analyzed regional data, will lead to a decrease in corn yield by 0.24 units for human energy and 0.06 units for nitrogen fertilizer. In agricultural production modeling studies, machinery, irrigation (electricity), chemical fertilizers, and labor were reported as determining inputs in modeling and explaining yield changes (Hatirli, Ozkan, & Fert, 2006; Mobtaker *et al.,* 2010). The calculated sum of the coefficients for the CEnC-based model reached approximately 0.93, indicating that the yield in the studied area reflects diminishing returns to scale regarding CEnC. Model 2, which was obtained based on CExC, shows that about 94% (R^2) of yield changes can be explained by changes in 5 inputs of diesel fuel, electricity, nitrogen fertilizer, phosphate fertilizer, and biocides. Exergy consumption of inputs of fuel, electricity, and phosphorus fertilizer, respectively, has the greatest impact on corn production yield. The exergy of nitrogen fertilizer in this model has a negative coefficient, and it shows that the yield will decrease with the increase of exergy input of nitrogen fertilizer.

Table 2- Estimated coefficients of corn production function based on Cobb-Douglas function

Independent variables	Coefficient (α)	Sig
Model 1 (CEnC): $\ln Y_i = a_0 + a_1 lnX_{1i} + a_2 lnX_{2i} + a_3 lnX_{3i} + a_4 lnX_{4i} + a_5 lnX_{5i} + a_6 lnX_{6i} + e_i$		
Constant	0.737	0.037
Electricity	0.578	0.000
Phosphate fertilizer	0.242	0.000
Fuel	0.185	0.015
Labor	-0.242	0.000
Machinery	0.228	0.001
Nitrogen fertilizer	-0.065	0.009
Durbin‑Watson	1.87	
R^2	0.941	
Returns to scale	0.926	
Model 2 (CExC): $\ln Y_i = a_1 lnX_{1i} + a_2 lnX_{2i} + a_3 lnX_{3i} + a_4 lnX_{4i} + a_5 lnX_{5i} + e_i$		
Fuel	0.469	0.000
Electricity	0.403	0.000
Nitrogen fertilizer	-0.103	0.000
Phosphate fertilizer	0.284	0.000
Pesticides	0.007	0.001
Durbin‑Watson	1.73	
R^2	0.938	
Returns to scale	1.06	

Investigating the efficiency of corn production

To optimize the corn production system and determine efficient and inefficient fields based on input and output exergy values using the DEA method, all 214 farms were considered as DMUs, and the input-output exergy for all farms was analyzed based on input-oriented constant returns to scale (CCR-I) and input-oriented variable returns to scale (BCC-I) models. The efficiency results of corn production fields in terms of CExC based on CCR-I and BCC-I models are shown in Table 3. In terms of CExC in the CCR model, about 57% of corn production farms are technically inefficient, and 92 of the 214 surveyed farmers are technically efficient in this model, which shows that the activity of these farmers is constant returns to scale, and operate at the optimal scale of performance. The average efficiency of all farms in the CCR model is 94.7% and the most inefficient farm has a technical efficiency of 74.3%. The obtained efficiency values show that many of the farms in the studied area are significantly inefficient in terms of exergy consumption and do not use inputs correctly and efficiently or do not use the appropriate production methods. In the BCC model, the average efficiency is 97.8%, and 51.87% of farms have pure technical efficiency. Nearly all inefficient farms experience diminishing returns to scale, meaning that each additional unit of exergy input results in less than a one-unit increase in exergy output. Therefore, increasing the use of inputs does not increase exergy efficiency, and in the current method of corn production, inputs are used more than the optimal amount. Understanding the returns to scale associated with redistributing inputs among farms can significantly enhance performance outcomes (Chauhan *et al.,* 2006; Mousavi-Avval *et al.,* 2011a). The SE of farms was 0.968. The units were ranked based on the efficiency values obtained, so that the higher the efficiency value, the higher the farm ranked. One of the valid methods for ranking the efficient units is the benchmarking method, in which an efficient unit is ranked highly if it appears frequently in the reference sets of inefficient DMUs. The information of these DMUs can be used to determine the amounts of inputs used in inefficient units (Adler *et al.,* 2002; Mousavi-Avval *et al.,* 2011a). In this study, the 10 efficient farms with the highest values were DMUs No. 5, 74, 60, 50, 214, 12, 111, 8, 152, and 22, which appeared 55, 53, 39, 37, 36, 23, 20, 20, 19, and 18 times, in the CCR model reference set, respectively.

Table 3- The overall results of the input-oriented DEA method for CExC

Model	Average efficiency	The lowest efficiency	Number of inefficient units	Number of efficient units	Number of reference units
CCR	0.947±0.0683	0.743	122 (57.01%)	92 (42.99%)	16
BCC	0.978±0.0389	0.787	103	111	19
Scale Efficiency	0.968±0.0459	0.946	-	-	-

The highest CExC saving was related to diesel fuel and nitrogen fertilizer with about 1407 (21.21%) and 902 (24.95%) MJ ha^{-1}, respectively. However, the highest percentage of saving in CExC was related to potassium and phosphate fertilizers with 66.51 (34.51 MJ ha^{-1}) and 46.02% (201.70 MJ ha^{-1}), respectively. This shows that inputs, especially potassium and phosphate fertilizers, are used more than required.

The values of CExC and its components based on the input-oriented fixed and variable returns to scale model are shown in Fig. **3**. Based on the analysis of CCR and BCC models, it is possible to reduce the exergy consumption of all inputs in these two models while maintaining the production level. Based on the results of the CCR model and the target values obtained, savings of 6.47, 10.42, 7.40, 13.32, 31.29, 3.25, and 78.6% can be achieved in the exergy consumption of diesel fuel, electricity, machinery, chemical fertilizers,

biocides, seeds, and irrigation, respectively, while maintaining the current level of corn production yield. These values in the BCC model were 3.28, 7.22, 5.41, 6.64, 15.31, 1.12, and 6.04%, respectively. The CExC target value, based on the CCR model analysis, is 26833.5 MJ/ha, which represents 2776.6 MJ ha^{-1} (9.38%) of exergy saving. The highest amount of cumulative exergy savings based on the pure technical efficiency model with 1437.2, 484.8, and 429.4 MJ ha^{-1} is related to electricity, nitrogen fertilizer, and diesel fuel, respectively. Meanwhile, the highest percentage of exergy savings of 31.64, 31.29, and 13.41% was related to phosphate fertilizer, biocides, and nitrogen fertilizer, respectively. This suggests an overutilization of inputs within the production system. In face-to-face interviews, most of the farmers believed that the increase in inputs increased the yield, and on this basis, they use more inputs to increase production without improving the production methods. Excessive irrigation and low efficiency of water pumping systems in the study area have led to an increase in the consumption of more than the required amount of water in corn production, which, in addition to wasting water and electricity, often aggravates drainage problems, and reduces soil quality (Mousavi-Avval *et al.,* 2011b; Singh, Gursahib Singh, & Singh, 2004). The lowest percentage of saving in exergy consumption is related to seed input (1.12%), which shows that the farmers of the region use seeds more efficiently than other inputs. The DEA analysis, along with the insights from the reference set and the findings depicted in Fig. **3**, provides valuable recommendations for inefficient farms. By adopting the superior operational practices employed by the reference farms of their peers, these less efficient farms can reduce exergy consumption to align with the target values identified through the DEA method, all while sustaining their current yield levels.
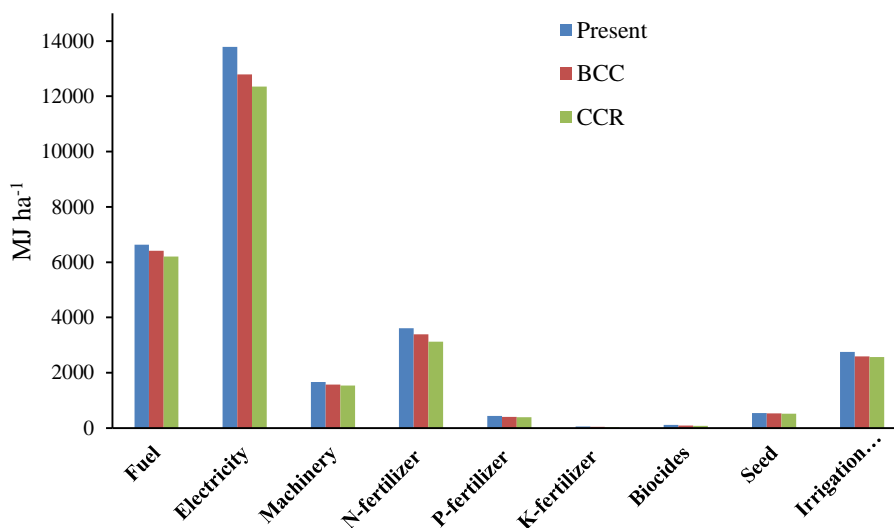
Fig. 3. CExC values of different inputs in the current mode, BCC, and CCR models

Energy, exergy, and environmental indicators

Table 4 shows the values of energy and exergy evaluation indices in the current condition (default), and optimal states based on CCR and BCC models. According to DEA analysis, it is possible to reduce CEnC and CExC by 9.76 and 9.38%, respectively, while maintaining the current production level, by optimally using inputs and improving management and promoting methods used by efficient farms (reference set). The ER index shows that the total system energy output is

2.75 times higher than CEnC. Also, in general, the studied system produces about 121 GJ ha^{-1} of energy (Cumulative Net Energy Gain-CNEnG). As mentioned before, in the analysis of energy and exergy in a production system of agricultural crops (Cumulative net energy gain), only inputs for which costs and energy have been spent are considered. For this reason, ER and CNEnG can be greater than one and zero, respectively. EI and EP indices show that 6.64 MJ of energy is consumed to produce each kilogram of corn, or in other words, about 0.15 kg of corn is produced for each MJ of energy consumed. In similar studies in Iran, ER for corn production has been reported as 4.78 (Pishgar-Komleh *et al.,* 2012), 1.69 to 2.17 (Banaeian & Zangeneh, 2011), and 2.67 (Yousefi, Mahdavi, *et al.,* 2014). Based on the optimization results, an improvement of about 11% in the ER and EP indices of the corn production system is possible only based on following the way of input management by efficient units. CDP, which is often used to check the efficiency of exergy consumption and system stability, was obtained around 7.6. This index for different types of corn production systems in Mexico has been calculated from 1.6 to 1.14

(Juárez-Hernández *et al.,* 2019). The obtained CDP is also higher than that of some agricultural products such as wheat (2.9, (Yildizhan & Taki, 2019)), black tea (0.43, (Pelvan & Özilgen, 2017), rapeseed (2.19, (EsmaeilpourTroujeni *et al.,* 2021)), and strawberry (0.29, (Yildizhan, 2018)), which is mostly due to the high yield and higher exergy output of corn in this study. The larger these indicators are, the more stable the production system and the less environmental consequences. The RI of about 0.87 in this study shows that corn production is a relatively renewable process. The obtained RI index is higher than that of other agricultural products in similar studies (EsmaeilpourTroujeni *et al.,* 2021; Pelvan & Özilgen, 2017; Yildizhan & Taki, 2018, 2019), which is mainly due to the higher output exergy in the corn production system.

Optimum use of non-renewable inputs, especially electricity, diesel fuel, and chemical fertilizers, increases the process's RI. As shown in Figure 2, the highest CExC belongs to these three inputs, which are produced from non-renewable sources.

Table 4- Energy and exergy evaluation indicators in default scenario and optimized scenarios

Items	Unit	Current	CCR		BCC	
			Target	Change (%)	Target	Change (%)
CEnC	MJ ha^{-1}	68924.7	62200.5	-9.76	64537.7	-6.36
ER	-	2.75	3.05	+10.81	2.94	+6.80
EI	MJ kg^{-1}	6.64	5.99	-9.76	6.22	-6.36
EP	kg MJ^{-1}	0.150	0.167	+10.81	0.161	+6.80
CNEnG	MJ ha^{-1}	120923.3	127653.5	+5.56	125316.2	+3.63
DCEnC[a]	MJ ha^{-1}	46867.7 (68.00%)	42266.5 (67.95%)	-9.82	43762.9 (67.81%)	-6.63
ICEnC[b]	MJ ha^{-1}	22057.0 (32.00%)	19934.0 (32.05%)	-9.63	20774.8 (32.19%)	-5.81
RCEnC[c]	MJ ha^{-1}	2662.7 (3.86%)	2570.5 (4.23%)	-3.46	2627.6 (4.07%)	-1.32
NRCEnC[d]	MJ ha^{-1}	66261.9 (96.14%)	59629.9 (95.87%)	-10.01	61910.2 (95.93)	-6.57
CExC	MJ ha^{-1}	29610.0	26833.5		27843.1	
CDP	-	7.60	8.40	+10.35	8.09	+6.35
RI	-	0.871	0.883	+1.41	0.879	+0.90
DCExC[e]	MJ ha^{-1}	20424.6 (68.98%)	18557.9 (69.16%)	-9.24	19210.4 (68.99%)	-05.95
ICExC[f]	MJ ha^{-1}	9185.5 (31.02%)	8275.5 (30.84%)	-9.91	8632.7 (31.01%)	-6.02
RCExC[g]	MJ ha^{-1}	542.5 (1.83%)	524.87 (1.97%))	-3.25	536.4 (1.93%))	-1.12
NRCExC[h]	MJ ha^{-1}	29067.5 (98.17%)	26308.6 (98.04%)	-9.49	27306.7 (98.07%)	-6.06

[a] Direct CEnC, [b] Indirect CEnC, [c] Renewable CEnC, [d] Non- renewable CEnC, [e] Direct CExC, [f] Indirect CExC, [g] Renewable CExC, and [h] Non-renewable CExC

Therefore, their optimal use increases the renewable index. Supplying input from

renewable sources will also increase the sustainability and renewability of the system.

Based on the analysis of DEA method, CDP and RI can be improved by about 10.3% and 1.4%, respectively, with optimal and appropriate use of inputs based on existing conditions and facilities. By increasing the efficiency of irrigation and water pumping systems, an effective step can be taken in reducing electricity consumption, which is the main exergy input, and of course increase exergy efficiency. The conventional tillage system in corn production in Iran involves the intensive use of energy-intensive tillage machines such as moldboard plow and deep tillage tolls.

This has caused an increase in the use of agricultural machinery and diesel fuel. As reported in several studies, conservation tillage methods reduce the use of agricultural machinery and reduce fuel consumption compared to conventional tillage (Filipovic, Kosutic, Gospodaric, Zimmer, & Banaj, 2006; Ordikhani et al., 2021). Also, the use of better machinery management techniques can reduce diesel fuel consumption and its harmful effects on the environment (Mousavi-Avval et al., 2011a).

As can be seen from Table 4, the main components of energy consumption and cumulative exergy in the corn production system are direct and non-renewable types of energy. The share of about 96% of non-renewable energies in CEnC and 98% in CExC has caused the strong dependence of corn production on non-renewable resources. In many similar studies, the ratio of DCExC and DCEnC is higher than that of ICEnC and ICExC, and the ratio of NRCEnC and NRCExC is much higher than that of RCEnC and RCExC (Erdal et al., 2007; EsmaeilpourTroujeni et al., 2021; Juárez-Hernández et al., 2019; Mousavi-Avval et al., 2011a; Ordikhani et al., 2021; Rahman & Hasan, 2014; Yildizhan & Taki, 2018). The agricultural production system based on the intensive use of non-renewable resources is not sustainable in the long term and has harmful consequences on human health and the environment (Khan, Khan, Hanjra, & Mu, 2009). Electricity is the main component of

CEnC and CExC in the production of corn (to pump water and irrigate fields) and its production in Iran is mainly based on non-renewable fossil resources (Anonymous, 2018). Using renewable electricity instead of fossil electricity in corn production processes like other processes can be one of the ways to reduce environmental consequences and increase RI.

In Iran, mainly due to the lack of economic competition with fossil fuels, renewable energy sources, except for hydropower plants, are still not developed much. However, in recent years, efforts and plans have been made to promote the use of renewable resources for energy production. For example, the production of electricity from wind has increased in recent years, and efforts are underway to make more use of solar energy. It is expected that the share of energy from renewable sources in electricity production in Iran will increase in the future (Anonymous, 2018). Also, promising researches have been conducted on harnessing wind (Jalalvand, Bakhoda, & Almassi, 2014) and solar energy (Parvaresh Rizi & Ashrafzadeh, 2018; Shojaei & Akhavan, 2020) for water pumping, that accounts for the majority of electricity consumption in agriculture. Animal manures and organic fertilizers are currently used commercially in Iran's agricultural sector, and in the past few years, the production of animal manures has increased as a result of the increase in livestock and poultry farms. This way, the renewability index in the default scenario increases to 0.93 and according to the CCR model, it increases to about 0.94. Another suggestion to increase the renewability of the system is to use renewable fuels such as biodiesel instead of diesel and organic fertilizers instead of chemical fertilizers (EsmaeilpourTroujeni et al., 2021; Khan et al., 2009; Mousavi-Avval et al., 2011a; Soltanali, Nikkhah, & Rohani, 2017).

Life cycle assessment
Life cycle assessment based on default (current) values, and optimized values based on BCC model and CCR model was

performed, and the results were compared. Natural resources like minerals and fossil fuels are classified as abiotic resources. However, the extraction of these resources often leads to their depletion. Energy production is one of the biggest and most important consumers of natural resources and one of the main factors of consumption and depletion of abiotic resources (Milà I Canals, Burnip, & Cowell, 2006). In agricultural production, the depletion of minerals such as phosphate and potash, alongside fossil fuels, are among the most important subsets of the Abiotic Depletion (AD). From Table 5, it can be seen that to produce one kilogram of corn, 9.513 g Sb *eq* is discharged from abiotic resources. Based on the results of the DEA model, by optimizing input consumption, there is a potential of 10.38% reduction in the effects of depletion of abiotic resources caused by corn production with the current facilities and conditions in the study area. Fig. **4** shows the contribution of the corn production system inputs in the impact categories. About 91% of the "abiotic depletion" category is due to electricity consumption, followed by diesel fuel and chemical fertilizers. Therefore, increasing the efficiency of electrical systems in pumping irrigation water, as well as the use of electricity from renewable sources, is very effective in reducing the depletion of abiotic resources. In a study that assessed the life cycle of the wheat production system, electricity, diesel fuel, and chemical fertilizers were reported as the most important consumers of abiotic resources (Houshyar & Grundmann, 2017).

Acidification, particularly in the form of acid rain, negatively affects terrestrial or aquatic ecosystems (Jacob-Lopes, Zepka, & Deprá, 2021). According to Table 5, the "Acidification" potential is 0.019 g SO_2 eq per 1 kg of corn production. The highest acidification potential due to corn production is related to electricity and on-farm emissions, respectively, which are responsible for about 98% of the total acidification potential. The potential of acidification due to the production of 1 kg of corn based on the optimized values of BCC and CCR models was found to be 17.76 and 17.06 g SO_2 eq, respectively, which shows a reduction of 7.06 and 10.71 percent, respectively.

Enrichment of water environments with dissolved compounds that leads to excessive growth of some living organisms is called eutrophication. In fact, eutrophication is the response of the ecosystem to the excessive increase of natural or artificial substances in a terrestrial or aquatic environment (Houshyar & Grundmann, 2017). The eutrophication potential for the production of each kilogram of corn is about 3.73 g PO_4^{3-} eq. On-farm emissions, mainly due to the loss of chemical fertilizers, especially nitrogen, are responsible for 89.42% of eutrophication. An effective way to reduce eutrophication is to minimize losses of nitrogen and phosphate fertilizers (Bechmann & Stålnacke, 2005; Houshyar & Grundmann, 2017). Life cycle assessment based on DEA model values showed that there is a potential to reduce eutrophication effects by 8.38%.

Table 5- Values of the environmental impacts for 1 kg of corn production

Impact category	Unit	Current condition	BCC model		CCR model	
			BCC	Change (%)	CCR	Change (%)
Abiotic depletion	kg Sb eq	0.009513	0.008844	-7.03248	0.008526	-10.38
Acidification	kg SO_2 eq	0.019105	0.017757	-7.05574	0.017059	-10.71
Eutrophication	kg PO_4^{3-} eq	0.003727	0.003571	-4.18567	0.003398	-8.83
Global warming (GWP100)	kg CO_2 eq	1.36434	1.272863	-6.70485	1.227315	-10.04
Ozone layer depletion	kg CFC-11 eq	1.58E-09	1.46E-09	-7.59494	1.34E-09	-15.19
Human toxicity	kg 1,4-DB eq	0.391071	0.333648	-14.6835	0.321487	-17.79
Fresh water aquatic ecotoxicity	kg 1,4-DB eq	0.095594	0.089181	-6.70858	0.085796	-10.25
Marine aquatic ecotoxicity	kg 1,4-DB eq	304.9183	282.9338	-7.20996	273.1014	-10.43
Terrestrial ecotoxicity	kg 1,4-DB eq	0.002271	0.001815	-20.0793	0.001725	-24.04
Photochemical oxidation	kg C_2H_4 eq	0.000685	0.000635	-7.29927	0.000613	-10.51

Global warming is one of the harmful effects of greenhouse gases, which has led to an increase in the Earth's average temperature and ocean levels. The capacity of gases in absorbing and trapping solar radiation is not the same, and it is evaluated relative to the potential of 1 kg of CO_2 over a period of 100 years. Hence, the global warming potential of a greenhouse gas is expressed in terms of kg carbon dioxide equivalent (kg CO_2 eq). The main cause of the ozone layer depletion is the chemicals produced by human activities, which are called Ozone-Depleting Substances (ODS). As can be seen from Figure 4, electricity has the highest load on GWP with 83.12%, followed by on-farm emissions and diesel fuel with a share of 9.72% and 4.55%, respectively. Diesel fuel, biocides, and chemical fertilizers have the highest load on OLD with 42.67, 31.50, and 17.78%, respectively, and the share of electricity is insignificant (less than 1%). Diesel fuel and on-farm emissions, which are mostly due to the consumption of diesel fuel in agricultural machinery, and chemical fertilizers and biocides, are major contributors to GWP and OLD. Tillage is the main consumer of diesel fuel, followed by harvesting. In the study of the impact of wheat production system on global warming, the most effective factor was fuel consumption in plowing, planting, and harvesting operations (Fallahpour, Aminghafouri, Ghalegolab Behbahani, & Bannayan, 2012; Houshyar & Grundmann, 2017). Optimizing tillage operations and optimal use of plowing tools will reduce fuel consumption and thus reduce its impact on GWP (Lovarelli, Bacenetti, & Fiala, 2017). The results show that the GWP of 1 kg of corn production is about 1.346 kg CO_2 eq. However, based on the findings of DEA, with the optimal use of available resources through the pursuit of efficient farms in the study area (reference group), it is possible to reduce the GWP of corn production by 10.04%. This way, a 15.19 percent reduction in the load on OLD is also achieved.

Another major impact category is photochemical oxidation, which is a dangerous chemical air pollutant that causes various problems such as eye irritation and damage to some materials and products. This phenomenon mostly occurs in the presence of emissions from the combustion of fossil fuels, sunlight, and low humidity (Baumann & Tillman, 2004). The production of 1 kg of corn may cause a photochemical oxidation potential of 0.685 g C_2H_4 eq, 98% of which is due to the use of electricity (Fig. **4**). Life cycle assessment based on optimized values using DEA showed that there is a potential to reduce 10.51% of the potential of photochemical oxidation caused by corn production through optimizing the input consumption of inefficient farms.

In toxicity categories that include Human Toxicity (HT), Fresh Water Aquatic Eco-toxicity (FWAE), Marine Aquatic Eco-toxicity (MAE), and Terrestrial Eco-toxicity (TE), electricity is one of the most influential inputs. The share of electricity in the MAE impact category is about 99%. In the TE category, on-farm emissions have the highest share with 51.09%, while in the BCC and CCR models, its share decreases to 42.83% and 41.86%, respectively, but the share of electricity increases. The contribution of inputs in different subcategories of toxicity impact category is shown in Fig. **5**. The DEA results show that with the optimal use of inputs, 10.25 to 24.05% of the effects of toxicity categories caused by corn production can be reduced.

The comparison of the normalized environmental effects of producing 1 kg of corn under current conditions (default scenario) and the optimized values using the input-oriented BCC and CCR models based on the CML 2 baseline 2000 V2.05 / Netherlands, 1997 model is shown in Fig. **5**. It can be seen that corn production has the highest load on MAE, AC, and FWAE impact categories, respectively, while the lowest load is on OLD. This figure also shows that the DEA method can reduce all environmental impact categories by 9% to 24% by optimizing inputs.

Conclusion

Relatively high yield of corn and higher exergy output in the corn production system have led to the achievement of a production system with efficient exergy consumption (CDP=7.6). Additionally, according to the obtained RI index (0.87), in general, the corn production process in the study area is relatively renewable. However, it can be improved by optimal use of inputs, especially non-renewable inputs such as electricity, diesel fuel, and chemical fertilizers. Electricity is the main component of CEnC and CExC in corn production, and replacing non-renewable sources of electricity with renewable sources can lead to reduced environmental consequences and improved energy indicators. Other important inputs affecting the renewability and sustainability of the corn production system, which must be used very carefully and efficiently, are diesel fuel and chemical fertilizers.
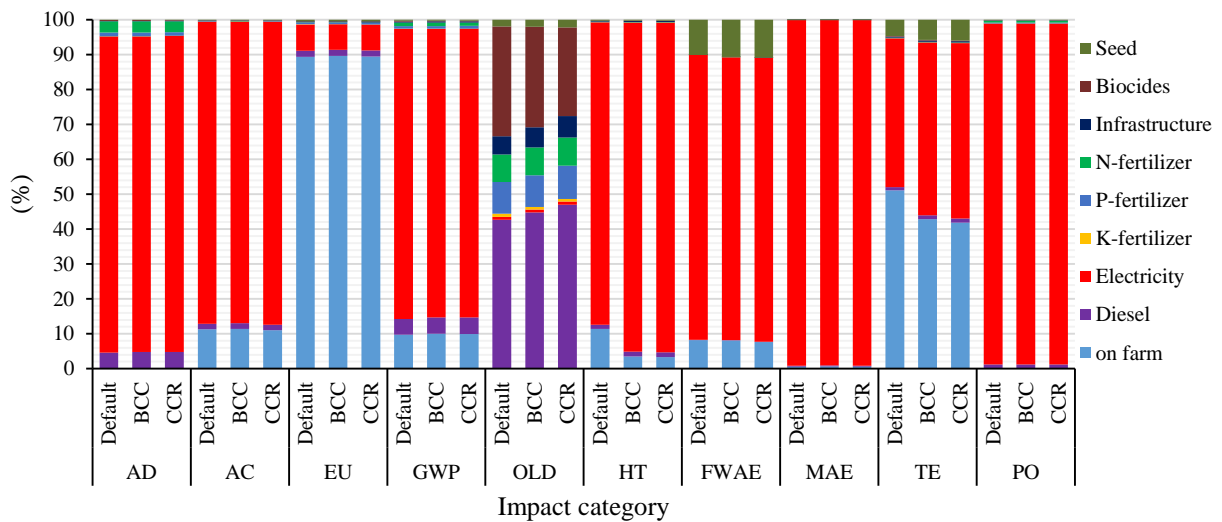

Fig. 4. The contribution of inputs in different impact categories in corn production system
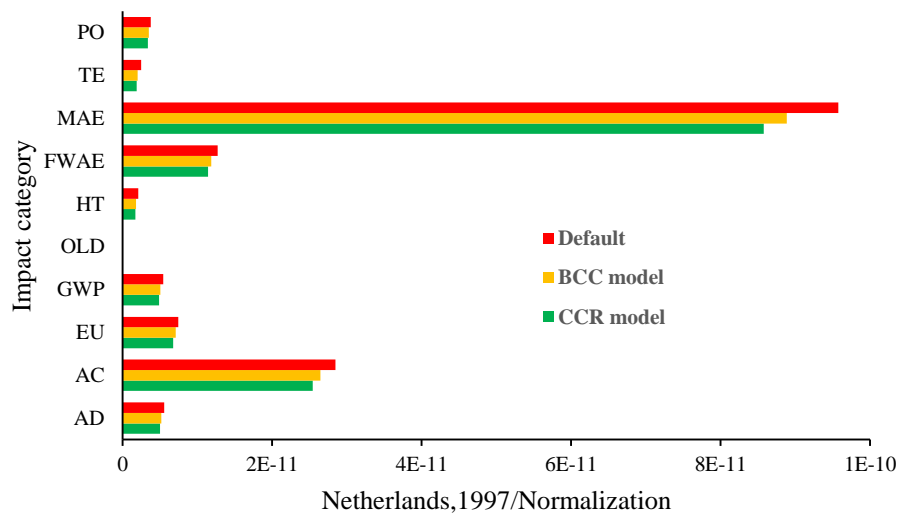

Fig. 5. Comparison of environmental impact categories of 1 kg of corn production in three scenarios (Method: CML 2 baseline 2000 V2.05/the Netherlands,1997/Normalization)

DEA is an effective method for finding efficient farms and recommending best practices aimed at minimizing exergy consumption to meet specified targets. Results showed that the average efficiency of all farms in terms of CExC in CCR and BCC models was 94.7 and 97.8%, respectively. Based on the DEA results, it was possible to save 6.47, 10.42, 7.40, 13.32, 31.29, 3.25, and 78.6%, respectively, in the exergy consumption of diesel fuel, electricity, machinery, chemical fertilizers, biocides, seeds, and irrigation, while maintaining the current yield level, only by promoting methods used by efficient farms. Consequently, CEnC and CExC have decreased by 9.76 and 9.38%, respectively. Furthermore, there was a potential for reductions of about 10, 17, 8, 10, and 11% respectively in the impact categories of "depletion of abiotic resources", "acidification", "eutrophication", "GWP", and "photochemical oxidation". The improvement of ER, EP, CDP, and RI energy indices was also about 11, 11, 10.3, and 1.4%, respectively.

Conflicts of interest/Competing interests

The authors declare they have no financial interests.

Availability of data and materials

The datasets used and analyzed during the current study are available from the corresponding author on reasonable request.

Authors Contribution

M. Soleymani: Responsible for conceptualization, Methodology, Analysis, and Writing the manuscript

A. Asakereh: Provided technical advice and guidance throughout the research process and assisted with exergy and environmental analysis

M. Safaieenejad: Responsible for Study design, and Data collection

References

1. Adler, N., Friedman, L., & Sinuany-Stern, Z. (2002). Review of ranking methods in the data envelopment analysis context. In *European Journal of Operational Research*, *140*, 249-265. North-Holland. https://doi.org/10.1016/S0377-2217(02)00068-1
2. Ahamed, J. U., Saidur, R., Masjuki, H. H., Mekhilef, S., Ali, M. B., & Furqon, M. H. (2011). An application of energy and exergy analysis in agricultural sector of Malaysia. *Energy Policy*, *39*(12), 7922-7929. https://doi.org/10.1016/j.enpol.2011.09.045
3. Al-Ghandoor, A., & Jaber, J. O. (2009). Analysis of energy and exergy utilisation of Jordan's agricultural sector. *International Journal of Exergy*, *6*(4), 491-508. https://doi.org/10.1504/IJEX.2009.026674
4. Alam, M. S., Alam, M. R., & Islam, K. K. (2005). Energy Flow in Agriculture: Bangladesh. *American Journal of Environmental Sciences*, *1*(3), 213–220. https://doi.org/10.3844/ajessp.2005.213.220
5. Amiri, Z., Asgharipour, M., Campbell, D. E., & Armin, M. (2020). Extended exergy analysis (EAA) of two canola farming systems in Khorramabad, Iran. *Agricultural Systems*, *180*, 102789. https://doi.org/10.1016/j.agsy.2020.102789
6. Anonymous. (2018). *Energy Balance Sheet of Iran*. Tehran: Iran Ministry of Energy Deputy of Electricity and Energy Affairs.
7. Apazhev, A. K., Fiapshev, A. G., Shekikhachev, I. A., Khazhmetov, L. M., Khazhmetova, A. L., & Ashabokov, K. K. (2019). Energy efficiency of improvement of agriculture optimization technology and machine complex optimization. In *E3S Web of Conferences* (Vol. 124, p. 05054). EDP Sciences. https://doi.org/10.1051/e3sconf/201912405054

8. Arts, W., Ruijten, D., Aelst, K. Van, Trullemans, L., & Sels, B. (2021). The RCF biorefinery: Building on a chemical platform from lignin. *Advances in Inorganic Chemistry*, 77, 241-297. https://doi.org/10.1016/BS.ADIOCH.2021.02.006

9. Ashby, M. F. (2013). Eco-audits and eco-audit tools. *Materials and the Environment*, 175-191. https://doi.org/10.1016/B978-0-12-385971-6.00007-5

10. Banaeian, N., & Zangeneh, M. (2011). Study on energy efficiency in corn production of Iran. *Energy*, *36*(8), 5394-5402.

11. Baumann, H., & Tillman, A. M. (2004). *The Hitch Hiker's Guide to LCA. An orientation in life cycle assessment methodology and application*. *Studentlitteratur Lund*. Studentlitteratur AB.

12. Bechmann, M., & Stålnacke, P. (2005). Effect of policy-induced measures on suspended sediments and total phosphorus concentrations from three Norwegian agricultural catchments. *Science of the Total Environment*, *344*(1-3 SPEC. ISS.), 129-142. https://doi.org/10.1016/j.scitotenv.2005.02.013

13. Beheshti Tabar, I., Keyhani, A., & Rafiee, S. (2010, February). Energy balance in Iran's agronomy (1990-2006). *Renewable and Sustainable Energy Reviews*. Pergamon. https://doi.org/10.1016/j.rser.2009.10.024

14. Berthiaume, R., Bouchard, C., & Rosen., M. A. (2001). Exergetic evaluation of the renewability of a biofuel. *Exergy, An International Journal*, *1*(4), 256-268.

15. Bhunia, S., Karmakar, S., Bhattacharjee, S., Roy, K., Kanthal, S., Pramanick, M., …, & Mandal, B. (2021). Optimization of energy consumption using data envelopment analysis (DEA) in rice-wheat-green gram cropping system under conservation tillage practices. *Energy*, *236*, 121499. https://doi.org/10.1016/j.energy.2021.121499

16. Bösch, M. E., Hellweg, S., Frischknecht, M. A. J., & Huijbregts, R. (2007). Applying cumulative exergy demand (CExD) indicators to the ecoinvent database. *The International Journal of Life Cycle Assessment*, *12*(181).

17. Brentrup, F., Küsters, J., Lammel, J., Barraclough, P., & Kuhlmann, H. (2004). Environmental impact assessment of agricultural production systems using the life cycle assessment (LCA) methodology II. The application to N fertilizer use in winter wheat production systems. *European Journal of Agronomy*, *20*(3), 265-279. https://doi.org/10.1016/S1161-0301(03)00039-X

18. Cao, C. (2017). Sustainability and life assessment of high strength natural fibre composites in construction. *Advanced High Strength Natural Fibre Composites in Construction*, 529-544. https://doi.org/10.1016/B978-0-08-100411-1.00021-2

19. Chauhan, N. S., Mohapatra, P. K. K. J., & Pandey, K. P. (2006). Improving energy productivity in paddy production through benchmarking—An application of data envelopment analysis. *Energy Conversion and Management*, *47*(9-10), 1063-1085. https://doi.org/10.1016/j.enconman.2005.07.004

20. Dincer, I., & Cengel, Y. A. (2001). Energy, entropy and exergy concepts and their roles in thermal engineering. *Entropy*, *3*(3), 116-149. https://doi.org/10.3390/e3030116

21. Erdal, G., Esengün, K., Erdal, H., & Gündüz, O. (2007). Energy use and economical analysis of sugar beet production in Tokat province of Turkey. *Energy*, *32*(1), 35-41. https://doi.org/10.1016/j.energy.2006.01.007

22. EsmaeilpourTroujeni, M., Rohani, A., & Khojastehpour, M. (2021). Optimization of rapeseed production using exergy analysis methodology. *Sustainable Energy Technologies and Assessments*, *43*, 100959. https://doi.org/10.1016/j.seta.2020.100959

23. Fallahpour, F., Aminghafouri, A., Ghalegolab Behbahani, A., & Bannayan, M. (2012). The environmental impact assessment of wheat and barley production by using life cycle assessment (LCA) methodology. *Environment, Development and Sustainability*, *14*(6), 979-992. https://doi.org/10.1007/s10668-012-9367-3

24. Filipovic, D., Kosutic, S., Gospodaric, Z., Zimmer, R., & Banaj, D. (2006). The possibilities of fuel savings and the reduction of CO_2 emissions in the soil tillage in Croatia. *Agriculture, Ecosystems and Environment*, *115*(1-4), 290-294. https://doi.org/10.1016/j.agee.2005.12.013

25. Finkbeiner, M., Inaba, A., Tan, R. B. H., Christiansen, K., & Klüppel, H. J. (2006, January). The

new international standards for life cycle assessment: ISO 14040 and ISO 14044. *International Journal of Life Cycle Assessment*. Springer. https://doi.org/10.1065/lca2006.02.002

26. Gezer, I., Acaroğlu, M., & Haciseferoğullari, H. (2003). Use of energy and labour in apricot agriculture in Turkey. *Biomass and Bioenergy*, *24*(3), 215-219. https://doi.org/10.1016/S0961-9534(02)00116-2

27. Gurdeep Singh, P., Sodhi, G. P. S., & Tiwari, D. (2021). Energy auditing and data envelopment analysis (DEA) based optimization for increased energy use efficiency in wheat cultivation (*Triticum aestium* L.) in north-western India. *Sustainable Energy Technologies and Assessments*, *47*, 101453. https://doi.org/10.1016/j.seta.2021.101453

28. Hai, Q., Zhiliang, D., Xinshang, Y., Li, Y., Zhao, Y., & Xiaotian, S. (2023). Extended exergy accounting for assessing the sustainability of agriculture: A case study of Hebei Province, China. *Ecological Indicators*, *150*, 110240.

29. Hatirli, S. A., Ozkan, B., & Fert, C. (2005, December). An econometric analysis of energy input-output in Turkish agriculture. *Renewable and Sustainable Energy Reviews*. Pergamon. https://doi.org/10.1016/j.rser.2004.07.001

30. Hatirli, S. A., Ozkan, B., & Fert, C. (2006). Energy inputs and crop yield relationship in greenhouse tomato production. *Renewable Energy*, *31*(4), 427-438.

31. Hernandez, P., Oregi, X., Longo, S., & Cellura, M. (2019). Life-Cycle Assessment of Buildings. *Handbook of Energy Efficiency in Buildings: A Life Cycle Approach*, 207-261. https://doi.org/10.1016/B978-0-12-812817-6.00010-3

32. Houshyar, E., & Grundmann, P. (2017). Environmental impacts of energy use in wheat tillage systems: A comparative life cycle assessment (LCA) study in Iran. *Energy*, 122, 11-24. https://doi.org/10.1016/j.energy.2017.01.069

33. IPCC. (2006). *IPCC guidelines for national greenhouse gas inventories.* Hayama, Japan.: Institute for Global Environmental Strategies.

34. Jacob-Lopes, E., Zepka, L. Q., & Deprá, M. C. (2021). Methods of evaluation of the environmental impact on the life cycle. In *Sustainability Metrics and Indicators of Environmental Impact* (pp. 29–70). Elsevier. https://doi.org/10.1016/b978-0-12-823411-2.00003-7

35. Jalalvand, M., Bakhoda, H., & Almassi, M. (2014). Wind Energy Potential Assessment for Electric Pumps of Agriculture in Broujerd. *Journal of Agricultural Machinery*, *4*(2), 368-377. (in Persian). https://doi.org/10.22067/jam.v4i2.34821

36. Jat, H. S., Jat, R. D., Nanwal, R. K., Lohan, S. K., Yadav, A. K., Poonia, T., …, & Jat, M. L. (2020). Energy use efficiency of crop residue management for sustainable energy and agriculture conservation in NW India. *Renewable Energy*, *155*, 1372-1382. https://doi.org/10.1016/j.renene.2020.04.046

37. Juárez-Hernández, S., Usón, S., & Pardo, C. S. (2019). Assessing maize production systems in Mexico from an energy, exergy, and greenhouse-gas emissions perspective. *Energy*, *170*, 199-211. https://doi.org/10.1016/j.energy.2018.12.161

38. Kaab, A., Sharifi, M., Mobli, H., Nabavi-Pelesaraei, A., & Chau, K. wing. (2019). Use of optimization techniques for energy use efficiency and environmental life cycle assessment modification in sugarcane production. *Energy*, *181*, 1298-1320. https://doi.org/10.1016/j.energy.2019.06.002

39. Khan, S., Khan, M. A., Hanjra, M. A., & Mu, J. (2009). Pathways to reduce the environmental footprints of water and energy inputs in food production. *Food Policy*, *34*(2), 141-149.

40. KhojastehpourTroujeni, M., Esmailpour, M., Vahedi, A., & Emadi, B. (2018). Sensitivity analysis of energy inputs and economic evaluation of pomegranate production in Iran. *Information Processing in Agriculture*, *5*(1), 114-123. https://doi.org/10.1016/j.inpa.2017.10.002

41. Kitani, O. (1999). *Energy and biomass engineering, CIGR handbook of agricultural engineering*. American Society of Agricultural and Biological Engineers. https://doi.org/10.13031/2013.36411

42. Komleh Pishgar, S. H., Keyhani, A., Rafiee, S., & Sefeedpary, P. (2011). Energy use and economic analysis of corn silage production under three cultivated area levels in Tehran province of Iran.

Energy, *36*(5), 3335-3341.

43. Kylili, A., Seduikyte, L., & Fokaides, P. A. (2018). Life Cycle Analysis of Polyurethane Foam Wastes. *Recycling of Polyurethane Foams*, 97-113. https://doi.org/10.1016/B978-0-323-51133-9.00009-7

44. Leiva, F. R., & Morris, J. (2001). Mechanization and sustainability in arable farming in England. *Journal of Agricultural and Engineering Research*, *79*(1), 81-90. https://doi.org/10.1006/jaer.2000.0686

45. Lovarelli, D., Bacenetti, J., & Fiala, M. (2017). Effect of local conditions and machinery characteristics on the environmental impacts of primary soil tillage. *Journal of Cleaner Production*, *140*, 479-491. https://doi.org/10.1016/j.jclepro.2016.02.011

46. Malana, N. M., & Malano, H. M. (2006). Benchmarking productive efficiency of selected wheat areas in Pakistan and India using data envelopment analysis. *Irrigation and Drainage*, *55*(4), 383-394. https://doi.org/10.1002/ird.264

47. Mani, I., Kumar, P., Panwar, J. S., & Kant, K. (2007). Variation in energy consumption in production of wheat-maize with varying altitudes in hilly regions of Himachal Pradesh, India. *Energy*, *32*(12), 2336-2339. https://doi.org/10.1016/j.energy.2007.07.004

48. Michalakakis, C., Fouillou, J., Lupton, R. C., Gonzalez Hernandez, A., & Cullen, J. M. (2021). Calculating the chemical exergy of materials. *Journal of Industrial Ecology*, *25*(2), 274-287. https://doi.org/10.1111/jiec.13120

49. Milà I Canals, L., Burnip, G. M., & Cowell, S. J. (2006). Evaluation of the environmental impacts of apple production using Life Cycle Assessment (LCA): Case study in New Zealand. *Agriculture, Ecosystems and Environment*, *114*(2-4), 226-238. https://doi.org/10.1016/j.agee.2005.10.023

50. Mobtaker, H. G., Keyhani, A., Mohammadi, A., Rafiee, S., & Akram, A. (2010). Sensitivity analysis of energy inputs for barley production in Hamedan Province of Iran. *Agriculture, Ecosystems and Environment*, *137*(3-4), 367-372. https://doi.org/10.1016/j.agee.2010.03.011

51. Mohammadi, A., Rafiee, S., Jafari, A., Dalgaard, T., Knudsen, M. T., Keyhani, A., …, & Hermansen, J. E. (2013). Potential greenhouse gas emission reductions in soybean farming: A combined use of Life Cycle Assessment and Data Envelopment Analysis. *Journal of Cleaner Production*, *54*, 89-100. https://doi.org/10.1016/j.jclepro.2013.05.019

52. Mohammadi, A., Rafiee, S., Jafari, A., Keyhani, A., Mousavi-Avval, S. H., & Nonhebel, S. (2014, February). Energy use efficiency and greenhouse gas emissions of farming systems in north Iran. *Renewable and Sustainable Energy Reviews*. Pergamon. https://doi.org/10.1016/j.rser.2013.11.012

53. Mousavi-Avval, S. H., Rafiee, S., Jafari, A., & Mohammadi, A. (2011a). Improving energy use efficiency of canola production using data envelopment analysis (DEA) approach. *Energy*, *36*(5), 2765-2772. https://doi.org/10.1016/j.energy.2011.02.016

54. Mousavi-Avval, S. H., Rafiee, S., Jafari, A., & Mohammadi, A. (2011b). Optimization of energy consumption for soybean production using Data Envelopment Analysis (DEA) approach. *Applied Energy*, *88*(11), 3765-3772. https://doi.org/10.1016/j.apenergy.2011.04.021

55. Nemecek, T., Dubois, D., Huguenin-Elie, O., & Gaillard, G. (2011). Life cycle assessment of Swiss farming systems: I. Integrated and organic farming. *Agricultural Systems*, *104*(3), 217-232. https://doi.org/10.1016/j.agsy.2010.10.002

56. Nikkhah, A., Khojastehpour, M., Emadi, B., Taheri-Rad, A., & Khorramdel, S. (2015). Environmental impacts of peanut production system using life cycle assessment methodology. *Journal of Cleaner Production*, *92*, 84-90. https://doi.org/10.1016/j.jclepro.2014.12.048

57. Ordikhani, H., Parashkoohi, M. G., Zamani, D. M., & Ghahderijani, M. (2021). Energy-environmental life cycle assessment and cumulative exergy demand analysis for horticultural crops (Case study: Qazvin province). *Energy Reports*, *7*, 2899-2915. https://doi.org/10.1016/j.egyr.2021.05.022

58. Papapetrou, M., & Kosmadakis, G. (2022). Resource, environmental, and economic aspects of SGHE. *Salinity Gradient Heat Engines*, 319-353. https://doi.org/10.1016/B978-0-08-102847-6.00006-1

59. Parihar, C. M., Jat, S. L., Singh, A. K., Kumar, B., Rathore, N. S., Jat, M. L., …, & Kuri, B. R. (2018). Energy auditing of long-term conservation agriculture based irrigated intensive maize systems in semi-arid tropics of India. *Energy*, *142*, 289-302. https://doi.org/10.1016/j.energy.2017.10.015

60. Parvaresh Rizi, A., & Ashrafzadeh, A. (2018). Techno-economic Analysis of Solar Irrigation: Comparison with Conventional Energy Sources for Irrigation. *Journal of Energy Planning And Policy Research*, *4*(2), 201-228.

61. Pelvan, E., & Özilgen, M. (2017). Assessment of energy and exergy efficiencies and renewability of black tea, instant tea and ice tea production and waste valorization processes. *Sustainable Production and Consumption*, *12*, 59-77. https://doi.org/10.1016/j.spc.2017.05.003

62. Pishgar-Komleh, S. H., Keyhani, A., Mostofi-Sarkari, M. R., & Jafari, A. (2012). Energy and economic analysis of different seed corn harvesting systems in Iran. *Energy*, *43*(1), 469-476. https://doi.org/10.1016/j.energy.2012.03.040

63. Powar, R. V., Mehetre, S. A., Patil, P. R., Patil, R. V., Wagavekar, V. A., Turkewadkar, S. G., & Patil, S. B. (2020). Study on Energy Use Efficiency for Sugarcane Crop Production Using the Data Envelopment Analysis (DEA) Technique. *Journal of Biosystems Engineering*, *45*(4), 291-309. https://doi.org/10.1007/s42853-020-00070-x

64. Prasad, S., Singh, A., Korres, N. E., Rathore, D., Sevda, S., & Pant, D. (2020, May). Sustainable utilization of crop residues for energy generation: A life cycle assessment (LCA) perspective. *Bioresource Technology*. Elsevier. https://doi.org/10.1016/j.biortech.2020.122964

65. Ptasinski, K. J. (2016). *Efficiency of Biomass Energy: An Exergy Approach to Biofuels, Power, and Biorefineries*. *Hoboken, NJ: Wiley*. https://doi.org/10.1002/9781119118169

66. Rahman, S., & Hasan, M. K. (2014). Energy productivity and efficiency of wheat farming in Bangladesh. *Energy*, *66*, 107-114. https://doi.org/10.1016/j.energy.2013.12.070

67. Royan, M., Khojastehpour, M., Emadi, B., & Mobtaker, H. G. (2012). Investigation of energy inputs for peach production using sensitivity analysis in Iran. In *Energy Conversion and Management 64*, 441-446. Pergamon. https://doi.org/10.1016/j.enconman.2012.07.002

68. Sartor, K., & Dewallef, P. (2017). Exergy analysis applied to performance of buildings in Europe. *Energy and Buildings*, *148*, 348-354. https://doi.org/10.1016/j.enbuild.2017.05.026

69. Shah, S. M., Liu, G., Yang, Q., Casazza, M., Agostinho, F., & Giannetti, B. F. (2021). Sustainability assessment of agriculture production systems in Pakistan: A provincial-scale energy-based evaluation. *Ecological Modelling*, *455*, 109654. https://doi.org/10.1016/j.ecolmodel.2021.109654

70. Shahhoseini, H. R., Ramroudi, M., Kazemi, H., & Amiri, Z. (2021). Sustainability assessment of autumn and spring potato production systems using extended exergy analysis (EEA). *Energy, Ecology and Environment*, 1-12. https://doi.org/10.1007/s40974-021-00222-5

71. Shojaei, M., & Akhavan, S. (2020). Economic assessment of photovoltaic (PV) water pumping system in drip-irrigated fields. *Iranian Water Researches Journal*, *14*(1), 19-28.

72. Singh, A., Pant, D., Korres, N. E., Nizami, A. S., Prasad, S., & Murphy, J. D. (2010). Key issues in life cycle assessment of ethanol production from lignocellulosic biomass: Challenges and perspectives. *Bioresource Technology*, *101*(13), 5003-5012. https://doi.org/10.1016/j.biortech.2009.11.062

73. Singh, Gursahib, Singh, S., & Singh, J. (2004). Optimization of energy inputs for wheat crop in Punjab. *Energy Conversion and Management*, *45*(3), 453-465. https://doi.org/10.1016/S0196-8904(03)00155-9

74. Singh, P., Singh, G., & Sodhi, G. P. S. (2019). Applying DEA optimization approach for energy auditing in wheat cultivation under rice-wheat and cotton-wheat cropping systems in north-western India. *Energy*, *181*, 18-28. https://doi.org/10.1016/j.energy.2019.05.147

75. Soltanali, H., Nikkhah, A., & Rohani, A. (2017). Energy audit of Iranian kiwifruit production using intelligent systems. *Energy*, *139*, 646-654. https://doi.org/10.1016/j.energy.2017.08.010

76. Su, X., Shao, X., Tian, S., Li, H., & Huang, Y. (2021). Life cycle assessment comparison of three

typical energy utilization ways for corn stover in China. *Biomass and Bioenergy*, *152*, 106199.

77. Thankappan, S., Midmore, P., & Jenkins, T. (2006). Conserving energy in smallholder agriculture: A multi-objective programming case-study of northwest India. *Ecological Economics*, *56*(2), 190-208. https://doi.org/10.1016/j.ecolecon.2005.01.017

78. Tzilivakis, J., Warner, D. J., May, M., Lewis, K. A., & Jaggard, K. (2005). An assessment of the energy inputs and greenhouse gas emissions in sugar beet (*Beta vulgaris*) production in the UK. *Agricultural Systems*, *85*(2), 101-119. https://doi.org/10.1016/j.agsy.2004.07.015

79. Vlontzos, G., Niavis, S., & Manos, B. (2014, December). A DEA approach for estimating the agricultural energy and environmental efficiency of EU countries. *Renewable and Sustainable Energy Reviews*. Pergamon. https://doi.org/10.1016/j.rser.2014.07.153

80. William G. Cochran. (1991). *Sampling Techniques* (3rd Editio). New York: John Wiley and Sons.

81. Yildizhan, H. (2018). Energy, exergy utilization and CO_2 emission of strawberry production in greenhouse and open field. *Energy*, *143*, 417-423. https://doi.org/10.1016/j.energy.2017.10.139

82. Yildizhan, H., & Taki, M. (2018). Assessment of tomato production process by cumulative exergy consumption approach in greenhouse and open field conditions: Case study of Turkey. *Energy*, *156*, 401-408. https://doi.org/10.1016/j.energy.2018.05.117

83. Yildizhan, H., & Taki, M. (2019). Sustainable management and conservation of resources for different wheat production processes; cumulative exergy consumption approach. *International Journal of Exergy*, *28*(4), 404-422. https://doi.org/10.1504/IJEX.2019.099295

84. Yilmaz, I., Akcaoz, H., & Ozkan, B. (2005). An analysis of energy use and input costs for cotton production in Turkey. *Renewable Energy*, *30*(2), 145-155. https://doi.org/10.1016/j.renene.2004.06.001

85. Yousefi, M., Khoramivafa, M., & Mondani, F. (2014). Integrated evaluation of energy use, greenhouse gas emissions and global warming potential for sugar beet (*Beta vulgaris*) agroecosystems in Iran. *Atmospheric Environment*, *92*, 501-505. https://doi.org/10.1016/j.atmosenv.2014.04.050

86. Yousefi, M., Mahdavi, A., & Mahmud, D. K. (2014). Energy consumption, greenhouse gas emissions and assessment of sustainability index in corn agroecosystems of Iran. *Science of the Total Environment*, *493*, 330-335.

87. Yuan, S., Peng, S., Wang, D., & Man, J. (2018). Evaluation of the energy budget and energy use efficiency in wheat production under various crop management practices in China. *Energy*, *160*, 184-191. https://doi.org/10.1016/j.energy.2018.07.006

بهینه‌سازی مصرف انرژی و اکسرژی تجمعی و ارزیابی چرخه حیات زیست‌محیطی تولید ذرت در استان لرستان

محسن سلیمانی ۱*، عباس عساکره ۱، مجتبی صفایی‌نژاد۲

چکیده

بهینه‌سازی مصرف نهاده، کاهش مصرف انرژی و اثرات مختلف زیست‌محیطی سیستم تولید ذرت در استان لرستان بر اساس تحلیل اکسرژی و ارزیابی چرخه حیات زیست‌محیطی مورد بررسی قرار گرفت. بر اساس نتایج به‌دست‌آمده و با توجه به معادله کاب–داگلاس، برق، سوخت دیزل و کود نیتروژن، بیشترین سهم را در مصرف اکسرژی تجمعی در سیستم تولید ذرت داشته‌اند. نتایج DEA نشان داد که میانگین راندمان تمام مزارع از نظر مصرف اکسرژی تجمعی در مدل‌های CCR و BCC، به‌ترتیب ۹۴/۷ و ۹۷/۸ درصد است. همچنین نتایج نشان داد که نهاده‌ها به‌ویژه کودهای پتاسیم و فسفات بیش از نیاز مصرف می‌شوند. همچنین می‌توان ۶/۴۷، ۱۰/۴۲، ۷/۴۰، ۱۳/۳۲، ۳۱/۲۹، ۳/۲۵ و ۶/۷۸ درصد به‌ترتیب در مصرف اکسرژی سوخت دیزل، برق، ماشین‌ها، کودهای شیمیایی، سموم، بذر و انرژی آبیاری، با حفظ سطح عملکرد فعلی و تنها با ترویج روش‌های مورد استفاده توسط مزارع کارآمد، صرفه‌جویی کرد.

واژه‌های کلیدی: LCA، DEA، انرژی در کشاورزی، پایداری، تجدیدپذیری

۱- گروه مهندسی بیوسیستم، دانشکده کشاورزی، دانشگاه شهید چمران اهواز، اهواز، ایران
۲- گروه مدیریت مکانیزاسیون کشاورزی، جهاد کشاورزی استان لرستان، خرم‌آباد، ایران
(*- نویسنده مسئول: Email: m.soleymani@scu.ac.ir)

IoT Stingless Bee Colony Monitoring System

R. J. Arendela[1], R. A. Ebora[1], E. Arboleda [iD][1, 2], J. L. M. Ramos [iD][1*], M. Bono[2], D. Dimero[2]

1- Department of Computer, Electronics and Electrical Engineering (DCEE), College of Engineering and Information Technology, Cavite State University, Indang (Main Campus), Indang, Cavite, Philippines
2- CvSU Bee Research, Innovation, Trade, and Extension (BRITE) Center, Cavite State University, Indang, Cavite, Philippines
(*- Corresponding Author Email: josephlouismichael.ramos@cvsu.edu.ph)

Abstract

The IoT monitoring system for stingless bee colonies aims to provide real-time information about temperature, humidity, and hive weight in response to the issue of colony collapse disorder (CCD) caused by human intervention in beekeeping. It also aims to improve the current monitoring methods for the bees more effectively and efficiently. The monitoring system features a water-cooling control system to maintain an optimal temperature for Tetragonula Biroi (Stingless Bees). The system also includes a user dashboard for remote monitoring and alerts the beekeeper when it is time to harvest. It's primarily built around the ESP8266-MOD microcontroller, with an Arduino Mega 2560 R3 for the water valve control system. Data were collected from a DHT22 sensor for temperature and humidity, and load cells connected to an HX711 amplifier for hive weight. The system was tested by comparing samples from the system and actual measuring instruments using MAPE for two months, and it demonstrated 98.74% and 97.89% accuracy for surrounding temperature and humidity, respectively. An accuracy of 95.92% for the weight scale and 93% for the water valve control system was also obtained. Hives equipped with the IoT system gained 3.414% more weight than those without it, indicating that the project succeeded in achieving its objectives.

Keywords: Environmental parameters, Hive weight, IoT monitoring system, Remote monitoring, Stingless bee colony

Introduction

The stingless bees known as "Kiwot" are similar in size to ants but share many characteristics with honeybees, excluding the absence of a stinger. These bees play a crucial role in primary healthcare by producing medicinal hive products like honey, propolis, and beebread (Kwapong, Aidoo, Combey, & Karikari 2010). According to research conducted by the National Library of

Medicine, it was asserted that the application of propolis can expedite the healing process of cold sores compared to not receiving any treatment (Sforcin, 2016). Carcinogens contained in honey are proven to fight cancer development with the ability to mitigate toxicity through antioxidant properties in honey (Afrin *et al.,* 2019). Beekeeping, also known as Apiculture, has ancient origins, as evidenced by prehistoric art depicting humans harvesting honey from bee colonies. In the early days of beekeeping, honey and wax were the primary products obtained from hives. However, in contemporary times, honey production is viewed as a secondary outcome of the western honeybee (*Apis mellifera*),

whose most crucial role is pollinating plants. Today, up to 79% of the global food supply relies on pollination, making the honeybee the predominant and highly active pollinator species across the world (Fitzgerald, Murphy, Wright, Whelan, & Popovici 2015). Among these pollinators are stingless honeybees, which also serve for commercial honey production, albeit at a lower scale. Research suggests that the honey produced by these bees could potentially aid wound healing by promoting processes like angiogenesis and oxygen circulation (Jalil, Kasmuri, & Hadi, 2017). Honey is most frequently used as a sweetener. Honey is also renowned for its healing properties (Chan-Rodríguez *et al.,* 2012). Additionally, stingless bee honey has demonstrated promise in the realm of medicine due to its phenolic content that enhances antioxidant levels and may help mitigate diseases related to oxidative stress (Yaacob, Rajab, Shahar, & Sharif, 2017). Stingless bee honey showcases unique physicochemical properties that distinguish its composition from honey produced by other species (Özbalci, Boyaci, Topcu, Kadılar, & Tamer 2013). These stingless honeybees are significant not only for their contribution to pollination and honey production but also for their suitability in urban environments due to their non-aggressive behavior and lack of stinging capability in comparison to common honey bees (Honeybees Vs Stingless Bees-The Real Difference, 2020).

In the Philippines, various species of stingless bees play an essential role as pollinators for agriculture in certain regions, often nesting in old bamboo and wooden structures. These bees inadvertently pollinate flowers while collecting pollen for nourishment and produce small amounts of honey. They have a wide foraging range but prefer high-quality pollen sources nearby, visiting numerous flowering plants and potentially contributing to the pollination of around 60 crop species. Despite their importance, their small size often leads to their neglect and confusion with other insects, contributing to declining populations due to habitat loss and pesticide use (Roubik, 2014). Research shows that the population of bees is declining at an alarming rate due to various natural and human-induced factors (Fitzgerald *et al.,* 2015). Researches also show that the understanding of humans of various stingless bee biology and ecological topics continues to lag behind the understanding of honeybees and bumblebees (Biesmeijer, Hartfelder, & Imperatriz-Fonseca, 2006). One research aims to solve this problem and come up with an idea of utilizing useful sensors to monitor the beehive (internal and ambient temperature, humidity, and weight of the hives). These sensors enable beekeepers to effectively evaluate and respond to the bees' needs based on changes in parameters (Zabasta, Zhiravetska, Kunicina, & Kondratjevs 2019). Most of these researchers have utilized a weighing scale to measure and document the hive's weight as part of their approach (Johannsen, Senger, & Kluss, 2020). The researchers aim to follow the same goal but with the use of IoT to monitor the beehive of Stingless honeybees. This study has the potential to support the preservation of bee populations while minimizing stress on the bees, all while enabling remote monitoring of hive conditions. There is a pressing need to comprehensively assess environmental factors affecting stingless bee colonies. By focusing on critical parameters such as temperature, humidity, and light intensity, the study shed light on the influence of the monitoring system on hive health and honey production (Harun *et al.,* 2015).

Beekeepers employ various hive management strategies, including inspection, to check hive occupancy, protect it against enemies, and facilitate honey harvesting (Kwapong *et al.,* 2010). Beekeepers from the Hadiya zone in Southern Ethiopia believe that inspecting hives during the rainy season could lead to disease (Jalil *et al.,* 2017). While external inspections are conducted year-round, caution is advised regarding the timing and frequency of internal inspections. Hive visits serve diverse purposes such as confirming occupation, observing bee activity, and

ensuring hive cleanliness (Kiros & Tsegay, 2017; Alebachew, 2018). Yet, internal inspections are less common except for honey assessment (Tesfa & Kebede, 2013). Beekeeping practices and harvesting frequency are influenced by agro-ecology, with higher-frequency harvesting in highland areas due to better forage availability and climate. A study showed that stingless bee activity was intense on warmer days, particularly when the temperature exceeded $30°C$. Humidity had minimal impact on flight activities. The study demonstrated the potential of IoT applications in monitoring stingless bee conditions and understanding climate effects on their activities (Yunus, 2017). Also, a study presents an IoT-based strategy that focuses on individual monitoring of bee colonies to enhance resource efficiency and maximize productivity (Ochoa, Gutierrez, & Rodriguez, 2019).

The technology known as "Wireless Sensor Networks" (WSN) is a result of recent developments in embedded sensing, downsizing, wireless communications, low-power operation, and energy harvesting. The Internet of Things (IoT), a new idea, is not complete without WSN. In several fields, such as healthcare (Kulkarni & Ozturk, 2011), smart homes (Edwards-Murphy *et al.*, 2013), and security (Magno, Tombari, Brunelli, Di Stefano, & Benini, 2009), WSN are quickly becoming a necessary component of daily life. A study by Fitzgerald *et al.* (2015), used NodeMCU ESP8266 as a Controller. NodeMCU is an open-source firmware and development kit renowned for its advantages in prototyping IoT (Internet of Things) products with minimal Lua script lines. This versatile controller offers several benefits, including its cost-effectiveness, integrated support for WiFi networks, compact board size, and low energy consumption. They are now a focus of both academic and industrial study, and there are numerous ready-made solutions. Researchers aimed to develop an autonomous smart sprinkler system that responds to real-time soil moisture levels and incorporates Internet of Things (IoT)

technology. This system allows users to remotely control watering, offering advantages such as conserving water and preventing overwatering, especially useful in situations like impending thunderstorms. Their research showcases the potential of cost-effective IoT-enabled smart sprinklers as a replacement for traditional sprinkler systems (Chowdhury & Raghukiran, 2017).

The field of agro-industry and the environment are well-suited for implementing Internet of Things (IoT) solutions. This is because they encompass expansive regions requiring constant surveillance and management. Concurrently, IoT introduces fresh possibilities that extend beyond basic operational automation. Utilizing the gathered data to fuel machine learning algorithms for predictive purposes simplifies the process of strategic decision-making and planning for proprietors, supervisors, and policymakers (Talavera *et al.*, 2017).

The current beekeeping method at the International Islamic University Malaysia (IIUM) relies on manual inspections, which can stress stingless bee colonies and potentially lead to colony collapse disorder (CCD). To address this issue, a prototype of an intelligent apiary system using IoT technology is introduced, allowing real-time monitoring of stingless bee health through parameters like weight, temperature, and humidity. The system integrates with a mobile app and employs various sensors, including an HX711 load cell and an FSR402 force sensor, to provide valuable insights and issue alerts for emergencies (Rosli, Malik, & Ahmad, 2022). In another implementation of IoT based monitoring system, an artificial hive was created and a NodeMCU ESP8266 was implemented, along with temperature and humidity sensors, and load cell sensors. The setup monitors various parameters such as the weight of the honey compartment and temperature and humidity inside and outside the stingless beehive. The data collected from these sensors is uploaded to IoT platforms, allowing users to conveniently monitor it via their computers or mobile phones. However,

the IoT monitoring system recorded a high-temperature reading of 39.4 degrees Celsius, highlighting the urgency for developing future hives integrated with heat-resistant materials and advanced heat management systems to mitigate the risk of Colony Collapse Disorder (Ali *et al.,* 2023). Numerous IoT-based monitoring systems monitor mainly the temperature, humidity, and weight using different kinds of sensors and methods. Some systems have additional features such as a smoke-gas sensor (Yusof, Billah, Kadir, Ali, & Ahmad, 2019), and GPS for monitoring a large number of colonies (Man, Bakar, & Razak, 2019).

The authors aim to follow existing studies by creating an IoT-based monitoring system that would monitor surrounding temperature, surrounding humidity, and weight at high accuracies for reliability. Additionally, the researchers aim to improve current studies by adding a water-cooling system in an effort to control the surrounding parameters and maintain it at a desired level. The system is designed to minimize human interaction to further explore the impact of the monitoring system compared to colonies without the monitoring system.

Materials and Methods

Design and construction of the monitoring system circuit

The Internet of Things monitoring system for the stingless bee colony was composed of two circuits and both were designed using the EasyEDA software application. The first circuit was responsible for the online system. In this circuit, the microcontroller unit used was the ESP8266. The sensors and components that were integrated were the DHT22 temperature and humidity sensor, load cells which were connected in a Wheatstone bridge circuit and then to the HX711 amplifier module, and the light emitting diode (LED) light indicator for weight. Figure 1a shows the actual schematic diagram of the IoT system including the specific pin mode mentioned. The second circuit that was developed is responsible for the water valve control system.

The water valve control system works by opening the valve of a water mister to increase the surrounding humidity or decrease the surrounding temperature when it detects that the surrounding temperature and/or humidity is not at the desired level. Once the sensors detect that the parameters are back to the desired level, it closes the valve. Although the control valve is located beside the stingless bee hive, the water mister is installed on the roof of the shed of the beehive to prevent direct contact of the water with the bees. The water-cooling system is designed to be very passive so as not to disturb the stingless bees. The MCU used in this circuit was the Arduino Mega 2560 R3. The components that were integrated were the DHT22 temperature and humidity sensor, the 12V solenoid water valve, and the 5V relay. The power supply needed for the Arduino Mega and ESP8266 to operate was also taken from the 12V battery via a 12V to 5V converter. Figure 1b shows the actual schematic diagram of the circuit for the water valve control system.

Development of the program for the IoT system

The IoT monitoring system was composed of two programs. The first program was made using Arduino IoT Cloud for the online part of the system responsible for updating the real-time parameters via the user dashboard. The second program is for the water valve control system, an offline part of the monitoring system, made using an Arduino Integrated Development Environment (IDE) sketch editor. To create the program, it was essential to initially declare the variables for temperature, humidity, and weight. This step ensured that the system could recognize and process their inputs. Libraries were also included in the sketch such as the ESP8266, DHT22, and the HX711. The input data underwent calibrations before being displayed on the user dashboard. The calibration factor was achieved through trial and error basis, by measuring the parameter with a trusted measuring device such as a weighing scale or temperature humidity meter, and comparing it to the result of the system. The calibration factor was adjusted until the system and the

measuring instrument displayed the same readings. The sketch was set to a specific threshold weight of 2500 grams that will trigger the light-emitting diode (LED) indicator to light up as a signal that the colony is ready for harvest. This feature will be visible on the physical chassis via LED and on the user's dashboard by the color status in which red means not ready and green means ready for harvest. Lastly, the data was expected to show the actual reading on the end user using a dashboard via widget gauge for the temperature, humidity, weight, and color status of the LED.
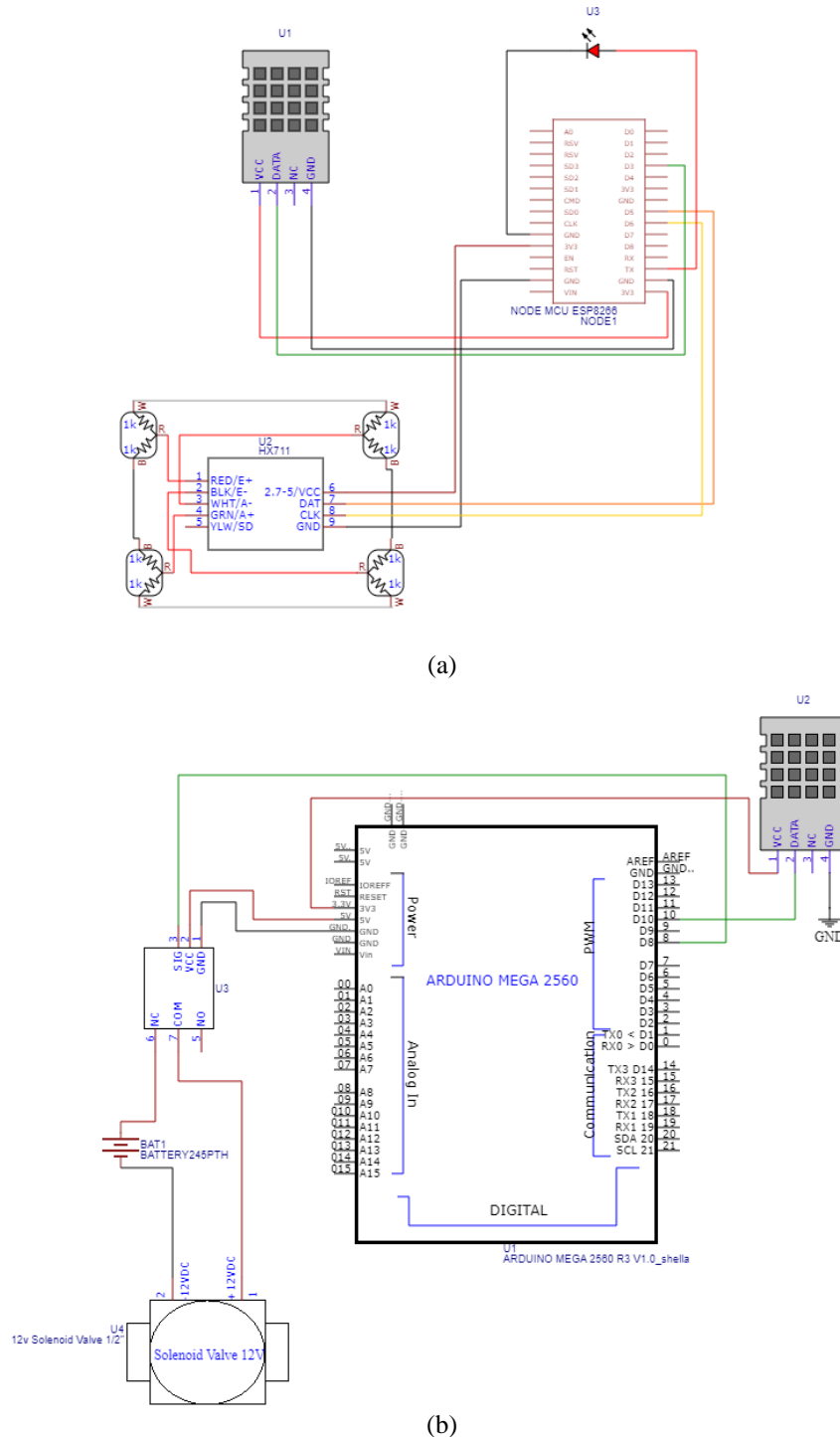

(a)

(b)

Fig. 1. Circuit diagram of the system (a) online part of the system, and (b) water valve control system

For the second program, the sketch was edited with a specific threshold temperature and humidity that will trigger the water valve to work during the hot season that reaches high temperatures of 35 degrees Celsius and higher and humidity levels at or below 50 percent.

Figure 2 illustrates the flowchart of the IoT system program from the start, which was to read the temperature, humidity, and weight values as an input. For the first condition which was the temperature, as it reaches 35 degrees Celsius and above or as the humidity reading is less than or equal to 50 percent, the solenoid valve would open, otherwise it would remain closed. The next condition was the weight, as the weight reaches the predetermined weight of the hive which in this case was 2500 grams and above, the LED will light up, otherwise it would remain off.
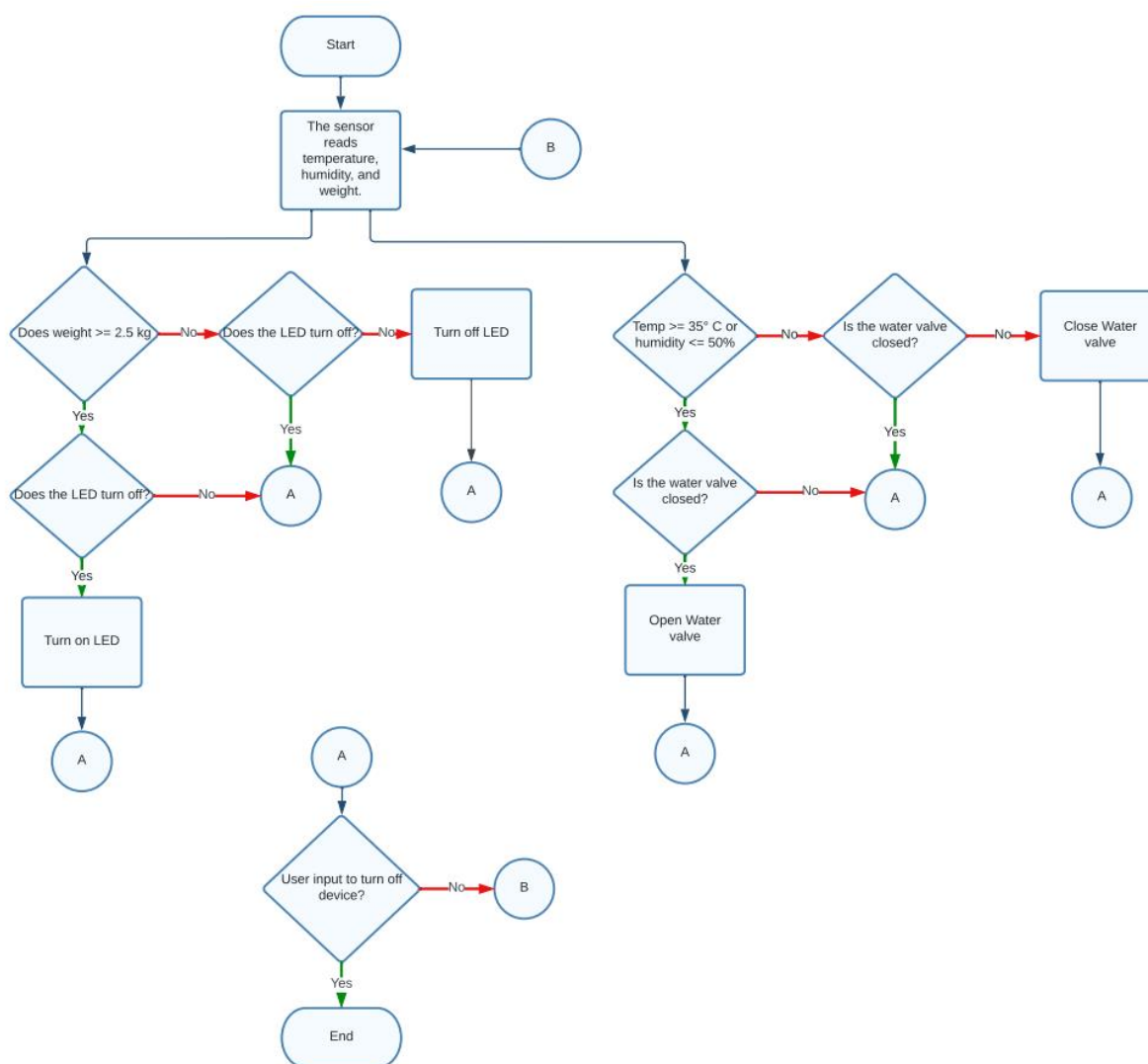
Fig. 2. Flowchart of the IoT system program

Development of the system user's dashboard

The user dashboard for the IoT System was created using the Arduino IoT cloud. The Arduino cloud service also has a user dashboard that could be modified by adding widgets that are suitable for each variable. This was made possible by assigning appropriate data types to the properties such as float for the temperature and humidity readings, integer for weight, and Boolean for

the light emitting diode (LED). After assigning these variables, it can be represented by adding suitable widgets such as gauge for temperature, humidity, and weight readings, and color status for the LED. A sticky note was also added to the dashboard with a short description of the critical temperature, and how the light indicator works to inform the beekeeper of the harvest status. The user dashboard editor is web-based and can be arranged easily on Arduino Create Agent. The mobile view is also available and can be positioned just like the desktop view.
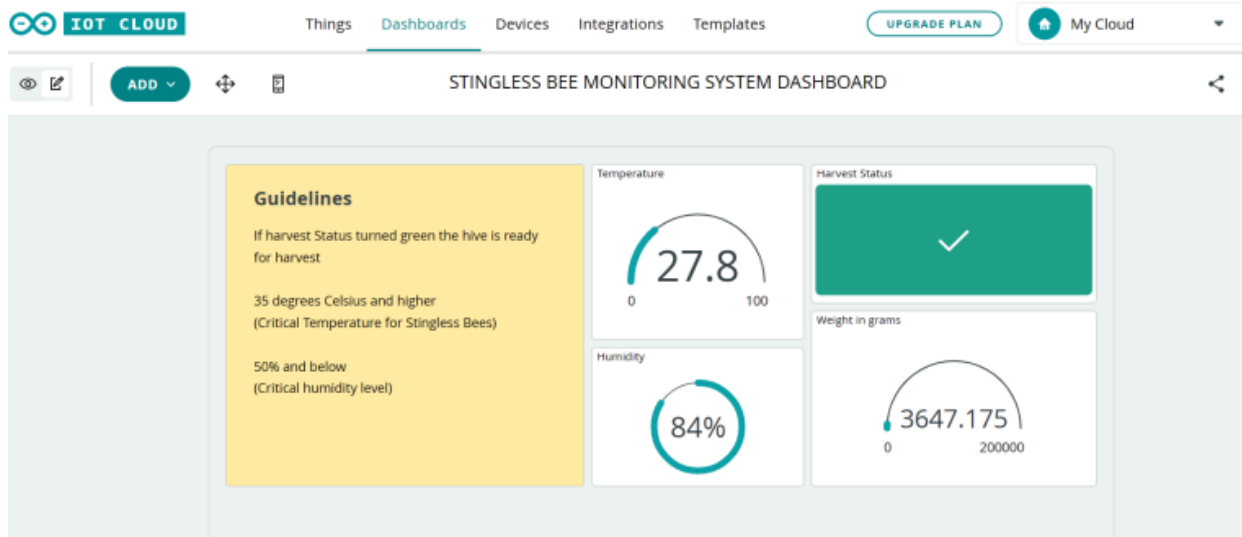

Fig. 3. Desktop view of the user dashboard

Design and construction of the chassis

The IoT system device includes a protective chassis made of 3mm plywood measuring 14.5 x 19.88 x 16 cm to safeguard its components, sensors, and microcontroller unit from potential damage by the bees. The chassis containing the system is placed beside the stingless bee hive, and it features a hinge on the top cover for easy access, holes for sensor connectors and wiring, and an additional hole for a rocker switch. Additionally, a weighing platform constructed from 5.2mm plywood, measuring 21 x 26 cm, was created with load cells installed underneath on a Wheatstone bridge circuit. The weighing platform is placed under the hive for continuous measurement of the weight. Both the chassis and weighing platform were painted with yellow wood paint after construction.

Fig. 4. Actual device installed on a beehive

Evaluating the system

Accuracy of the system parameters reading

To test the monitoring system's accuracy with its reading capabilities for the temperature, humidity, weight, and water valve control system, the device was used to take 100 sample data for each parameter and then calculated for accuracy in comparison to the readings of 100 sample data of the actual measuring instrument in the same environment the sensors were being tested. The actual measuring instrument used to calibrate and determine the accuracy of the temperature and humidity is the UT333 Mini Temperature Humidity Meter of Uni-Trend. The weights used for the calibration and accuracy test of the weight parameter are iPhone 6 (130g), 500g of rice, and 1000g of rice. The formula used for obtaining the accuracy is mean absolute percentage error.

The Mean Absolute Percentage Error (MAPE) shown in Equation 1 was particularly useful in assessing the performance of such models for obtaining data that have varying scales or magnitudes. To determine the degree of prediction inaccuracy in relation to the actual results, MAPE calculates the average percentage difference between the predicted values and the actual values. This is advantageous because quantifying errors as a percentage makes it easier to analyze accuracy more understandably.

$$MAPE = \frac{1}{n}\sum_{i=1}^{n}\left|\frac{A_i - F_i}{A_i}\right| x \ 100\%$$

$$= 1.26\%$$

(1)

Where:
- n represents the total number of data points
- A_i is the actual value of the observation
- F_i is the forecasted/predicted value for observation
- $|\cdot|$ denotes the absolute value

To test the water valve control system's accuracy for working performance, the device was taken out of the shed for the authors to blow hot air at the sensors and simulate 50 samples of 35 degrees and above. The authors also conducted further analysis by evaluating the response of the water valve control system with an additional 50 temperature samples at or below 34 degrees Celsius. A confusion matrix was utilized to calculate the accuracy of the system when it comes to the water valve control system. A confusion matrix is a tabular representation used to assess the performance of a classification model. It helps in understanding the accuracy. The matrix displays the actual and predicted classifications of a dataset, providing insights into the true positives (TP), true negatives (TN), false positives (FP), and false negatives (FN). The confusion matrix table displays a summary of the classifiers' actual versus projected results.

A confusion matrix resides in its capacity to offer a thorough and in-depth evaluation of a classification model's performance. When evaluating the correctness of models in situations involving numerous classes or categories, a confusion matrix is very helpful.

Fig. 5. Confusion matrix

Accuracy is calculated by taking the total of all entries in the confusion matrix as the denominator and using the sum of the true positive and true negative values as the numerator. Equation 2 shows the formula used to obtain the accuracy of the water valve control system reaction to changes in temperature and humidity.

$$Accuracy = \frac{TP + TN}{TP + TN + FP + FN} \quad (2)$$

Hive health comparison

A pair of typical beehives was chosen for the comparison. One of these beehives had a monitoring system installed, but the other one was left without any such modernization. This data-gathering technique, which was based on a week-specific indicator of honey harvest readiness, made it easier to focus on the effect of the monitoring system on the hive's internal environment. Every afternoon, the researchers manually weighed the unmonitored hive using a weighing scale while also gathering the weight of the monitored hive through the system. The unmonitored beehive was manually cooled as part of the manual monitoring process by transporting it to a cooler location during peak noon temperature. The monitored hive's use of modern sensors allowed for the collection of a substantial dataset and a thorough analysis of how the monitoring system affected and possibly improved the conditions favorable to productive honeybee activity. As a result, this analytical approach enabled a nuanced investigation of the advantages of integrating monitoring systems into beehives and their potential contribution to improving hive production and health.

Figure 6 shows the manual weight data collection for the IoT-based and non-IoT-based monitoring of beehives. It also shows the bee shed housing the beehive used for non-IoT-based monitoring.

<table>
<tr><td>(a)</td><td>(b)</td></tr>
</table>

Fig. 6. Beehive weight data gathering (a) w/o IoT system, and (b) w/ IoT system

To calculate the percentage difference between the health of the monitored beehive to the other without the monitoring system, the percent increase of the monitored hive was subtracted from the percent increase of the unmonitored hive using the formula shown in Equation 3. On the other hand, the percent increase formula used for obtaining the percent increase in both hives is presented in Equation 4.

$$PercentIncrease of Monitored Hive - Percent Increase of Normal Hive$$
$$= Percentage Difference \tag{3}$$

$$PercentIncrease = \frac{FinalValue - InitialValue}{InitialValue} x\ 100\% \tag{4}$$

Results and Discussion

System Evaluation

Parameter Accuracies

For the accuracy percentage results, which were obtained using mean absolute percentage error for the parameter readings, the temperature's accuracywas 1.26 percent. This means that the temperature accuracy was

98.74 percent in comparison to the reading of the actual temperature measured by a temperature humidity meter in the same environment. This accuracy percentage result tells that the system obtained its objective of providing an acceptable temperature reading to be used by the beekeeper for remote monitoring as shown in Figure 7.
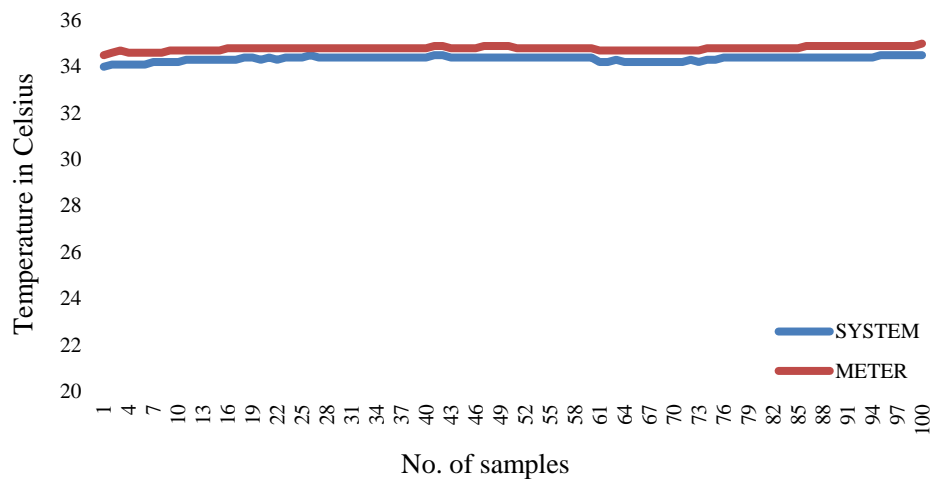

Fig. 7. Temperature reading comparison of the system
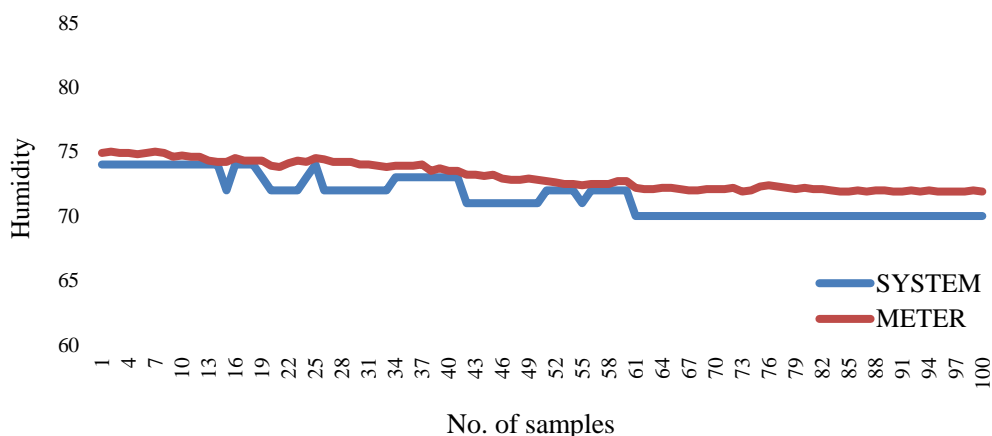

Fig. 8. Humidity reading comparison of the system

The second parameter was the surrounding humidity, which has a mean absolute

percentage of 2.11 percent and an accuracy of 97.89 percent (Figure 8). This accuracy result concludes that the humidity reading could also be reliable data that could be helpful for the beekeepers in monitoring the health and optimal humidity of the stingless bee's colony.

The weight parameter was tested using the weighing platform of the monitoring system to weigh three known weights: 130g, 500g, and 1000g. These weights were used to make sure that the monitoring system could weigh light, medium, and heavy objects. The test resulted in 95.92 percent accuracy with a mean

absolute percentage error of 4.08 percent. This accuracy result concludes that the weighing platform could accurately provide the weight parameter that the beekeepers could use as they remotely monitor the bee colony. This weight parameter could tell several facts about the health of the colony. As the weight increases day by day, the beekeeper canconclude that the hive is in good condition which means that the stingless bees were continuously growing and collecting honey and pollen.
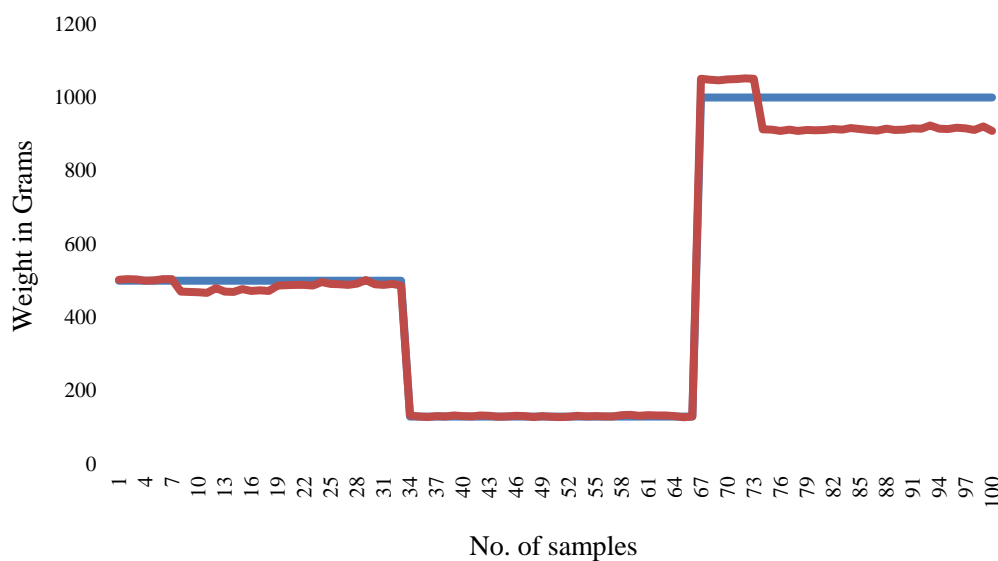

Fig. 9. Weight reading comparison of the system

The water valve control system had 93.46 percent accuracy using the confusion matrix. The true positive (TP) was 43, the true negative (TN) was 50, the false positive (FP) was 0, and the false negative (FN) was 7. The water valve accurately reacted to the 43 true positives by turning on 50 times as the temperature reached 35 degrees and above. There was no recorded false positive from the water valve testing and evaluation. During the testing, the authors found that the false negative results were caused by the direct blowing of hot air in the sensors which caused the DHT222 to fail a few times.

The accuracy percentages were acceptable and efficient in comparison to manually checking the temperature, humidity, and

weight of the hive which causes disturbances to the bees affecting their behavior that leads to several issues specifically the colony collapse disorder. Also, the cooling system was more efficient than the traditional way, which was manually lifting the beehive and moving it to another area with optimal or lower temperature.

Table 1 shows the system accuracy for parameters reading in temperature, humidity, weight, and water valve control system. The results indicate that the objectives were successfully met, achieving high accuracy percentages that the system can offer to beekeepers for effective monitoring.

Table 1- Summary of accuracy results of the system

Parameter	System accuracy (%)
Surrounding temperature	98.74
Surrounding humidity	97.89
Colony's weight	95.92
Water valve control	93.46

Table 2 presents a concise summary of the manually tallied measurements for true positives, true negatives, false positives, and false negatives, reflecting the performance of the water valve in response to temperature variations. TP corresponds to the value of temperature 35 degrees Celsius and above, TN corresponds to the value of temperature 34 degrees and below, FN for the false negative, and FP for the false positive. It shows that the water control system functioned well and was able to achieve its objective which was to maintain the hive's temperature within optimal and safe limits.

Table 2- Performance of valve control TP, TN, FP, and FN of the system

	System Valve Off	System Valve On
Actual Off	TN = 50	FP = 0
Actual On	FN = 7	TP = 43

Hive Health Comparison

The monitored hive consistently exhibited more stable internal conditions, with narrower fluctuations in temperature and humidity compared to the normal hive. Additionally, the Monitored Hive provided real-time data on the colony's weight changes, allowing for early detection of potential issues such as swarming or food shortages.

The monitored hive produced a 3.414 percent higher weight gain compared to the normal hive. This difference in weight gain can be attributed to the Monitored Hive's ability to maintain optimal hive conditions, thereby promoting better foraging efficiency and colony health. Also, there was no need for unnecessary inspections thus promoting continued production and less stress for the stingless bees. The weight values provided by the system were a useful reflection of the beehive's health, which was fundamental in beekeeping. The weight provided by the system reflects whether the bee had continuous production by accumulating an expected daily weight. On the other hand, decreasing weight could alarm the beekeeper and he/she could immediately respond to investigate and solve the problem effectively. Manual checking of the beehive's internal condition leads to stress in the stingless bees' behavior and could cause colony collapse and other problems such as fermentation of honey, pest invasion, and low honey production.

Table 3 shows the daily weight data comparison of the bee colony with the IoT monitoring system in comparison to the beehive without the system. The total weight gain for the whole week is also included in the last row.

Table 3- Daily weight comparison of the beehives

Date	Beehive With IoT System Weight In (g)	Beehive W/O IoT System Weight In (g)
August 16, 2023	3433.882	3417.691
August 17, 2023	3699.107	3644.327
August 18, 2023	3913.446	3838.196
August 19, 2023	4157.259	3961.348
August 22, 2023	4381.764	4141.234
August 23, 2023	4509.876	4371.928
Total weight gained	1075.94	954.237

The results of this study highlight the benefits of integrating monitoring systems into

beekeeping practices. The Monitored Hive's ability to maintain stable internal conditions contributed to its higher weight gain. By offering real-time insights, monitoring systems empower beekeepers to intervene promptly in response to changes in hive dynamics, potentially preventing issues that could otherwise negatively impact hive health and productivity.

Cost Computation

Table 4 presents a detailed breakdown of the cost computation for the IoT System. It includes quantity, description, unit cost, and the total cost per material. The overall cost amounted to P10, 004 (Philippine Peso).

Table 4- Cost computation of the IoT system

Quantity	Description	Unit cost (PHP)	Total cost (PHP)
1	ESP8266MOD	300.00	300.00
1	NodeMCU Arduino Mega 2560 R3	500.00	500.00
5	Arduino IoT Cloud Subscription Plan	400.00	2000.00
1	HX711 Load Cell	250.00	250.00
2	DHT22	250.00	500.00
1	Tem and Hum 12V Battery	700.00	700.00
1	Rocker Switch	9.00	9.00
1	5V relay	50.00	50.00
1	12V Solenoid Valve	300.00	300.00
1	LED	5.00	5.00
4	Female hose connectors	70.00	280.00
3	Male connectors	70.00	210.00
2	Water hose (10m)	300.00	600.00
1	12V to 5V DC adapter	300.00	300.00
1	Paint/brush	300.00	300.00
1	Wooden Chassis	500.00	500.00
	Miscellaneous	3 200.00	3 200.00
Total			10 004.00

Conclusion

The study was able to accomplish high-accuracy readings which were acceptable and can be used by the beekeepers. Using the mean absolute percentage error subtracted from 100 for each parameter, accuracy values of 98.74 percent for the surrounding temperature, 97.89 percent for the surrounding humidity, 95.92 percent for the weight scale, and 93 percent for the water valve control system were obtained. These accuracy percentage results mean that the system was reliable in providing valuable information to the beekeeper through the sensors that were integrated. The weight difference was also higher at 3.414 percent in the hive with the IoT system in comparison to the weight of the stingless bee colony without the IoT system. The automatic water valve control also helped in optimizing the temperature and humidity, specifically during the hot season. The total cost of the IoT monitoring system amounted to P10,004 (Philippine Peso). While this was only used on one beehive colony, further expansion of the monitoring system will be more cost-effective, as some components have the capabilities for expansion.

In conclusion, the IoT monitoring system for stingless bee colonies was a success. It demonstrated the capability to deliver satisfactory parameter accuracy while contributing to the overall health of the hive. Utilizing the monitoring system for the remote oversight of stingless bee colonies is a highly effective strategy for preventing potential issues. This approach empowers beekeepers to take prompt action in response to any changes in the colony's environment. Using the IoT monitoring system could also prevent colony collapse disorder by decreasing stress on the

bees caused by human intervention and could help in optimizing the temperature as it reaches the critical level to prevent deaths of the stingless bees' larvae.

The authors recommend that in future studies, the use of more compatible Arduino IoT Cloud boards would be better to fully maximize the programming and avoid errors and incompatibilities. It is advisable to use boards that support over-the-air code updates to reduce the necessity of disturbing the stingless bees whenever issues arise. The authors suggest adding a messaging feature to alert beekeepers about their colony's health, eliminating the need to frequently open the app. The implementation of a camera on the monitoring system is also recommended to provide more data to the end user and track the health of the colony. The authors recommend an alternative source of power supply due to the fact the available source of power is limited, especially in secluded and remotely located areas. Lastly, the authors also recommend longer periods of actual testing to further understand the reliability and effectiveness of the system. This would also help in identifying if the monitoring system, although non-moving, affects the colonies itself. Longer periods of observation would also provide a way for an in-depth economic analysis of the system.

Declaration of competing interests

The authors declare that they have no conflict of interest.

Authors Contribution

R. J. Arendela: The author constructed the circuit for IOT Stingless Bee monitoring system. He also tested and evaluated the developed system.

R. A. Ebora: The author constructed the circuit for IOT Stingless Bee monitoring system. He also tested and evaluated the developed system.

E. R. Arboleda: The author contributed the following: conceptualization of the research idea, supervision in the conduct of the study, provided technical advice as well as devised the methodology for this study.

J. L. M. Ramos: The author performed the writing, review and editing of the manuscript in a publishable format. He also contributed in data acquisition, data pre and post processing, statistical analysis, numerical/computer simulation, validation and visualization

M. Bono: Provided technical advice in the behavior of the sting less bees and how the process of taking care of them can be automated.

D. Dimero: Provided technical advice in the behavior of the sting less bees and how the process of taking care of them can be automated.

References

1. Afrin, S., Haneefa, S. M., Fernandez-Cabezudo, M. J., Giampieri, F., Al-Ramadi, B. K., & Battino, M. (2019). Therapeutic and preventive properties of honey and its bioactive compounds in cancer: an evidence-based review. *Nutrition Research Reviews*, *33*(1), 50-76. https://doi.org/10.1017/s0954422419000192
2. Alebachew, G. W. (2018). Economic Value of Pollination Service of Agricultural Crops in Ethiopia: Biological pollinators. *Journal of Apicultural Science*, *62*(2), 265-273. https://doi.org/10.2478/jas-2018-0024
3. Ali, N. M. a. a. C., Ilias, N. B., Rahim, N. N. A., Shukor, N. S. a. A., Adom, N. a. H., Saad, N. M. A., & Hassan, N. M. F. A. (2023). Development of Artificial Stingless Bee Hive Monitoring using IoT System on Developing Colony. *Journal of Advanced Research in Applied Sciences and Engineering Technology*, *33*(2), 254-268. https://doi.org/10.37934/araset.33.2.254268
4. Biesmeijer, J. C., Hartfelder, K., & Imperatriz-Fonseca, V. L. (2006). Stingless bees: biology and management. *Apidologie*, *37*(2), 121-123. https://doi.org/10.1051/apido:2006020
5. Chan-Rodríguez, D., Ramón-Sierra, J., Lope-Ayora, J., Sauri-Duch, E., Cuevas-Glory, L., &

Ortiz-Vázquez, E. (2012). Antibacterial properties of honey produced by Melipona beecheii and Apis mellifera against foodborn microorganisms. *Food Science and Biotechnology*, *21*(3), 905-909. https://doi.org/10.1007/s10068-012-0118-x

6. Chowdhury, B. S., & Raghukiran, N. (2017). Autonomous Sprinkler System with Internet of Things. 12, 5430-5432.

7. Edwards-Murphy, F., Magno, M., Frost, A., Long, A., Corbett, N., & Popovici, E. (2013). Demo Abstract: SmartSync; When Toys meet wireless sensor Networks. In *Lecture notes in electrical engineering* (pp. 91–96). https://doi.org/10.1007/978-3-319-03071-5_11

8. Fitzgerald, D. W., Murphy, F. E., Wright, W. M. D., Whelan, P. M., & Popovici, E. M. (2015). Design and development of a smart weighing scale for beehive monitoring. *2015 26th Irish Signals and Systems Conference (ISSC)*. https://doi.org/10.1109/issc.2015.7163763

9. Harun, A., Zaaba, S., Kamarudin, L. M., Zakaria, A., Farook, R. S. M., Ndzi, D. L., & Shakaff, A. Y. M. (2015). Stingless Bee Colony Health Sensing Through Integrated Wireless System. *Journal Teknologi*, *77*(28). https://doi.org/10.11113/jt.v77.6798

10. *Honeybees vs stingless bees - The real difference* (2020) *mybeeline*. https://doi.org/10.1007/978-3-642-72649-1_2

11. Jalil, M. a. A., Kasmuri, A. R., & Hadi, H. (2017). Stingless Bee Honey, The Natural Wound Healer: a review. *Skin Pharmacology and Physiology*, *30*(2), 66-75. https://doi.org/10.1159/000458416

12. Johannsen, C., Senger, D., & Kluss, T. (2020). A DIY sensor kit, Gaussian processes and a multi-agent system fused into a smart beekeeping assistant. *2020 16th International Conference on Intelligent Environments (IE)*, 92-99. https://doi.org/10.1109/ie49459.2020.9154974

13. Kiros, W., & Tsegay, T. (2017). Honey-bee production practices and hive technology preferences in Jimma and Illubabor Zone of Oromiya Regional State, Ethiopia. *Acta Universitatis Sapientiae Agriculture and Environment*, *9*(1), 31-43. https://doi.org/10.1515/ausae-2017-0003

14. Kulkarni, P., & Ozturk, Y. (2010). mPHASiS: Mobile patient healthcare and sensor information system. *Journal of Network and Computer Applications*, *34*(1), 402-417. https://doi.org/10.1016/j.jnca.2010.03.030

15. Kwapong, P., Aidoo, K., Combey, R., & Karikari, A. (2010). *Singless Bees Importance, Management and Utilisation* (1st ed.), Unimax Macmillan Ltd. http://zoologie.umons.ac.be/hymenoptera/biblio/01500/KwapongStinglessbeebookpdf.pdf

16. Magno, M., Tombari, F., Brunelli, D., Di Stefano, L., & Benini, L. (2009). Multimodal Abandoned/Removed Object detection for low power video surveillance systems. *2009 Sixth IEEE International Conference on Advanced Video and Signal Based Surveillance*, 188-193. https://doi.org/10.1109/avss.2009.72

17. Man, M., Bakar, W. a. W. A., & Razak, M. a. B. B. A. (2019). An Intelligent Stingless Bee System with Embedded IoT Technology. *International Journal of Recent Technology and Engineering (IJRTE)*, *8*(3), 264-269. https://doi.org/10.35940/ijrte.c4124.098319

18. Ochoa, I. Z., Gutierrez, S., & Rodriguez, F. (2019). Internet of Things: Low cost monitoring BeeHive system using wireless sensor network. *2019 IEEE International Conference on Engineering Veracruz (ICEV)*. https://doi.org/10.1109/icev.2019.8920622

19. Özbalci, B., Boyaci, İ. H., Topcu, A., Kadılar, C., & Tamer, U. (2012). Rapid analysis of sugars in honey by processing Raman spectrum using chemometric methods and artificial neural networks. *Food Chemistry*, *136*(3-4), 1444-1452. https://doi.org/10.1016/j.foodchem.2012.09.064

20. Rosli, H. A., Malik, N. A., & Ahmad, Y. A. (2022). IoT based monitoring system for stingless bees colony in IIUM. *Journal of Physics Conference Series*, *2312*(1), 012088. https://doi.org/10.1088/1742-6596/2312/1/012088

21. Roubik, D. W. (2014). Stingless bees (Kiwot) in the Philippines Pollination by Honeybees in the Philippines. http://beephilippines.info/stingless-bees/

22. Sforcin, J. M. (2016). Biological properties and therapeutic applications of propolis. *Phytotherapy Research*, *30*(6), 894-905. https://doi.org/10.1002/ptr.5605

23. Talavera, J. M., Tobón, L. E., Gómez, J. A., Culman, M. A., Aranda, J. M., Parra, D. T., Quiroz, L. A., Hoyos, A., & Garreta, L. E. (2017). Review of IoT applications in agro-industrial and environmental fields. *Computers and Electronics in Agriculture*, *142*, 283-297. https://doi.org/10.1016/j.compag.2017.09.015

24. Tesfa, A., & Kebede, A. (2013). Assessment of Current Beekeeping Management Practice and Honey Bee Floras of Western Amhara, Ethiopia', *Research Gate.*

25. Yaacob, M., Rajab, N., Shahar, S., & Sharif, R. (2017). Stingless bee honey and its potential value: a systematic review. *Food Research*, *2*(2), 124-133. https://doi.org/10.26656/fr.2017.2(2).212

26. Yunus, M. a. M. (2017). Internet of Things (IoT) application in meliponiculture. *International Journal of Integrated Engineering*, *9*(4). https://penerbit.uthm.edu.my/ojs/index.php/ijie/article/download/2016/1222

27. Yusof, Z. M., Billah, M. M., Kadir, K., Ali, A. M. M., & Ahmad, I. (2019). Improvement of honey production: A smart honey bee health monitoring system. *2019 IEEE 6th International Conference on Smart Instrumentation, Measurement and Applications (ICSIMA 2019)*, 1-5. https://doi.org/10.1109/icsima47653.2019.9057336

28. Zabasta, A., Zhiravetska, A., Kunicina, N., & Kondratjevs, K. (2019). Technical implementation of IoT concept for bee colony Monitoring. *2022 11ᵗʰ Mediterranean Conference on Embedded Computing (MECO)*, 1-4. https://doi.org/10.1109/meco.2019.8760180

سیستم نظارت بر کلونی زنبورهای بدون نیش با کمک اینترنت اشیا

راس جان آرندلا[۱]، رابرت آلن ابورا[۱]، ادوین آربولدا [iD] [۱، ۲]، جوزف لوئیس مایکل راموس [iD] [۱]*، میشل بونو[۲]، دیکسون دیمرو[۲]

چکیده

هدف از توسعه سیستم نظارت بر کلونی‌های زنبورهای بدون نیش با اینترنت اشیا، ارائه اطلاعات در لحظه درباره دمـا، رطوبـت و وزن کنـدو بـرای مقابله با اختلال فروپاشی کلونی (CCD) ناشی از مداخله انسان در زنبورداری است. همچنین بهبود روش‌های فعلی نظارت بر زنبورها و نظارت مـوثرتر و کارآمدتر از دیگر اهداف این سیستم هستند. سیستم نظارتی همچنین دارای یک سیستم خنک‌کننده آب برای حفظ دمای مطلوب زنبورهای بدون نیش (*Tetragonula Biroi*) است. این سیستم همچنین دارای داشبورد کاربر برای نظارت از راه دور بوده و هنگام فرارسیدن زمـان برداشـت بـه زنبـوردار اطلاع می‌دهد. این دستگاه بر روی میکروکنترلر ESP8266MOD ساخته شده و از Arduino Mega 2560 R3 برای سیستم کنتـرل دریچـه آب استفاده شده است. داده‌های دما و رطوبت با سنسور DHT22 و وزن کندو با لودسل‌های متصل به آمپلیفایر HX711 جمـع‌آوری شـدند. بـرای تسـت سیستم، داده‌های به‌دست‌آمده از سیستم با اندازه‌گیری دستی به مدت دو ماه و با استفاده از MAPE مقایسه شدند و در نتیجه، دقت سیسـتم بـه‌ترتیب ۹۸/۷۴ و ۹۷/۸۹ درصد برای دما و رطوبت محیط اندازه‌گیری شد. همچنین دقت ۹۵/۹۲ درصد برای وزن کندو و ۹۳ درصد برای سیستم کنترل شیر آب به‌دست آمد. کندوهای مجهز به سیستم نظارت اینترنت اشیا ۳/۴۱۴ درصد وزن بیشتری نسبت به کندوهای عادی بهدسـت آوردنـد کـه نشـان‌دهنده‌ی موفقیت پژوهش در دستیابی به اهداف خود می‌باشد.

واژه‌های کلیدی: پارامترهای محیطی، پایش از راه دور، سیستم نظارت اینترنت اشیا، کلونی زنبورهای بدون نیش، وزن کندو

۱- گروه کامپیوتر، الکترونیک و مهندسی برق، دانشکده مهندسی و فناوری اطلاعات، دانشگاه ایالتی کاویت، ایندانگ (پردیس اصلی)، ایندانگ، کاویت، فیلیپین

۲- مرکز تحقیقات، نوآوری، تجارت و توسعه زنبور عسل (BRITE)، دانشگاه ایالتی کاویت، ایندانگ، کاویت، فیلیپین

(*- نویسنده مسئول: Email: josephlouismichael.ramos@cvsu.edu.ph)

Diagnosis and Classification of Two Common Potato Leaf Diseases (Early Blight and Late Blight) Using Image Processing and Machine Learning

H. Koroshi Talab[1], D. Mohammadzamani (iD)**[1*], M. Gholami Parashkoohi** (iD)**[2]**

1- Department of Biosystems Engineering, Takestan Branch, Islamic Azad University, Takestan, Iran
2- Department of Mechanical Engineering, Shahr-e-Qods Branch, Islamic Azad University, Tehran, Iran
(*- Corresponding Author Email: dr.dmzamani@iau.ac.ir)

Abstract

Diagnosing plant diseases is an important part of crop management and can significantly affect the quantity and quality of production. Traditional methods of visual assessment by human observers are time-consuming, costly, and error-prone, making accurate diagnosis and differentiation between various diseases difficult. Advances in agriculture have enabled the use of non-destructive machine vision systems for plant disease detection, and color imaging sensors have demonstrated great potential in this field. This study presents a framework for diagnosing early blight and late blight diseases in potatoes using a combination of Relief feature selection algorithms and Random Forest classification, along with color, texture, and shape features in three color spaces: RGB, HSV, and CIELAB (Lab*). The results indicated that the diagnostic accuracy for the early blight and late blight disease groups, as well as the healthy leaf group, were 94.71%, 95%, and 95.2%, respectively. The overall accuracy for disease classification was 95.99%. Additionally, the diagnostic accuracy for the early blight and late blight disease groups, along with the healthy leaf group, was 91.07%, 98.36%, and 98.93%, respectively, with an overall classification accuracy of 96.12%. After separating the diseased area from the healthy part of the leaf, a total of 150 features were extracted, including 45 color, 99 textural, and 6 shape features. The most effective features for disease detection were identified using a combination of all three feature sets. This study demonstrated that integrating these three sets of features can lead to a more accurate classification of potato leaves and provide valuable insights into the diagnosis and classification of potato diseases. This approach can help farmers and other plant disease specialists to accurately diagnose and manage potato diseases, and ultimately lead to an increase in product quality and yield.

Keywords: Artificial intelligence, Disease diagnosis, Feature extraction, Feature selection, Potato diseases

Introduction

Potatoes are one of the products that occupy a wide area of production in Iran. As a staple food, potato has its priority in cultivation all over the world. However, several diseases such as late blight and early potato blight

affect the production of this product and destroy agricultural development. Therefore, diagnosing the disease in the early stages can be a better solution for successful crop cultivation (Abdulridha, Ampatzidis, Kakarla, & Roberts, 2019). The early blight and late blight, as the most destructive foliage diseases of potato crops, could cause major losses in most potato-growing areas in the world. On potato leaves, late blight appears as light green or olive green areas that rapidly turn brownish-

black, water-soaked, and oily. Likewise, early blight is round or irregular, which shows dark brown or black spots. Overall, early blight and late blight can occur in all stages of potato growth (Da Silva Silveira Duarte, Zambolim, Machado, Pereira Porto, & Rodrigues, 2019). To control and prevent diseases effectively and timely, it is of great significance to identify and detect the diseases of potato leaves.

In general, the traditional diagnosis of crop diseases is performed by experienced experts, but manual diagnosis is inefficient, subjective, and unsuitable for large regional scenarios. Traditional diagnostic techniques of crop diseases tend to include polymerase chain reaction (PCR), fluorescence in situ hybridization (FISH), enzyme-linked immunosorbent assay (ELISA), thermal imaging, and hyperspectral imaging (Fang & Ramasamy, 2015; Madufor, Perold, & Opara, 2018; Xie, Shao, Li, & He, 2015). In real-life production, farmers need simple, rapid, and accurate ways to identify potato diseases. Therefore, it is crucial to develop a fast, low-cost, time-saving, and labor-saving automatic identification system for potato diseases. In terms of image analysis, the application of machine learning techniques has shown great potential in the effective monitoring and identification of plant diseases. The visible patterns on the leaves of plants can be captured and processed through various image processing techniques to obtain specific patterns related to a particular disease. By comparing the obtained features or patterns with historical data, it is possible to classify different diseases. Machine learning techniques such as the combination of image processing and machine learning are highly effective in identifying and classifying diseases.

One of the potential advantages of machine learning is its ability to identify various diseases such as bacterial, fungal, and viral diseases. Intelligent diagnostic systems based on machine learning algorithms can automatically detect diseases in plants based on symptoms observed in their leaves. This technique can assist in monitoring large farms

and diagnosing diseases earlier to minimize the adverse effects caused by such diseases (Barbedo, 2018).

Machine learning models, however, have a limitation in that a large and high-quality data set is required for model training and testing. Additionally, most of the existing machine learning and deep learning methods are unable to determine the most effective features extracted from images of plants for disease classification. Deep learning models, in particular, are complex and their functioning is not fully understood, which makes it difficult to determine why they perform better using different methods or models. Another challenge in the diagnosis of plant diseases is identifying and classifying diseases with similar symptoms, especially in the early stages of development. To overcome these challenges, it's crucial to develop a comprehensive system that can effectively extract features for accurate diagnosis and classification of diseases, particularly when comparing diseases and disorders with similar symptoms.

In recent years, significant research has been conducted in the field of machine vision in agriculture, particularly for fruit ripeness classification and quality ratings (Lopez, Aguilera, & Cobos, 2009; Mohamadzamani, Sajadian, & Javidan, 2020). This research has extended to include a range of sensors, such as color, multispectral, and hyperspectral cameras. Typically, the sensor used for these applications records information in the visible spectral range. This indicates the extent to which machine vision technology has progressed in the agriculture industry, with a focus on improving the effectiveness of farmers' decision-making processes.

Xiao and Liu, (2017) presented an adaptive feature combination and rapid diagnosis method for potato diseases. As proved by the detection test of three potato diseases, the average detection rate of the modified adaptive feature fusion method is at least 1.8% higher than the traditional adaptive method. Meanwhile, the average detection rate of the detection method was 92.5%. Fan and Li,

(2019) proposed a keypoint-based detection method that can quickly detect disease in target regions by combining the color and Textural Features. Although this method detects 10 types of potato diseases with high speed and accuracy, it does not perform well for diagnosis in complex environments. The detection accuracy in this method was 80%. Yang, Feng, Zhang, Sun, and Wang (2020) proposed a potato leaf disease detection method based on the combination of deep CNN and composite feature dictionary, adopted the faster R-CNN to detect disease areas, and built a composite feature dictionary through image feature extraction. The disease diagnosis model was trained by support vector machine and its average diagnosis accuracy can reach 84.16%. However, the background of the image was relatively simple. In research by Singh and Kaur (2021), an automatic system for potato leaf image disease detection was developed, and it was investigated using SVM algorithm on two well-known potato leaf diseases such as late blight and early blight. The proposed model achieved 91% accuracy.

Automatic plant disease detection system uses various techniques including: image acquisition, processing, segmentation, feature extraction, and machine learning to achieve quick and accurate diagnosis of plant diseases for farmers. The implementation of this automatic system eliminates the need for manual inspection, reducing the time and effort required for crop disease detection. As a result, farmers can focus on more critical tasks, such as ensuring optimal plant health, yields, and productivity.

This study presents a framework for potato leaf disease diagnosis. For this purpose, a dataset was compiled from farms in Qazvin province, Iran, consisting of one class of healthy potato leaves and two classes of diseased leaves, specifically late blight and early blight. A total of 300 images were prepared, with 100 images for each group. Subsequently, a combination of the Relief feature selection algorithm and the Random Forest classification algorithm was developed to diagnose and classify these diseases while also identifying the best and most effective features for recognizing common potato leaf diseases.

Materials and Methods

Machine learning has played a significant role in automating various systems, particularly in the field of agriculture, specifically in the classification and detection of plant diseases based on images. The proposed framework includes various steps, including system requirements, data collection, image segmentation, feature extraction, and classification. Each step is designed to achieve the ultimate goal of diagnosing and classifying images into different categories of diseases using the advantages of machine learning methods. The discussion will be organized to cover each of these steps, including their details and importance in achieving the desired results. Figure 1 shows the research process.

Creating the database of images

The creation of accurate and reliable image classifiers for plant disease detection is a crucial and challenging task. A large validated dataset of diseased and healthy plant images is highly necessary to develop effective classifiers. However, the lack of such a dataset has been one of the key barriers to achieving this goal. Previously, researchers had to create their own image datasets, which was a time-consuming and labor-intensive process. In this study, a data set of images of infected leaves including late blight and early blight will be prepared and analyzed by a Samsung mobile phone model (model A32) equipped with a 64 megapixel camera and in an environment with natural light. The images of the studied diseases are shown in Figure 2. The obtained dataset includes 300 leaves of potato plants, which were classified into 3 categories. The image database contains 100 healthy leaves and 200 diseased leaves. The image database was divided into two training databases and test databases. The training database contains 80% of the image database, i.e. 240 images, and the test database contains the remaining 20% of the image database, i.e. 60 images. The

proposed framework was implemented on Windows 10 operating system with Intel®Core™ i3-8130U processor @ 2.20 GHz -2.21 GHz with 8 GB RAM. The proposed algorithm has been implemented in order to diagnose and classify potato diseases using Matlab2018 software.
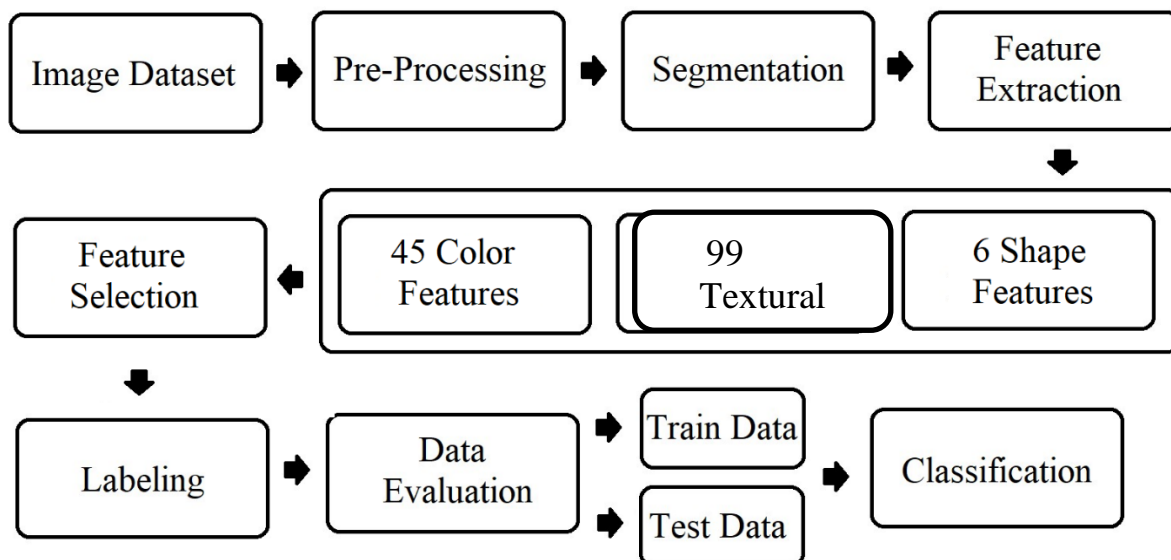

Fig. 1. The process of the proposed method to diagnose and classify potato diseases

Disease Name	Late Blight	Early Blight	Healthy
Leaf Image			
Symptoms	Early symptoms of late blight are small, light to dark green, circular to irregular spots soaked in water.	Symptoms of premature burn occur in the fruit, stem and foliage of potato and the stem, foliage and tubers of potato.	-

Fig. 2. Pictures of diseases along with their symptoms

Preprocessing

K-means clustering is used to classify objects based on a set of features into a total of K classes. The objects are classified by minimizing the sum of squares of the distance between the object and the corresponding cluster. The K-means clustering algorithm can be described by four steps (Mohammadi & Asefpour Vakilian, 2023): (1) picking the center of the K-th cluster either randomly or based on some heuristics; (2) assigning each pixel to a cluster that minimizes the distance between the pixel and the cluster center; (3) computing the cluster centers by averaging all the pixels in the cluster; and finally, (4) repeating steps 2 and 3 until convergence is obtained.

Generally, the selection of the value of K and also the selection of Region of Interest (ROI) are made manually, depending on the

skill of the user. Sometimes, ROI may not be selected correctly by the user. This means that for each number of images in the database, the ROI number should be manually selected to determine the desired area of the disease. This is very time-consuming and error-prone. Therefore, automatic clustering can be useful for the reliable diagnosis of the disease area in the plant leaves. In this study, *K*-means clustering was used to automatically separate the disease symptoms from the healthy areas of a leaf. Therefore, the ROI in the *K*-means clustering (cluster number indicating the

disease), which had to be selected by the user in other methods, was done automatically by thresholding between the color of the disease area (i.e., symptoms) and the color of the healthy leaf area. For this purpose, in the leaf image, the pixels in which the red color is less than the blue and green values were masked. After that step, in the rest of the image, only the diseased area of the leaf will remain. Figure 3 shows the steps of preparing and separating the image from the background and detecting the disease area of potato leaves.
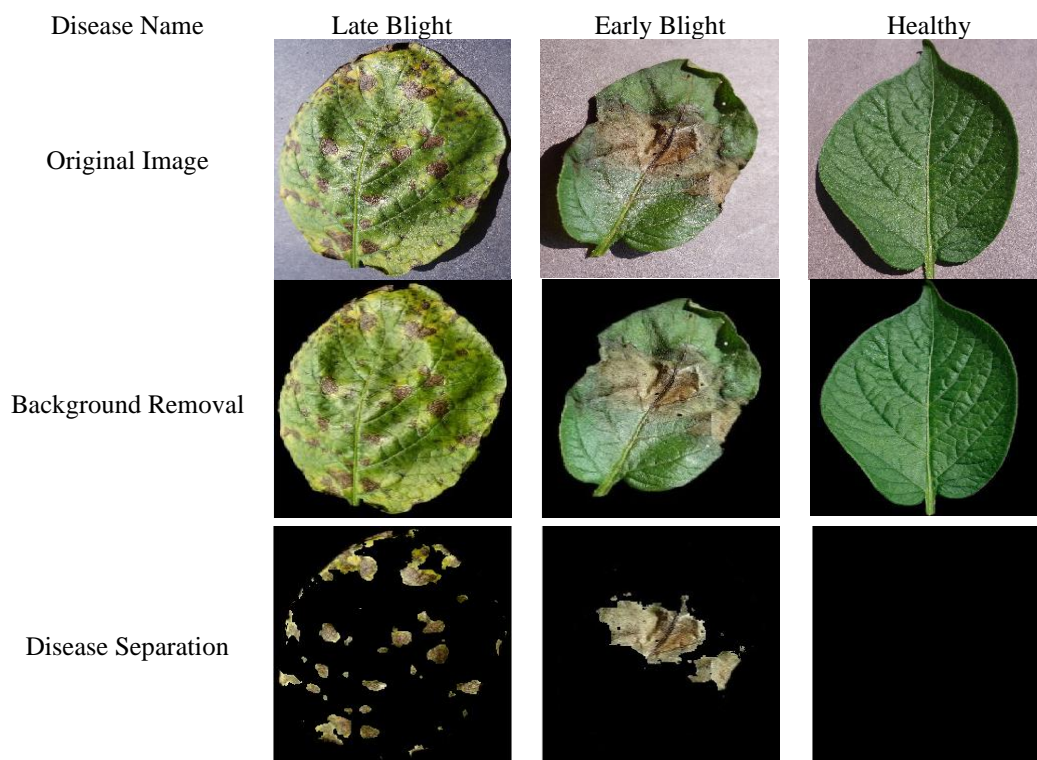

Fig. 3. Separation of the diseased area from the healthy leaf image

Feature extraction

The process of feature extraction involves transforming raw data into numerical features that can be understood and analyzed by machine learning models. Compared to directly using raw data, feature extraction can greatly improve the performance of machine learning models. In this case, after segmenting the disease area and extracting the damaged part of the leaf from input image, a variety of features such as colors, texture, and shapes were extracted (Ampatzidis, Partel, & Costa,

2020). In this study, after dividing the disease area, which means extracting the damaged part of the leaf from the input image, features such as color, shape, and texture were extracted. Color features (mean, maximum, minimum, standard deviation, and median) and Textural Features from GLCM (contrast, correlation, energy, homogeneity, mean, standard deviation, entropy, variance, smoothness, kurtosis, and skewness) in each band of three color spaces RGB, Lab*, and HSV, 45 color features and 99 Textural Features.

Furthermore, 6 shape features including: area, perimeter, number of spots, length of major and minor axis of points, and eccentricity index were extracted from images. Table 1 shows a description of the extracted features.

Table 1- Extracted features to diagnose and classify the diseases

Feature	Description	Equation	Reference
Color Features			
Mean	The average value is computed as the sum of all the observed outcomes from the sample, divided by the total number of events	$\overline{x} = \dfrac{1}{n} \sum\limits_{i=1}^{n} x_i$	Ashfaq *et al.* (2019)
Max	Assign the maximum amount of neighborhood grays to the center pixel	-	Ashfaq *et al.* (2019)
Min	Assign the minimum amount of neighborhood grays to the center pixel	-	Ashfaq *et al.* (2019)
Standard Deviation	The measure of how far the data values lie from the mean	$s = \sqrt{\dfrac{1}{n-1} \sum\limits_{i=1}^{n} (x - \overline{x})^2}$	Ashfaq *et al.* (2019)
Median	The middle value of a series of values is equal to the middle value of a series of numbers	-	Ashfaq *et al.* (2019)
Textural Features			
Contrast	The measure of the difference between the brightness of the objects or regions and other objects within the same field of view	$\sum\limits_{i,j} \lvert i-j \rvert^2 p(j,j)$	Haralick, Shanmugam, and Dinstein (1972)
Correlation	The measure of degree and type of relationship between adjacent pixels	$\sum\limits_{i,j} \dfrac{(i-\mu i)(j-\mu j)p(i,j)}{\sigma_i \sigma_j}$	Haralick *et al.* (1972)
Energy	The sum of squared elements in the gray level co-occurrence matrix	$\sum\limits_{i,j} p(i,j)^2$	Haralick *et al.* (1972)
Homogeneity	The closeness of the distribution of elements in the GLCM	$\sum\limits_{i,j} \dfrac{p(i,j)}{1+\lvert i-j \rvert}$	Haralick *et al.* (1972)
Mean	The measure of the average intensity value of the pixels present in the region	$\dfrac{1}{n}\left(\sum\limits_{i=1}^{n} X_i \right)$	Haralick *et al.* (1972)
Standard Deviation	The measure of how much the gray levels differ from the mean	$\sqrt{\dfrac{1}{n}\left(\sum\limits_{i=1}^{n} (X_i - \overline{X})^2 \right)}$	Haralick *et al.* (1972)

Entropy	The measure of differences in gray levels	E=sum(p.*log2(p))	Haralick *et al.* (1972)
Variance	The measure of variance value of an image	$\frac{1}{n}\left(\sum_{i=1}^{n}\left(X_i-\bar{X}\right)^2\right)$	Haralick *et al.* (1972)
Smoothness	A measure of relative smoothness of intensity in a region	-	Haralick *et al.* (1972)
Kurtosis	A measure of peaks distribution related to the normal distribution	$K=\dfrac{E(x-\mu)^4}{\sigma^4}$	Haralick *et al.* (1972)
Skewness	A measure of asymmetry in a statistical distribution	$S=\dfrac{E(x-\mu)^3}{\sigma^3}$	Haralick *et al.* (1972)
Shape Features			
Area	Mean number of pixels in each segmented region in the image	$a=\sum_{u=1}^{M}\sum_{v=1}^{N}A[u,v]$	Vishnoi, Kumar, and Kumar (2021)
Perimeter	Mean of number of boundary pixels on each segmented region in the image	2 (length + width)	Vishnoi *et al.* (2021)
Number of objects	Number of disease spots in the leaf image	-	-
Major axis length	Length of the major axis of the ellipse that has the same normalized second central moments as the region	$M=x_1+x_2$	Vishnoi *et al.* (2021)
Minor axis length	Length of the minor axis of the ellipse that has the same normalized second central moments as the region	$m=\sqrt{((x_1+x_2)^2-d)}$	Vishnoi *et al.* (2021)
eccentricity index	The eccentricity of the ellipse that has the same second-moments as the region	$\dfrac{\text{Major axis length}}{\text{Minor axis length}}$	Vishnoi *et al.* (2021)

The Textural Features include energy, standard deviation, entropy, mean, and median, which are usually used to describe the texture of an image. Also, the selected band for each feature is specified in Table 1. The energy feature measures the amount of energy at a given pixel location based on the contrast of adjacent pixels, and higher values indicate more contrast. The standard deviation feature measures the deviation of the intensity values of neighboring pixels from the mean, with higher values indicating greater variability in the texture. The entropy property measures the amount of information at a given pixel location, with higher values indicating more random patterns (Ashfaq *et al.,* 2019). The average property represents the average intensity of all pixels in an image, while the

mean property represents the average gray level of a given pixel.

The color features include median in two RGB bands, the maximum in Lab* band, and the average in two RGB bands, which are usually used to describe the color of an image. The median feature takes the middle value of the intensity values of the three color bands, and higher values indicate darker colors. The maximum feature in the Lab* band takes the highest intensity value of the Lab* color space and higher values indicate brighter colors. The average attribute represents the average intensity of all colors in an image, while the Lab* attribute captures the hue, saturation, and brightness values of a specific color (Zhou, Gao, Zhang, & Lou, 2020). Finally, color properties indicate the degree of red, green or blueness of a color.

The shape features include perimeter, area, and number of spots in the image, minor axis length and main axis length, which are usually used to describe the shape of an object in an image. The perimeter attribute indicates the distance around the perimeter of a given object, with higher values indicating larger objects. The area property represents the area value of an object, with higher values representing larger objects. The number of points features indicates the amount of variation in a given object, with higher values indicating more complex shapes. The minor axis length and major axis length indicate the length of the shortest and longest lines that can be drawn within an object, with higher values indicating longer or irregular shapes.

Feature selection

Feature selection is crucial for developing effective and reliable machine learning models for plant disease detection. Research has shown that selecting the right features can significantly impact the performance and accuracy of these models. Choosing the optimal set of features can also reduce the computational time required for training the system, particularly in cases where the number of features is large. One way to identify the most effective features is by using the Relief feature selection method, which reduces the redundancy of data features. This method randomly selects samples from the dataset and updates the score of each feature based on its correlation with the selected samples. Features with high scores are considered to be effective in the diagnosis and classification of plant diseases, making them ideal candidates for inclusion in machine learning models. This research applies the Relief method to extract the most important features for the detection and classification of potato diseases, making it a valuable resource for researchers in this field who are seeking to improve the accuracy and efficiency of their models.

Using Random Forest for classification

The Random Forest method is one of the comprehensive methods of machine learning that has competitive predictive application in various fields such as biological sciences, earth sciences, finance, chemical engineering, etc. The Random Forest can be introduced as a flexible and easy-to-use machine learning algorithm for different prediction and classification, which produces very good results most of the time even without setting too many parameters (Mohammadzamani, Javidan, Zand, & Rasouli, 2023). This new and powerful method has provided significant improvements in data mining technology. It is also one of the most widely used algorithms, because it can be used for classification and regression due to its simplicity and variety. Random Forest technique is a developed model of tree regression and classification method.

Performance evaluation in the classification of potato diseases

One of the most important criteria for evaluating the performance of a classification model is the confusion matrix. This matrix shows the relationship between the predicted and actual classes, where TP stands for the number of true positives, TN stands for the number of true negatives, FP stands for the number of false positives, and FN stands for the number of false negatives. In this research,

the performance of the model was evaluated by classification accuracy, as well as other metrics such as Precision, Sensitivity, Specificity, and F-Measure (Equations 1 to 5).

$$Accuracy = \frac{(TP+TN)}{(TP+TN+FP+FN)} \quad (1)$$

$$Precision = \frac{TP}{TP+FP} \quad (2)$$

$$Sensitivity = \frac{TP}{TP+FN} \quad (3)$$

$$Specificity = \frac{TN}{TN+FP} \quad (4)$$

$$F\text{-}Measure = \frac{2 \times (Precision \times Sensitivity)}{(Precision + Sensitivity)} \quad (5)$$

Results and Discussion

Image classification results

The proposed method for potato leaf diseases classification consists of several stages: segmentation of diseased region, feature extraction, feature selection (Relief algorithm), and classification (Random Forest algorithm). Finally, classification of diseases and healthy leaves before using feature selection algorithm and using random forest classification algorithm with 95.99% accuracy, 96.12% precision, 96.25% recall, and 96.16% F1 score. The classification criteria for diseases are presented in Table 2. The proposed method provides a promising approach for the precise and accurate diagnosis of potato diseases.

According to Figure 4, the late blight class achieved a lower accuracy than the other two classes. Additionally, the healthy leaves category obtained a higher accuracy compared to the other classes. The proposed model showed a satisfactory overall performance in terms of precision, recall, and F1 score. It was evident that the healthy leaves class performed better than the other two classes. This suggests that more attention should be paid to increasing the accuracy of the late blight class in future research. The proposed framework provides a promising and efficient approach for the accurate diagnosis of plant diseases.
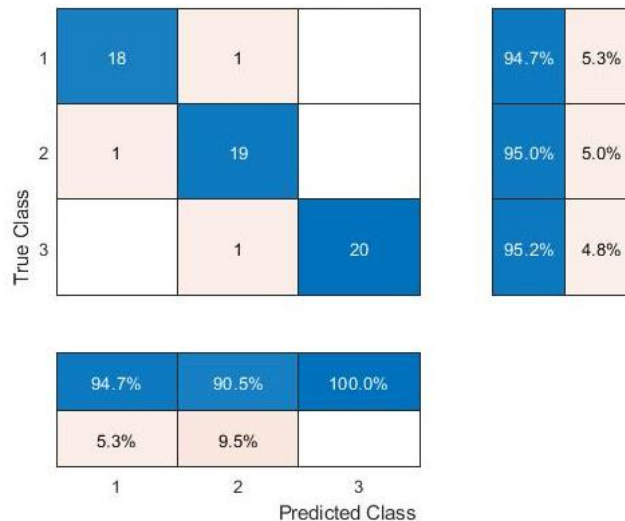

Fig. 4. Confusion matrix for classification (1- early blight group, 2- late blight group, and 3- healthy leaf group)

Table 2- Evaluation criteria for the classification of potato diseases

Category Name	Precision (%)	Recall (%)	F1-score (%)	Accuracy (%)
Late Blight	91.07	95.41	93.29	94.71
Early Blight	98.36	94.71	96.43	95
Healthy	98.93	98.62	98.76	95.2
Overall	96.12	96.25	96.16	95.99

According to Figure 5, the proposed model has performed well in identifying late blight and early blight in potato plants with accuracy rates of 94.71 and 95% and precision of 91.07 and 98.36%, respectively. In addition, it was able to accurately identify healthy leaves with an accuracy rate of 95.2%. The overall accuracy rate of the model was 95.99%, which shows that it had a relatively low error and was able to accurately identify plant diseases in most cases. The high model accuracy and good overall accuracy are promising indicators of its potential in plant disease diagnosis. However, it is important to note that the performance of the model is affected by the size and quality of the training dataset, and the scope of the specific application may also affect its performance (Zhai, Qiu, Weckler, He, & Jabran, 2023). In addition, there may be cases where the model misclassifies healthy or diseased plants, which can lead to false positives or negatives. These mistakes can potentially lead to incorrect treatment or lack of intervention, which can lead to financial losses for farmers or reduce the quality and quantity of crops (Jaisakthi, Mirunalini, & Thenmozhi, 2019). Therefore, it is important to continue validating the model performance in a larger dataset with different plant types. The results of these validation experiments provide valuable insights into model strengths and limitations and help guide the development of more accurate and robust models for plant disease diagnosis.
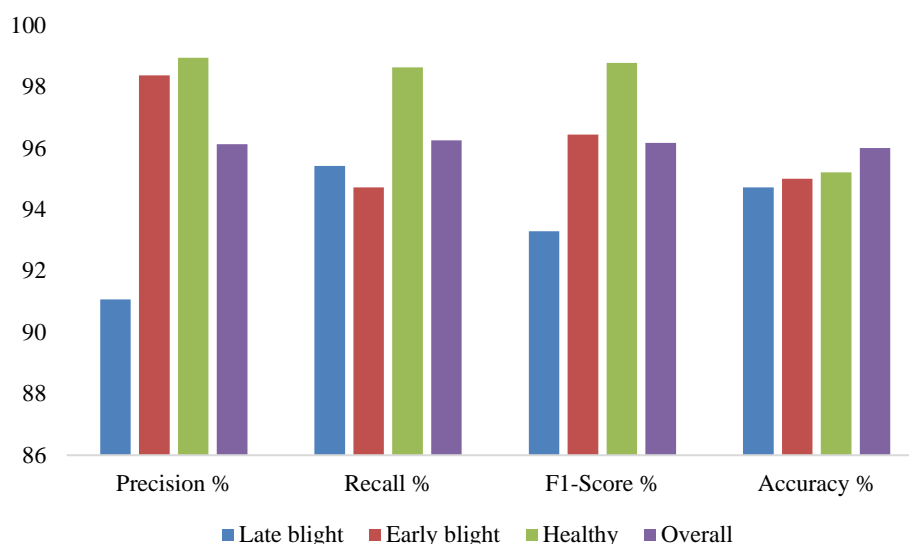

Fig. 5. A representation of evaluation criteria for the classification of potato diseases

Results of feature selection for potato disease diagnosis

After separating the diseased area from the healthy part of the leaf, a total of 150 features were extracted. These features included 45 color features, 99 Textural Features, and 6 shape features. To identify and classify each group, the most effective features were selected. This selection process included a combination of all three feature sets. The analysis of each feature set showed the features that had the greatest impact in the classification process. The final results showed that the combination of these three sets of features led to the most accurate classification.

The classification accuracy of individual feature sets was 70.45% for color features, 82.50% for Textural Features, and 70% for shape features. On the other hand, the classification accuracy of the combined feature set of the Random Forest classifier was

95.99%. In Table 3, five effective features for recognizing and classifying potato leaves are listed along with their descriptions, weights, and scores. In general, this study shows that the combination of three sets of features can lead to a more accurate classification of potato leaves. The selected features can also provide valuable insights into the diagnosis and classification of potato diseases. This approach can help farmers and other plant disease specialists to accurately diagnose and manage potato diseases, and ultimately lead to an increase in product quality and yield.

According to Table 3, the most important features selected by the Relief algorithm for diagnosing and classifying potato diseases based on texture, color and shape can be summarized as follows:

In general, these selected features represent the most important features that can be extracted from the leaves affected by potato-potato disease and can help in the diagnosis and classification of potato diseases. Textural features describe the structure and texture of the leaf, while color features describe the color and brightness of the leaf. Shape features describe leaf shape, including perimeter, area, number of spots in the image, minor axis length, and major axis length. These features (texture, color, and shape), when combined, can provide valuable information about the presence and nature of potato diseases and help farmers and plant disease specialists to identify and manage potato diseases more effectively.

Table 3- The results of the best and most important features selected for the diagnosis of potato leaf diseases

Row	1	2	3	4	5	Accuracy%
Color	Median (RGB) (G)	Median (RGB) (B)	Max (Lab*) (b)	mean (RGB) (G)	mean (RGB) (B)	70.45
Texture	Energy (Lab*) (l)	Standard Deviation (RGB) (B)	Entropy (Lab*) (b)	Mean (HSV) (H)	Median (Lab*) (l)	82.50
Shape	Area	Perimeter	Number of objects	Minor axis length	Major axis length	70
All Features	Skewness (HSV) (S)	Homogeneity (Lab*) (b)	Correlation (Lab*) (b)	Energy (RGB) (R)	Entropy (RGB) (R)	95.99

Compared to the research done by other researchers, what is more visible is the difference in classification accuracy, the number of extracted features, the classification method, and the number of data available in the diagnosis of diseases, which is one of the most important things that make the classification different (Padol & Yadav, 2016). The most important challenge in past research is the limited availability of diverse image datasets in various deep learning methods and convolutional neural networks, which weakens the performance of classifiers (Liu, Tan, Li, He, & Wang, 2020; Xie *et al.,* 2020). In such cases, using machine learning and correctly and effectively extracting the main features such as texture, color, and shape from images of diseased leaves can be a more effective approach (Jaisakthi *et al.,* 2019; Singh & Kaur, 2021). The weakness of fewer data can be

overcome by using classification in machine learning, but the condition of high classification accuracy is the extraction of features that also increase classification accuracy (Padol & Yadav, 2016). Comparing the results with research that used machine learning shows that the use of different groups of features has a great impact on classification accuracy (Padol & Yadav, 2016). In this research, it was shown that an algorithm can be used to diagnose and classify the common diseases of potato plants, which determined the exact location of the disease by processing color images. In addition, researchers were introduced to features that are highly accurate in diagnosis. They are most effective in the classification of diseases with almost identical symptoms in the leaves of the potato plant. Also, the results obtained by a feature selection algorithm showed that different

feature groups such as texture, and color in different color and shape spaces have almost the same importance in classification, so removing or ignoring each of the feature groups in the algorithm's performance will reduce the classification of the disease. On the other hand, there are cases such as not diagnosing the disease in the early days within two or three days after contracting the disease. Also, the limited spectrum in the color camera can be solved by using hyperspectral cameras, but using them and taking pictures cost a lot, and it will be difficult for farmers to carry out, as well as the small number of diseases, which will be increased in future research or can be suggested to be carried out by other researchers. Finally, the limited number of images used in deep learning algorithms can be considered as the limitation of this research.

A practical application of the proposed method can help plant breeders and farmers identify and diagnose potato diseases early in the crop cycle. This can help farmers to take timely measures and take measures to reduce disease outbreaks that can reduce yield and profitability. The proposed method can also be used to diagnose potato diseases alongside the knowledge of plant pathologists.

One of the challenges facing breeders and farmers in diagnosing potato diseases is the large number of diseases that can affect potato crops. Potato disease can be caused by viruses, bacteria, fungi, and other pathogens, and each disease can cause unique symptoms that can make identification and diagnosis difficult. Another challenge is the lack of reliable diagnostic tools such as laboratories and experienced plant pathologists in rural areas. This can make it difficult for farmers to access accurate diagnoses and effective treatments, which can lead to reduced yields and profitability.

Conclusion

This study presents a framework for detecting late blight and early blight diseases using a combination of Relief feature selection algorithms and Random Forest classification,

along with color features (in three color spaces: RGB, HSV, and CIELAB), Textural Features, and shape features. After separating the diseased area from the healthy part of the leaf, a total of 150 features were extracted, including 45 color features, 99 textural features, and 6 shape features. The most effective features for disease detection were identified using a combination of all three feature sets. This study demonstrated that integrating these three sets of features can lead to more accurate classification of potato diseases than using each group of features separately and can provide valuable insights into the diagnosis and classification of potato diseases. The results indicated that the diagnostic accuracy for the early blight and late blight disease groups, as well as the healthy leaf group, was 94.71%, 95%, and 95.2%, respectively, with an overall accuracy for disease classification of 95.99%. Additionally, the diagnostic accuracy for the two disease groups (early blight and late blight) and the healthy leaf group was 91.07%, 98.36%, and 98.93%, respectively, with an overall classification accuracy of 96.12%.

This approach can help farmers and plant disease specialists accurately diagnose two important potato diseases: early blight and late blight. It assists farmers and plant pathologists in making informed decisions for managing these diseases. By providing a quick, accurate, and convenient method for diagnosing early blight and late blight using digital images of leaves, this automated method reduces the time and effort required for disease diagnosis and can be utilized by farmers and plant breeders with minimal training. Furthermore, this method can be integrated with existing digital technologies, such as drones and remote sensing, to monitor large areas of potato crops for disease symptoms, ultimately saving time and money.

Competing Interests

The authors declare that they have no conflict of interest in the publication of this article. There are no copyrights relevant to this work. There are no relationships or activities

to disclose that could be perceived to have influenced the submitted work.

Authors Contribution

H. Koroshi Talab: Conceptualization, Study design, Data collection, Methodology and analysis.

D. Mohammad Zamani: Supervision, Writing the manuscript.

M. Gholami Parashkoohi: Thesis advisor.

References

1. Abdulridha, J., Ampatzidis, Y., Kakarla, S. C., & Roberts, P. (2019). Detection of target spot and bacterial spot diseases in tomato using UAV-based and benchtop-based hyperspectral imaging techniques. *Precision Agriculture, 21*(5), 955-978. Springer Science and Business Media LLC. https://doi.org/10.1007/s11119-019-09703-4

2. Ampatzidis, Y., Partel, V., & Costa, L. (2020). Agroview: Cloud-based application to process, analyze and visualize UAV-collected data for precision agriculture applications utilizing artificial intelligence. *Computers and Electronics in Agriculture, 174*, 105457. Elsevier BV. https://doi.org/10.1016/j.compag.2020.105457

3. Ashfaq, M., Minallah, N., Ullah, Z., Ahmad, A. M., Saeed, A., & Hafeez, A. (2019). Performance Analysis of Low-Level and High-Level Intuitive Features for Melanoma Detection. *Electronics, 8*(6), 672. https://doi.org/10.3390/electronics8060672

4. Barbedo, J. G. A. (2018). Factors influencing the use of deep learning for plant disease recognition. *Biosystems Engineering*, *172*, 84-91. https://doi.org/10.1016/j.biosystemseng.2018.05.013

5. Da Silva Silveira Duarte, H., Zambolim, L., Machado, F. J., Pereira Porto, H. R., & Rodrigues, F. A. (2019). Comparative epidemiology of late blight and early blight of potato under different environmental conditions and fungicide application programs. *Semina: Ciências Agrárias, Londrina, 40*, 1805-1818. https://doi.org/10.5433/1679-0359.2019v40n5p1805

6. Fan, Z., & Li, X. (2019). Recognition of potato diseases based on fast detection and fusion features of ROI. *Southwest China Journal of Agricultural Science*. 544-550. https://doi.org/10.16213/j.cnki.scjas.2019.3.015

7. Fang, Y., & Ramasamy, R. P. (2015). Current and prospective methods for plant disease detection. *Biosensors,* 5, 537-561. https://doi.org/10.3390/bios5030537

8. Haralick, R. M., Shanmugam, K., & Dinstein, I. (1972). On some quickly computable features for texture. *In Symposium of Computer Image Processing and Recognition*, University of Missouri, Columbia, *2*(2), 12-2.

9. Jaisakthi, S. M., Mirunalini, P., & Thenmozhi, D. (2019). Grape leaf disease identification using machine learning techniques, *in Proceedings of the 2019 International Conference on Computational Intelligence in Data Science (ICCIDS)*, Chennai, 1-6. https://doi.org/10.1109/ICCIDS.2019.8862084

10. Liu, B., Tan, C., Li, S., He, J., & Wang, H. (2020). A Data Augmentation Method Based on Generative Adversarial Networks for Grape Leaf Disease Identification. *IEEE Access, 8*, 102188-102198. Institute of Electrical and Electronics Engineers (IEEE). https://doi.org/10.1109/access.2020.2998839

11. Lopez, J. J., Aguilera, E., & Cobos, M. (2009). Defect Detection and Classification in Citrus Using Computer Vision. *In Neural Information Processing* (pp. 11-18). Springer Berlin Heidelberg. https://doi.org/10.1007/978-3-642-10684-2_2

12. Madufor, N. J. K., Perold, W. J., & Opara, U. L. (2018). detection of plant diseases using biosensors: a review. *Acta Horticulturae, 1201*, 83-90. https://doi.org/10.17660/ActaHortic.2018.1201.12

13. Mohamadzamani, D., Sajadian, S., & Javidan, S. M. (2020). DDetection of *Callosobruchus*

maculatus F. with image processing and artificial neural network. *Applied Entomology and Phytopathology*, *88*(1), 103-112. https://doi.org/10.22092/jaep.2020.341684.1324

14. Mohammadi, P., & Asefpour Vakilian, K. (2023). Machine learning provides specific detection of salt and drought stresses in cucumber based on miRNA characteristics. *In Plant Methods, 19*(1). Springer Science and Business Media LLC. https://doi.org/10.1186/s13007-023-01095-x

15. Mohammadzamani, D., Javidan, S. M., Zand, M., & Rasouli, M. (2023). Detection of Cucumber Fruit on Plant Image Using Artificial Neural Network. *Journal of Agricultural Machinery*, *13*(1), 27. https://doi.org/10.22067/jam.2022.73827.1077

16. Padol, P. B., & Yadav, A. A. (2016). SVM classifier based grape leaf disease detection, in *Proceedings of the 2016 Conference on Advances in Signal Processing (CASP)*, April 12-15. Lisbon,

17. Singh, A., & Kaur, H. (2021). Potato Plant Leaves Disease Detection and Classification using Machine Learning Methodologies. *In IOP Conference Series: Materials Science and Engineering, 1022*(1), 012121. IOP Publishing. https://doi.org/10.1088/1757-899x/1022/1/012121

18. Vishnoi, V. K., Kumar, K., & Kumar, B. (2021). A comprehensive study of feature extraction techniques for plant leaf disease detection. *Multimedia Tools and Applications, 81*, 367-419. https://doi.org/10.1007/s11042-021-11375-0

19. Xiao, Z., & Liu, H. (2017). Adaptive features fusion and fast recognition of potato typical disease images. *Transactions of the Chinese Society for Agricultural Machinery*, *48*(12), 26-32. https://doi.org/10.6041/j.issn.1000-1298.2017.12.003

20. Xie, C., Shao, Y., Li, X., & He, Y. (2015). Detection of early blight and late blight diseases on tomato leaves using hyperspectral imaging. *Scientific Reports,* 5, 1-11. https://doi.org/10.1038/srep16564

21. Xie, X., Ma, Y., Liu, B., He, J., Li, S., & Wang, H. (2020). A Deep-Learning-Based Real-Time Detector for Grape Leaf Diseases Using Improved Convolutional Neural Networks. *Frontiers in Plant Science, 11*(2). Frontiers Media SA. https://doi.org/10.3389/fpls.2020.00751

22. Yang, S., Feng, Q., Zhang, J., Sun, W., & Wang, G. (2020). Identification method for potato disease based on deep learning and composite dictionary. *Transactions of the Chinese Society for Agricultural Machinery, 51*(7), 22-29. https://doi.org/10.6041/j.issn.1000-1298.2020.07.003

23. Zhai, C., Qiu, W., Weckler, P., He, X., & Jabran, K. (2023). Editorial: Advanced application technology for plant protection: Sensing, modelling, spraying system and equipment. *Frontiers in Plant Science, 14*. Frontiers Media SA. https://doi.org/10.3389/fpls.2023.1113359

24. Zhou, W., Gao, S., Zhang, L., & Lou, X. (2020). Histogram of Oriented Gradients Feature Extraction from Raw Bayer Pattern Images. *In IEEE Transactions on Circuits and Systems II: Express Briefs, 67*(5), 946-950). Institute of Electrical and Electronics Engineers (IEEE). https://doi.org/10.1109/tcsii.2020.2980557

تشخیص و طبقه‌بندی دو بیماری شایع برگ سیب‌زمینی (لکه‌موجی زودرس و سفیدک داخلی) با استفاده از پردازش تصویر و یادگیری ماشینی

حسن کوروشی طلب¹، داود محمدزمانی ۱*، محمد غلامی پرشکوهی ۲

چکیده

تشخیص بیماری‌های گیاهی بخش مهمی از فرآیند مدیریت مزرعه است و می‌تواند تـاثیر قابـل‌توجهی بـر کمیـت و کیفیـت تولیـد داشـته باشـد. روش‌های سنتی ارزیابی چشمی توسط ناظران انسانی زمان‌بر، پر هزینه و مستعد خطا هستند و تشخیص دقیق و تمایز بین بیماری‌های مختلف را دشوار می‌سازند. پیشرفت‌های کشاورزی امکان استفاده از سامانه‌های بینایی ماشین غیرمخرب را برای تشـخیص بیماری‌هـای گیـاهی فـراهم کـرده اسـت و حسگرهای تصویربرداری رنگی توانایی بالایی در این زمینه از خود بروز داده‌اند. این مطالعه چارچوبی را برای تشـخیص بیمـاری لکـه مـوجی زودرس و سفیدک داخلی سیب‌زمینی با استفاده از ترکیبی از الگوریتم‌های انتخاب ویژگی Relief و طبقه‌بندی تصادفی جنگل و ویژگی‌های رنگ، بافت و شـکل در سه فضای رنگی HSV ،RGB و Lab* توصیف کرد. نتایج این بررسی نشان داد که دقت تشـخیص بـرای گـروه بیمـاری لکـه مـوجی زودرس و سفیدک داخلی و گروه برگ سالم به‌ترتیب ۹۴/۷۱، ۹۵ و ۹۵/۲ درصد و دقت کلی برای طبقه‌بندی بیماری ۹۵/۹۹ درصد بود. همچنین دقـت تشـخیص برای دو گروه بیماری لکه موجی زودرس و سفیدک داخلی و گروه برگ سالم به‌ترتیب ۹۱/۰۷، ۹۸/۳۶ و ۹۸/۹۳ درصد و دقـت کلـی بـرای طبقه‌بنـدی بیماری‌ها ۹۶/۱۲ درصد بود. پس از جداسازی ناحیه بیمار از قسمت سالم برگ، در مجموع ۱۵۰ ویژگی شامل ۴۵ ویژگی رنگی، ۹۹ ویژگی بافتی و شش ویژگی شکلی استخراج شد. مؤثرترین ویژگی‌ها برای تشخیص بیماری با استفاده از ترکیبی از هر سه مجموعه ویژگی شناسایی شدند. این مطالعه نشان داد که ترکیب این سه مجموعه از ویژگی‌ها می‌تواند منجر به طبقه‌بندی دقیق‌تر برگ‌های سیب‌زمینی شود و بینش ارزشمندی در تشخیص و طبقه‌بندی بیماری‌های سیب‌زمینی ارائه دهد. این رویکرد می‌تواند به کشاورزان و سایر متخصصان بیماری‌های گیاهی کمک کنـد تـا بیماری‌هـای سـیب‌زمینی را به‌طور دقیق تشخیص داده و مدیریت کنند و در نهایت منجر به افزایش کیفیت و عملکرد محصول شود.

واژه‌های کلیدی: انتخاب ویژگی، استخراج ویژگی، بیماری‌های سیب زمینی، تشخیص بیماری، هوش مصنوعی

۱– گروه مهندسی بیوسیستم، واحد تاکستان، دانشگاه آزاد اسلامی، تاکستان، ایران

۲– گروه مهندسی مکانیک، واحد شهر قدس، دانشگاه آزاد اسلامی، تهران، ایران

(Email: dr.dmzamani@iau.ac.ir :نویسنده مسئول –*)

Evaluations of Cereal Combine Harvester Head Attachment for Harvesting of Sunflower and Comparison with Conventional Harvesting Methods

M. Safari [ID][1*], **P. Ghiasi** [ID][2], **A. Rohani** [ID][3]

1- Department of Farm Machinery and Mechanization, Agriculture Engineering Research Institute, Agriculture Research Education, Extention Organization, Karaj, Iran
2- Department of Biosystem Engineering, Faculty of Agriculture, Tarbiat Modares University, Tehran, Iran
3- Department of Biosystems Engineering, Faculty of Agriculture, Ferdowsi University of Mashhad, Mashhad, Iran
(*- Corresponding Author Email: m.safary@areeo.ac.ir)

Abstract

In Iran, more than 50,000 hectares of sunflowers (oil and nuts) are cultivated annually. Conventional grain combine harvesters are not compatible with the unique characteristics of sunflowers, leading to significant grain losses during harvesting. Therefore, it is currently being harvested manually. Manual harvesting increases labor hardships, energy and time consumption, and production costs. In this research, to harvest sunflower seeds, modifications were made on conventional head of a combine harvester (John deer 1055) to allow simultaneous harvesting, threshing, and cleaning of the sunflower seeds. After designing and fabricating the accessory, the improved head in field conditions was evaluated and compared with conventional harvesting methods. The field evaluation of the improved head was based on a randomized complete block design with three replications. The treatments involved three different harvesting methods: 1) using a modified combine head, 2) employing a combine equipped with pan attachment, and 3) manual harvesting. In each of the machine treatments, beating and cleaning units were set up for sunflower harvest. The results showed that there was a significant difference between the treatments concerning machine losses, field capacity, and harvesting costs, all at the 5% significance level. In the modified combine, combine with pans attachment, and manual method, combine losses were 0.72, 4.85, and 6%, and field capacity was 1.2, 1.13, and 0.12 ha h^{-1}, respectively. The profit-to-cost ratio was 13.97, 13.3, and 3.01, respectively. The grain breakage percentage was 3, 3.3, and 0.56, respectively. According to the results, due to lower losses, appropriate field capacity, and lower harvesting costs, the use of John deer 1055 combine with the modified head is recommended for harvesting of the sunflower.

Keywords*: Attachment, Combine head, Harvesting, Improvement, Sunflower

Introduction

The sunflower plant is one of the most important oilseeds in the world. The origin of this plant is North America; this plant was

brought to Europe by the Spaniards in the 19th century and about 80 to 90 years ago was imported to Iran. The most important countries producing sunflower in the world are Russia, the USA, China, and Argentina, respectively. In recent years, the high imports of this oilseed to Iran have been for oil production (Mozaffari & Hassanpour Darvish, 2012). The sunflower is an annual crop. The plant is physiologically ripe when the back color of the head changes

from green to yellow and is ready for harvesting; this time is routinely before drying of heads. Many farmers prefer to harvest sunflowers at grain moisture between 20-25% with a combine harvester or by hand to reduce the loss time and birds damage. Harvesting of the sunflower with high humidity causes molding on the heads, increases the percentage of lean and wrinkled grains, as well as complications during the threshing process. The sunflower is cultivated over 59,531 hectares of Iran's lands every year (Ahmadi, Ebadzadeh, Hatami, Abdshah, & Kazemian, 2020). One of the critical stages of production of this crop is harvesting operation which is done manually by workers. Manual harvesting has problems like formidable work, labor shortages, and high labor costs; therefore, mechanized harvesting of this crop is essential.

There is no economic justification for constructing a head attachment of sunflower harvester in combine factories, so local workshops make this attachment. Modifications are applied to the cutter bar and the reels. The conventional reel is replaced by a reel with three thin arms attached to a plate. In the case of the cutter bar, 7.5 cm wide long pans are attached and act as the stripper. The plates attached to the reel pass through two pans and push the plant straw to the auger. Pans guide the stem and prevent seeds loss (Grower, 1971). Researchers evaluated various brands of different harvesting mechanisms for sunflower crops in one study; these mechanisms consist of four essential components including: the dividers, the pans, the reel, and the plates attached to the reel (Nyborg, Thauberger, Gregory, & Pool, 1980). The conventional cutter bar and reel can be used, but long pans should be used to guide the stems and reduce the loss (Husiman, 1977). The cereal combine harvesters can be used to harvest sunflower and most of the combines used for this crop follow the principles of stripper harvester (Hoffman, Berglund, & Hellevarge, 1982). Another study showed that conventional fine-grains cutter bars can be used to harvest sunflower by modifying the dividers and reel (Dekalb, 1987). The

sunflower harvesting losses using the conventional head were higher than the row crop head and the head equipped with the pans. The conventional head loss was between 24-30%, while under the similar conditions, these losses in the head equipped with the attachment were between 4-5% (Thierstin, 1990). The Prairie Institute tested the tractor sunflower harvester. The special pans (pentagonal plates) were used for row spacing. A small reel equipped with a hydraulic motor with feeder's fingers was implemented above the cutter bar. The pans wide were considered according to the distance between the rows of sunflower cultivation. The plant passed between the pans and was delivered to the reel. The pans were long enough to collect any fallen seeds. The working width was 3.8 m and the distance between the pans (center to center) was 76 mm. The performance of pans and dividers was appropriate. The flow of the crop was smooth and there was a suitable match between the reel speed and forward speed. Optimal speed is dependent on crop conditions (especially moisture). The ideal speed was 7km.h^{-1}. The grain losses were low and pans covered 84% of the cutter bar; however, the reel with dry grains increased grain losses (ZACH, 1981). The fine-grained combine harvesters can be modified to harvest sunflowers. The kinds of head attachments are available, and many of them work according to the operating principles of strippers. Attachments were designed to collect only sunflower heads (non-harvested stems). The most important components of the attachments were the pans, the deflectors, and the reels. The deflector was positioned atop the pans, guiding the stems inward and delivering them directly to the cutter bar. The pans were available in different widths, from narrow (23 cm) that were suitable for 30 cm row spacing to 94 cm for 102 cm row spacing. The deflector was a curved sheet metal with a combine work width that was mounted on the reel retaining arm. The reels usually had 3-4 arms with 41-51cm diameter and were installed at 10-13 cm above the pans; thus, when the sunflower heads were in contact with

the reel, they were directed towards the auger (NDSU, 2014). A study was conducted to evaluate the effectiveness of a combine harvester in the sunflower crop harvest. The effects of some important parameters such as forward speed, threshing cylinder speed, and concave distance were studied; the results showed that the favorable conditions in terms of low grain losses and energy consumption, and high field capacity were achieved at a forward speed of 3.3 km h^{-1} and grain moisture content of 15.15% (based on dry weight). The grain losses, energy consumption, and field capacity were 3.12%, 11.38 kW ton^{-1}, and 1739 kg h^{-1}, respectively. In this situation, the fuel consumption was 5.5 liters per hour (Sayed & Abd El Maksoud, 2012). In one study, the effects of forward and reel speed on the sunflower harvest losses were studied. The results showed that the combine forward speed did not have a significant effect on the total losses, but the effect of the reel speed on the loss was significant. Finally, the most suitable forward speed and reel speed in terms of low losses were 6 km h^{-1} and 30 rpm, respectively; under these conditions, the reel index was five (Elfatih Mohammed, 2014). In a study to harvest the sunflower, a combine equipped with a four-row crop head, the grain purity was 96.64%, the number of damaged seeds at a moisture content of 5.1%, was 1.5% and the total loss was less than 1%. One of the reasons for the low losses in this type of head was the lack of sunflower stems entering threshing units. On the other hand, the high percent of purity and the low percent of breakage indicated the proper performance of the combine cleaning and threshing units (Shaforostov & Makarov, 2019). In a study in the Ukraine region, a new head for the sunflower harvesting was introduced and evaluated. The results showed that the most important factor in reducing crop losses was the forward speed. The minimum losses were achieved at 2.5-5 km h^{-1}, the cutting height was 0.5-0.7 m, and the harvesting period was less than five days. Using this technology, the loss rate was reduced by 1.4 times. In this technology, the sunflower crop was directed to a special channel by the dividers. Two rollers were installed on the head that made the stem stable, and with the lower fingers, the plant stem was cut and directed backward. At the end of the head was another blade that cut the head from the bottom. In the next step, it was guided backward and inside the combine by the elevator belt (Nalobina *et al.,* 2019).In a study titled Modeling Grain Losses in Mechanized Harvesting of Oilseed Sunflower, the effect of the height of the crop's sleeper rod on head and combine grain losses was significant at the 1% and 5% levels, respectively, but the effect of head height and the interaction effect of head height × rod height was significant only on head grain losses at the 5% level. With increasing rod height from 20 to 70 cm, the average head and combine losses increased from 4.7 to 18.6% and 3.4 to 4.5%, respectively, but with increasing cutting height from 60 to 120 cm; the average grain losses in the combine decreased from 3.4 to 1.5% and the average head grain losses increased from 10.8 to 12.4%. The regression model showed the relationship between the independent and dependent parameters. The output of the regression model showed that by adjusting the cutting height and the crop-laying bar, the total losses of the combine, including losses at the head and rear of the combine, can be reduced to less than 5% (Ghiasi & Safari, 2021). According to the researches mentioned, different mechanisms have been used for the mechanized harvesting of the sunflower. Conventional harvesting methods primarily fall into two categories. The manual method faces numerous challenges, particularly concerning labor costs and operational difficulties. The other method involves using a wheat harvesting combine that has been equipped with pans. This method has high loss due to using reel during sunflower harvesting. In this research, the conventional head was modified with minimum cost and evaluated in the field for harvesting of sunflower (Fig.1).
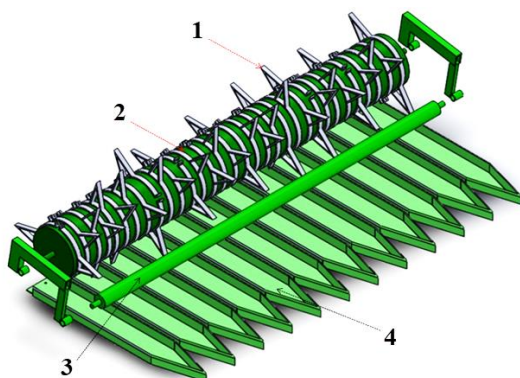
(a)   (b)

Fig. 1. (a) Components of the new system attached to the grain combine head:
1- Reel finger, 2 - Reel cylinder, 3 - Plant sleeper rods, and 4 - Seed pans.
(b) Combine harvester with modified header and combine harvester with conventional header equipped with pans

Materials and Methods

Cereal combine harvesters have a reel to guide the crop inward, a cutter bar to cut the crop, an auger to move the crop to the feeder elevator, a threshing unit to beat the crop, and a cleaning unit to clean the crop. The heads of these combine harvesters were designed for cereal harvesting and wasn't suitable for sunflower crops, so the necessary modifications were carried out on the head, and adjustments applied to the combine threshing and cleaning units to reduce harvest losses. In this research, an attachment was designed and constructed, and installed on the John deer combine (1055). This research was carried out in two phases: the development of the attached system and the field evaluation of its effectiveness.

Construction of the prototype attachment

This system consists of separate components as follows:

Crop guidance pans mechanism

The spacing for the sunflower plants was set at 60 cm between the rows and 15 cm between the plants within each row. Therefore, inter-row seed pans on the combine head were designed based on a coefficient of 30 cm. The length and width of the seed pans were 140

and 25 cm, respectively (Fig.1). The head width was 4.27 m and included 16 pans. The pan's thickness was 1.5 mm with suitable shapes that provided minimum friction with the crop. The position of the pans was such that the crop was guided to the cutter bar with minimal loss. Under the pans were the retaining metal belts, which connected the pans to the cutter bar. The pans prevented heads from falling and controlled crop losses.

Feeder cylinder and crop sleeper rod mechanism

The sleeper rod consisted of a steel pipe with 4m long and 10cm diameter, which is supported by a reel retaining rod on both sides (Fig.1). The sleeper rod was positioned on the pans, ensuring that the cutting unit effectively severed the plant's stem. The same conditions existed in the combine that was equipped with pans made in the local workshops of Shiraz, Iran. To guide the sunflower heads, the reel was released from the head, and the feeder cylinder with 30 cm diameter and radial appendages with 30 cm length were installed. The sleeper rod was bending the crop and the feeder drum moved the crop towards the auger. Additional walls were installed in the sidewalls of the head to stop the crop from falling outside.

Evaluation of head attachment

This mechanism was compared with other methods in an oil sunflower field in Kermanshah, Iran. The experiment design was completely randomized blocks with three replications. The variety of sunflower was Azargol. The harvesting methods studied were as follows:

1- Manual harvesting (MH)

2. Equipped Machine Harvester (EMH): Harvesting with a conventional wheat combine harvester with conventional head equipped with seed pans (Fig1-b)

3- Improved Machine Harvester (IMH): Harvesting with grain combine equipped with a new improved head

The combine threshing and cleaning units were set up for sunflower harvesting before field harvesting. The threshing clearance distance was 3 cm at the front and 1.5 cm at the rear. Rotational cylinder speed was 750 rpm. The straw sieves in the cleaning unit were completely open. The grain sieve holes were selected according to sunflower seed size. The dimensions of each experimental plot were 5×20 m.

In the manual method, the sunflower heads were removed from the plant by the laborer and then transferred to the place where the heads were pounded (Fig. 2).

Fig. 2. Manual harvesting method and separating the grain from heads

The studied important technical indicators included the natural and combine losses. The grain damage percentage and grain purity were measured as well. The sampling included measuring grain moisture at harvest time, plant height, and height of harvest residues, field capacity, natural losses, hand-harvested grain losses, combine losses (cutting platform and combine end losses), and quality losses. Combine losses were considered equal to the total losses of the threshing unit, separating unit, and cleaning unit. By measuring the time required for harvesting 20 meters in 3 repetitions, the average forward speed was calculated. To determine the harvesting height, the height of the standing sunflower stems from the ground was measured. The rotational speed of the threshing cylinder was obtained by the combine panel. By determining the

cutting width (4.27 m) and the forward speed and considering field efficiency of 80%, the field effective capacity was calculated. Grain moisture content was assessed using 100 g samples, which were then transported to the laboratory for analysis. The average grain moisture content was 10.49% (based on the wet weight of grain).

Grain losses in manual harvesting

In manual method, natural loss was determined before harvesting. Then, the sunflower heads were harvested manually and put in special bags for threshing and cleaning. The grains that were left inside the sunflower heads during the threshing and cleaning stages were considered as post-harvest losses. All manual method losses included grain losses

during field harvesting and grain losses after harvesting.

$$P_n = \frac{W_b}{W_a + W_b} \times 100 \qquad (1)$$

Where:

P_n: Natural grain losses (%)

W_a: Mass of grains in standing classes per unit area (g)

W_b: Mass of grains shed per unit area - shed before the combine entered the field (g)

$$Y_t = \frac{10 \times (W_a + W_b)}{A_k} \qquad (2)$$

Where:

Y_t: total grain produced per unit area (kg ha^{-1})

A_k: Sampling area (m^2)

Natural grain losses

The natural losses included grains and sunflower heads that were dropped on the ground before harvesting. The cause of this loss was the wind, hail, rain, pests, diseases, birds, crop lodge, and rodents. At a distance of 20 m in each experimental plot, the number of heads and grains shed before harvesting were collected. The total weight of grains in the sheds and the grains on the ground was considered as natural losses. The field yield was determined in three replications by the plots with dimensions of 2×1. The sunflower seeds from these plots were harvested and subsequently weighed to calculate the percentage of natural loss.

$$P_i = \frac{W_q \times 1000}{Y_t \times A_k} - p_n \qquad (3)$$

Where:

P_i: Percentage of grain losses per head (%)

W_q: Total mass of grains collected at a distance of 20 meters (g)

Head losses

The head losses included sunflower heads and grains that fell before being transferred to the threshing and cleaning units. This loss was attributed to the incorrect operation of the cutter bar, feeder speed, and an improper distance between the feeding unit and the cutter bar. Fallen seeds and heads were collected inside experimental plots after harvesting at a distance of 20 meters.

Combine rear losses (threshing, separating, and cleaning units)

The losses of the threshing unit included the grains in the sunflower head and semi-threshed seeds that came out of the end of the combine. A rectangular wood frame with an internal dimension of 33 x 61 cm was placed under the combine while the combine harvester was normally harvesting. The floor of this frame was covered with fine wire mesh that collected uncut and semi-crushed sunflower heads. Then the healthy and breakage grains separated, and their net weight was recorded. The threshers, cutter bar, and sieve losses were recorded as end-of-combine losses.

$$P_z = \frac{K + M + N + R}{T} \times 100 \qquad (4)$$

Where:

P_z: Percentage of impurities (%)

K: Mass of broken grains in the sample (g)

M: Mass of straw in the sample (g)

N: Mass of weed in the sample (g)

R: Mass of gravel and soil in the sample (g)

T: Total sample mass (g)

Percentage of impurities and quality loss

During the harvesting by the combine, part of the grains are broken down and transferred to the combine tank, which is known as quality loss. Impurities from the harvested crop also included weed seeds, soil, pebbles, and straw. The percentage of qualitative loss was obtained from the ratio of the weight of broken grains to the healthy grain weight. The percentage of impurities was obtained from the ratio of the weight of total impurities (weed seeds, soil, pebbles, and straw) to the total weight of the sample.

Theoretical capacity

This factor indicates the number of surfaces covered by the machine regardless of the wasted time. This index is a function of the forward speed and width of the machine and can be calculated from Equation 5:

$$C_t = (V \times W)/10 \qquad (5)$$

Where:

V = Forward speed (km h^{-1})

W = Working width (m)

C_t = Theoretical capacity (ha h^{-1})

To determine the forward speed, the time required for a distance of 20 meters was measured.

Effective field capacity

This capacity represents the actual operating hours of the machine with considering wasting time (some time is wasted during operation for turning, adjustments, lubrication, repairs and service, rest, etc.) and is a function of theoretical capacity and field efficiency:

$$C_e = C_t \times \eta \qquad (6)$$

Where:

η = field efficiency (%)

C_e = effective field capacity (ha h^{-1})

Another method for determining the effective field capacity is to determine the time required to harvest one hectare, which has been used manually method.

Economic assessments

In the economic evaluation, harvesting methods were compared using the partial budgeting method, and factors such as additional income and costs arising from the new technology were determined (Roth & Heyde, 2002). The results were statistically analyzed by SPSS software using Duncan's test method at 5% and 1% levels.

Results and Discussion

Field capacity

There was a significant difference between the used machines and manual methods in terms of field capacity at the level of 5%. There was no significant difference between a combine equipped with a pan and an improved combine (Table 1). The capacity of the improved combine, combine equipped with pans, and manual method were 1.2, 1.13, and 0.12 hectares per hour, respectively. These

results that are presented in Fig. 3 showed that the sunflower harvesting capacity in machine methods was 10 and 9.4 times of the manual method (Table 2). Although the working width of the combine was the same, the slight difference between the machine methods could be due to the different speeds or the field efficiency (Fig. 3).

Grain fracture rate

There was a significant difference between the machine and manual methods in terms of grain fracture percentage at the level of 5%. In the improved machine and equipped with pans, the fracture percent was 3% and 3.3%, respectively. There was no significant difference between these methods (Fig. 4). In the manual method, the fracture rate was 0.56%, which showed a significant difference with the machine methods. In a study on a combine equipped with a 4-row head for sunflower harvest, the purity percentage was 96.64% and the number of damaged seeds at a moisture content of 5.1% was 1.5%, which indicates the proper performance of the threshing and cleaning units (Shaforostov & Makarov, 2019). In this study, one of the reasons for the low loss and grain fracture (twice the fracture rate of this study compared to the study mentioned), may be due to the type of hammer, which in the current study was rasp bar type, but these researchers used nail studs for sunflower harvesting. However, the amount of breakage in oily sunflower seeds does not matter much and a high percentage of purity that is the removal of the input stem in the combine has been reported.

Purity

There was no significant difference between harvesting methods in terms of purity percentage (Table 1). The percentage of impurities in the improved head methods, machine with the pans equipped, and manual method was 6.19, 6.67, and 4.67 percent, respectively (Fig. 5). These results showed that in terms of quality, the quality of grains in the combine tank has the same conditions and the necessary settings have been applied to the

crusher and anti-crusher cleaning units. Threshing and purity have been acceptable. In the manual method, the beating and cleaning steps have been done properly. The maximum acceptable impurity in oil sunflower mill factories was 10% (Anonymous, 2019), so all harvesting methods in this study were acceptable purity. The results of a study conducted by Shaforusto and Macro (2019) on a four-row combine for sunflower harvesting showed the impurity rate was 1.38%, which was less than the results of this study. The

harvesting head used by these researchers was similar to corn harvesting machines and had feed rollers that were sloping on the dividers and guided the crop from the bottom according to the harvest to the feeding elevators (Shaforusto & Macro, 2019). A key factor contributing to the low impurity observed in this study was the separation of the head from the stem prior to its entry into the thresher. The efficiency of these units has increased because the stems do not enter the threshing and cleaning units.

Table 1- Analysis of variance of the effect of levels of the sunflower harvesting methods

Variation source	Degree of Freedom	Head loss	Back loss	Total loss	Grain fractures	Seed purity	Field capacity
Replication	2	1.29^{ns}	0.34^{ns}	2.74^{ns}	0.35^{ns}	0.74^{ns}	0.05^{ns}
Harvesting method	2	15.56^{**}	24.65^{**}	23.14^{**}	6.74^{ns}	3.27^{ns}	1.10^{**}
Error	2	0.39	0.33	0.68	11.80	1.24	0.02
Coefficient of change	C.V	29.05	34.09	21.34	9.54	1.18	16.06

** Significant difference at 1% level, and ns: No significant difference

Table 2- Comparison and classification of the mean of studied traits in different harvesting methods

Harvesting method	Head loss (%)	Back loss (%)	Total loss (%)	Grain fractures (%)	Seed purity (%)	Field capacity (ha.h^{-1})
Modified head	0.70^{b}	0.02^{b}	0.72^{b}	3.00^{a}	93.81^{a}	1.20^{a}
Pans head	4.78^{a}	0.05^{b}	4.85^{a}	3.30^{a}	93.33^{a}	1.13^{a}
Manual method	1.00^{b}	5.00^{a}	6.00^{a}	0.56^{b}	95.33^{a}	0.12^{b}

In each column, the difference between the means that have at least one common letter, is not significant.

Tall stems that remain in the field after harvesting sunflower can interfere with the cultivation of subsequent crops. Therefore, if the combine can be equipped with stem shredding units, the problem of the remaining residues in the field will also be solved. The highest losses in combines were in their header part. Unlike natural losses, this factor was a function of combine performance. According to Tables 1 and 2, there was a significant difference between machine methods in terms of losses in the header of the combine. The combine equipped with pans experienced the most significant loss, reaching 4.78%. The average loss of the improved header was 0.7%.

In a study, the effect of reel rpm on the rate of sunflower harvesting losses was significant. The appropriate rpm and proper forward

speeds were 30 rpm and 6 km h^{-1}, respectively. Therefore, one of the reasons for the high losses in the combine harvester equipped with pans was the high rpm of the reel (Elfatih Mohammed, 2014). In the current study, the average speed of the reel in the combine equipped with pans was 20 rpm and the speed of the reel was low. So, it can not be considered as the cause of grain loss.

Rear combine losses

The rear combine losses weren't significant in combine harvesters, but there was a significant difference between the combine harvesters and manual methods at the level of 5%. On the other hand, the rate of the rear of combine losses in the tested combines was very low and insignificant.

Total combine losses

The average natural loss was 0.9%, which showed that the field crop was not affected by natural loss factors such as storms and excessive drought. There was a significant difference between the experimental methods in terms of total losses at the level of 5%. The rate of losses of the improved combine harvester, combine equipped with pans, and manual method were 0.72, 4.85, and 6%, respectively. These results indicate that the losses in the improved combine were low (Fig 6). Efficient hybrid operations should be applied to minimize harvest losses. Natural losses play a major role in reducing losses. Total product losses should not exceed 5% of the yield. These losses include pre-harvest, header, beating, and cleaning losses. In one study, pre-harvest sunflower harvesting losses, header, thresher, cleaner, and total loss (including natural losses) were 2.2, 5.3, 0.1, 1.8, and 9.4%, respectively (Anonymous, 2005). The loss, without natural loss, was 7.2%, which was lower than the current research.

In one study, a major factor in increasing grain losses was the combine forward speed. The rate of loss was directly proportional to the rate of forwarding speed. Increasing the forward speed from 3.2 km h^{-1} to 5.6 km h^{-1} increased grain losses by 4% (Nalobina *et al.,* 2019). In the current study, the average forward speed was 3.51 km h^{-1}, which did not have a significant effect on the grain losses.

In another study, using a 4-row sunflower harvesting header, the grain loss rate at 5.1% grain moisture content was less than 1%. The heads were cut from the lower parts by sloping dividers. It reduced the entry of the plant stem into the threshing and cleaning units. Reduced plant entry increased the threshing and threshing efficiency, and reduced the overall grain losses in combine harvesting (Shaforostov & Makarov, 2019). The results of these researches in terms of overall combine losses were consistent with the results of this study for harvesting sunflower with the help of the modified header.

Economic assessment

The yield per hectare of the farm was 2200 kg.ha^{-1}. The guaranteed purchase price of oil sunflower seeds was $0.128 (Anonymous, 1397) and the net income was $281.6. The renting cost of the combine for sunflower harvesting was $20. The harvesting costs were $88 in the manual method including 22 people per day per hectare for harvesting, threshing, and cleaning. The net income of the improved combine methods equipped with pans and manual method were $279.6, $267.9, and $264.7, respectively (Figs 7 and 8). The costs per hectare were $20, $20, and $88, respectively, and the benefit-to-cost ratio in these methods was 13.97, 13.3, and 3.01, respectively.

Conclusion

1- The field capacity of sunflower combine was about nine times that of the manual method; therefore, harvesting by combine in a short time can effectively prevent pre-harvest losses such as birds attack, pests, and grain loss.

2- The percentage of fractures in the manual harvesting method was lower than harvesting by machine methods. One of the reasons for the increase in grain fracture in combine harvesters is due to the abrasive threshing unit.

3- The variations in grain purity percentages were not significant across the improved combine harvesting method, the combine equipped with pans, and the manual harvesting method. These percentages were 93.93, 93.33, and 95.33%, respectively.

4- The lowest and highest grain losses were related to the use of improved combine and manual methods, respectively.

5- Using the combine harvesters with the new improved header and equipped with pans reduced costs compared to the manual method by 76.3% and 74.46%, respectively.

Finally, the use of an improved combine (equipped with a new improved header) was recommended for sunflower harvesting due to reducing harvesting costs, grain losses, grain

impurity, and suitable field capacity.

Declaration of competing interests

The authors declare that they have no conflict of interest.

Authors Contribution

M. Safari: Corresponding author and conductor of the research

P. Ghiasi: Contribution in conducting the project in the field

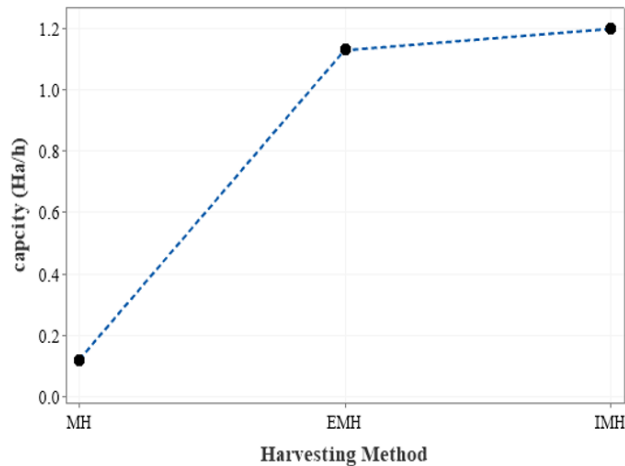A. Rohani: Contribution to writing and editing the article

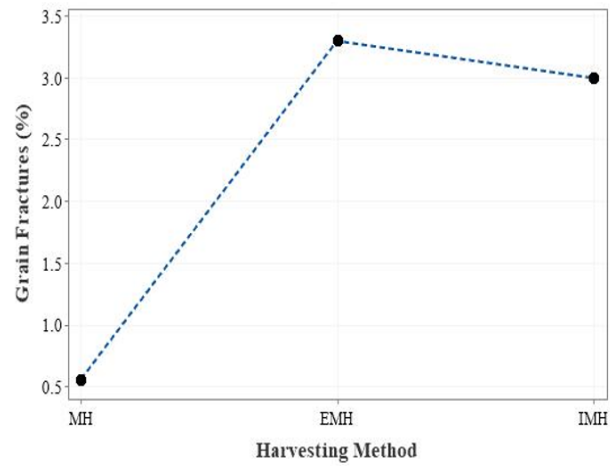**Fig. 3.** Farm capacities in various harvesting methods
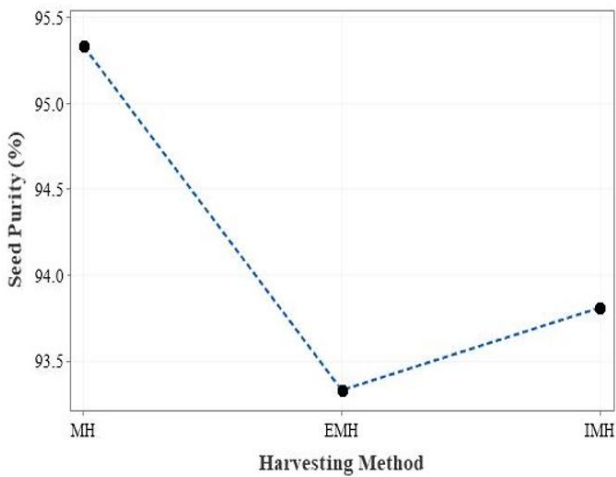

Fig. 4. Grain fractures in various harvesting methods

Fig. 5. Seed purity in various harvesting method
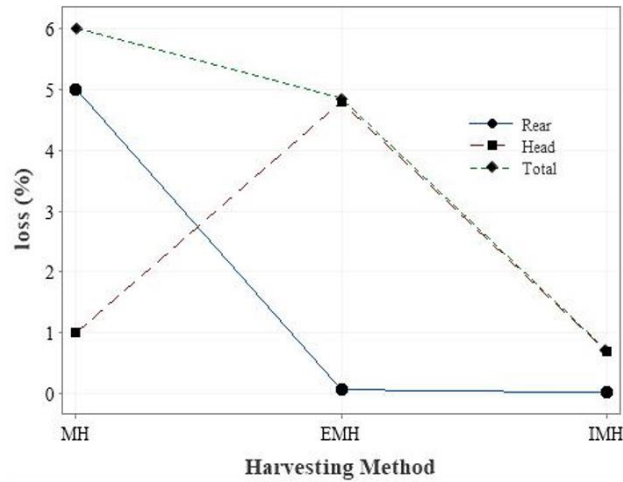
Fig. 6. Loss in various harvesting methods for three parts of Rear, Head, and Total
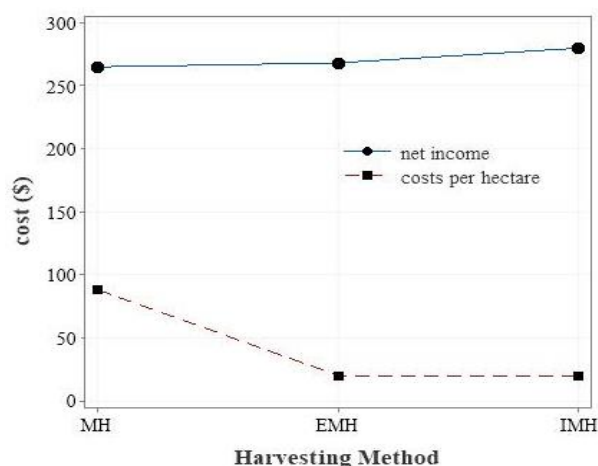
Fig. 7. Net income and costs per hectare for harvesting methods
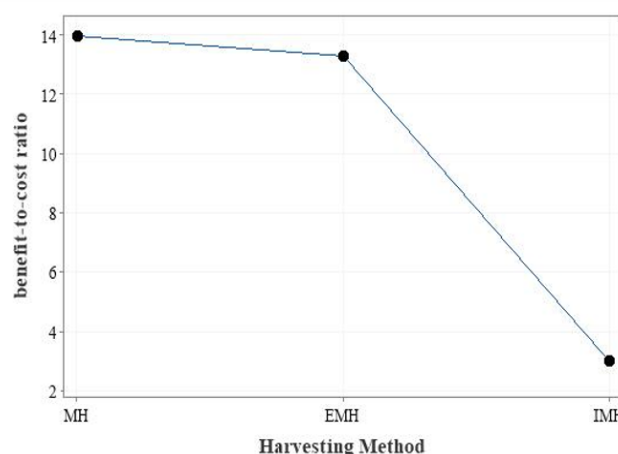
Fig. 8. Benefit-to-cost ratio for three harvesting methods

References

1. Ahmadi, K., Ebadzadeh, H. R., Hatami, F., Abdshah, H., & Kazemian, A. (2020). Agricultural statistic letter. Ministry of Agriculture Jihad. Planning and Economic Deputy, Information and Communication Technology Center. Vol: 1.
2. Anonymous. (2005). High plains sunflower production. Handbook. Kansas state university, Agricultural Experimentation and Cooperative Extension Service.
3. Anonymous. (2019). Instructions for sampling, determination of moisture and impurities of oilseeds (sunflower seeds and soybeans). *Cereals Research Center, Purchasing and Maintenance Group.* https://zakhiresazigroup.blogfa.com/post/94
4. Dekalb, D. P. (1987). Sunflower. Culture and Management. Agriculture Research Inc. Illinois DK 79660, 87591, ISF-2-Ih. Harvest and Storage.
5. Elfatih Mohammed, A. H. (2014). Effect of combine harvester forward and reel speeds on sunflower harvesting losses in Gadarif Area (Sudan). Khartoum.
6. Ghiasi, P., & Safari, M.(2021). Modeling grain losses in mechanized harvesting of oily sunflower. *Journal of Agricultural Machinery*, *11*(2), 399-408. (in Persian with English abstract). https://doi.org/10.22067/jam.v11i2.84191
7. Grower, G.(1971). Sunflower Attachment for Combines. *Field Crops,* 145-745.
8. Hoffman, V., Berglund, D., & Hellevarge, K. (1982). Sunflower Production, Harvesting, Drying and Storage. *ASAE*, 33-41.
9. Husiman, V. (1977). Combine Adjustment for Harvesting Sunflowers Cooperative Extension Service. North Dakota State.
10. Mozaffari, H., & Hassanpour Darvish, H. (2012). Investigation of Different Methods of Combined Irrigation with Saline and Sweet Water on the Percentage and Yield of Oil and the Fatty Acid Composition of Sunflower Oil. *Journal of Food Science and Nutrition,* 10.
11. Nalobina, O. O., Vasylchuk, N. V., Bundza, O. Z., Holotiuk, M. V., Veselovska, N. R., & Oshchuk, N. V. Z. (2019). A New Technical Solution of a Header for Sunflower Harvesting in MATEH *Agricultural Engineering* 58. https://doi.org/10.35633/inmateh-58-14
12. NDSU. (2014). Sunflower Production. *Extension Publication* A-1331 EB-25 revised, 101.
13. Nyborg, E. O., Thauberger, Gregory, J. C., & Pool, L. (1980). Stanley Sunflower Harvesting Attachment. Pami Evaluation Report. *Prairie Agricultural Machinery Institute*. ISSN:0383-3445.
14. Roth, S., & Heyde, J. (2002). Partial Budgeting for Agricultural Businesses. Penn State University, University Park, PA, CAT UA366 7.

15. Sayed, E., & Abd El Maksoud, G. H. SF. (2012). Evaluating the Performance of a Modified Grain Combine Harvester Used for Sunflower Crops. *AGRIS*, *87*, 73.
16. Shaforostov, V. D., & Makarov, S. S. (2019). The Header for a Breeding Plot Combines for Sunflower Harvesting, *Acta Technologica Agriculturae,* 2. Slovaca Universitas Nitra, Slovaca Universitas Agriculturae Nitriae, 60-63. https://doi.org/10.2478/ata-2019-0011
17. Thierstin, G. (1990). Header Loss in Harvesting. Sunflower. ASAE 90-6049, 12.
18. ZACH. (1981). Evaluation Report of Zach Sunflower Harvesting Attachment, in: E0280B, N. (Ed.), *Tested at Portage*, Prairie ISSN 0383-3445.

ارزیابی ضمیمه هد کمباین غلات برای برداشت آفتابگردان و مقایسه با روش‌های برداشت مرسوم

محمود صفری ⁱᴰ ۱*، پدرام قیاسی ⁱᴰ ۲، عباس روحانی ⁱᴰ ۳

چکیده

در ایران هرساله بیش از ۵۰ هزار هکتار آفتابگردان روغنی و آجیلی، کشت می‌شود. به علت سازگار نبودن کمباین‌های غـلات موجـود در کشـور بـا ویژگی‌های بوته و طبق آفتابگردان، مقدار زیادی دانه توسط کمباین تلف می‌شود. لذا، هم‌اکنون برداشت آن به‌صورت دسـتی انجـام می‌شـود. برداشـت دستی باعث افزایش مشقت‌های کارگری، انرژی مصرفی و هزینه تولید گردیده است. در این تحقیق، به‌منظور برداشت مکانیزه این محصول، اصـلاحاتی بر روی هد موجود کمباین غلات (جاندیر ۱۰۵۵)، اعمال گردید تا بتوان با آن عملیات برداشت، کوبش و بوجاری آفتابگردان را به‌طور هم‌زمان انجام داد. پس از طراحی و ساخت الحاقیه، هد به‌سازی‌شده در شرایط مزرعه، ارزیابی و با روش‌های برداشت مرسوم مقایسه شد. ارزیابی هد به‌سازی‌شده در قالب طرح بلوک‌های کامل تصادفی با سه تکرار بود. تیمارها شامل: ۱) برداشت توسط کمباین غلات مجهز به هـد اصلاح‌شـده، ۲) برداشـت توسـط کمباین غلات مجهز به قایقی و ۳) برداشت به روش دستی بود. در هرکدام از تیمارهـای ماشـینی، واحـدهای کوبنـده و تمیزکننـده بـه‌منظور برداشت آفتابگردان تنظیم گردید. نتایج نشان داد که بین تیمارهای آزمایشی از نظر تلفات کمباینی، ظرفیت مزرعه‌ای و هزینه‌های برداشت، اخـتلاف معنـی‌داری در سطح ۵٪ وجود دارد. در کمباین اصلاح‌شده، کمباین شیراز و روش دستی، تلفات کمباینی به‌ترتیب ۰/۷۲، ۴/۸۵ و ۶ درصد، ظرفیت مزرعه‌ای به‌ترتیب ۱/۲، ۱/۱۳ و ۰/۱۲ هکتار بر ساعت و نسبت سود به هزینه به‌ترتیب ۱۳/۹۷، ۱۳/۳ و ۳/۰۱ بود. بین تیمارها از نظر افت طبیعی و درصد خلوص اخـتلاف معنی‌داری در سطح ۵٪ وجود نداشت. با توجه به نتایج به‌دست‌آمده، به دلیل پایین بودن تلفات، ظرفیت مزرعه‌ای مناسب و هزینه برداشت پایین، استفاده از کمباین جاندیر ۱۰۵۵ مجهز به هد اصلاح‌شده برای برداشت آفتابگردان روغنی قابل‌توصیه است.

واژه‌های کلیدی: آفتابگردان، برداشت، به‌سازی، ضمیمه، هد کمباین

۱- بخش تحقیقات ماشین‌های کشاورزی و مکانیزاسیون، موسسه تحقیقات فنی و مهندسی کشاورزی، سازمان تحقیقات، آموزش و ترویج کشاورزی، کرج، ایران

۲- گروه مهندسی بیوسیستم، دانشکده کشاورزی، دانشگاه تربیت مدرس، تهران، ایران

۳- گروه مهندسی بیوسیستم، دانشکده کشاورزی، دانشگاه فردوسی مشهد، مشهد، ایران

(Email: m.safary@areeo.ac.ir :نویسنده مسئول -*)

Developing a Service Management Framework in the Agricultural Supply Chain with Fuzzy Weighted Average

M. Zangeneh [iD] [1*]

1- Department of Biosystems Engineering, Faculty of Agricultural Sciences, University of Guilan, Rasht, Iran
(*- Corresponding Author Email: zanganeh@guilan.ac.ir)

Abstract

The main objective of this research is to create a comprehensive and adaptable framework for assessing performance in agricultural supply chains and develop two improving approaches. The most relevant performance measures are selected to assess the current status of services in agricultural supply chains (ASCs). The contribution of this research is related to the selection of key performance indicators (KPIs) and approaches for enhancing ASC performance. The proposed framework comprises performance measurement and a service selection process. Two approaches have been developed based on the selected KPIs of services in ASC to identify which services require improvement. The proposed approaches are robust and versatile tools for agricultural managers to strategize and enhance their supply chains. A case study is also presented from Iran. For this region, selection approaches prioritize agricultural services such as postproduction consulting, financial support, mechanization, business consulting, and input supply. The framework shows that these services should be improved in order to better meet the needs of the region under study.

Keywords: Agriculture, Fuzzy, Performance measure, Service, Supply chain

Introduction

The term "agricultural supply chains" (ASC) refers to some activities involved in bringing agricultural or horticultural products from the farm to the table, including production, distribution, and marketing (Aramyan, Ondersteijn, Kooten, & Lansink, 2006). The ASC has recently received considerable attention due to emerging public health concerns. It has become apparent that in the near future, the design and operation of ASCs will be subject to more stringent regulations and closer monitoring, especially for products intended for human consumption,

such as agrifoods (Ahumada & Villalobos, 2009). Designing agrifood supply chain (SC) networks becomes more challenging when sustainability is incorporated into the traditional economic oriented models (Allaoui, Guo, Choudhary, & Bloemhof, 2018). The literature highlights the growing interest in developing agricultural supply chain performance management frameworks using operation research methods. These studies emphasize the need for comprehensive evaluation methods that consider various criteria such as cost, quality, delivery, sustainability, and flexibility. Different studies integrated the techniques like fuzzy logic, Fuzzy Delphi, AHP, PROMETHEE, and MCDM, offering effective decision-making support and aids in developing optimized agricultural supply chains.

van der Vorst, Peeters, and Bloemhof

(2013) presented a sustainability research framework for food supply chains logistics including drivers, strategies, performance, and indicators. The study provides insights into the development of a sustainability assessment framework for food supply chain logistics. Routroy and Behera (2017) provided a comprehensive review of literature on the agriculture supply chain. Rehman, Al-Zabidi, AlKahtani, Umer and Usmani (2020) used a fuzzy multicriteria method to assess the agility of a supply chain. While it does not focus on agricultural supply chains, it provides insights into the use of fuzzy logic for evaluating supply chain performance. Oubrahim, Sefiani, and Happonen (2022) presented a review of supply chain performance evaluation models. It provides insights into the different methods and models used for evaluating supply chain performance. Evangelista, Aro, Selerio, and Pascual (2023) proposed an integrated Fermatean fuzzy multiattribute evaluation method for evaluating digital technologies for circular public sector supply chains. Thumrongvut, Sethanan, Pitakaso, Jamrus, and Golinska-Dawson (2022) addressed the problem of designing tourist trips and planning tour routes to improve the competitiveness of community tourism. The study proposed the use of Industry 3.5 approach for planning more sustainable supply chain operations for tourism service providers. Banaeian, Zangeneh, and Golinska-Dawson (2022) proposed a multicriteria sustainability performance assessment of horticultural crops using Data Envelopment Analysis (DEA) and Elimination and Choice Translating Reality IV (ELECTRE IV) methods. The study aimed to evaluate the sustainability performance of horticultural crops and identify the most sustainable crops. These studies provide insights into the sustainability of agricultural production and supply chains and propose frameworks and approaches for achieving sustainability goals.

Generally, there are three types of commodities in the agricultural sector: (1) farm based commodities, (2) animal commodities, and (3) natural resource commodities. Each commodity requires various services, which can be categorized as follows: (a) input supply services, (b) consulting services, (c) business services, and (d) technical services. In this study, we focus on commodities and services that are based on farms.

In the context of the ASC, four main functional areas are identified: production, harvest, storage, and distribution (Ahumada & Villalobos, 2009). The subservices within each service type were identified by analyzing the activities of agricultural service companies in multiple countries. Consulting services are available in both the production and postproduction phases.

Literature review
Challenges of ASC

Farmers around the world face numerous constraints, such as limited access to financing, inputs, and technologies, which hinder their ability to improve production (Graham, Kaboli, Sridharan, & Taleghani, 2012). The challenges of ASC can be managed through different levels of management practices, including strategic, tactical, and operational approaches. In this study, we consider the strategic challenges that are almost exclusively related to services in ASCs. To focus the research, a summary of challenges mentioned in the literature will serve as a frame. This summary is presented in Table 1. Recently, most of the current research has focused on improving individual firms or processes rather than designing an entire supply chain (Allaoui *et al.,* 2018). In the current study, a smart service management procedure is being investigated.

Ganeshkumar, Pachayappan, and Madanmohan (2017) presented a critical review of prior literature relating to agrifood supply chain management. The study identifies gaps to be explored about agricultural supply chain management practices and provides a comprehensive understanding of the different aspects of agricultural supply chains.

Despoudi, Spanaki, Rodriguez-Espindola, and Zamani (2021) suggested a framework for

achieving sustainability in agricultural supply chains using Industry 4.0 technologies. The study provides insights into the challenges and opportunities for achieving sustainability goals in agricultural supply chains. Singh, Biswas, and Banerjee (2023) used bibliometric analysis tools to identify obstacles in the agricultural supply chain and proposes future directions for research. Morkūnas, Rudienė, and Ostenda (2022) investigated the potential of climate-smart agriculture to enhance food security through short supply chains. The literature review suggests that achieving sustainability in agricultural supply chains and services is an important area of research. The use of Industry 4.0 technologies and climate-smart agriculture are emerging areas that can help achieve sustainability goals in agricultural supply chains.

Table 1- Challenges of ASC

Subject	Challenges	Reference
Rice Supply Chain in Iran	Damages from pesticides and fertilizers, price, demand, permissible cultivation area, guaranteed purchase of government, and direct sales of farmers	(Kazemi & Samouei, 2024)
Rice Supply Chain in Iran	Total profit, integrating different decisions of the rice supply chain, including supplier selection, cropping, fertilizing, pest control, harvesting, milling, transportation, and distribution	(Jifroudi et al., 2020)
Organic Agri-Products SC in Iran	lack of direct communication or online communication platform to communicate with customers, and lack of procedure for collecting and documenting information	(Ghazinoori, Olfat, Soofi, & Ahadi, 2020)
Shea in Africa	Labor shortage, poor storage, suboptimal postharvest processing, the lake of access to financing, low adaptation of grafting, absence of effective controls and sorting processes, and low awareness among international buyers	(Graham et al., 2012)
Palm oil in Africa	Low access to reliable market information, trade –offs between food and cash crop production, access to financing, low productivity and quality from smallholder farmers, lack of access to processing mills, certification adherence, and environmental issues	(Graham et al., 2012)
Cashew in Africa	Poor seed/tree stock, lack of fertilizer and pesticides, little weeding, limited labor for fruit picking, lack of certification/standards, poor postharvest, poor grading techniques, and bad marketing	(Graham et al., 2012)
Food distribution	Low profit margins, food safety, food quality, and sustainability	(Akkerman, Farahani, & Grunow, 2010)
Food SC in Europe	Design and development of ICT solutions and expert systems and decision support systems to support decisions on the strategic planning of land use, facilities sites, and operation management within a food SC	(Manzini & Accorsi, 2013)

Performance measurement in ASC

Various perspectives can be found in the literature for evaluating the performance of supply chains (SCs). The evaluation of service center performance in service delivery can be complex and may vary even within the same sector (Cho *et al.,* 2012). Numerous techniques, encompassing both qualitative and quantitative approaches, are discussed in the literature pertaining to the service sector (Buyukozkan, Cifci, & Guleryuz, 2011). These selection models include both statistical and decision theory models. For instance, Chang, Hung, Wong, and Lee (2013) focused on constructing and implementing SCs to determine ways to overcome SC barriers and evaluate SC integration performance using the balanced scorecard approach. Vorst (2005) proposed a framework for developing innovative food supply chain networks and discussed the implications of implementing a performance measurement system and addressing respective bottlenecks. Aramyan *et al.* (2006) developed a conceptual framework for the existing performance indicators in ASC. These indicators are classified into four

primary categories: efficiency, flexibility, responsiveness, and food quality. Each category includes more specific performance indicators.

Improving the performance of agricultural supply chains requires comprehensive approaches that include performance evaluation systems, metrics, responsible guidelines, and advanced analytics. The proposed frameworks and approaches can help agricultural managers to make informed decisions to improve the sustainability and smartness of their supply chains. Trivellas, Malindretos, and Reklitis (2020) conducted a study on the implications of green logistics management on sustainable business and supply chain performance in the Greek agrifood sector. The study also proposed a conceptual framework for understanding the relationship between green logistics management and sustainable performance. Zangeneh, Nielsen, Akram and Keyhani (2014) proposed a performance evaluation system for agricultural services in supply chains. The study compares all possible scenarios to improve the performance of agricultural supply chains. Ramos, Coles, Chavez, and Hazen (2022) suggested metrics for measuring agrifood supply chain performance. The study provides insights into the factors that can improve supply chain performance in the agricultural sector.

Despite the importance of supply chain management (SCM), only a few researches have focused on the services it offers (Sengupta, Heiser, & Koll, 2006; Baltacioglu, Ada, Kaplan, Yurt, & Kaplan, 2007; Ellram, Tate, & Billington, 2007; Buyukozkan *et al.,* 2011; Cho, Lee, Ahn, & Hwang, 2012). Several studies emphasize the improvement of supply chain performance (Joshi, Banwet, Shankar, & Gandhi, 2012; Uysal, 2012; Cho *et al.,* 2012). Ulutas, Shukla, Kiridena, and Gibson (2016) proposed an integrated solution framework that can be used to evaluate both tangible and intangible attributes of potential suppliers in supply chains. This framework combines three individual methods: the Fuzzy Analytic Hierarchy Process, Fuzzy Complex Proportional Assessment, and Fuzzy Linear Programming. According to the literature, a comprehensive approach is necessary to identify and prioritize relevant criteria for developing a systematic performance measurement process for SCM.

While there are few research works specifically focused on this topic, insights from related fields suggest that fuzzy logic can be a valuable tool for evaluating supply chain performance. Generally, the literature suggests that incorporating smart and sustainable practices in agricultural supply chains is essential for achieving sustainable and efficient agricultural services. The proposed framework and approaches for improving the performance of agricultural services in supply chains can be used by agricultural managers to enhance the sustainability and competitiveness of their supply chains.

In this study, we propose a portfolio of agricultural services aimed at improving the overall performance of ASC. The goals of providing services in an ASC should be defined based on the ASC's objectives. In this study, we considered the following goals for service supply that influence the ASC targets: (1) Optimize the service delivery performance, including service order lead time and customer query time, (2) Minimize the service cost, including cost paid by customers to receive the services, (3) Maximize the service quality, view point of technical, health and environmental aspects, and (4) Maximize the service flexibility, including innovation, reflect customer needs etc.

Materials and Methods

Performance measures for services in ASC

In this section, we present a framework for performance measures and metrics to investigate the current status of services implemented in ASC for farm based commodities, including farming and horticulture (Table 2).

Table 2- Framework of KPIs of services in ASC

Production phase	Type of Service	Performance measures	#PM	References
Preproduction (PP)	1. Input supply (PP1)	Supplier's delivery performance (on time delivery and delivery reliability performance)	PM1	(Gunasekaran, Patel, & McGaughey, 2004)
		Supplier's pricing against market	PM2	(Gunasekaran et al. 2004)
		Quality of supplier's inputs	PM3	(Mapes, New, & Szwejczewski, 1997)
		Supplier's auxiliary services (booking, cash flow method, purchase order cycle time, and back order)	PM4	(Gunasekaran et al. 2004)
Production (PR)	1. Mechanization services (PR1)	Quality of services	PM5	(Mapes et al., 1997)
		Customer query time	PM6	(Bigliardi & Bottani, 2010)
	2. Consulting services (PR2)	Service pricing against market	PM7	(Gunasekaran et al., 2004)
		Customer satisfaction	PM8	(Aramyan et al., 2006)
		The flexibility of services to meet customer needs	PM9	(Gunasekaran et al., 2004)
	3. Financial services (PR3)	Customer query time	PM10	(Bigliardi & Bottani, 2010)
		The flexibility of services to meet customer needs	PM11	(Gunasekaran, Patel, et al. 2004)
Post production (PO)	1. Consulting services (PO1)	Customer satisfaction	PM12	(Aramyan et al., 2006)
		The flexibility of service systems to meet customer needs	PM13	(Gunasekaran et al., 2004)
	2. Inspection services (PO2)	Customer query time	PM14	(Bigliardi & Bottani, 2010)
		Reliability of performance	PM15	(Bhagwat & Sharma, 2007)
	3. Business services (PO3)	Purchase order cycle time	PM16	(Bhagwat & Sharma, 2007)
		Shipping errors	PM17	(Aramyan et al., 2006)
		Service pricing against market	PM18	(Gunasekaran et al., 2004)

Proposed approaches to select best alternatives to improve the ASC performance

There are a total of seven types of services available in ASCs. The combination of these services forms alternatives for improving ASCs. In this research, substituting the current service suppliers with new service centers that offer better services is considered an improvement action. Making decisions to choose an alternative that can enhance performance measures and improve the main targets of ASC is very difficult due to the complex relationships and inherent complexity of services in SCs. Therefore, an effective procedure is needed to select the best agricultural services alternatives. There are several scenarios which can improve the performance of agricultural services in ASC. Scenario I offers the most services, while scenario 4 offers the least. In the first scenario,

all services are distributed in the region through service centers, but budget and time constraints make this impossible. This scenario may lead to short term economic losses because the older service providers in the region have more competitive capabilities than the new service center. In the long term, if the service center's performance and quality of services exceed those of its competitors and satisfy its customers, the center may consider adding additional services to its service package. Therefore, the first scenario does not meet the aims of our research and will be disregarded. The fourth scenario considers services that are deemed necessary in the region based on the performance measure survey and have the greatest impact on ASC performance. As this scenario overlooks the necessary services in the region, it should only

be considered when managers are under tight budget and time constraints and must choose the most efficient services from the required ones. This type of scenario will not be investigated in the current study.

This research focuses on Scenario II, and two different approaches have been designed to evaluate this scenario. To begin, an integrated algorithm must be designed. Next, thresholds for performance measures of service types should be determined in order to select the best service packages as alternatives to improve the overall performance of the supply chain. Strategic level managers can specify the threshold for each performance measure. If the value of a performance measure for a service falls below/above the threshold (based on whether the character should be maximized or minimized), then another service supplier should implement that service in the supply chain. The next section describes the formulation of the service selection procedure based on the relevant performance measurements.

First approach: Fuzzy Weighted Average (FWA)

The first approach for evaluating the PM and proposing improvement actions uses FWA. Some definitions of fuzzy numbers, the fuzzy pairwise comparison, has been illustrated completely in several kinds of literature (Zimmermann, 2001; Wu, Pu, Shao, & Fang, 2004); Zadeh, 1965; Cho *et al.,* 2012; Zheng, Zhu, Tian, Chen, & Sun, 2012)). The concept of FWA and related formulas are described in the following section. The Fuzzy Weighted Average (FWAs) (Dong & Wong,1987; Liou & Wang,1992) is a process that may be defined as whereby via obtaining the fuzzy ratings A_{ji} of some objects S_j with respect to a set of criteria, attributes or factors $i \in \{1,2,\dots,n\}$ of a problem. Also, the fuzzy weighting or importance of the criteria, W_i, $i \in \{1,2,\dots,n\}$, reaches the objective function that aggregates the fuzzy ratings of the objects S_j and the fuzzy weights into the fuzzy aggregated outcomes M_j. The linguistic variables and related trapezoidal fuzzy numbers for both fuzzy weighting and fuzzy rating are given in Tables 3 and 4, respectively. Relich & Pawlewski (2017) used FWA to assist managers in making portfolio selection decisions for ranking new product projects and artificial neural networks for estimating project performance.

Table 3- Scale of relative importance of performance measurements of each service type

The scale of the relative importance	Trapezoidal fuzzy number	Linguistic variable
1	$(1,1,1,1)$	Equally important
3	$(2,2.5,3.5,4)$	Weakly important
5	$(4,4.5,5.5,6)$	Essentially important
7	$(6,6.5,7.5,8)$	Very strongly important
9	$(8,8.5,9,9)$	Absolutely important

Table 4- Linguistic variable and trapezoidal fuzzy numbers for the evaluation of each PM in the studied region

Scale of evaluation	Trapezoidal fuzzy number	Linguistic variable
1	$(0,0.1,0.2,0.3)$	Very poor
3	$(0.1,0.2,0.3,0.4)$	Poor
5	$(0.3,0.4,0.5,0.6)$	Medium
7	$(0.5,0.6,0.7,0.8)$	Good
9	$(0.7,0.8,0.9,1.0)$	Very good

Therefore, FWAs serve as an aggregation process for multiple criteria decision-making problems. Objects can be ranked using a ranking method based on their outcomes.

Thus, an FWA can be defined as a system that includes both fuzzy criteria ratings and fuzzy weightings (Cho *et al.,* 2012; Chang, Hung, Lin, & Chang, 2006). More information about

the efficient fuzzy weighted average can be found in the publication by Chang, Lee, Hung, Tsai, and Perng (2009).

Second approach for selecting agricultural services

In this paper, a multistep procedure has been developed to investigate the performance measurement of ASSC and improve the ASC's performance. This approach comprises three main steps. The first two steps involve studying the current situation of ASC, while the last step focuses on improving ASC. A schematic diagram of the approach developed in this research is presented in Figure 1.
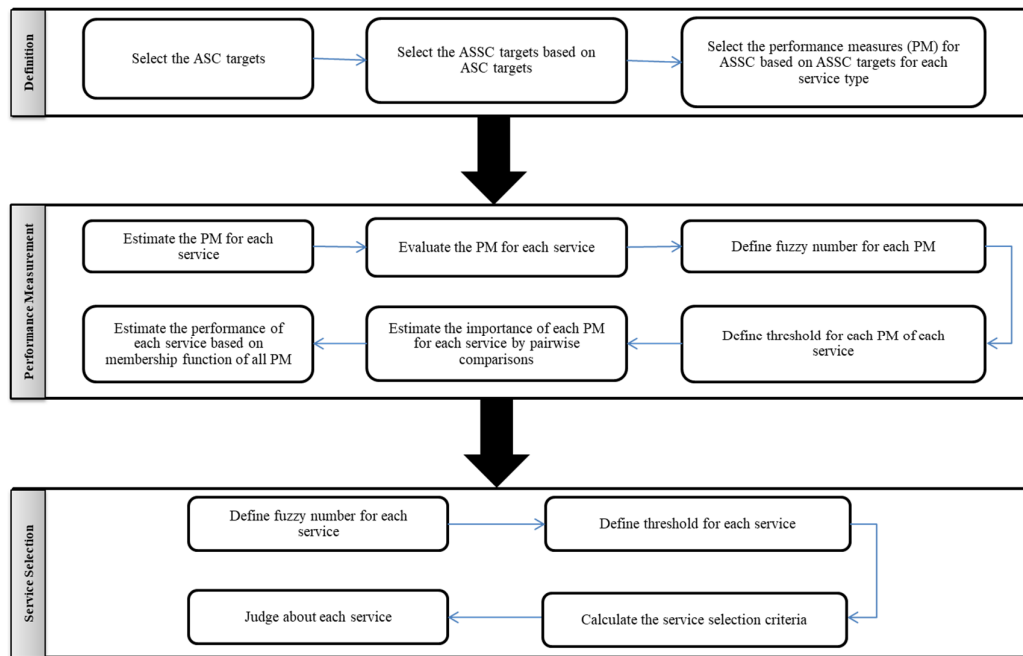
Fig.1. The summary of the second service selection approach

The proposed approach utilizes the fuzzy decision process. This is because when the estimation of a system coefficient is imprecise and only vague knowledge about the actual value of the parameters is available, it may be convenient to represent some or all of them with fuzzy numbers (Zadeh, 1965). The use of fuzzy theory in analyzing supply chains is relevant due to the inherent characteristics of this field. For instance, Mangla *et al.* (2018) employed a combined framework of Interpretive Structural Modeling (ISM) and fuzzy Decision-Making Trial and Evaluation Laboratory (DEMATEL) to analyze the factors that enable sustainability in agrifood supply chains. The desirability of each service performance measurement is represented as a unique left trapezoidal (or right trapezoidal)

fuzzy number. The left trapezoidal numbers are used for performance measurement when a lower value is preferred, while the right trapezoidal numbers are used when a higher value is preferred. In other words, a higher value of the membership function for a PM indicates a higher level of undesirability for that PM. For example, a value of 1 indicates that the PM is highly undesirable. If the membership function for service performance measurement is lower/higher than the threshold for the left and right fuzzy numbers, then the service can be considered as an option for improving performance. The value of the membership function and the relative importance of all performance metrics for each service type is used to determine the worst service viewpoint based on their performance.

These services will be selected for distribution by service centers to improve the quality of service in the region. The proposed selection procedure is formulated as equation (1):

$$A_i = \sum_{j=1}^{m} w_{ij} X_{ij} \quad \forall i \tag{1}$$

Where parameters: w_{ij}, X_{ij} are:
$\sum_{j=1}^{m} w_{ij} = 1 \quad \forall i \qquad 0 \le w_{ij} \le 1$

The value of w_{ij} for performance measurement, j of service i will be estimated using pairwise comparison survey between the performance measurements of service i.

X_{ij}: The membership function value of performance measurement j of service i.

Indices: i, j

i: The index of services $i = 1, 2, \dots, n$.

j: The index of performance measurement $j = 1, 2, \dots, m$. $\qquad 0 \le w_{ij} X_{ij} \le 1$
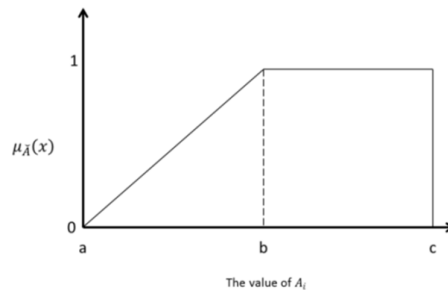
Fig.2. Left trapezoidal Fuzzy number for the A_i

Using the proposed procedure, the service i will be selected to import the service center if the value of $A_i = w_{ij} X_{ij}$ is greater than b (b is a threshold for service i), otherwise, it will not be selected. The left trapezoidal fuzzy number (Fig. 2) is selected here to select the worst services, because A_i was calculated using X_{ij} and a bigger value of X_{ij} indicates more membership degree to the undesirable service set. So whenever A_i is bigger, the chance of service i being selected will increase. So an algorithm is developed to choose which services must be imported to the service center, to create the solution space (Fig.3).

The framework proposed in this paper is a preliminary step towards improving the performance of ASC. After designing the best service packages, a crucial issue is their distribution to evaluate their effectiveness.

The required data for running the developed framework for selecting services is estimated according to the characteristics of the studied region via local database and interviews with farmers.

Results and Discussion

A case study is presented to demonstrate the application of the methodology for resolving ASC performance issues. The region under study is Razan, a county situated in the northern part of Hamedan province in Iran.

Table 5 presents the efficiency criteria values for the studied region, which were derived from local databases and interviews with farmers from the area. The value of each performance measure indicates the current status of that measure in the agricultural supply chain of the region. This criterion can take a value between zero and 100. In each criterion, a larger number indicates a better situation for positive criteria and a worse situation for negative criteria in terms of the efficiency of that service. For example, the number 40, concerning the input supplier's delivery efficiency criterion (PM1) as a negative criterion, whose fuzzy number is of the left type, indicates the relatively good condition of the input suppliers in the region. The higher this number is, the worse the supply services in the region will be. On the

other hand, there are criteria that determine whether the type of fuzzy number associated with them is appropriate. The higher these criteria are, the better the performance. For example, the value of the input quality criterion (PM3) as a positive criterion is equal to 30. By referring to its fuzzy number, it can be concluded that the quality of the input provided in the studied region is not optimal and there is a need to review and correct it. The values of other performance criteria can be judged similarly.
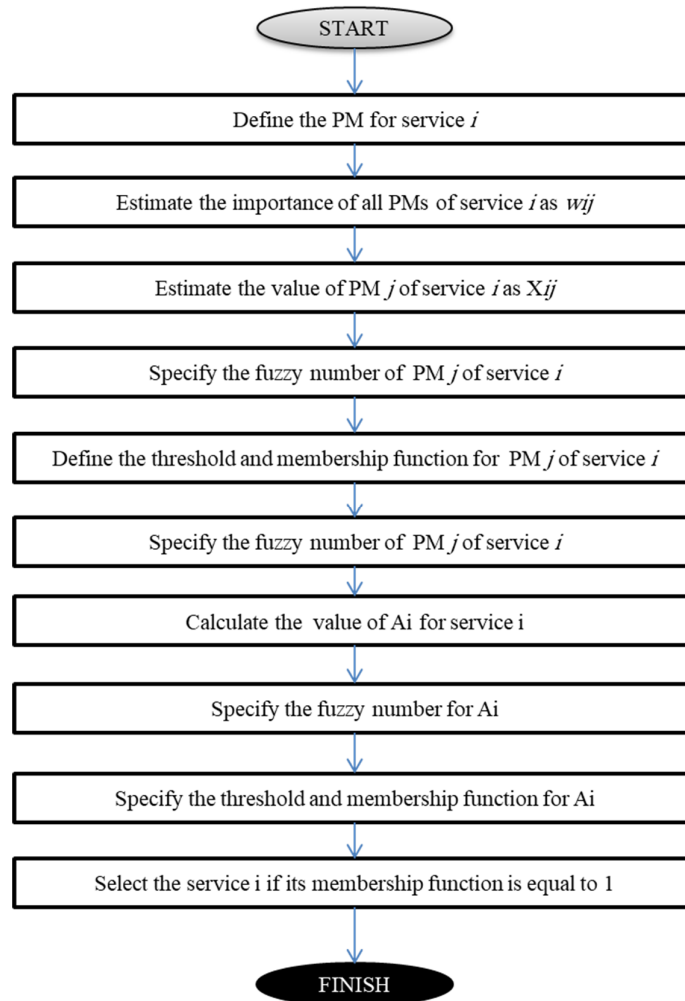

Fig.3. The service selection procedure

Table 5- The value of agricultural supply chain efficiency indicators in the study area

Service	PP1					PR1			PR2	PR3		PO1		PO2		PO3		
#PM	1	2	3	4	5	6	7	8	9	10	11	12	13	14	15	16	17	18
Value	40	60	30	50	70	100	40	70	10	30	60	70	80	100	60	40	20	50

FWA procedure results

The FWA procedure requires determining the fuzzy weights of decision criteria (performance measurements) and decision objects (service types). The fuzzy numbers resulting from the PMs' pairwise comparisons are obtained and represented as a vector of fuzzy weights for each service type in Table 6. The results of the fuzzy weight calculation are shown in Table 7, and these values can be

applied to other case studies. The values of the fuzzy rating in each case study vary. Therefore, we utilized the proposed approach to demonstrate its computation details and results for a region in Iran.

Table 6- Pairwise comparison matrix of the PMs

PP1	CI	PM1	PM2	PM3	PM4
PM1		$(1,1,1,1)$	$(2,2.5,3.5,4)$	$(8,8.5,9,9)^{-1}$	$(2,2.5,3.5,4)$
PM2	0.1	$(2,2.5,3.5,4)^{-1}$	$(1,1,1,1)$	$(6,6.5,7.5,8)^{-1}$	$(2,2.5,3.5,4)$
PM3		$(8,8.5,9,9)$	$(6,6.5,7.5,8)$	$(1,1,1,1)$	$(8,8.5,9,9)$
PM4		$(2,2.5,3.5,4)^{-1}$	$(2,2.5,3.5,4)^{-1}$	$(8,8.5,9,9)^{-1}$	$(1,1,1,1)$
PR1		**PM5**		**PM6**	**PM7**
PM5	0.09	$(1,1,1,1)$		$(6,6.5,7.5,8)$	$(8,8.5,9,9)$
PM6		$(6,6.5,7.5,8)^{-1}$		$(1,1,1,1)$	$(4,4.5,5.5,6)$
PM7		$(8,8.5,9,9)^{-1}$		$(4,4.5,5.5,6)^{-1}$	$(1,1,1,1)$
PR2		**PM8**		**PM9**	
PM8	0.00	$(1,1,1,1)$		$(8,8.5,9,9)$	
PM9		$(8,8.5,9,9)^{-1}$		$(1,1,1,1)$	
PR3		**PM10**		**PM11**	
PM10	0.00	$(1,1,1,1)$		$(6,6.5,7.5,8)$	
PM11		$(6,6.5,7.5,8)^{-1}$		$(1,1,1,1)$	
PO1		**PM12**		**PM13**	
PM12	0.00	$(1,1,1,1)$		$(6,6.5,7.5,8)$	
PM13		$(6,6.5,7.5,8)^{-1}$		$(1,1,1,1)$	
PO2		**PM14**		**PM15**	
PM14	0.00	$(1,1,1,1)$		$(8,8.5,9,9)^{-1}$	
PM15		$(8,8.5,9,9)$		$(1,1,1,1)$	
PO3		**PM16**		**PM17**	**PM18**
PM16	0.08	$(1,1,1,1)$		$(8,8.5,9,9)$	$(6,6.5,7.5,8)$
PM17		$(8,8.5,9,9)^{-1}$		$(1,1,1,1)$	$(2,2.5,3.5,4)$
PM18		$(6,6.5,7.5,8)^{-1}$		$(2,2.5,3.5,4)^{-1}$	$(1,1,1,1)$

Table 7- Evaluated performance measurement of the services and related αcut ($\alpha = 0.5$)

#PM	PM importance			Service evaluation		
	Fuzzy weight	αcut value		Fuzzy rating	αcut value	
PM1	(0.11,0.13,0.17,0.20)	0.12	0.185	(0.3,0.4,0.5,0.6)	0.35	0.55
PM2	(0.07,0.08,0.11,0.13)	0.075	0.12	(0,0.1,0.2,0.3)	0.05	0.25
PM3	(0.60,0.65,0.77,0.84)	0.625	0.805	(0,0.1,0.2,0.3)	0.05	0.25
PM4	(0.03,0.04,0.06,0.07)	0.035	0.065	(0.5,0.6,0.7,0.8)	0.55	0.75
PM5	(0.66,0.72,0.83,0.89)	0.69	0.86	(0.5,0.6,0.7,0.8)	0.55	0.75
PM6	(0.14,0.16,0.19,0.21)	0.15	0.2	(0.3,0.4,0.5,0.6)	0.35	0.55
PM7	(0.04,0.05,0.06,0.07)	0.045	0.065	(0.3,0.4,0.5,0.6)	0.35	0.55
PM8	(0.84,0.87,0.92,0.95)	0.855	0.935	(0.5,0.6,0.7,0.8)	0.55	0.75
PM9	(0.09,0.09,0.10,0.11)	0.09	0.105	(0.7,0.8,0.9,1.0)	0.75	0.95
PM10	(0.73,0.76,0.84,0.89)	0.745	0.865	(0.3,0.4,0.5,0.6)	0.35	0.55
PM11	(0.10,0.11,0.12,0.13)	0.105	0.125	(0.1,0.2,0.3,0.4)	0.15	0.35
PM12	(0.73,0.76,0.84,0.89)	0.745	0.865	(0.3,0.4,0.5,0.6)	0.35	0.55
PM13	(0.10,0.11,0.12,0.13)	0.105	0.125	(0.5,0.6,0.7,0.8)	0.55	0.75
PM14	(0.09,0.09,0.10,0.11)	0.09	0.105	(0.3,0.4,0.5,0.6)	0.35	0.55
PM15	(0.84,0.87,0.92,0.95)	0.855	0.935	(0.5,0.6,0.7,0.8)	0.55	0.75
PM16	(0.66,0.72,0.83,0.87)	0.69	0.85	(0,0.1,0.2,0.3)	0.05	0.25
PM17	(0.11,0.12,0.15,0.17)	0.115	0.16	(0.5,0.6,0.7,0.8)	0.55	0.75
PM18	(0.05,0.06,0.08,0.09)	0.055	0.085	(0.1,0.2,0.3,0.4)	0.15	0.35

Table 8- Overall FWA scores of the agricultural services

Service type	ℓ_0	ρ_0	$\bar{X}$
PP1	0.111858	0.311858	0.211858
PR1	0.496032	0.696032	0.596032
PR2	0.567561	0.767561	0.667561
PR3	0.321264	0.521264	0.421264
PO1	0.371649	0.571649	0.471649
PO2	0.528125	0.728125	0.628125
PO3	0.112319	0.312319	0.212319
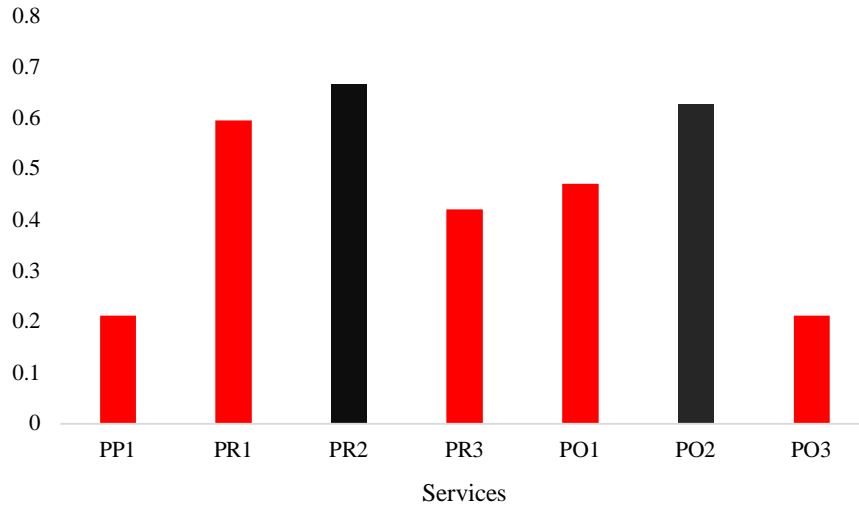
Fig.4. The values of $\bar{X}$ for agricultural services at $\alpha = 0.5$

According to the algorithm developed by Chang *et al.* (2009), the calculation of the benchmark should continue to improve the values of ℓ and ρ until the stop condition is satisfied. Since in this research, the number of evaluation criteria for each service type is small, no sensible improvement has been seen after calculating the ℓ_1 and ρ_1. So we reported the values computed in the first round of calculation in Table 9.

Using the αcut based method, from Fig.4, it can be concluded that red color services have smaller values $\forall \alpha \in (0.5, 1]$. Services with lower values are identified as the poorest quality services. Based on the study, it can be concluded that the services PO3, PP1, PR3, PO1, and PR1 are the worst performing services, in that order. Sustainable development requires sustainable enablers throughout the entire region. In the current supply chain, various services are assumed to

be enablers for sustainable development. To implement any supply chain strategy, it is crucial to establish procedures for it (Mangla *et al.,* 2018). The procedure recommended in current research is to replace underperforming service providers with new ones.

Results of the second approach

To calculate A_i for each service, two parameters must be estimated, i.e. w_{ij} and X_{ij}. The first parameter is estimated using pairwise comparisons, but the second must be estimated in each case study. The value of X_{ij} is the value of PM membership function. Initially, it is essential to calculate the fuzzy number parameters and membership function. After that, based on the PM which was measured in the studied region, the value of X_{ij} can be calculated. The best type of fuzzy number in this study is trapezoidal, because of our aim to

select the worst services using several PMs. For each PM, a unique trapezoidal fuzzy number is defined. The variable $\mu_{\tilde{A}}(x)$ is the membership function of each PM to the undesirable set, i.e. the value of 1 is completely undesirable while the value of zero is completely desirable performance. The direction of desirability differs for each project manager. The desirability of certain PMs has a positive correlation with their value (refer to Fig. 5), while for others, right and left trapezoidal fuzzy numbers are used to represent their desirability. The PM value in the studied region was estimated through a questionnaire administered to experts in the area. With the obtained values for PMs, the computation details of each PM membership function can be calculated as follows:

$$X_{11}(PM1) = \begin{cases} 0, & x < 30 \\ \frac{x-30}{80-30}, & 30 \le x \le 80 \\ 1, & 80 < x < 100 \\ 0, & 100 < x \end{cases}$$

$$X_{11}(50) = \frac{50-30}{80-30} = (0.4)$$

$$X_{12}(PM2) =$$

$$\begin{cases} 0, & x < 0 \\ \frac{x}{20}, & 0 \le x \le 20 \\ 1, & 20 < x < 100 \\ 0, & 100 < x \end{cases}$$

$$X_{12}(10) = \frac{10}{20} = (0,0.5,1,0)$$

$$X_{23}(PM7) = X_{23}(5) = \frac{5}{20} = (0,0.25,1,0)$$

$$X_{13}(PM3) =$$

$$\begin{cases} 0, & x < 0 \\ 1, & 0 \le x \le 80 \\ \frac{100-x}{100-80}, & 80 < x < 100 \\ 0, & 100 < x \end{cases}$$

$$X_{13}(0) = 1 \qquad X_{14}(PM4) = \begin{cases} 0, & x < 0 \\ 1, & 0 \le x \le 50 \\ \frac{100-x}{100-50}, & 50 < x < 100 \\ 0, & 100 < x \end{cases} \qquad X_{14}(70) = \frac{100-70}{100-50} = 0.6$$

$$X_{31}(PM8) = X_{31}(100) = 0$$
$$X_{32}(PM9) = X_{32}(100) = 0 \qquad X_{52}(PM13) = X_{52}(45) = 1 \qquad X_{21}(PM5) =$$

$$\begin{cases} 0, & x < 0 \\ 1, & 0 < x \le 70 \\ \frac{100-x}{100-70}, & 70 < x < 100 \\ 0, & 100 < x \end{cases}$$

$$X_{21}(75) = \frac{100-75}{100-70} = 0.84 \qquad X_{22}(PM6) = \begin{cases} 0, & x < 0 \\ \frac{x}{70}, & 0 < x \le 70 \\ 1, & 70 < x < 100 \\ 0, & 100 < x \end{cases} \qquad X_{22}(50) = \frac{50}{70} = 0.71$$

$$X_{41}(PM10) = X_{41}(60) = \frac{60}{70} = 0.86 \qquad X_{42}(PM11) = \begin{cases} 0, & x < 0 \\ 1, & 0 < x \le 60 \\ \frac{100-x}{100-60}, & 60 < x < 100 \\ 0, & 100 < x \end{cases}$$

$$X_{42}(70) = \frac{100-70}{100-60} = 0.75$$

$$X_{51}(PM12) = X_{51}(50) = 1 \qquad X_{61}(PM14) = \begin{cases} 0, & x < 0 \\ \frac{x}{80}, & 0 < x \le 80 \\ 1, & 80 < x < 100 \\ 0, & 100 < x \end{cases} \qquad X_{61}(80) = \frac{80}{80} = 1$$

$$X_{72}(PM17) = X_{72}(15) = \frac{15}{80} = 0.19 \qquad X_{73}(PM18) = X_{73}(15) = \frac{15}{80} = 0.19 \qquad X_{62}(PM15) =$$

$$\begin{cases} 0, & x < 0 \\ 1, & 0 < x \le 90 \\ \frac{100-x}{100-90}, & 90 < x < 100 \\ 0, & 100 < x \end{cases}$$

$$X_{62}(95) = \frac{100-95}{100-90} = 0.5 \qquad X_{71}(PM16) = \begin{cases} 0, & x < 0 \\ \frac{x}{60}, & 0 < x \le 60 \\ 1, & 60 < x < 100 \\ 0, & 100 < x \end{cases} \qquad X_{71}(70) = 1$$

After this, the value of A_i can be calculated. For example, the value of A_1 is calculated as follows:

$$A_1 = \sum_{j=1}^{4} w_{1j}X_{1j} = (0.56 * 0.4) + (0.08 * 0.5) + (0.32 * 1) + (0.04 * 0.6) = 0.61$$

Similar to A_1, values for all A_i are calculated. The details of the computation for the service selection procedure have been summarized in Table 8. A unique fuzzy number is defined for each PM. The scale of each fuzzy number is specified by three values: a, b, and c. The values of the fuzzy number elements are selected based on the characteristics of each performance measure. For example, let PM1 have a value of 30 for variable a, 80 for variable b, and 100 for variable c. For this PM, the value of 100 represents the maximum time period available for the supplier to deliver inputs to the farmers. The value of a=30 indicates that there is no undesirability in delivering inputs during the first 30% of the designated period. Over time, the level of undesirability will continue to increase. After 80% of the time period has elapsed, the inputs become useless for the farmer. Similar to PM1, we assume fuzzy scales for other performance measures (PMs) ranging from 0 to 100. This simplifies computation and facilitates comparisons. The values of the fuzzy number may change in different conditions and case studies, requiring the definition of new values.

The related fuzzy number of PMs has been shown in Fig. 5. There are both left and right trapezoidal fuzzy numbers and their thresholds are different.

In the final step, after calculating the parameters of the model, the selected services that need to be imported to the service center are determined. A threshold is necessary for the procedure of selecting a service. The procedure involves a fuzzy decision-making process as one needs to consider the vague relationships in service selection. The proposed threshold can be determined based on the input of ASC's strategic managers, and it may vary across different regions. In this case study, a threshold of 0.6 has been selected. Services with a score above 0.6 will be selected and imported to service centers for more efficient distribution. The membership function in a fuzzy number represents the degree of membership of a service to the undesirable service set. This step will select the services that have a membership value of 1. According to the values of A_i, which are illustrated in Fig.6, the services PP1, PR1, PR3, PO1, and PO3 are selected.

Table 9- The values of the service selection procedure

Type of Service	Performance measures	Fuzzy number	Trapezoidal fuzzy scale				The value of PM	Membership function (X_{ij})	w_{ij}	A_i
			a	b	c	d				
(PP1)	PM1	LT*	0.3	0.8	1	1	50	0.40	0.56	
	PM2	LT	0.2	0.5	1	1	10	0.50	0.08	0.61
	PM3	RT**	0	0	0.8	1	0	1.00	0.32	
	PM4	RT	0	0	0.5	1	70	0.60	0.04	
(PR1)	PM5	RT	0	0	0.7	1	75	0.84	0.79	
	PM6	LT	0.35	0.7	1	1	50	0.71	0.14	0.78
	PM7	LT	0.2	0.5	1	1	5	0.25	0.07	
(PR2)	PM8	RT	0	0	0.5	1	100	0	0.83	0
	PM9	RT	0	0	0.5	1	100	0	0.17	
(PR3)	PM10	LT	0.3	0.7	1	1	60	0.86	0.75	0.83
	PM11	RT	0	0	0.6	1	70	0.75	0.25	
(PO1)	PM12	RT	0	0	0.6	1	50	1.00	0.75	1.00
	PM13	RT	0	0	0.5	1	45	1.00	0.25	
(PO2)	PM14	LT	0.3	0.8	1	1	80	1.00	0.13	0.57
	PM15	RT	0	0	0.9	1	95	0.5	0.87	
(PO3)	PM16	LT	0.2	0.6	1	1	70	1.00	0.63	
	PM17	LT	0.5	0.8	1	1	15	0.19	0.26	0.70
	PM18	LT	0.2	0.8	1	1	15	0.19	0.11	

*Left Trapezoidal (LT)   **Right Trapezoidal (RT)
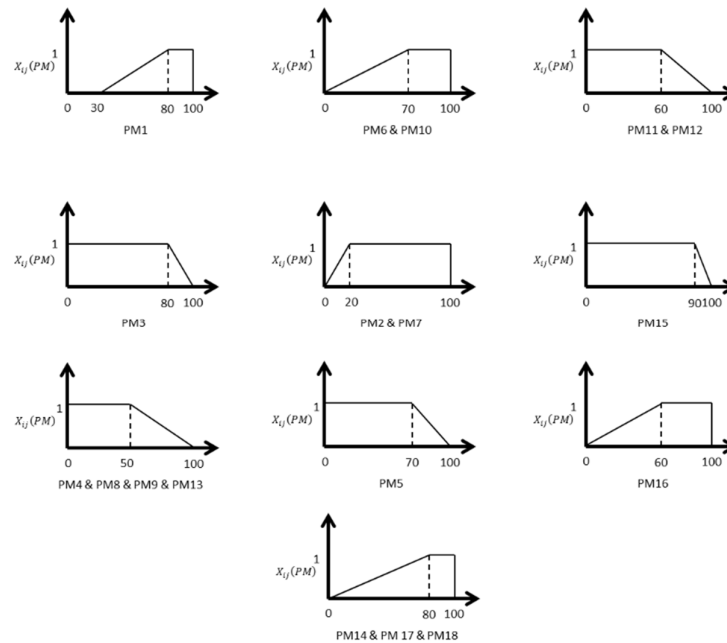
Fig.5. The schematic figure of PMs fuzzy number
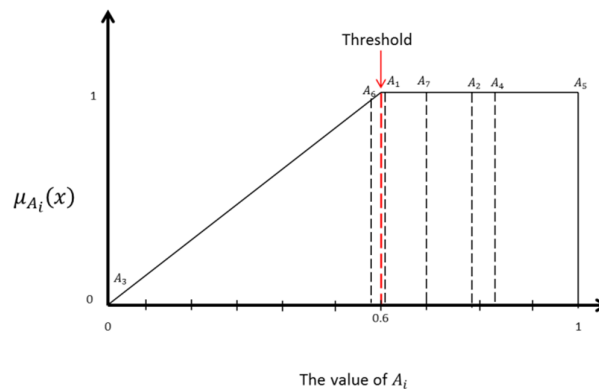
Fig.6. The fuzzy number of A_i

Conclusion

In this research, a new framework has been developed to investigate the performance measurement of agricultural services. The study focuses on seven types of agricultural services and conducts surveys on performance measures for each service type. Two fuzzy-based approaches are proposed to identify services in need of improvement. Improvement actions are suggested to address low performance in professional agricultural service centers, including resource allocation and replacing substandard service providers. Managerial implications include identifying service types and performance measures, utilizing fuzzy-based approaches for service selection, and implementing improvement actions and resource distribution. The research findings and framework can guide decision-makers in the agricultural sector to prioritize actions and allocate resources effectively. Implementing a feedback system is important for improving the results of service package implementation in service centers. Further research is needed to investigate budget and time allocation for improving low-performing services and the location of agricultural service centers.

Declaration of competing interests

The author declares that he has no conflict of interest.

Authors Contribution

M. Zangeneh: Conceptualization, Methodology, Data acquisition, Data pre and post processing, Statistical analysis, Writing and Editing

References

1. Ahumada, O., & Villalobos, J. R. (2009). Application of planning models in the agri-food supply chain: A review. *European Journal of Operational Research, 195*(1), 1-20. https://doi.org/10.1016/j.ejor.2008.02.014
2. Akkerman, R., Farahani, P., & Grunow, M. (2010). Quality, safety and sustainability in food distribution: A review of quantitative operations management approaches and challenges. *OR Spectrum, 32*(4), 863-904. https://doi.org/10.1007/s00291-010-0223-2
3. Allaoui, H., Guo, Y., Choudhary, A., & Bloemhof, J. (2018). Sustainable agro-food supply chain design using two-stage hybrid multi-objective decision-making approach. *Computers & Operations Research, 89*, 369-384. https://doi.org/10.1016/j.cor.2016.10.012
4. Aramyan, C., Ondersteijn, O., van Kooten, O., & Lansink, A. O. (2006). Performance indicators in agri-food production chains. In *Quantifying the agri-food supply chain* (pp. 49–66). Springer.

5. Baltacioglu, T., Ada, E., Kaplan, M. D., Yurt, O., & Kaplan, Y. C. (2007). A new framework for service supply chains. *The Service Industries Journal, 27*(2), 105-124. https://doi.org/10.1080/02642060601122629

6. Banaeian, N., Zangeneh, M., & Golinska-Dawson, P. (2022). Multi-criteria sustainability performance assessment of horticultural crops using DEA and ELECTRE IV methods. *Renewable Agriculture and Food Systems, 37*(6), 649-659. https://doi.org/10.1017/s1742170522000242

7. Bhagwat, R., & Sharma, M. K. (2007). Performance measurement of supply chain management: A balanced scorecard approach. *Computers and Industrial Engineering, 53*(1), 43-62. https://doi.org/10.1016/j.cie.2007.04.001

8. Bigliardi, B., & Bottani, E. (2010). Performance measurement in the food supply chain: A balanced scorecard approach. *Facilities, 28*(5/6), 249-260. https://doi.org/10.1108/02632771011031493

9. Buyukozkan, G., Cifci, G., & Guleryuz, S. (2011). Strategic analysis of healthcare service quality using fuzzy AHP methodology. *Expert Systems with Applications, 38*(8), 9407-9424. https://doi.org/10.1016/j.eswa.2011.01.103

10. Chang, H. H., Hung, C.-J., Wong, K. H., & Lee, C.-H. (2013). Using the balanced scorecard on supply chain integration performance—a case study of service businesses. *Service Business, 7*(4), 539-561. https://doi.org/10.1007/s11628-012-0175-5

11. Chang, P.-T., Hung, K.-C., Lin, K.-P., & Chang, C.-H. (2006). A comparison of discrete algorithms for fuzzy weighted average. *IEEE Transactions on Fuzzy Systems, 14*(5), 663-675. https://doi.org/10.1109/tfuzz.2006.878253

12. Chang, P.-T., Lee, J.-H., Hung, K.-C., Tsai, J.-T., & Perng, C. (2009). Applying fuzzy weighted average approach to evaluate office layouts with Feng-Shui consideration. *Mathematics and Computers in Simulation, 79*(4), 1514-1537. https://doi.org/10.1016/j.mcm.2008.07.038

13. Cho, D. W., Lee, Y. H., Ahn, S. H., & Hwang, M. K. (2012). A framework for measuring the performance of service supply chain management. *Computers & Industrial Engineering, 62*(3), 801-818. https://doi.org/10.1016/j.cie.2011.11.014

14. Despoudi, S., Spanaki, K., Rodriguez-Espindola, O., & Zamani, E. D. (2021). Sustainability in Agricultural 4.0 supply chains. In *Agricultural supply chains and Industry 4.0* (pp. 95-113). Palgrave Macmillan. https://doi.org/10.1007/978-3-030-72770-3_6

15. Dong, W. M., & Wong, F. S. (1987). Fuzzy weighted averages and implementation of the extension principle. *Fuzzy Sets and Systems, 21*(2), 183-199. https://doi.org/10.1016/0165-0114(87)90163-1

16. Ellram, L. M., Tate, W. L., & Billington, C. (2007). Services supply management: The next frontier for improved organizational performance. *California Management Review, 49*(4), 44-66. https://doi.org/10.2307/41166405

17. Evangelista, S. S., Aro, J. L., Selerio, E., & Pascual, R. (2023). An integrated Fermatean fuzzy multi-attribute evaluation of digital technologies for circular public sector supply chains. *International Journal of Computational Intelligence Systems, 16*, Article 122. https://doi.org/10.1007/s44196-023-00294-7

18. Ganeshkumar, C., Pachayappan, M., & Madanmohan, G. (2017). Agri-food supply chain management: Literature review. *Intelligent Information Management, 9*(2), 68-96. https://doi.org/10.4236/iim.2017.92004

19. Ghazinoori, S., Olfat, L., Soofi, J., & Ahadi, R. (2020). Investigating the organic agricultural products supply chain in Iran. *Journal of Agricultural Science and Technology, 20*, 71-85.

20. Graham, M., Kaboli, D., Sridharan, M., & Taleghani, S. (2012). Creating value and sustainability in agricultural supply chains. *MIT Sloan School of Management*.

21. Gunasekaran, A., Patel, C., & McGaughey, R. E. (2004). A framework for supply chain performance measurement. *International Journal of Production Economics, 87*(3), 337-347. https://doi.org/10.1016/j.ijpe.2003.08.003

22. Jifroudi, S., Teimoury, E., & Barzinpour, F. (2020). Designing and planning a rice supply chain: A case study for Iran farmlands. *Decision Science Letters, 9*(2), 163-180. https://doi.org/10.5267/j.dsl.2020.1.001

23. Joshi, R., Banwet, D. K., Shankar, R., & Gandhi, J. (2012). Performance improvement of cold chain in an emerging economy. *Production Planning & Control, 23*(11), 817-836. https://doi.org/10.1080/09537287.2011.642187

24. Kazemi, M. J., & Samouei, P. (2024). A new bi-level mathematical model for government-farmer interaction regarding food security and environmental damages of pesticides and fertilizers: Case study of rice supply chain in Iran. *Computers and Electronics in Agriculture, 219*, Article 108771. https://doi.org/10.1016/j.compag.2024.108771

25. Liou, T. S., & Wang, M. J. J. (1992). Fuzzy weighted average: An improved algorithm. *Fuzzy Sets and Systems, 49*(1), 105-118. https://doi.org/10.1016/0165-0114(92)90282-9

26. Mangla, S. K., Luthra, S., Rich, N., Kumar, D., Rana, N. P., & Dwivedi, Y. K. (2018). Enablers to implement sustainable initiatives in agri-food supply chains. *International Journal of Production Economics, 203*, 379-393. https://doi.org/10.1016/j.ijpe.2018.07.012

27. Manzini, R., & Accorsi, R. (2013). The new conceptual framework for food supply chain assessment. *Journal of Food Engineering, 115*(2), 251-263. https://doi.org/10.1016/j.jfoodeng.2012.10.026

28. Mapes, J., New, C., & Szwejczewski, M. (1997). Performance trade-offs in manufacturing plants. *International Journal of Operations & Production Management, 17*(9), 1020-1033. https://doi.org/10.1108/01443579710177031

29. Morkūnas, M., Rudienė, E., & Ostenda, A. (2022). Can climate-smart agriculture help to assure food security through short supply chains? A systematic bibliometric and bibliographic literature review. *Business, Management and Economics Engineering, 20*(2), 207-223. https://doi.org/10.3846/bmee.2022.17101

30. Oubrahim, I., Sefiani, N., & Happonen, A. (2022). Supply chain performance evaluation models: A literature review. *Acta Logistica, 9*(2), 207-221. https://doi.org/10.22306/al.v9i2.298

31. Ramos, E., Coles, P. S., Chavez, M., & Hazen, B. (2022). Measuring agri-food supply chain performance: Insights from the Peruvian kiwicha industry. *Benchmarking: An International Journal, 29*(5), 1484-1512. https://doi.org/10.1108/BIJ-10-2020-0544

32. Rehman, A. U., Al-Zabidi, A., AlKahtani, M., Umer, U., & Usmani, Y. S. (2020). Assessment of supply chain agility to foster sustainability: Fuzzy-DSS for a Saudi manufacturing organization. *Processes, 8*(5), Article 577. https://doi.org/10.3390/pr8050577

33. Relich, M., & Pawlewski, P. (2017). A fuzzy weighted average approach for selecting portfolio of new product development projects. *Neurocomputing, 231*, 19-27. https://doi.org/10.1016/j.neucom.2016.05.104

34. Routroy, S., & Behera, A. (2017). Agriculture supply chain: A systematic review of literature and implications for future research. *Journal of Agribusiness in Developing and Emerging Economies, 7*(3), 275-302. https://doi.org/10.1108/jadee-06-2016-0039

35. Sengupta, K., Heiser, D., & Koll, L. (2006). Manufacturing and service supply chain performance: A comparative analysis. *Journal of Supply Chain Management, 42*(4), 4-15. https://doi.org/10.1111/j.1745-493x.2006.00018.x

36. Singh, N., Biswas, R., & Banerjee, M. (2023). A systematic review to identify obstacles in the agricultural supply chain and future directions. Journal of Agribusiness in Developing and Emerging Economies. Advance online publication. https://doi.org/10.1108/JADEE-12-2022-0262

37. Thumrongvut, P., Sethanan, K., Pitakaso, R., Jamrus, T., & Golinska-Dawson, P. (2022). Application of Industry 3.5 approach for planning of more sustainable supply chain operations for tourism service providers. *International Journal of Logistics Research and Applications.* Advance online publication. https://doi.org/10.1080/13675567.2022.2090529

38. Trivellas, P., Malindretos, G., & Reklitis, P. (2020). Implications of green logistics management on sustainable business and supply chain performance: Evidence from a survey in the Greek agri-food sector. *Sustainability, 12*(24), Article 10515. https://doi.org/10.3390/su122410515

39. Ulutas, A., Shukla, N., Kiridena, S., & Gibson, P. (2016). A utility-driven approach to supplier evaluation and selection: Empirical validation of an integrated solution framework. *International Journal of Production Research, 54*(5), 1554-1567. https://doi.org/10.1080/00207543.2015.1098787

40. Uysal, F. (2012). An integrated model for sustainable performance measurement in supply chain. *Procedia Engineering, 62*, 689-694. https://doi.org/10.1016/j.sbspro.2012.09.117

41. van der Vorst, J. G. A. J., Peeters, L., & Bloemhof, J. M. (2013). Sustainability assessment framework for food supply chain logistics: Empirical findings from Dutch food industry. *International Journal on Food System Dynamics, 4*(2), 130-139. https://doi.org/10.18461/ijfsd.v4i2.424

42. Vorst, J. G. A. J. (2005). Performance measurement in agri-food supply chain networks. In C. J. Ondersteijn (Ed.), *Quantifying the agri-food supply chain* (pp. 13–24). Springer.

43. Wu, X. Q., Pu, F., Shao, S. H., & Fang, J. N. (2004). Trapezoidal fuzzy AHP for the comprehensive evaluation of highway network programming schemes in Yangtze River Delta. *Proceedings of the 5th World Congress on Intelligent Control and Automation, Hangzhou, 15-19 June 2004* (pp. 4114-4118). IEEE. https://doi.org/10.1109/wcica.2004.1343719

44. Zadeh, L. A. (1965). Fuzzy sets. *Information and Control, 8*(3), 338-353. https://doi.org/10.1016/S0019-9958(65)90241-X

45. Zangeneh, M., Nielsen, P., Akram, A., & Keyhani, A. (2014). A performance evaluation system for agricultural services in agricultural supply chain. *Management and Production Engineering Review, 5*(3), 70-80.

46. Zheng, G., Zhu, N., Tian, Z., Chen, Y., & Sun, B. (2012). Application of a trapezoidal fuzzy AHP method for work safety evaluation and early warning rating of hot and humid environments. Safety Science, 50(2), 228-239. https://doi.org/10.1016/j.ssci.2011.08.042

47. Zimmermann, H. J. (2001). *Fuzzy set theory—and its applications* (4th ed.). Springer. https://doi.org/10.1007/978-94-010-0646-0

توسعه چارچوب مدیریت خدمات در زنجیره تامین کشاورزی با میانگین موزون فازی

مرتضی زنگنه [iD] [1]*

چکیده

هدف اصلی این تحقیق ایجاد چارچوبی جامع برای ارزیابی عملکـرد در زنجیـره تـامین کشـاورزی و توسـعه دو رویکـرد بـرای بهبـود آن می‌باشـد. مرتبط‌ترین معیارهای عملکرد برای ارزیابی وضعیت فعلی خدمات در زنجیره تامین کشاورزی (ASC) انتخاب شدند. نـوآوری ایـن تحقیـق بـه انتخـاب شاخص‌های کلیدی عملکرد (KPI) و رویکردهایی برای افزایش عملکرد ASC مربوط می‌شود. چارچوب پیشنهادی شامل اندازه‌گیری عملکرد و فرآیند انتخاب خدمات است. دو رویکرد بر اساس KPIهای منتخب از خدمات در ASC توسعه داده شده است تا مشخص شود کـدام خـدمات نیـاز بـه بهبـود دارند. رویکردهای پیشنهادی ابزارهای قوی و همه‌کاره‌ای برای مدیران کشاورزی هستند تا زنجیره‌های تامین خود را ارتقا دهند. یک مطالعه مـوردی نیـز از ایران ارائه شده است. چارچوب پیشنهادی برای این منطقـه، رویکردهـای انتخـاب خـدمات کشـاورزی ماننـد مشـاوره پـس از تولیـد، حمایـت مـالی، مکانیزاسیون، مشاوره تجاری و تامین نهاده را در اولویت قرار می‌دهند. این چارچوب نشان می‌دهد که این خـدمات بایـد بـه‌منظور پاسـخ‌گویی بهتـر بـه نیازهای منطقه مورد مطالعه بهبود یابد.

واژه‌های کلیدی: خدمات، زنجیره تامین، سنجش عملکرد، فازی، کشاورزی

1- گروه مهندسی بیوسیستم، دانشکده علوم کشاورزی، دانشگاه گیلان، رشت، ایران

(Email: zanganeh@guilan.ac.ir :نویسنده مسئول -*)

Qualitative Analysis of Apple Fruit during Storage using Magnetic Resonance Imaging

R. Khodabakhshian Kargar [ID][1*], **R. Baghbani** [ID][2]

1- Department of Biosystems Engineering, Faculty of Agriculture, Ferdowsi University of Mashhad, Mashhad, Iran
2- Department of Agricultural Engineering, National University of Skills (NUS), Tehran, Iran
(*- Corresponding Author Email: Khodabakhshian@um.ac.ir)

Abstract

Magnetic resonance imaging (MRI) is a non-destructive technique for determining the quality of fruits which, with different protocols, shows the density and structure of hydrogen atoms in the fruit in which it is placed. This study compared MRI images of healthy and bruised apple flesh tissues, both with and without pests, using various protocols to identify the best one. For this purpose, magnetic resonance imaging (MRI) using two protocols: T_1 (Spin-lattice relaxation time) and T_2 (Spin-spin relaxation time), was carried out on 200 apple fruits that were loaded during storage. The loading of fruits was performed at four levels: 150, 300, 450, and 600 N in a quasi-static manner, and then stored for periods of 25, 50, and 75 days at 4 °C. At the end of each storage period, imaging was carried out. Then, the contrast of T_1 and T_2 images of healthy and bruised tissue of apple fruit with and without pests using ImageJ software was determined. It was concluded that the healthy tissue of apple fruit without pests was clearer in T_1 images than in T_2 images. It has also been seen that the bruised area of fruits without pests in T_2 images is more recognizable than in T_1 images.

Keywords: Apple fruit, Histogram analysis, Magnetic resonance imaging, Quality

Introduction

The apple fruit with the scientific name Malus Domestica is a widely consumed fruit known for its rich content of sugars, vitamins, anthocyanins, minerals, and various other nutrients (Zhang *et al.,* 2019). Nowadays, apples are regarded as one of the most important sources of health benefits due to their components, which include antioxidants, antimicrobial agents, and wound-healing properties (Zhang *et al.,* 2022). One of the factors that caused the drop in the quality of

apple fruit is pest. Also, the risk of quality loss is increased by the fact that fresh fruit is highly perishable during storage and transportation (Shicheng, Youwen, Ping, Kuan, & Shiyuan, 2019). Due to the prevalence of pests in apple fruit, as well as compressive forces and external stresses during harvest, transportation, etc., detection of decayed fruit is essential. However, detection of decayed apple fruit mostly relies on manual work. Manual work is inefficient and unreliable (Leiva-Valenzuela & Aguilera, 2013). Therefore, to ensure the minimum acceptability of the fruit's quality to consumers, a healthy, non-destructive, high-accuracy method should be used in the quality sorting of apple fruit.

During the last decade, many researchers have used non-destructive methods to study

the quality of foods and fruits such as electronic tongue and electronic nose (Lu, Hu, Hu, Li, & Tian, 2022); x-ray computed tomography (Olakanmi, Karunakaran, & Jayas, 2023); ultrasonic wave propagation (Mierzwa, Szadzinska, Gapinski, Radziejewska-Kubzdela, & Biegańska-Marecik, 2022); hyperspectral imaging (Khodabakhshian & Emadi, 2017; Wieme et al., 2022); nuclear magnetic resonance (Ozel & Oztop, 2021; Perez-Palacios et al., 2023); near infrared spectroscopy (Lan et al., 2022) and Raman spectroscopy (Khodabakhshian, 2022). Among these methods, magnetic resonance imaging (MRI) has become well known due to its advantages, such as reliable online quality assessment, excellent soft tissue differentiation compared to X-ray imaging, and its applications in studying the ripening stage and ripening of fruits, pathogen invasion, tissue chemistry, water transfer and diffusion, and oxygen diffusion in agricultural products (Srivastava, Talluri, Beebi & Kumar, 2018; Perez-Palacios et al., 2023). On the other hand, this non-destructive technique can analyze the distribution and motility of protons in water molecules and other metabolites concentrated in biological tissue. So, it is usable to determine the change in the concentration of oil and water in food and agricultural products, which is usually associated with maturity, damage and fruit rot (Perez-Palacios et al., 2023).

Usually, three types of protocols are used in magnetic resonance imaging: T_1, T_2, and proton density-weighted images. T_1 and T_2 are two completely separate time parameters that can be detected and measured after RF pulse excitation. The comparison between these two times and their ratio in different states is the basis of magnetic resonance imaging (Perez-Palacios et al., 2023). The MRI imaging protocol is determined by considering the structure of the tissue being imaged in terms of the density of water and hydrocarbon molecules.

Many researchers have used magnetic resonance imaging to study agricultural products (Defraeye et al., 2013; Galed,

Fernández-Valle, Martinez, & Heras, 2004; Gonzalez et al., 2001; Herremans et al., 2014; Mazhar et al., 2015; Ozel & Oztop, 2021; Perez-Palacios et al., 2023; Razavi, Asghari, Azadbakh, & Shamsabadi, 2018; Shicheng et al., 2019; Zhang & McCarthy, 2012). In one research, the effect of force and storage time on the distribution of bruising volume of Darghazi pears was studied with the help of image data obtained from magnetic resonance imaging, and they concluded that the applied force leads to a linear increase in the bruising volume during the storage period, while the effect of storage time on the diffusion of distribution of bruising is non-linear (Razavi et al., 2018). Shicheng et al. (2019) used low-field nuclear magnetic resonance (LF-NMR) data to detect decayed blueberry fruit from healthy. Also, in another experiment, Gonzalez et al. (2001) investigated the development of internal tissue browning due to high levels of carbon dioxide in the storage of Fuji apples in a controlled atmosphere, and it was concluded that T_2 measurements of images produced better contrast between normal tissue and tissue with intrinsic browning compared to the image produced using differences in proton density or T_1 measurements.

Therefore, the aim of the current research was to determine which MRI protocol performed best for different parts of the apple fruit. The two imaging protocols, T_1 and T_2, were compared across various areas of the apple, including the healthy tissue, bruised areas, and the fruit core, using the desired protocols for both pest-free and pest-infested apples.

Materials and Methods

Sample collection and preparation

In this experiment, a total of 200 apple fruits of the same size, grown in 2021 from a commercial orchard in Mashhad, Khorasan Razavi province, Iran were randomly collected. The physico-chemical properties of the studied apple variety are shown in Table 1. The fruits were divided into two groups, based on the subjective evaluation of their skin

texture: (i) Healthy fruits without pests, and (ii) Infected fruits infested with pests. Then all samples were individually washed, numbered and placed in plastic boxes. After selection, apples were transported to the physical properties laboratory and stored in periods of 25, 50, and 75 days at 4 °C. Before starting the experiment, the samples were taken out of the refrigerator and placed at room temperature (22°C) for approximately 2 hours in order to reach temperature equilibrium (Khodabakhshian *et al.,* 2017). MRI experiments were performed on all samples.

Table 1- Physico-chemical properties of the studied apple variety

Variety	Soluble Solids (Brix)	Titratable Acidity (gL^{-1})	pH	Geometric mean diameter (mm)	Fruit density (gcm^{-3})	Moisture (% w.b.)
Golden Delicious	13.2 ± 0.4	0.6 ± 0.1	3.5 ± 0.2	65.09 ± 5.2	0.94 ± 0.12	86.68 ± 0.13

In order to study apple susceptibility to bruising during the storage period, the quasi–static compression was used to create the bruised area. The quasi– static compression force was exerted on equatorial regions of samples of each group by the same probe (plunger) using Mechanical Testing Machine (Model H5KS, Tinius Olsen Company) with a load cell of 5 4903.33 N. Each individual sample was loaded at pretest speed 1.5 mm min^{-1}, the test speed of 0.5 mm min^{-1}, four levels 150, 300, 450, and 600 N (Khodabakhshian, Emadi, Khojastehpour, & Golzarian, 2019). These four levels were selected to load the samples (in three replications) according to the initial tests on the fruit. It was observed that a force higher than this amount caused the complete failure of the fruit and on the other hand, a force less than about 150 Newtons did not have a significant effect on the fruit. In this experiment, samples were positioned horizontally (Figure 1) during loading, and the amount of force-deformation of the fruits were recorded.

MRI measurements

Magnetic resonance imaging was performed with two protocols T$_1$ and T$_2$ to examine the differences between these types of imaging and to detect healthy, infected, and bruised areas of the samples, as well as the ability to detect its various components and tissues. T$_1$ imaging differentiates between adipose tissue and water, showing water as lighter than adipose tissue. T$_2$ imaging, similar to T$_1$-weighted imaging, separates fat and water but with the difference that fat appears lighter and water appears darker in the image (McRobbie, Moore, Graves, & Prince 2009; Perez-Palacios *et al.,* 2023). As it was stated in section 2.1, the samples were stored for periods of 25, 50, and 75 days at 4 °C in a refrigerator. At the end of each period of storage, magnetic resonance imaging with T$_1$ and T$_2$ protocols was performed using Alltech EchoStar 1.5T magnetic resonance imaging device in Aref Imaging Medical Center in Mashhad, Khorasan Razavi province, Iran (Figure 2). These images were acquired with a field of view of 350×350 mm, thickness of 3 mm, pixel depth of 3 mm, recovery time (TR) of 905 ms, effective echo time (TE) of 10 ms for T$_1$, and TR of 5598 ms and TE f 100 ms for T$_2$. The total acquisition time was 4 min 2s for all the slices, for all experiments (Herremans *et al.,* 2014; Noshad, Asghari, Azadbakht, & Ghasemnezhad, 2020). For each fruit, approximately 45 slices were obtained, ranging from 43 to 47, depending on the apple size. ImageJ software was used to compare the contrast in T$_1$ and T$_2$ images. With help of this software, samples of healthy tissue, infected tissue, and bruised tissue due to quasi-static compression were studied and the histogram of these samples were compared.

Data Analysis

A completely randomized design (CRD) in factorial with two experimental factors was employed, studying two factors: loading force

and storage period. These two factors were tested across both healthy and infected fruit groups, with three replications. All data were subjected to one-way analysis of variance, ANOVA using SPSS19 software. The F test was used to determine the significance of independent factors (loading force and storage period), and significant differences of means were compared using the Duncan's multiple ranges test at 5% significant level.

Results and Discussion

The results of variance analysis which was carried out to examine the effect of loading variables, storage time and their interaction on the amount of light intensity in images taken with protocols T_1 and T_2 for flesh tissue and bruised part of apple fruit without pests and with pests is shown in Table 2.

Table 2- Analysis of variance of factors considered on the T_1 and T_2 images of apple fruit

Factors	df	T_1 image of flesh tissue without pests	T_2 image of flesh tissue without pests	T_1 image of bruised tissue without pests	T_2 image of bruised tissue without pests
		Mean squares			
Loading force	3	1597.72*	2896.51**	88.91 ns	205.11 ns
Storage period	2	1884.51**	314.23 ns	8652.13**	3096.22**
Loading force × Storage period	6	625.23*	481.22 ns	65.11 ns	29.53 ns
Error		118.12	156.62	97.15	42.84
Coefficient of variation		10.25	12.26	19.42	20.72

	df	T_1 image of bruised tissue with pests	T_2 image bruised tissue with pests	T_1 image of flesh tissue with pests	T_2 image flesh tissue with pests
Loading force	3	682.42**	47.62*	432.86 ns	1976.85*
Storage period	2	9586.22**	3982.27**	38.56 ns	2453.22**
Loading force × Storage period	6	212.91**	38.52 ns	796.22 ns	352.91 ns
Error		31.25	22.47	683.57	501.22
Coefficient of variation		15.76	18.74	19.49	22.05

** Significant at the 1% level, * Significance at the 5% level, and ns Non – significant

Histogram analysis of T_1 and T_2 images of flesh tissue of apple fruits without pests

A sample of images with T_1 and T_2 protocols related to flesh tissue of pest-free apple fruits without applying force and also the histogram of a sample of their selected area are shown in Figure 1. As can be seen in this figure, the intensity of brightness in the T_1 images is higher than in the T_2 images. Also, the standard deviation of the sample histogram with T_2 protocol is more than T_1 protocol, which indicates more fluctuations in images with T_2 protocol. Therefore, it can be concluded that the weighted images taken with protocol T_1 are completely different. That is, tissues with a long T_1 have the weakest signal, which causes the T_1 images to be brighter. In

other words, the bright pixels in the images with the T_1 protocol are related to short T_1 (1500-2000 ms) (Li, Li, & Zhang, 2018; Shicheng et al., 2019).

According to the results obtained for flesh tissue of apple fruits without pests with T_1 protocol, loading force (p<0.05), storage period (p<0.01), and their interaction (p<0.05) were significant (Figure 2a). Additionally, on the basis of the acquired results, with increasing storage time and loading force, the brightness (from 0 to 255) of flesh tissue of pest-free apple fruits decreased with T_1 protocol and its value became darker (got closer to zero), which means a change in tissue color due to pressure. No statistically significant differences were observed in the loading forces during the storage periods of 25

and 50 days, nor in the forces of 450 and 600 N across the storage durations of 1, 25, 50, and 75 days. Also, as can be found from Table 2, only the loading force was significant ($p<0.01$) and the storage period and their interaction were not significant for flesh tissue of apple fruits without pests with T_2 protocol.

According to Figure 2b, it is apparent that there is a significant difference between all four loading forces and the brightness significantly decreased with increasing of loading force so the maximum and minimum of brightness belonged to loading forces of 150 N and 600 N, respectively.
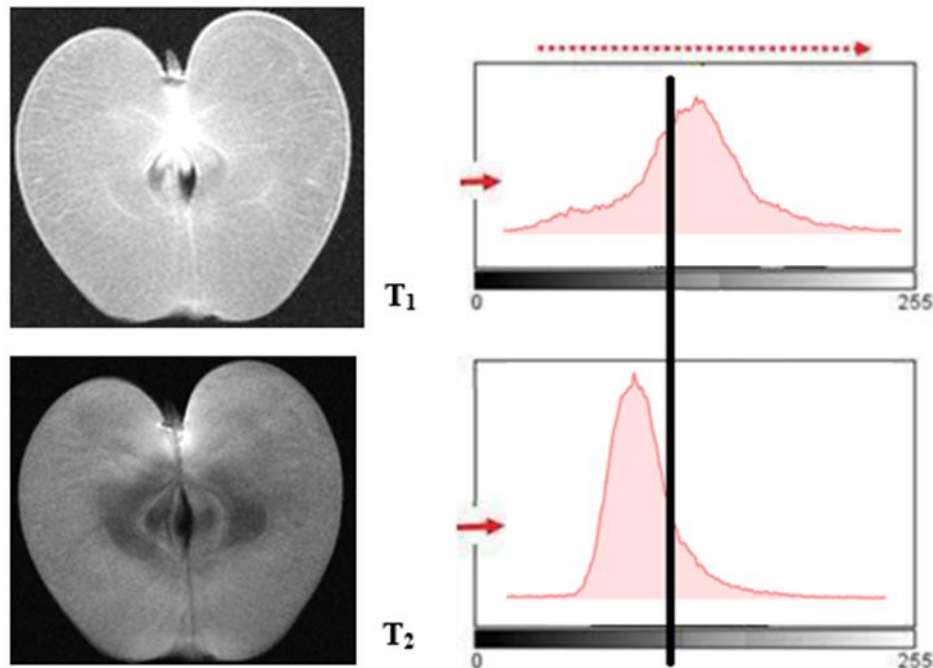
Fig. 1. Histogram of magnetic resonance imaging with T_1 and T_2 protocol of pest-free apple fruits without applying force
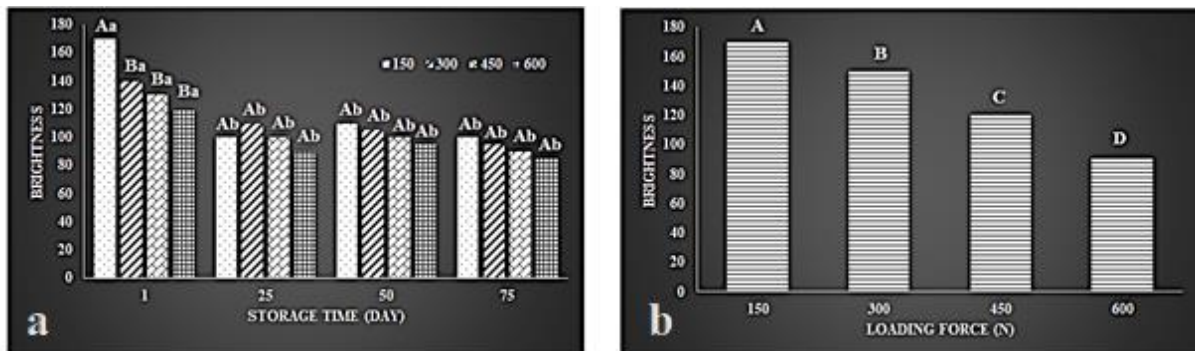
Fig. 2. **a:** Interaction effect of loading force and storage time on light intensity of flesh tissue of apple fruits without pests with T_1 protocol. **b:** Comparison of the mean effect of loading force on the brightness of flesh tissue of apple fruits without pests with T_2 protocol. Uppercase letters indicate insignificance in a fixed storage period and lowercase letters indicate insignificance in a fixed loading force

Histogram analysis of T_1 and T_2 images of flesh tissue of apple fruits with pests

Figure 3 shows an example of images with T_1 and T_2 protocols related to flesh tissue of

apple fruits with pests. As it can be seen, the track of the pest passage in T_1 and T_2 images is quite clear, although due to the presence of

hydrocarbon residues of the pest, fewer details of the track were detectable in T_1 images. At first, the pupae of the "Apple" fruit pest enter the "Apple" seeds, and since the "Apple" seeds are seen in T_1 images, the details of the pest infestation of the seeds are more specific in this type of imaging. Similarly, Haishi, Koizumi, Arai, Koizumi, and Kano (2011) investigated the contamination of apple fruits harvested by peach fruit moth (*Carposina sasakii Matsumura*) using non-destructive magnetic resonance imaging (MRI) and T_1 and T_2 protocols. Similar researches were also done by Herremans *et al.* (2014), Mazhar *et al.* (2015), Shicheng *et al.* (2019), and Noshad *et al.* (2020) on apple, avocado, blueberry, and quince fruits, respectively, using low field nuclear magnetic resonance and T_1 and T_2 images.
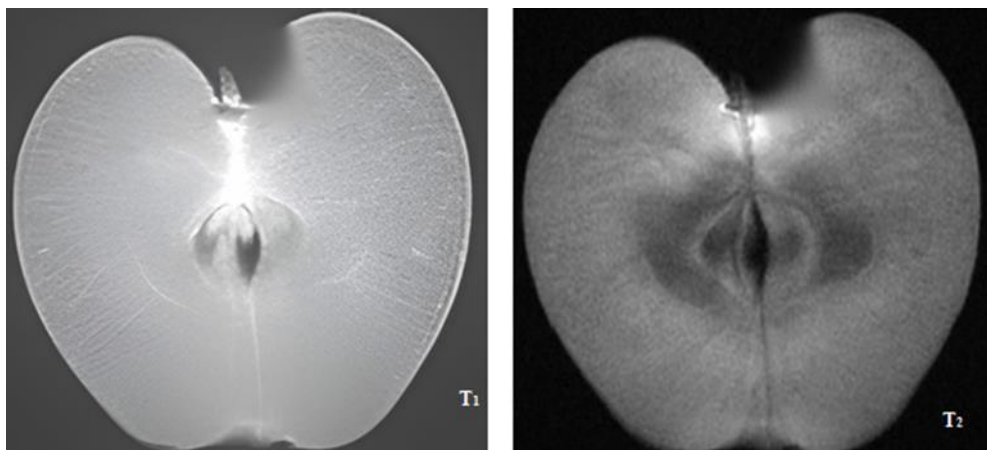
Fig. 3. Comparison of magnetic resonance images of T_1 and T_2 protocols related to flesh tissue of apple fruits with pests

According to the results (Table 2), none of the factors were significant for the flesh tissue of infected apple fruits with T_1 protocol, but with T_2 protocol, the effect of two factors of loading force and storage period were significant ($p<0.01$). As it can be found from Figure 4, the light intensity of flesh tissue of infected apple fruits "goes" to the blurred, of course, there was no statistically significant difference between 300, 450, and 600 N forces, but these three forces had a significant difference with the force of 150 N. It can also be seen that with increasing storage period, the light intensity of flesh tissue of pest infested apple fruits become darker and of course there is no statistically significant difference between samples of storage period after 25, 50, and 75 days. However, there are statistically significant differences between these three storage periods and the samples taken on the first day.

Histogram analysis of T_1 and T_2 images of bruised tissue of apple fruits without pests

As shown in Figure 5, the bruised area is clearer in the T_2 protocol image. This is due to the exit of more water molecules and the decrease of moisture from the cells of this area and absorption by other areas during 75 days of storage, but in the image with the T_1 protocol, there is not much difference in the area bruised compared to other areas because the loaded areas show lower water content (shorter T_2 time) compared to unloaded areas with higher water content (longer T_2 time). This justification was also presented by McRobbie *et al.* (2009).
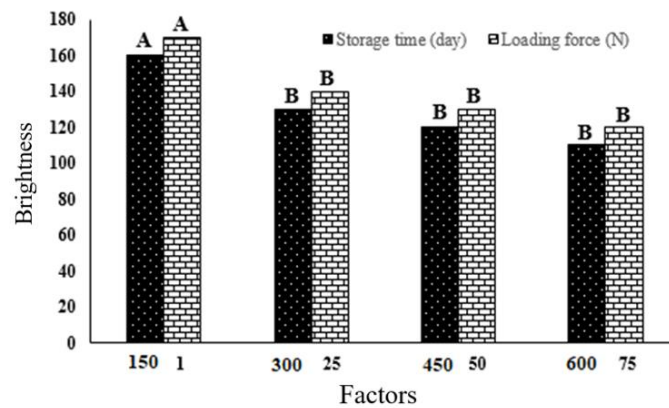
Fig. 4. Mean Comparison of the effect of loading force and storage period on the brightness of the T_2 images of flesh tissue of pest infested apple fruits
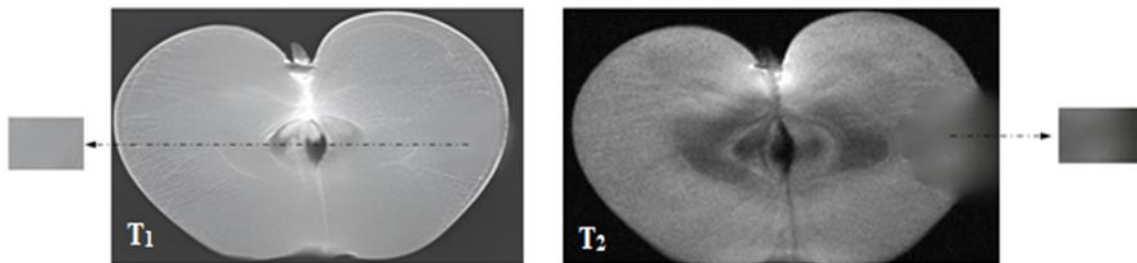
Fig. 5. Difference between T_1 and T_2 magnetic resonance images of the bruised tissue of apple fruits without pests after 75 days of storage

For the bruised tissue of apple fruit without pest with T_1 protocol only the storage period was significant (p<0.01) and their loading force and interaction were not significant (Table 2). The results of comparing the mean in Figure 6 show that as the storage period increases, the brightness of the bruised fruit with the T_1 protocol becomes darker and there is a statistically significant difference between them. Only the storage period was significant (p<0.01) for the pest-free bruised tissue of apple fruit with T_2 protocol and the loading force and the interaction of these two factors were not significant. According to Figure 8, with increasing storage period, the amount of darkness for the bruised tissue increases and a significant difference is observed between the

two storage periods of 50 and 75 days. In a similar experiment on Fuji apples, Gonzalez et al. (2001) studied the development of internal tissue bruising due to high levels of carbon dioxide in controlled atmospheric storage and concluded that T_2 measurements of images with better contrast provide a contrast between normal tissue and tissue with internal browning relative to the image produced using differences in proton density or T_1 measurements. These results were also similar to the results of Hernández-Sánchez, Hills, Barreiro, & Marigheto (2007), Defraeye et al. (2013), and Noshad et al. (2020) on internal browning of pear, apple, and quince fruits using T_2 protocol, respectively.
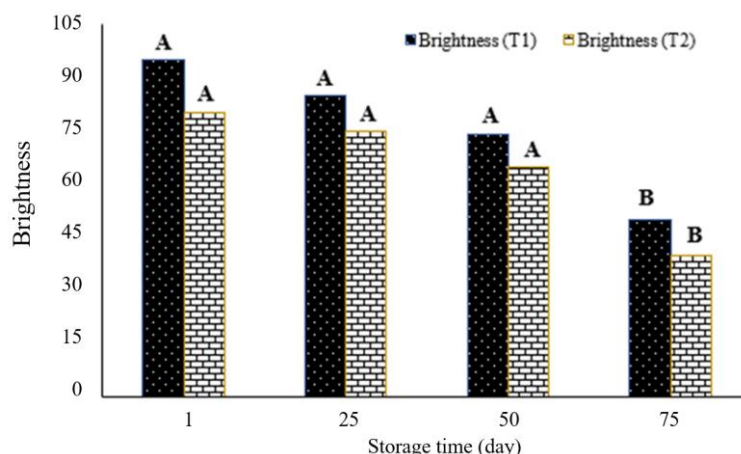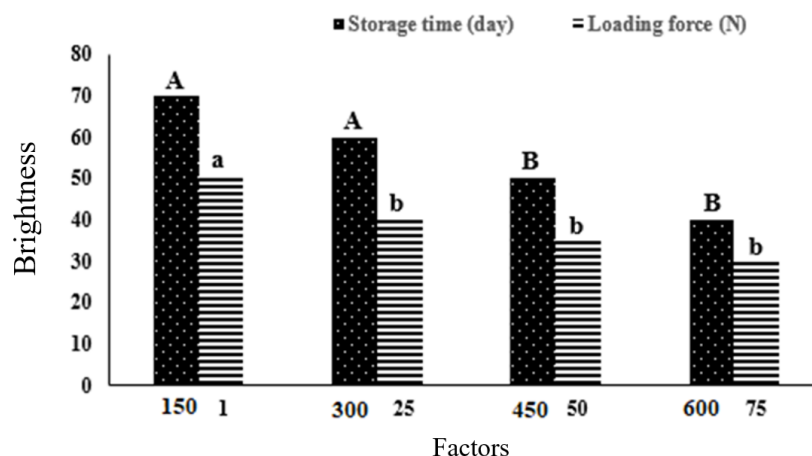
Fig. 6. Mean Comparison of the effect of storage period on the brightness of T_1 and T_2 images of bruised tissue of apple fruit without pest

Histogram analysis of T_1 and T_2 images of bruised tissue of apple fruits with pests

Figure 7 shows the difference between the magnetic resonance images with the T_1 and T_2 protocols of bruised tissue of apple fruits with pests. As shown in the figure, the bruised tissue with the T_1 protocol is clearer, because the infected tissue loses its moisture by creating an empty space by the pest over time. Also, the loaded area is darkened due to the decrease in moisture because with increasing interval the humidity decreases after loading

(Diels *et al.,* 2017; Noshad *et al.* 2020). According to the results (Table 2), the contaminated tissue of apple fruit bruised with T_1 protocol was significant for both loading force and storage period (p<0.01) and the interaction of these two factors was also significant. Furthermore, based on Figure 8, it can be concluded that the light intensity of the bruised tissue of apple fruit decreased with increasing storage period and this was observed for all four loading forces.
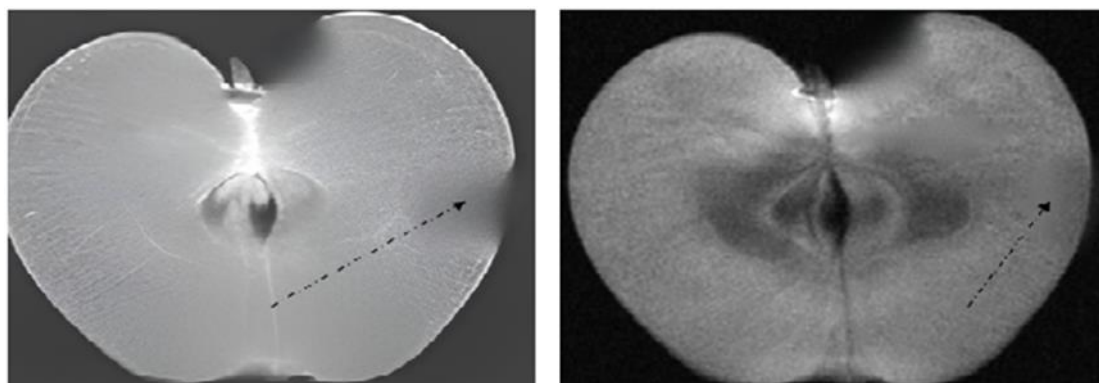
Fig. 7. Difference between T_1 and T_2 magnetic resonance images of the bruised area of apple fruit with pest
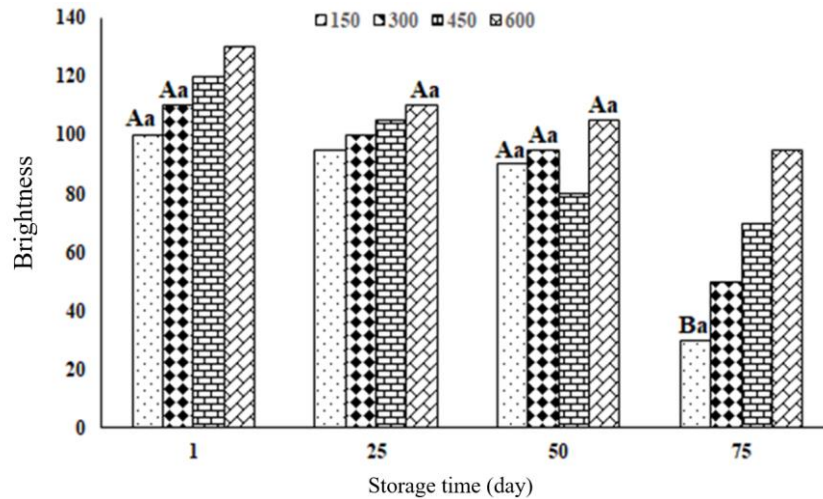
Fig. 8. Interaction effect of loading force and storage time on light intensity of bruised tissue of apple fruits with pests by T_1 protocol. Uppercase letters indicate insignificance in a fixed storage period and lowercase letters indicate insignificance in a fixed loading force

There was no statistically significant difference between loading forces for samples in the storage period of 25-day and also there was no statistically significant difference between loaded forces of 150 and 600 N for 50-day storage period, but a significant difference was observed between all four loading forces in 75-day storage period. In addition, the effect of loading force parameters ($p<0.05$) and storage period ($p<0.01$) on the bruised tissue of apple fruits with pests by T_2 protocol were significant and the interaction of these two factors was not significant. According to Figure 9, it is clear that with increasing loading force, the amount of bruised tissue in the infected fruit became darker and a statistically significant difference was observed between the forces of 150 and 600 N for the specified value. Also, with increasing the storage period from 25 to 75 days, the light intensity of the bruised fruit tissue becomes darker and there is a statistically significant difference between these storage periods. These results were also similar to the results of Noshad *et al.* (2020) on internal browning of quince fruit using low field nuclear magnetic resonance and T_1 and T_2 images.

Fig. 9. Mean Comparison of the effect of storage period and loading force on the brightness of T_1 images of bruised tissue of apple fruit with pest

Conclusion

This study investigates the application of magnetic resonance imaging (MRI) for qualitative analysis of apple fruit during storage, focusing on both healthy and pest-infected samples. The research employs T_1 (spin-lattice relaxation time) and T_2 (spin-spin relaxation time) MRI protocols to assess differences in tissue structure and water content over a storage period of 25, 50, and 75 days at 4°C. A total of 200 apples were subjected to quasi-static loading at four levels (150, 300, 450, and 600 N) to induce bruising, mimicking conditions encountered during handling and transportation.

The key findings indicate that T_1 imaging provides clearer differentiation of flesh tissue in pest-free apples, whereas T_2 imaging enhances the visibility of bruised areas, particularly in apples without pest. In the case of pest-infected apple fruits, both T_1 and T_2 MRI protocols revealed distinct characteristics of tissue integrity and pest infiltration. T_1 imaging showed identifiable tracks of pest pathways, particularly around seeds, where the infestation was more pronounced. Meanwhile, T_2 imaging provided clearer visualization. The study highlights significant effects of loading force and storage duration on MRI image contrast, revealing distinct patterns in tissue degradation and water distribution. Histogram analyses of T_1 and T_2 images further illustrate these differences, showing variations in brightness and standard deviation across different experimental conditions.

Overall, MRI proves to be effective in non-destructively assessing the quality of apple fruit, offering insights into structural changes, moisture loss, and pest-induced damage. This research underscores the potential of MRI as a robust tool for quality assessment in agricultural produce, contributing valuable data to improve storage and transportation practices.

Acknowledgment

Declaration of competing interests

The authors declare that they have no conflict of interest.

Authors Contribution

R. Khodabakhshian Kargar: Supervision and management, Data collection, Data processing, Statistical analysis, Validation, Extracting, and preparing the primary text

R. Baghbani: Conceptualization, Methodology, Technical consultation, Software services, Interpreting the results, Editing, and translating the text.

References

1. Defraeye, T., Lehmann, V., Gross, D., Holat, C., Herremans, E., Verboven, P., Verlinden, B. E., & Nicolai, B. M. (2013). Application of MRI for tissue characterisation of 'Braeburn' apple. *Postharvest Biology and Technology, 75*, 96-105. https://doi.org/10.1016/j.postharvbio.2012.08.009

2. Diels, E., Dael, M. V., Keresztes, J., Vanmaercke, S., Verboven, P., Nicolai, B., Saeys, W., Ramon, H., & Smeets, B. (2017). Assessment of bruise volumes in apples using X-ray computed tomography. *Postharvest Biology and Technology, 128*, 24-32. https://doi.org/10.1016/j.postharvbio.2017.01.013

3. Galed, G., Fernández-Valle, M. E., Martinez, A., & Heras, A. (2004). Application of MRI to monitor the process of ripening and decay in citrus treated with chitosan solutions. *Magnetic Resonance Imaging, 22*, 127-137. https://doi.org/10.1016/j.mri.2003.05.006

4. Gonzalez, J. J., Valle, R. C., Bobroff, S., Biasi, W. V., Mitcham, E. J., & McCarthy, M. J.

(2001). Detection and monitoring of internal browning development in 'Fuji' apples using MRI. *Postharvest Biology and Technology, 22*, 179-188. https://doi.org/10.1016/S0925-5214(00)00183-6

5. Haishi, T., Koizumi, H., Arai, T., Koizumi, M., & Kano, H. (2011). Rapid detection of infestation of apple fruits by the peach fruit moth, *Carposina sasakii* Matsumura, larvae using a 0.2-T dedicated magnetic resonance imaging apparatus. *Applied Magnetic Resonance, 41*, 1-18. https://doi.org/10.1007/s00723-011-0222-8

6. Hernández-Sánchez, N., Hills, B. P., Barreiro, P., & Marigheto, N. (2007). An NMR study on internal browning in pears. *Postharvest Biology and Technology, 44*, 260-270. https://doi.org/10.1016/j.postharvbio.2007.01.002

7. Herremans, E., Melado-Herreros, A., Defraeye, T., Verlinden, B., Hertog, M., Verboven, P., Val, J., Fernández-Valle, M. E., Bongaers, E., Estrade, P., Wevers, M., Barreiro, P., & Nicolai, B. M. (2014). Comparison of X-ray CT and MRI of watercore disorder of different apple cultivars. *Postharvest Biology and Technology, 87*, 42-50. https://doi.org/10.1016/j.postharvbio.2013.08.008

8. Khodabakhshian, R., & Emadi, B. (2017). Application of Vis/SNIR hyperspectral imaging in ripeness classification of pear. *International Journal of Food Properties, 20*(sup3). https://doi.org/10.1080/10942912.2017.1354022

9. Khodabakhshian, R., Emadi, B., Khojastehpour, M., & Golzarian, M. (2019). Instrumental measurement of pomegranate texture during four maturity stages. *Journal of Texture Studies, 50*. https://doi.org/10.1111/jtxs.12406

10. Khodabakhshian, R. (2022). Raman Spectroscopy for Fresh Fruits and Vegetables. In P. B. Pathare & M. S. Rahman (Eds.), *Nondestructive Quality Assessment Techniques for Fresh Fruits and Vegetables* (pp. 193–214). Springer. https://doi.org/10.1007/978-981-19-5422-1_8

11. Lan, W., Jaillais, B., Chen, S., Renard, M. G. C., Leca, A., & Bureau, S. (2022). Fruit variability impacts puree quality: Assessment on individually processed apples using the visible and near infrared spectroscopy. *Food Chemistry, 390*, 133088. https://doi.org/10.1016/j.foodchem.2022.133088

12. Leiva-Valenzuela, G. A., & Aguilera, J. M. (2013). Automatic detection of orientation and diseases in blueberries using image analysis to improve their postharvest storage quality. *Food Control, 33*(1), 166-173. https://doi.org/10.1016/j.foodcont.2013.02.025

13. Li, M., Li, B., & Zhang, W. J. (2018). Rapid and non-invasive detection and imaging of the hydrocolloid-injected prawns with low-field NMR and MRI. *Food Chemistry, 242*, 16-21. https://doi.org/10.1016/j.foodchem.2017.08.086

14. Lu, L., Hu, Z., Hu, X., Li, D., & Tian, S. (2022). Electronic tongue and electronic nose for food quality and safety. *Food Research International, 162*, 112214. https://doi.org/10.1016/j.foodres.2022.112214

15. Mazhar, M., Joyce, D., Cowin, G., Brereton, I., Hofman, P., Collins, R., & Gupta, M. (2015). Non-destructive 1H-MRI assessment of flesh bruising in avocado (*Persea americana* M.) cv. Hass. *Postharvest Biology and Technology, 100*, 33-40. https://doi.org/10.1016/j.postharvbio.2014.09.006

16. McRobbie, D. W., Moore, E. A., Graves, M. J., & Prince, M. R. (2009). *MRI from picture to proton*. Cambridge University Press. https://doi.org/10.1017/CBO9780511545405

17. Mierzwa, D., Szadzinska, J., Gapinski, B., Radziejewska-Kubzdela, E., & Biegańska-Marecik, R. (2022). Assessment of ultrasound-assisted vacuum impregnation as a method for modifying cranberries' quality. *Ultrasonics Sonochemistry, 89*, 106117. https://doi.org/10.1016/j.ultsonch.2022.106117

18. Noshad, F., Asghari, A., Azadbakht, M., & Ghasemnezhad, A. (2020). Comparison of different Magnetic Resonance Imaging (MRI) protocols from Quince fruit. *Iranian Journal of Biosystem*

Engineering, 51(3), 539-549. https://doi.org/10.22059/ijbse.2020.292847.665244

19. Olakanmi, S., Karunakaran, C., & Jayas, D. (2023). Applications of X-ray micro-computed tomography and small-angle X-ray scattering techniques in food systems: A concise review. *Journal of Food Engineering, 342*, 111355. https://doi.org/10.1016/j.jfoodeng.2022.111355

20. Ozel, B., & Oztop, M. H. (2021). A quick look to the use of time domain nuclear magnetic resonance relaxometry and magnetic resonance imaging for food quality applications. *Current Opinion in Food Science, 41*, 122-129. https://doi.org/10.1016/j.cofs.2021.03.012

21. Perez-Palacios, T., Avila, M., Antequera, T., Torres, J. P., González-Mohino, A., & Caro, A. (2023). MRI-computer vision on fresh and frozen-thawed beef: Optimization of methodology for classification and quality prediction. *Meat Science, 197*, 109054. https://doi.org/10.1016/j.meatsci.2022.109054

22. Razavi, M. S., Asghari, A., Azadbakh, M., & Shamsabadi, H. A. (2018). Analyzing the pear bruised volume after static loading by Magnetic Resonance Imaging (MRI). *Scientia Horticulturae, 229*, 33-39. https://doi.org/10.1016/j.scienta.2017.10.011

23. Shicheng, Q., Youwen, T., Ping, S., Kuan, H., & Shiyuan, S. (2019). Analysis and detection of decayed blueberry by low-field nuclear magnetic resonance and imaging. *Postharvest Biology and Technology, 156*, 110951. https://doi.org/10.1016/j.postharvbio.2019.110951

24. Srivastava, R. K., Talluri, S., Beebi, S. K., & Kumar, B. R. (2018). Magnetic resonance imaging for quality evaluation of fruits: A review. *Food Analytical Methods, 11*, 2943-2960. https://doi.org/10.1007/s12161-018-1262-6

25. Wieme, J., Mollazade, K., Malounas, L., Zude-Sasse, M., Zhao, M., Gowen, A., Argyropoulos, D., Fountas, S., & Van Beek, J. (2022). Application of hyperspectral imaging systems and artificial intelligence for quality assessment of fruit, vegetables and mushrooms: A review. *Biosystems Engineering, 222*, 156-176. https://doi.org/10.1016/j.biosystemseng.2022.07.013

26. Zhang, L., & McCarthy, J. M. (2012). Black heart characterization and detection in pomegranate using NMR relaxometry and MR imaging. *Postharvest Biology and Technology, 67*, 96-101. https://doi.org/10.1016/j.postharvbio.2011.12.018

27. Zhang, D., Xu, Y., Huang, W., Tian, X., Xia, Y., Xu, L., & Fan, S. (2019). Nondestructive measurement of soluble solids content in apple using near infrared hyperspectral imaging coupled with wavelength selection algorithm. *Infrared Physics & Technology, 98*, 297-304. https://doi.org/10.1016/j.infrared.2019.03.026

28. Zhang, Z., Liu, H., Chen, D., Zhang, J., Li, H., Shen, M., Pu, Y., Zhang, Z., Zhao, J., & Hu, J. (2022). SMOTE-based method for balanced spectral nondestructive detection of moldy apple core. *Food Control, 141*, 109100. https://doi.org/10.1016/j.foodcont.2022.109100

تجزیه و تحلیل کیفی میوه سیب در طول ذخیره‌سازی با استفاده از تصویربرداری تشدید مغناطیسی

رسول خدابخشیان کارگر [iD][1]*، **رضا باغبانی** [iD][2]

چکیده

تصویربرداری تشدید مغناطیسی (MRI)، یک روش غیرمخرب برای تعیین کیفیت میوه‌ها است که با پروتکل‌های مختلف، چگالی و ساختار اتم‌های هیدروژن را که در آن قرار می‌گیرد نشان‌می دهد. در این مطالعه تصاویر MRI گرفته‌شده با پروتکل‌های مختلف از بافت گوشـتی و قسـمت کبودشـده میوه سیب بدون آفت و با آفت مقایسه و بهترین پروتکل معرفی شد. برای این منظور، تصویربرداری تشدید مغناطیسی (MRI) با استفاده از دو پروتکـل T_1 و T_2 بر روی ۲۰۰ میوه سیب بارگذاری‌شده در حین نگهداری انجام شد. بارگیری میوه‌ها در چهار سـطح ۱۵۰، ۳۰۰، ۴۵۰ و ۶۰۰ نیـوتن به‌صورت شبه‌استاتیک انجام شد و سپس در دوره‌های ۲۵، ۵۰ و ۷۵ روزه در دمای ۴ درجه سانتی‌گراد نگهداری شد. در پایان هر دوره ذخیره‌سازی، تصویربرداری انجام شد. سپس کنتراست تصاویر T_1 و T_2 صدا و بافت کبودشده میوه سیب با و بدون آفت با استفاده از نرم‌افزار ImageJ تعیین شد. نتیجه‌گیری شـد که بافت صوتی میوه سیب بدون آفت در تصاویر T_1 واضح‌تر از تصاویر T_2 بود. همچنین دیده شده است کـه ناحیـه کبـودی میوه‌هـای بـدون آفت در تصاویر T_2 بیشتر از تصاویر T_1 قابل‌تشخیص است.

واژه‌های کلیدی: آنالیز هیستوگرام، تصویربرداری تشدید مغناطیسی، کیفیت، میوه سیب

۱- گروه مهندسی بیوسیستم، دانشکده کشاورزی، دانشگاه فردوسی مشهد، ایران

۲- گروه مهندسی کشاورزی، دانشگاه ملی مهارت، تهران، ایران

(Email: Khodabakhshian@um.ac.ir :نویسنده مسئول -*)

Hyperparameter Optimization of ANN, SVM, and KNN Models for Classification of Hazelnuts Images Based on Shell Cracks and Feature Selection Method

H. Bagherpour [iD][1*], **F. Fatehi** [iD][1], **A. Shojaeian** [iD][1], **R. Bagherpour** [iD][2]

1- Department of Biosystems Engineering, Faculty of Agriculture, Bu-Ali Sina University, Hamedan, Iran

2- Department of Computer Engineering, School of Computer Engineering, Iran University of Science and Technology, Tehran, Iran

(*- Corresponding Author Email: h.bagherpour@basu.ac.ir)

Abstract

In some countries, people commonly consume hazelnuts in their shells to extend shelf life or due to technological limitations. Therefore, open-shell hazelnuts are more marketable. At the semi-industrial scale, open-shell and closed-shell hazelnuts are currently separated from each other through visual inspection. This study aims to develop a new algorithm to separate open-shell hazelnuts from cracked or closed-shell hazelnuts. In the first approach, dimension reduction techniques such as Sequential Forward Feature Selection (SFFS) and Principal Component Analysis (PCA) were used to select or extract a combination of color, texture, and grayscale features for the model's input. In the second approach, individual features were used directly as inputs. In this study, three famous machine learning models, including Support Vector Machine (SVM), K-nearest neighbors (KNN), and Multi-Layer Perceptron (MLP) were employed. The results indicated that the SFFS method had a greater effect on improving the performance of the models than the PCA method. However, there was no significant difference between the performance of the models developed with combined features (98.00%) and that of the models using individual features (98.67%). The overall results of this study indicated that the MLP model, with one hidden layer, a dropout of 0.3, and 10 neurons using Histogram of Oriented Gradients (HOG) features as input, is a good choice for classifying hazelnuts into two classes of open-shell and closed-shell.

Keywords: Closed-shell, Dimension reduction, Machine learning, Open-shell, PCA

Introduction

Hazelnut is one of the garden products with the highest nutritional value for humans. It is utilized as snack, in baking and desserts, and in breakfast cereals like muesli. In confectionery, it is used for making pralines

and are combined with chocolate for truffles, alongside other popular treats like chocolate bars and hazelnut cocoa spreads like Nutella. It is also used in the cosmetics industry (FAOSTAT, 2021).

Hazelnuts are available in the market both in-shell and shelled. Although in many industrialized countries, hazelnuts are sold in the form of kernels, in many countries, including the Third World countries, a large amount of hazelnut is marketed in the form of open-shell. Shelled hazelnuts account for 5 to

10% of the global hazelnut market (FAOSTAT, 2021). During the cracking process undertaken to increase the marketability of hazelnuts, three different classes are produced after cracking: open-shell, cracked, and closed-shell. Among these, only the open-shell hazelnuts can be sold in the market. As a result, separating the cracked and closed-shell hazelnuts and making them open-shell is necessary. Since the cracks are very small, manual separation of closed-shell from open-shell hazelnuts is a tedious and time-consuming task. In commercial scale production, having a fast, non-destructive method and reliable classification is crucial.

Commercial hazelnut processing generally includes drying, sizing, cracking, and separating impurities (Menesatti *et al.,* 2008; Wang, Jung, McGorrin, & Zhao, 2018). By reviewing previous studies, few studies have been found in the field of hazelnut classification. In a study, sound signal was used to classify hazelnuts into two classes of underdeveloped and fully developed hazelnuts. The sound signals were obtained by dropping hazelnuts from a certain height onto a steel plate (Kalkan & Yardimci, 2006). In another study, a morphological method based on elliptic Fourier approximation to closed contours in a two-dimensional plane was applied to the RGB images to classify four local hazelnut cultivars in Italy. The coefficients of harmonic equations were obtained by PLS-DA. Menesatti *et al.* (2008) evaluated the potential use and efficacy of shape-based techniques in order to discriminate four traditional Italian hazelnut cultivars. The higher percentage of correct classification accuracy was reported between 77.5%- 98.8%. Seventeen hazelnut cultivars were classified using a developed convolutional neural network. This network had the highest accuracy (98.63%) as compared to other pre-trained models (Taner, Öztekin, & Duran, 2021).

A significant number of studies have presented the use of machine learning (ML) techniques for classification or qualitative evaluation of nuts and fruits. ML methods have been widely used for classification of various agricultural products, such as grading hazelnut kernels (Giraudo *et al.,* 2018), detection of hazelnut cultivars (Taner *et al.,* 2021), grading almond kernels (Vidyarthi , Singh, Xiao, & Tiwari, 2021), orange (Komal & Sonia, 2019), cucumber (Pourdarbani & Sabzi, 2022), apple (Lashgari, Imanmehr, & Tavakoli, 2020), classification of weed seeds (Luo *et al.,* 2023), and detection of abnormal lettuce leaves (Yang *et al.,* 2023). In a latest study on hazelnut classification based on shell crack detection, a deep convolutional neural network (DCNN) algorithm was employed (Shojaeian *et al.,* 2023). Although the results of their study were satisfactory, they did not assess the features individually, without providing any insights regarding the importance of the specific features.

To the best of our knowledge, there is currently no intelligent system available for the classification of hazelnuts based on the presence of shell cracks. Therefore, this research aims to classify the hazelnuts based on cracks in their shells, utilizing color and texture features extracted from RGB images, employing models such as MLP, SVM, and KNN.

Materials and Methods

Fig. 1a illustrates the schematic diagram of steps involved in modeling machine learning methods. In the first approach, images of the hazelnut samples were captured, and subsequently some preprocessing operations were performed. After extracting the color, grayscale, and texture features, their dimensions were reduced using Principal Component Analysis (PCA) technique, and Sequential Forward Feature Selection (SFFS) was employed for feature selection. As shown in Fig. 1b in the second approach, four investigated features were used individually as inputs to three classifiers. In this approach, the same optimized hyperparameters obtained in the first approach were utilized.
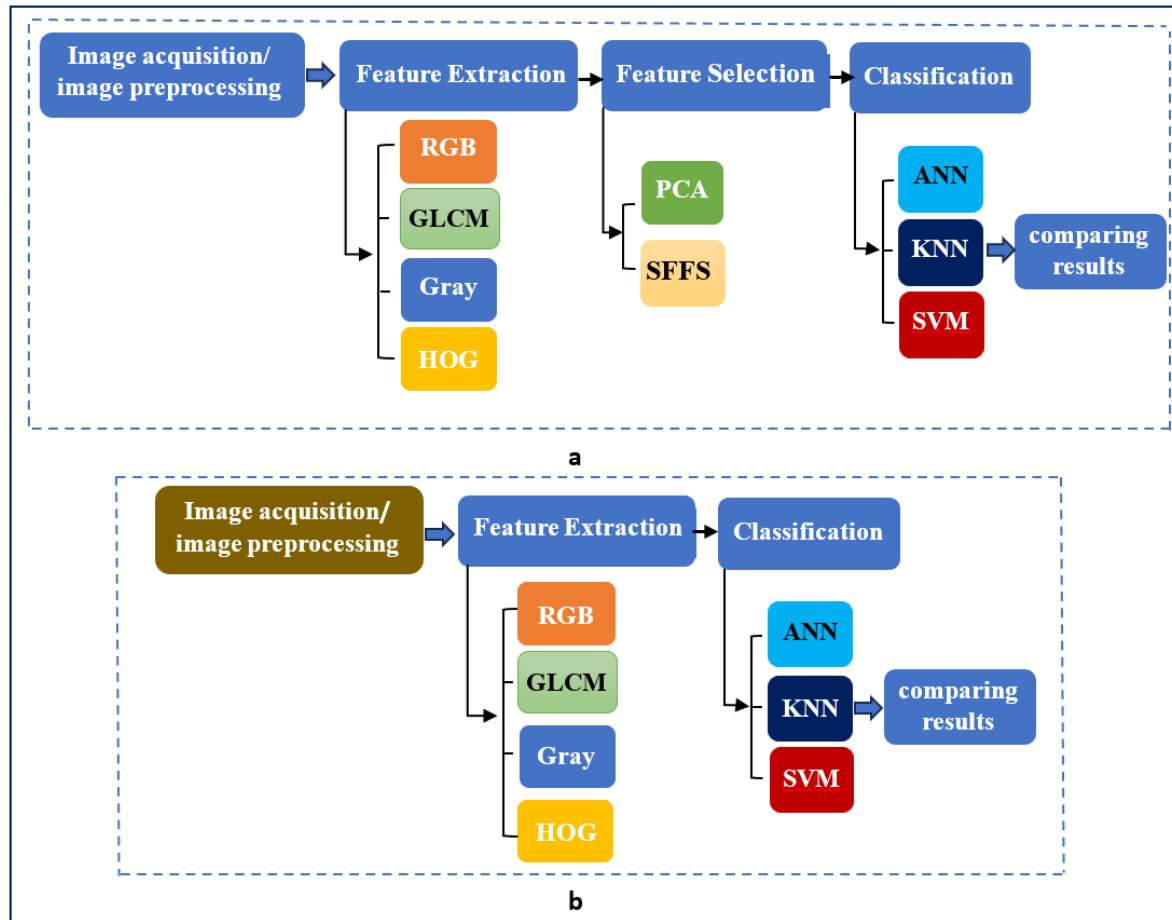
Fig. 1. Flowchart of hazelnut classification using machine learning algorithms. Two approaches were used: a) incorporating feature selection algorithms (first approach) and b) individual features used as input to three classifiers (second approach)

Sample preparation

Hazelnut samples were purchased during the summer of 2022 from Rahim Abad, located in Rudsar city, Gilan province, Iran. Five hundred samples were randomly selected for each class. The classes were as follows: 1) open-shell and 2) closed-shell hazelnuts (without cracks or with tiny cracks). Among these samples, 48% were open-shell, 32% were closed-shell, and 20% had tiny cracks.

To prepare images under consistent conditions and eliminate ambient effects, an imaging box was used. A camera (Samsung J5 smartphone) with a resolution of 2448 × 2448 pixels was positioned at the top of the box. Additionally, a 6-watt circular LED panel provided uniform illumination on the sample. The inner side walls of the box were covered with white cardboard, while blue cardboard was used as the background to increase the contrast between the hazelnuts and the background. Examples of captured hazelnut images from two different classes are shown in Fig. 2.

Feature Extraction

Crack Size

Five steps were carried out to identify cracks on the shell surface (Fig. 3). These steps include removing the background and converting the image to grayscale, implementing thresholding to create a mask, applying the mask to the original image using the concatenate function (cat (a, c)), and finally, applying a threshold to the R component of the RGB and the S component of the HSV to reveal the cracks in the hazelnuts (Fig. 3 f). An area threshold was then applied to separate open and cracked shell samples.
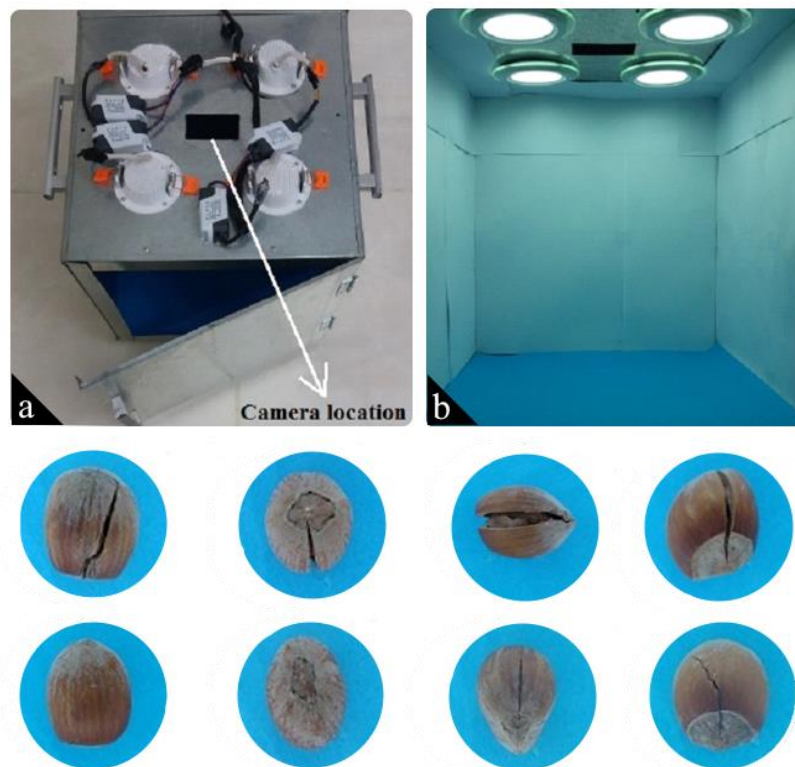
Fig. 2. The (a) exterior and (b) interior views of the imaging box. (c) The images in the first row and the second row show the open-shell (class 1) and closed-shell (class 2) hazelnuts, respectively
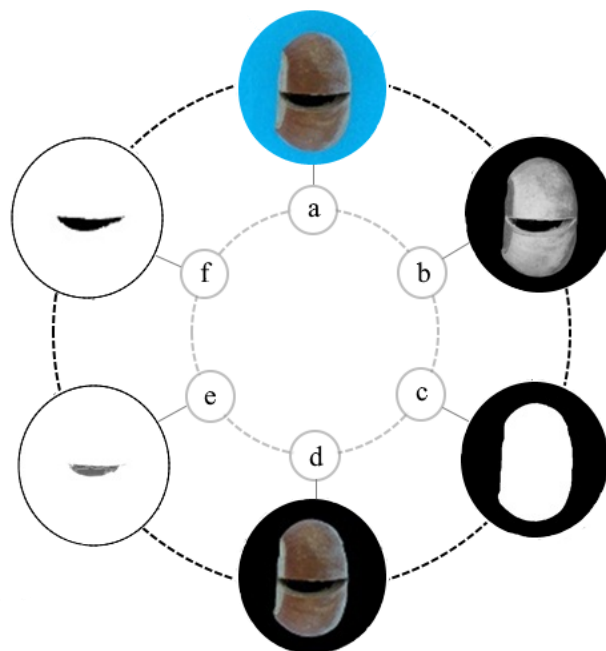
Fig. 3. Image processing for crack detection. a) Original RGB image, b) gray-scale image, c) binary image, d) concatenation of the original image and the corresponding masks, e) crack detection through a linear combination of the R component of the RGB color space and the S component of the HSV color space, and f) thresholding on image "e"

Color and Texture Features

The mean, standard deviation, skewness, and elongation of the color components were calculated using the image shown in Fig. 3 d. Table 1 shows these features, with R, G, and B representing the red, green, and blue components of the RGB image, respectively. Additionally, p, n, and i are the normalized color histogram, intensity, and number of color component levels, respectively.

To extract textural features, Fig. 3d was converted to a gray-scale image and the Gray-Level Co-Occurrence Matrix (GLCM) was derived from each image. Furthermore, all textural features were extracted from the gray-

scale image (Pourreza, Pourreza, Abbaspour-Fard, & Sadrnia, 2012). The gray features include the histograms of gray images and the aforementioned matrices as well as those mentioned in Table 1. The Gray-Level Co-Occurrence Matrix (GLCM) is a statistical method for analyzing the texture of an image. It considers the spatial relationship between pixels with specific intensity values. The GLCM functions characterize the texture by calculating how often pairs of pixels with certain values occur in a specified spatial relationship within the image.

Table 1- The features extracted from RGB, GLCM, and gray matrices

Features	Equation
Color Features	
Mean R	$\mu_R = \sum_i i p_R(i)$
Mean G	$\mu_G = \sum_i i p_G(i)$
Mean B	$\mu_B = \sum_i i p_B(i)$
Standard deviation R	$\sigma_R = \sqrt{\sum_i (i - \mu_R)^2 p_R(i)}$
Standard deviation G	$\sigma_G = \sqrt{\sum_i (i - \mu_G)^2 p_G(i)}$
Standard deviation B	$\sigma_B = \sqrt{\sum_i (i - \mu_B)^2 p_B(i)}$
Skewness R	$(\sum_{i=1}^{n}(i - \mu_R)^3)/(n-1)\sigma_R^3$
Skewness G	$(\sum_{i=1}^{n}(i - \mu_G)^3)/(n-1)\sigma_G^3$
Skewness B	$(\sum_{i=1}^{n}(i - \mu_B)^3)/(n-1)\sigma_B^3$
Kurtosis R	$(n\sum_I(i - \mu_R)^4/\sum_I(i - \mu_R^2)^2) - 3$
Kurtosis G	$(n\sum_I(i - \mu_G)^4/\sum_I(i - \mu_G^2)^2) - 3$
Extracted features from GLCM matrix	
Mean	$\mu = \sum_i i p(i)$
Standard deviation	$\sigma = \sqrt{\sum_i (i - \mu)^2 p(i)}$
Smoothness	$1 - 1/(1 + \sigma^2)$
Third moment	$\sum_i (i - \mu)^3 p(i)$
Uniformity	$\sum_i p(i)^2$
Entropy	$-\sum_{i,j} p(i,j) log\,(p(i,j))$
Uniformity	$\sum_{i,j} p(i,j)^2$
Homogeneity	$\sum_{i,j} p(i,j)/(1 + (i-j)^2)$
Inertia	$\sum_{i,j} (i-j)^2 p(i,j)$
Cluster shade	$\sum_{i,j} (i + j - 2\mu)^3 p(i,j)$
Cluster prominence	$\sum_{i,j} (i + j - 2\mu)^4 p(i,j)$
Maximum probability	$Max\,(p(i,j))$
Correlation	$\sum_{i,j} (i - \mu)(j - \mu)\sigma^2 p(i,j)$
Extracted features from gray matrices	
Mean	$\mu = \sum_i \text{ip}(i)$
Standard deviation	$\sigma = \sqrt{\sum_i (i - \mu)^2 \text{p}(i)}$
Third moment	$\sum (i - \mu)^3 p(i)$
Smoothness	$1 - 1/(1 + \sigma^2)$
Uniformity	$\sum_i \text{p}(i)^2$
Entropy	$-\sum_i \text{p}(i) log\,(p(i))$
Crack area	$\sum i_b \mid (i_b i = 1)$

In addition to the above features, the Histogram of Oriented Gradients (HOG) feature was also used as input of the proposed models to classify the hazelnuts according to their cracks. For this purpose, image sizes of 128×128 pixels were examined. HOG was calculated using 8×8 cell sizes and spread across 9 bins, resulting in an 8100-dimensional feature vector for each image.

Feature Selection

Feature selection is an important step in the process of building classifiers. It is a process that chooses a subset of features from the original set of features so that the features space is optimally reduced according to a certain criterion (Tan, Hoon, Yong, Kong, & Lin, 2005). Using the first approach in this study, a large number of features were initially extracted from the samples to identify the optimal features. The performance of the classifiers was then evaluated based on each category of input features. On the other hand, the extracted features may contain noise and irrelevant information, so the number of features should be reduced by employing feature conditioning methods (Garcia-Allende, Mirapeix, Conde, Cobo, & Lopez-Higuera, 2009). For this purpose, the PCA and SFFS algorithms were applied separately on the features to reduce the number of features based on their approach. In this research, six features were selected by SFFS for MLP, and eleven features were selected for SVM and KNN. In the PCA method, the six components that could explain 98% of variances were selected as inputs for the models.

Machine Learning Models

To achieve a simple structure, with the least complexity and the best performance without underfitting and overfitting, several MLP architectures were evaluated by changing the number of layers (one and two layers) and the number of neurons (3-12 neurons) in each hidden layer. As Fig. 4 shows, in the proposed network, six selected features by the SFFS method were considered as input of the network. The sigmoid active function was considered in the hidden layer neurons and the linear activation function was considered in the output layer neurons of the network. The Levenberg–Marquardt algorithm was used to train the network and the MSE criterion was also used to stop the training (Heaton, 2008).
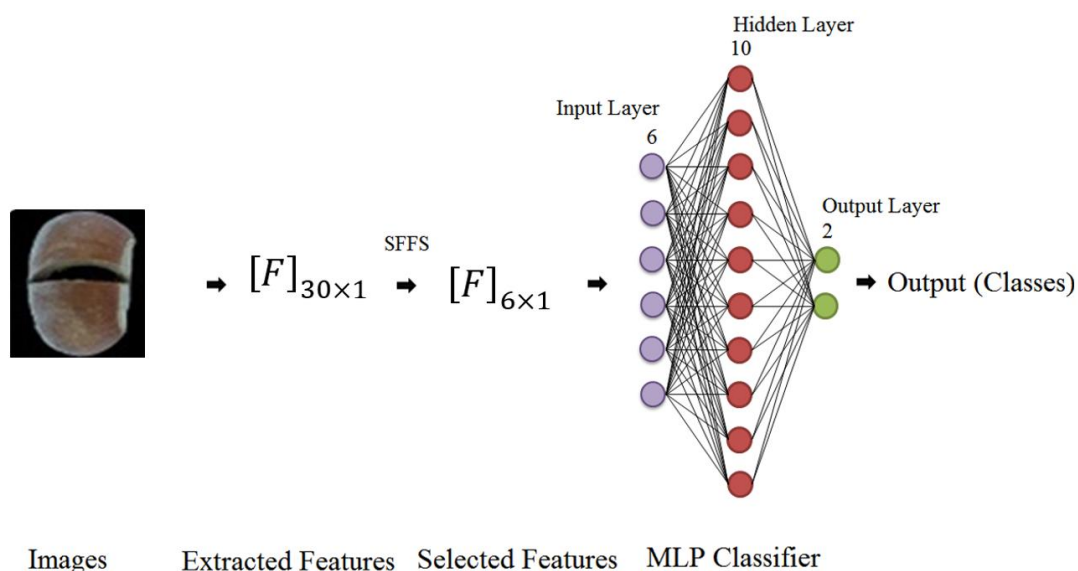
Fig. 4. The architecture of MLP model with one hidden layer containing 10 neurons

For each experiment, the initial learning rate was set as 0.001 and the number of iterations was 300. In data segmentation, 70%, 15%, and 15% of the data were used for training, validation, and testing of the network, respectively.

The KNN rule is one of the well-known supervised learning models in classification tasks. This rule simply retains all training sets during learning and assigns a class to each query represented by the majority label of its k-nearest neighbors in the training dataset (Gou, Du, Zhang, & Xiong, 2012). The main

problem is that the behavior of this model is affected by many parameters, including distance criteria, weights of neighborhoods (Table 2), and the number of neighbors (K) (Geler, Kurbalija, Radovanović, & Ivanović, 2016). Therefore, the effect of these factors was evaluated in this study. In these models as well as SVM, 80% of the dataset was considered for training and 20% of the dataset for testing. Note that the values of the neighborhood size k in the experiments vary from 3 to 11 by Step 2.

Table 2- Different weights of KNN model

Model	Weight (Sigma and C are constant)
KNN	-----
WKNN1	$1/D$
WKNN2	$1/D^2$
WKNN3	$1/(D^2 + C)$
WKNN4	$\exp(D^2/\text{Sigma})$

The SVM was another model investigated in this study. This model is a binary classifier which gives better performance in the classification tasks. SVM classifies two classes by constructing a hyperplane in high-dimensional feature space. A decision hyperplane is constructed in this higher dimension such that the distance between hyperplane and the support vectors of both classes is maximized (Way, Sahiner, Hadjiiski, & Chan, 2010). We evaluated the SVM model using the suggested RBF for the classification models (Manekar & Waghmare, 2014). There are two parameters in the RBF Kernel type of SVM: C (Cost) and g (gamma). The accuracy of the SVM for RBF type depends on these two parameters (Gopi, Jyothi, Narayana, & Sandeep, 2023).

Evaluation Metrics

The performance of the classifiers was evaluated considering the results obtained from the confusion matrix, along with key statistical metrics: accuracy (Eq. 1), sensitivity (Eq. 2), specificity (Eq. 3), precision (Eq. 4), and F1-Score (Eq. 5). MATLAB R2019a was

used to extract the features and implement the models.

$$Accuracy = \frac{TP+TN}{N} \tag{1}$$

$$Sensitivity\ (Recall) = \frac{TP}{TP+FN} \tag{2}$$

$$Specificity = \frac{TN}{TN+FP} \tag{3}$$

$$Precision = \frac{TP}{TP+FP} \tag{4}$$

$$F1\text{-}Score = 2 \times \frac{(Precision \times Recall)}{(Precision+Recall)} \tag{5}$$

where N is the total number of samples. TP is the number of true positives, FP is the number of false positives, and FN is the number of false negatives. The F1-score can have values between 0 and 1, with 1 being the best score.

Results and Discussion

Effect of dimension reduction methods on the model's performance

In this study, PCA and SFFS methods were used to assess the effect of dimension reduction methods. The results in Table 3 illustrates the confusion matrix obtained from the MLP results related to the proposed

method and PCA. These results indicated that the feature vectors obtained by SFFS outperform PCA. In the SFFS method, the F1-score for open-shell and closed-shell was 98.67 and 98.67%, respectively. While in the PCA method, this index was 78.67 and 80.00%, respectively. In a study to recognize facial expressions using RGB images, the feature selection method of SFFS and the ML (Machine Learning) approach suggested that

the selected subset of features not only enhances the classification performance, but also reduces computational complexity, making the system more practical for real-time applications (Li, Lu, & Liu, 2014). Furthermore, the SFFS method demonstrated superior performance in detecting stems and calyxes (SC) in apple stems using support vector classifiers (Unay, Gosselin, & Debeir, 2006).

Table 3- Confusion matrix of MLP model using SFFS and PCA method

		Predicted	
	Class	Open-Shell	Cracked or Closed-shell
		SFFS	
Actual	Open-Shell	74	1
	Cracked or Closed-shell	1	74
		PCA	
	Open-Shell	59	16
	Cracked or Closed-shell	15	60

In examining the performance of SVM and KNN classifiers with the feature subsets selected from SFFS, these models showed the classification accuracies of 96.67% and 98%, respectively. On the other hand, like the MLP classifier, in the SVM and KNN classifiers, using the features mapped by PCA, the accuracy of these models was less than 79% (Table 4). The low accuracy of the PCA

method suggests that using linear transformation to map features on the orthogonal directions can complicate the feature space and may not always be beneficial (Jolliffe, 2002). In the SFFS algorithm, the feedback of the desired classifier is considered to select the feature during feature selection (Lu, Wang, Wu, & Xie, 2016).

Table 4- Effect of dimension reduction methods on the performance of MLP, SVM, and WKNN2 models in the classification of hazelnut (WKNN2 results was obtained with k=7, criteria distance of Cityblock)

		Test data			
Method	Model	Precision (%)	Recall (%)	F1-Score (%)	Accuracy (%)
PCA	MLP	79.03	79.03	79.03	79.03
	SVM	50.00	100	66.67	50.00
	WKNN2	62.94	71.33	66.83	64.67
SFFS	MLP	98.67	98.67	98.67	98.67
	SVM	96.05	97.33	96.69	96.67
	WKNN2	96.15	100	98.04	98.00

Number of Neurons of the MLP Structure

In the MLP classifier, the number of neurons in the hidden layer has the highest impact on the performance of the network. Therefore, finding its optimal value is

important (Heaton, 2008). In examining the effect of the number of neurons, the artificial neural network (ANN) model with 10 neurons in the hidden layer had the highest accuracy (98.67%). In this selected network, the lowest

mean squared error (MSE = 0.08379) for validation data was obtained in the epoch of 17 (Fig. 5). Similar results have been published in studies that investigated the effect of the number of neurons in the hidden layer on the performance of artificial neural networks (Çolak, 2021; Liu, Starzyk, & Zhu, 2007). As

the results of table 5 show, using a dropout of 0.3 between input and hidden layers significantly improved the network accuracy. The decrease in accuracy with a dropout rate of 0.5 can be attributed to removing too many neurons during the training process.
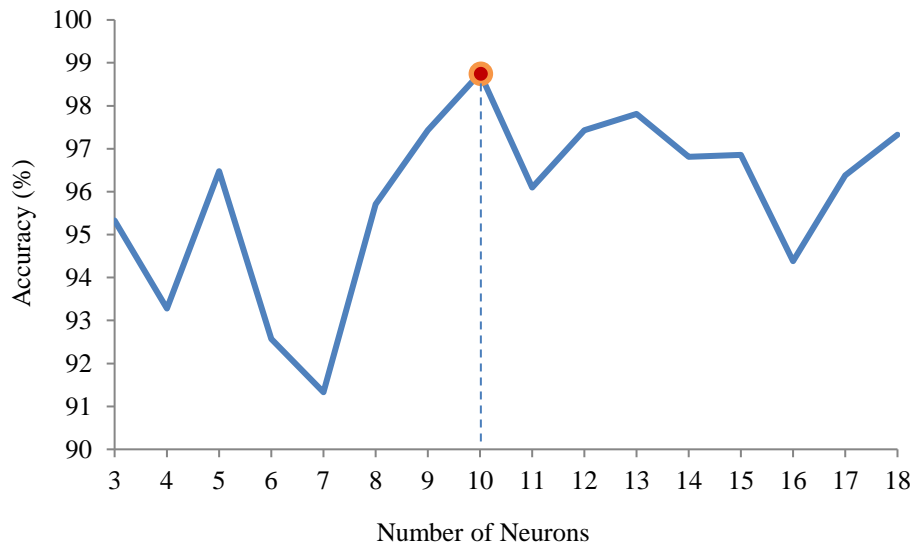
Fig. 5. Accuracy of MLP with different neurons in hidden layer

Table 5- Effect of dropout and the number of hidden layers on the accuracy of ANN model with HOG feature

Model	Number of layers	Dropout	Accuracy (%)
	1	-	0.955
	1	0.3	0.986
	1	0.5	0.930
ANN	2	-	0.940
	2	0.3	0.958
	2	0.5	0.942

KNN Classifier

The performance of various KNN classifier configurations was evaluated by considering different distance metrics (D), different neighborhood weighting schemes (w), and varying numbers of neighbors (k). The best average accuracy of the test data for each classifier was obtained with k=7 (Fig. 6) and the Cityblock distance metric (Table 6). In general, the weighted KNN models outperformed the unweighted model for different values of k. Although the accuracy of most weighted KNN configurations was above

95%, the classification accuracy of WKNN2 (98.00%) was the highest among the weighted KNNs. Therefore, the WKNN2 classifier was selected for further analysis. In the similar study to compare the performance of KNN and WKNN, the results of their comparison showed that the WKNN had higher performance than KNN (Tarakci & Ozkan, 2021). Evaluating the performance of KNN and WKNN in the classification of the UCI database revealed that the highest and lowest classification accuracy was related to WKNN and KNN, respectively (Gou *et al.,* 2012).

Table 6- Effect of distance criteria and weight of distance on the performance of the KNN model

Model	Distance criteria (with SFFS method and k=7)					
	Chebychev	Cityblock	Correlation	Cosine	Euclidean	Mincowski
KNN	89.67	95.31	94.33	93.67	92.42	89.33
WKNN1	93.33	97.33	96.33	97.33	95.23	92.67
WKNN2	**93.33**	**98.00**	**96.43**	**97.40**	**95.67**	**94.20**
WKNN3	90.07	96.33	94.33	93.67	93.14	89.67
WKNN4	90.15	97.33	94.33	93.67	95.33	90.33
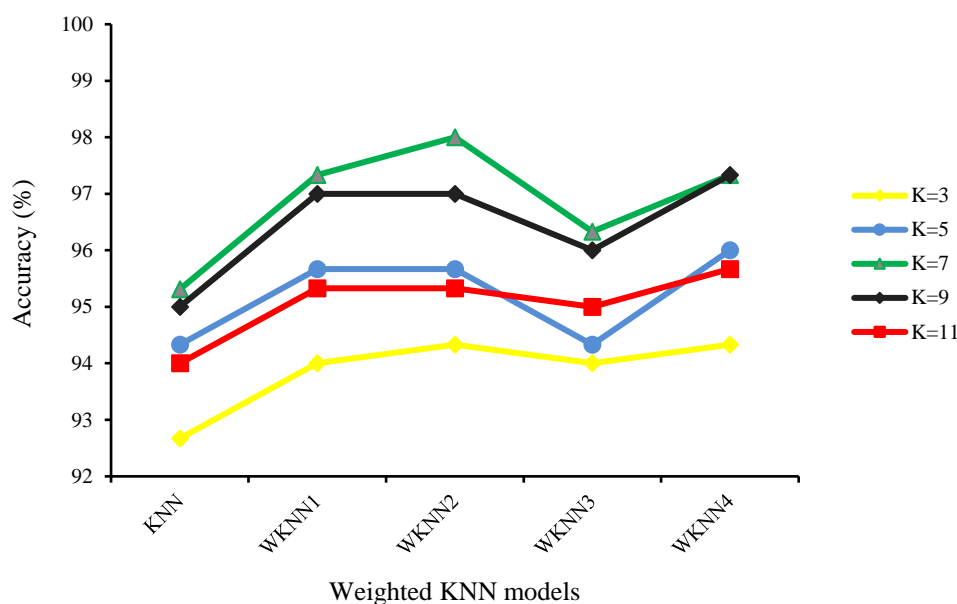
Fig. 6. Effect of number of neighborhood and weight of distance on the accuracy of the KNN model with the distance criteria of Cityblock and reduction method of SFFS

Effect of different individual features on the classifiers' accuracy

Fig. 7 shows the accuracy of MLP, SVM, and KNN classifiers based on different individual features. The results shown in this chart indicate that the color features (mean R, mean G, and mean B) and grayscale features performed well in the classification of hazelnuts. Conversely, the GLCM features yielded poor results. The high performance of the Color feature can be attributed to the presence of cracks on the Hazelnut surfaces. The larger the cracks, the greater the effect on the average value of the color indices. It should be mentioned that for all three feature types, the MLP model outperformed the SVM

and KNN models. However, by comparing the results, although the MLP model achieved the highest accuracy (98.67%) using the HOG feature, it shows little difference with color and gray features, and it can be said that these three methods exhibited similar performance. Additionally, in the overall comparison between the classifiers, the KNN classifier exhibited lower performance than the other classifiers. In a similar study to compare ANN, Fuzzy, EDT, and KNN models with the aim of developing a cherry fruit packing system, the ANN model with HOG feature showed the higher accuracy of 95% (Momeny, Jahanbakhshi, Jafarnezhad, & Zhang, 2020).
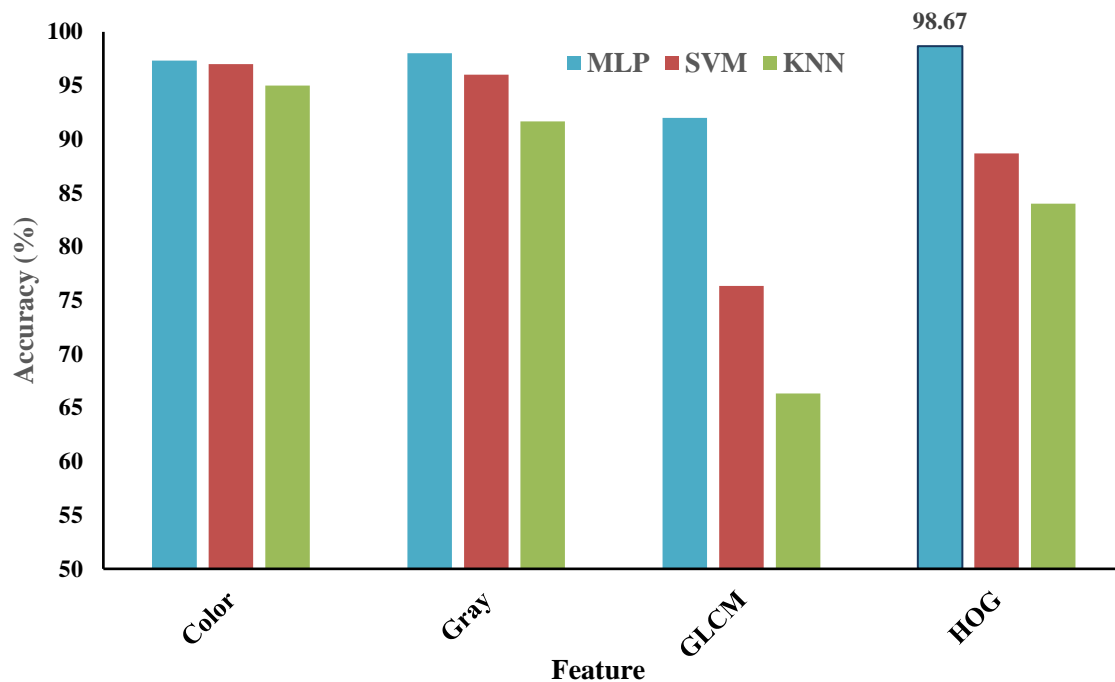
Fig. 7. Classification accuracy of MLP, SVM, and KNN using different features

The results of model evaluation are shown in Table 7. According to the F1-score measure, among the three features (HOG, Color, and Gray), the HOG is the best feature for the MLP model, while color features are recommended for the SVM and KNN models. Although all three models demonstrated satisfactory accuracy, the MLP showed better predictive capabilities for hazelnut classification based on surface cracks.

In the similar study that aimed to classify strawberry fruit into two classes of ripe and unripe, six classifiers including MLP, SVM, KNN, DT, NBC, and LR were investigated using bioimpedance data and surface color features. The classification results highlighted that, among all the tested models, MLP networks had the best performances (Ibba *et al.,* 2021). Four methods of SVM, KNN, and LDA (Linear Discriminant Analysis) were investigated to distinguish healthy and defective apples from each other. For this purpose, HOG and GLCM features were extracted. The SVM classifier was able to achieve 98.9% accuracy using these features. Additionally, applying PCA to these features

did not affect the accuracy of the SVM and KNN classifiers (Singh & Singh, 2019). In a study, different classifiers including MLP and SVM were used to detect cracks in the walls using features extracted from the grayscale images. The MLP classifier exhibited the best performance in detecting cracked walls (Hallee, Napolitano, Reinhart, & Glisic, 2021).

Compared to previously studies, there have been hardly any studies in the literature performing classification of nuts using machine learning models to compare our results. However, we found some similar research in literature on smart sorting of pistachio nuts and almonds based on acoustic signals and deep learning approaches. Omid (2011) proposed an expert system based on acoustic emission signal and fuzzy logic classifier for sorting open and closed-shell pistachio nuts and the overall accuracy of the sorting system was 95.56 % for test datasets. In the other study, the performance of feature learning from frequency spectrum was tested for sorting pistachio nuts. The accuracy of the MLP classifier with features extracted from wavelet domain data was 96.1% (Hosseinpour-

Zarnaq, Omid, Taheri-Garavand, Nasiri, & Mahmoudi, 2022). The results of our proposed ANN model are similar to those reported in these studies. It is worth noting that in the similar study, authors detected hazelnut based on their crack using deep convolutional neural network (DCNN) algorithm (Shojaeian *et al.,* 2023). While their approach demonstrated superior detection accuracy compared to ours, our study has transparently disclosed the specific features utilized, which was not the case in their work. Additionally, their model is highly elaborate and computationally intensive.

Table 7- Classification performance of MLP, SVM, and KNN models at different features

Feature	Color	Gray	GLCM	HOG	Crack
MLP					
Sensitivity	0.997	0.977	0.899	0.998	0.957
Specificity	0.944	0.984	0.775	0.976	0.763
precision	0.952	0.988	0.816	0.971	0.779
F1-Score	0.975	0.982	0.855	0.986	0.859
SVM					
Sensitivity	0.987	0.947	0.640	0.833	0.933
Specificity	0.953	0.980	0.613	0.940	0.807
precision	0.955	0.979	0.623	0.933	0.828
F1-Score	0.970	0.963	0.631	0.880	0.878
KNN					
Sensitivity	0.987	0.960	0.900	0.813	0.893
Specificity	0.913	0.973	0.727	0.867	0.333
precision	0.919	0.983	0.767	0.859	0.573
F1-Score	0.952	0.920	0.828	0.836	0.698

Conclusion

In countries where hazelnuts are sold in shell form, creating open-shell hazelnuts can increase the value of the product and the proportion of satisfied customers. The results of this study revealed that the well-known machine learning methods such as MLP, SVM, and KNN have great potential for the classification of hazelnuts. Although many features showed strong correlations with the hazelnut cracks, a greater number of them, especially HOG, exhibited higher accuracy. Meanwhile, the MLP model using the HOG feature achieved the highest accuracy, while GLCM features yielded low accuracy. The higher accuracy of the models using HOG features can be attributed to the fact that HOG can detect the object's edge and provide the outline of a shape, which can be effective features for representing different types of cracks. Additionally, SFFS as a feature selection method showed better results than PCA. The overall results of this study clearly indicate that it is feasible to monitor and classify hazelnuts based on shell cracks. While the developed machine learning models demonstrated a good ability in classifying nuts, the main drawback of this study is the lack of information about situations where the crack is on the side of the hazelnut, which should be considered in future studies. It is suggested to employ two cameras to capture images of the falling hazelnuts.

Conflict of Interest

The authors declare no competing interests.

Author Contributions

H. Bagherpour: Supervision, Conceptualization, Methodology, Software, Reviewing.

F. Fatehi: Software, Methodology, Data pre and post processing, Writing, Validation.

A. Shojaeian: Data curation, Methodology.

R. Bagherpour: Software, Validation.

References

1. Çolak, A. B. (2021). A novel comparative investigation of the effect of the number of neurons on the predictive performance of the artificial neural network: An experimental study on the thermal conductivity of ZrO_2 nanofluid. *International Journal of Energy Research*, *45*(13), 18944-18956. https://doi.org/10.1002/er.6989

2. FAOSTAT. (2021). Crops production data. http://wwwfaoorg/faostat/en/#data/QC. Accessed 20 March 2021

3. Garcia-Allende, P. B., Mirapeix, J., Conde, O. M., Cobo, A., & Lopez-Higuera, J. M. (2009). Spectral processing technique based on feature selection and artificial neural networks for arc-welding quality monitoring. *Ndt & E International*, *42*(1), 56-63. https://doi.org/10.1016/j.ndteint.2008.07.004

4. Geler, Z., Kurbalija, V., Radovanović, M., & Ivanović, M. (2016). Comparison of different weighting schemes for the k NN classifier on time-series data. *Knowledge and Information Systems*, *48*, 331-378. https://doi.org/10.1007/s10115-015-0881-0

5. Giraudo, A., Calvini, R., Orlandi, G., Ulrici, A., Geobaldo, F., & Savorani, F. (2018). Development of an automated method for the identification of defective hazelnuts based on RGB image analysis and colourgrams. *Food Control*, *94*, 233-240. https://doi.org/10.1016/j.foodcont.2018.07.018

6. Gopi, A. P., Jyothi, R. N. S., Narayana, V. L., & Sandeep, K. S. (2023). Classification of tweets data based on polarity using improved RBF kernel of SVM. *International Journal of Information Technology*, *15*(2), 965-980. https://doi.org/10.1007/s41870-019-00409-4

7. Gou, J., Du, L., Zhang, Y., & Xiong, T. (2012). A new distance-weighted k-nearest neighbor classifier. *J. Inf. Comput. Sci*, *9*(6), 1429-1436.

8. Hallee, M. J., Napolitano, R. K., Reinhart, W. F., & Glisic, B. (2021). Crack detection in images of masonry using cnns. *Sensors*, *21*(14), 4929. https://doi.org/10.3390/s21144929

9. Heaton, J. (2008). *Introduction to Neural Networks with Java*. Heaton Research, Inc.

10. Hosseinpour-Zarnaq, M., Omid, M., Taheri-Garavand, A., Nasiri, A., & Mahmoudi, A. (2022). Acoustic signal-based deep learning approach for smart sorting of pistachio nuts. *Postharvest Biology and Technology*, *185*, 111778. https://doi.org/10.1016/j.postharvbio.2021.111778

11. Ibba, P., Tronstad, C., Moscetti, R., Mimmo, T., Cantarella, G., Petti, L., ... & Lugli, P. (2021). Supervised binary classification methods for strawberry ripeness discrimination from bioimpedance data. *Scientific Reports*, *11*(1), 11202. https://doi.org/10.1038/s41598-021-90471-5

12. Jolliffe, I. T. (2002). *Principal component analysis for special types of data* (pp. 338-372). Springer New York. https://doi.org/10.1007/0-387-22440-8_13

13. Kalkan, H., & Yardimci, Y. (2006, September). *Classification of hazelnut kernels by impact acoustics*. In 2006 16th IEEE Signal Processing Society Workshop on Machine Learning for Signal Processing (pp. 325-330). IEEE. https://doi.org/10.1109/mlsp.2006.275569

14. Komal, K., & Sonia, D. (2019). GLCM algorithm and SVM classification method for Orange fruit quality assessment. *International Journal of Engineering Research & Technology (IJERT)*, *8*(9), 697-703.

15. Lashgari, M., Imanmehr, A., & Tavakoli, H. (2020). Fusion of acoustic sensing and deep learning techniques for apple mealiness detection. *Journal of Food Science and Technology*, *57*, 2233-2240. https://doi.org/10.1007/s13197-020-04259-y

16. Li, J., Lu, H., & Liu, X. (2014). Feature selection method based on SFFS and SVM for facial expression recognition. In 2014 *IEEE International Conference on Systems, Man, and Cybernetics (SMC)*. IEEE.

17. Liu, Y., Starzyk, J. A., & Zhu, Z. (2007). Optimizing number of hidden neurons in neural networks. *EeC*, *1*(1), 6.

18. Lu, F., Wang, D., Wu, H., & Xie, W. (2016). *A multi-classifier combination method using sffs algorithm for recognition of 19 human activities.* In Computational Science and Its Applications–ICCSA 2016: 16th International Conference, Beijing, China, July 4-7, 2016, Proceedings, Part II 16 (pp. 519-529). Springer International Publishing. https://doi.org/10.1007/978-3-319-42108-7_40

19. Luo, T., Zhao, J., Gu, Y., Zhang, S., Qiao, X., Tian, W., & Han, Y. (2023). Classification of weed seeds based on visual images and deep learning. *Information Processing in Agriculture*, *10*(1), 40-51. https://doi.org/10.1016/j.inpa.2021.10.002

20. Manekar, V., & Waghmare, K. (2014). Intrusion detection system using support vector machine (SVM) and particle swarm optimization (PSO). *International Journal of Advanced Computer Research*, *4*(3), 808.

21. Menesatti, P., Costa, C., Paglia, G., Pallottino, F., D'Andrea, S., Rimatori, V., & Aguzzi, J. (2008). Shape-based methodology for multivariate discrimination among Italian hazelnut cultivars. *Biosystems Engineering*, *101*(4), 417-424. https://doi.org/10.1016/j.biosystemseng.2008.09.013

22. Momeny, M., Jahanbakhshi, A., Jafarnezhad, K., & Zhang, Y. D. (2020). Accurate classification of cherry fruit using deep CNN based on hybrid pooling approach. *Postharvest Biology and Technology, 166*, 111204. https://doi.org/10.1016/j.postharvbio.2020.111204

23. Omid, M. (2011). Design of an expert system for sorting pistachio nuts through decision tree and fuzzy logic classifier. *Expert Systems with Applications, 38*(4), 4339-4347. https://doi.org/10.1016/j.eswa.2010.09.103

24. Pourdarbani, R., Sabzi, S. (2022). Detection of Cucumber Fruits with Excessive Consumption of Nitrogen using Hyperspectral imaging (With Emphasis on Sustainable Agriculture). *Journal of Environmental Sciences Studies*, *7*(4), 5485-5492.

25. Pourreza, A., Pourreza, H., Abbaspour-Fard, M. H., & Sadrnia, H. (2012). Identification of nine Iranian wheat seed varieties by textural analysis with image processing. *Computers and Electronics in Agriculture*, *83*, 102-108. https://doi.org/10.1016/j.compag.2012.02.005

26. Shojaeian, A., Bagherpour, H., Bagherpour, R., Parian, J. A., Fatehi, F., & Taghinezhad, E. (2023). The Potential Application of Innovative Methods in Neural Networks for Surface Crack Recognition of Unshelled Hazelnut. *Journal of Food Processing and Preservation*, 2023(1), 2177724. https://doi.org/10.1155/2023/2177724

27. Singh, S., & Singh, N. P. (2019). Machine learning-based classification of good and rotten apple. In *Recent Trends in Communication, Computing, and Electronics: Select Proceedings of IC3E 2018* (pp. 377-386). Springer Singapore. https://doi.org/10.1007/978-981-13-2685-1_36

28. Tan, S. S., Hoon, G. K., Yong, C. H., Kong, T. E., & Lin, C. S. (2005). *Mapping search results into self-customized category hierarchy.* In Intelligent Information Processing II: IFIP TC12/WG12. 3 International Conference on Intelligent Information Processing (IIP2004) October 21–23, 2004, Beijing, China 2 (pp. 311-323). Springer US. https://doi.org/10.1007/0-387-23152-8_41

29. Taner, A., Öztekin, Y. B., & Duran, H. (2021). Performance analysis of deep learning CNN models for variety classification in hazelnut. *Sustainability*, *13*(12), 6527. https://doi.org/10.3390/su13126527

30. Tarakci, F., & Ozkan, I. A. (2021). Comparison of classification performance of kNN and WKNN algorithms. *Selcuk University Journal of Engineering Sciences*, *20*(2), 32-37.

31. Unay, D., Gosselin, B., & Debeir, O. (2006, January). *Apple stem and calyx recognition by decision trees.* In Proceedings of the 6th IASTED International Conference on Visualization, Imaging, and Image Processing, VIIP (pp. 549-552).

32. Vidyarthi, S. K., Singh, S. K., Xiao, H. W., & Tiwari, R. (2021). Deep learnt grading of almond kernels. *Journal of Food Process Engineering*, *44*(4), e13662.

https://doi.org/10.1111/jfpe.13662

33. Wang, W., Jung, J., McGorrin, R. J., & Zhao, Y. (2018). Investigation of the mechanisms and strategies for reducing shell cracks of hazelnut (*Corylus avellana* L.) in hot-air drying. *Lwt*, *98*, 252-259. https://doi.org/10.1016/j.lwt.2018.08.053

34. Way, T. W., Sahiner, B., Hadjiiski, L. M., & Chan, H. P. (2010). Effect of finite sample size on feature selection and classification: a simulation study. *Medical Physics*, *37*(2), 907-920. https://doi.org/10.1118/1.3284974

35. Yang, R., Wu, Z., Fang, W., Zhang, H., Wang, W., Fu, L., ... & Cui, Y. (2023). Detection of abnormal hydroponic lettuce leaves based on image processing and machine learning. *Information Processing in Agriculture*, *10*(1), 1-10. https://doi.org/10.1016/j.inpa.2021.11.001

بهینه‌سازی هایپرپارامترهای مدل‌های ماشین بردار پشتیبان، k نزدیک‌ترین همسایه و شبکه عصبی مصنوعی برای طبقه‌بندی تصاویر فندق‌ها بر اساس روش انتخاب ویژگی‌ها

حسین باقرپور ۱*، فرهاد فاتحی ۱، علیرضا شجاعیان ۱، رضا باقرپور ۲

چکیده

در برخی کشورها، فندق‌ها به دلیل محدودیت‌های فناوری موجود و افزایش طول عمر نگهداری‌شان، معمولاً با پوسته مصرف می‌شوند. بنابراین، فندق‌های خندان مشتری پسندی بالاتری دارند. در مقیاس نیمه‌صنعتی، فندق‌های خندان و دهان بسته در حال حاضر از طریق بازرسی بصری از یکدیگر جدا می‌شوند. این مطالعه به‌منظور توسعه یک الگوریتم جدید برای جداسازی فندق‌های خندان از فندق‌های ترک‌خورده یا دهان بسته انجام شـده اسـت. در رویکرد اول، تکنیک‌های کاهش بعد مانند روش‌های مبتنی بر انتخاب ویژگی (SFFS) و تحلیل مؤلفه اصلی (PCA) بـرای انتخـاب یـا اسـتخراج ترکیبی از ویژگی‌های رنگ، بافت و خاکستری به‌عنوان ورودی مدل استفاده شدند. در رویکرد دوم، ویژگی‌هـا بـه شـکل انفـرادی مسـتقیماً بـه‌عنوان ورودی‌ها استفاده شدند. در این مطالعه، سه مدل معروف یادگیری ماشین، شامل ماشین بـردار پشـتیبان (SVM)، نزدیـک‌تـرین همسـایه‌ها (KNN) و پرسپترون چندلایه (MLP) مورد استفاده قرار گرفتند. نتایج نشان داد که روش SFFS تأثیر بیشتری در بهبود عملکرد مدل‌ها نسـبت بـه روش PCA دارد. با این حال، تفاوت معنی‌داری بین عملکرد مدل‌های توسعه‌یافته با ویژگی‌های ترکیبی (۹۸/۰۰٪) و عملکـرد مـدل‌هـا بـا اسـتفاده از ویژگی‌هـای انفرادی (۹۸/۶۷٪) وجود نداشت. نتایج کلی این مطالعه نشان داد که مدل MLP با یک لایه پنهان، دراپ اوت برابر با ۰/۳ و ۱۰ نورون، بـا اسـتفاده از ویژگی HOG به‌عنوان ورودی، انتخاب خوبی برای طبقه‌بندی فندق‌ها به دو دسته خندان و دهان بسته می‌باشد.

واژه‌های کلیدی: PCA، خندان، کاهش بعد، دهان بسته، یادگیری ماشین

۱- گروه مهندسی بیوسیستم، دانشکده کشاورزی، دانشگاه بو علی سینا، همدان، ایران

۲- گروه مهندسی کامپیوتر، دانشکده مهندسی کامپیوتر، دانشگاه علم و صنعت، تهران، ایران

(Email: h.bagherpour@basu.ac.ir :نویسنده مسئول -*)

مندرجات

نشریه ماشین های کشاورزی

عنوان مقالات